Pre-clinical evaluation and improvement of attenuated malaria sporozoite vaccine candidates

Dissertation

Zur Erlangung des akademischen Grades
Doctor rerum naturalium
(Dr. rer. nat)
im Fach Biologie

Eingereicht an der
Lebenswissenschaftlichen Fakultät
der Humboldt-Universität zu Berlin

von
Oriana Kay-Maria Kreutzfeld

Präsident der Humboldt-Universität zu Berlin
Prof. Dr.-Ing. Dr. Sabine Kunst

Dekan der Lebenswissenschaftlichen Fakultät
Prof. Dr. Bernhard Grimm

Gutachter:
1. Prof. Dr. Kai Matuschewski
2. Prof. Dr. Christian Schmitz-Linneweber
3. Dr. Julius Hafalla

Tag der mündlichen Prüfung: 15.2.2019

Eidesstattliche Erklärung

Hiermit erkläre ich an Eides statt, die vorliegende Dissertation selbständig angefertigt und keine anderen als die angegebenen Hilfsmittel verwendet zu haben.

Ich erkläre hiermit, dass ich an keiner anderen Universität ein Prüfungsverfahren beantragt bzw. die Dissertation in dieser oder anderer Form bereits anderweitig als Prüfungsarbeit verwendet oder einer anderen Fakultät als Dissertation vorgelegt habe. Wurden Ergebnisse in Kooperation produziert, ist dies entsprechend angegeben.

Die vorliegende Arbeit wurde am Max-Planck-Institut für Infektionsbiologie, Berlin und an der Humboldt Universität zu Berlin an der Fakultät für Lebenswissenschaften am Institut für Biologie im Department für molekulare Parasitologie, unter Leitung von Prof. Dr. Kai Matuschewski und Dr. Katja Müller durchgeführt.

Berlin, den 30.11.2018 Oriana Kreutzfeld

Erweiterte Eigenständigkeitserklärung

Hiermit versichere ich, Oriana Kreutzfeld, dass die folgenden Publikation:

- „Engineering of Genetically Arrested Parasites (GAPs) For a Precision Malaria Vaccine" (erschienen in Front. of cell and micro.)

maßgeblich von mir verfasst wurde. Mögliche Übereinstimmungen mit Textpassagen aus meiner Dissertation „Pre-clinical evaluation and improvement of attenuated sporozoite vaccine candidates" stellen somit keinen Plagiatsfall dar.

Dies wird bei Bedarf bestätigt durch den Betreuer der Dissertation und Co-Autoren der aufgeführten Publikation Prof. Dr. Kai Matuschewski und Dr. Katja Müller.

Berlin, den 30.11.2018 Oriana Kreutzfeld

Abstract

Stage conversion is a hallmark of parasites in general and permits unprecedented vaccine strategies. In the case of malaria, experimental immunizations with live genetically attenuated parasites (GAPs) preventing the development beyond the clinically silent liver stage have proven safe and efficacious against challenge infections in mice, primates, and humans. A number of GAPs have been engineered in *Plasmodium berghei, P. yoelii* and *P. falciparum* with varying safety and efficacy, however, a superior vaccine candidate providing both safety and efficacy and the underlying immune effector mechanisms against pre-erythrocytic stages remain elusive.

One GAP vaccine candidate, *SLARP*, provides the most robust life cycle arrest *in vivo* and *in vitro*. However, immunizations with *ΔSLARP* sporozoites do not elicit long-lasting immunity, most likely as a result of early liver stage arrest. In contrast, *ΔP36p/P36* sporozoites elicit long-lasting immunity, but lead to breakthrough infections during immunizations. This study gives a systematic pre-clinical evaluation of a triple knockout (tKO) GAP by combining *ΔSLARP* and *ΔP36p/P36*, which is a crucial step before translation to human clinical trials. Complete arrest of tKO parasites in cultured hepatoma cells and sporozoite-infected mice was confirmed. Animals immunized with tKO sporozoites elicit high antibody titers. Parasite load in the liver and the time to blood infection after a sporozoite challenge revealed reduced efficacy of the tKO vaccine.

While superior immunity can be achieved by a late developmental arrest at liver-to-blood stage conversion, the underlying molecular mechanisms remain elusive. An important question is whether parasite antigens are exposed to the hepatocyte cytoplasm. Protein translocation into the host cell cytoplasm mediated by PTEX, a protein translocon, is considered essential for blood stages. Strikingly, during liver stage maturation Heat-shock-protein 101 (HSP101), a core component of PTEX, is not expressed, suggesting that immune recognition of infected cells is severely reduced due to the lack of parasite-derived epitopes presented by MHCI.

To clarify the role of HSP101 in liver stage protein export and potential concomitant enhanced host immune responses, transgenic *P. berghei* parasites were generated expressing an extra copy of *HSP101* to commence parasite protein export in early liver stages. Parasites expressing elevated levels of HSP101 show severe liver stage growth defects *in vitro* and *in vivo* and in good agreement, inferior protection was observed in immunized animals. Surprisingly, parasites expressing low levels of HSP101 are able to complete the life cycle, but lack early liver stage protein export. Our results suggest that HSP101 expression is tightly controlled and PTEX-dependent early liver stage export cannot be restored solely by HSP101 overexpression.

Overall, pre-clinical analysis and improvement of GAP-based vaccine candidates can inform ongoing human vaccine trials and boost malaria vaccine development.

Zusammenfassung

Der Stadienwechsel ist ein Merkmal von Parasiten, welcher einen Angriffsbereich für potentielle Impfstoffkandidaten bildet. Im Fall von Malaria haben experimentelle Immunisierungsstudien mit genetisch attenuierten Leberstadien Parasiten (GAP), welche die Entwicklung über das klinisch asymptomatische Leberstadium hinaus verhindern, erwiesen, dass eine sichere und effiziente Immunisierung in Mäusen, Primaten und Menschen gewährleistet ist. Eine Reihe von GAPs mit unterschiedlicher Sicherheit und Wirksamkeit wurden in *Plasmodium berghei*, *P. yoelii* und *P. falciparum* generiert. Ein Impfstoffkandidat, der sowohl Sicherheit und Wirksamkeit als auch die zugrunde liegenden Prozesse der Immunerkennung und -antworten gegen prä-erythrozytische Stadien bietet, ist nach wie vor weitestgehend nicht in Sicht.

Zum jetzigen Zeitpunkt existiert nur ein GAP-basierter Kandidat *ΔSLARP,* welcher vollständig in der Leber arretiert. Jedoch haben Langzeitstudien gezeigt, dass der Kandidat keinen vollständigen und langanhaltenden Schutz bieten kann, höchstwahrscheinlich als Folge eines frühen Entwicklungsstillstandes in der Leber. Im Gegensatz dazu bieten Immunisierungen mit ΔP36p/P36 Sporozoiten einen langanhaltenden Schutz führen jedoch während des Immunisierungsprozesses gelegentlich zu Blutstadieninfektionen. Diese Studie liefert eine systematische vorklinische Bewertung eines dreifachen KO (tKO) GAP-Parasiten, durch die Kombination zweier Knockouts *ΔSLARP* und *ΔP36p/P36*. Dies ist ein entscheidender Schritt vor der Durchführung von humanen klinischen Studien. Die vollständige Arretierung von tKO Parasiten in kultivierten Hepatomzellen und mit Sporozoiten infizierten Mäusen konnte bestätigt werden. Mit tKO Sporozoiten immunisierte Tiere entwickeln ähnliche Antikörpertiter wie die Tiere, welche mit den ursprünglichen KOs immunisiert wurden. Die Parasitenlast in der Leber und die Zeit bis zur Blutinfektion nach einer Sporozoiteninfektion zeigten jedoch eine verminderte Wirksamkeit des tKO-GAP-Impfstoffs.

Während ein besserer Schutz durch einen späten Entwicklungsstillstand bei dem Parasitenstadienwechsel von Leber zu Blut erreicht werden kann, bleiben die zugrunde liegenden molekularen Mechanismen unklar. Eine weitere wichtige Frage ist, ob parasitäre Antigene im hepatozyten Zytoplasma sichtbar sind, eine Vorrausetzung für die Antigenpräsentation durch infizierten Leberzellen. Die Modifizierung der erythrozytären Wirtszelle ist ein überlebenswichtiger Mechanismus, der von dem Export von parasitären Proteinen durch PTEX, ein Proteintranslocon, in das Zytoplasma der Wirtszelle ermöglicht wird. Erste Studien konnten zeigen, dass der Proteinexportkomplex in Leberstadien nicht vollständig funktionstüchtig ist, da ein essentielles Protein, das Hitzeschockprotein 101 (HSP101), eine Kernkomponente von

PTEX, nicht exprimiert wird. Es lässt vermuten, dass die Immunerkennung infizierter Zellen, aufgrund der limitierten Präsentation von parasitären Epitopen über MHCI, stark reduziert ist.

Um die Rolle von HSP101 für den Export von Leberproteinen und die damit einhergehenden verstärkten Immunantworten des Wirts zu klären, wurden transgene *P. berghei* Parasiten erzeugt, die eine zusätzliche Kopie des HSP101 Proteins tragen, um den Parasitenproteinexport in frühen Leberstadien anzustoßen. Transgene Parasiten weisen *in vitro* und *in vivo* schwere Wachstumsstörungen im Leberstadium auf. Mäuse, die mit transgenen Parasiten immunisiert wurden, sind nicht gut gegen Neuinfektionen geschützt. Überraschenderweise können Parasiten, die geringe Mengen an HSP101 exprimieren, den Lebenszyklus abschließen, dabei konnte der frühe Export von Leberstadienproteinen nicht nachgewiesen werden. Die Ergebnisse legen nahe, dass die Expression von HSP101 streng kontrolliert wird und der PTEX-abhängige Export im frühen Leberstadien nicht durch die Überexpression von HSP101 wiederhergestellt werden kann, was auf ein multifaktorielles-System schließen lässt.

Insgesamt können prä-klinische Studien und die Weiterentwicklung von GAP-basierten Impfstoffkandidaten die laufenden humanen Impfstoffstudien beeinflussen und die Entwicklung von Malariaimpfstoffen vorantreiben.

Table of contents

Figure Index

Table Index

Supplementary Figure Index

Supplementary Table Index

Abbreviations

%	percent
°C	degree celsius
~	around
2D	two dimensional
µ	micro
µl	microliter
µm	micrometer
µM	micromolar
ACT	artemisinin-based combination therapies
APC	antigen presenting cell
AZ	Azythromycin
bp	basepairs
BSA	bovine serum albumin
C-terminal	carboxy-terminal
CD	cluster of differentiation
cDNA	Complementary DNA
$CD8^+$	Cluster of differentiation 8
$CD4^+$	Cluster of differentiation 4
CM	cerebral malaria
CQ	Chloroquine
CSP	Circum sporozoite protein
ddH_2O	distilled water
DHFR	dihydrofolate reductase
dKO	double knockout
DMSO	Dimethyl sulfoxide
DMEM	Dulbecco's modified Eagle's medium
DNA	Deoxyribonucleic acid
dNTP	deoxyribonucleotide triphosphate
E. coli	*Escherichia coli*
e.g.	exempli gratia
ECM	experimental cerebral malaria
EDTA	ethylenediaminetetraacetic acid
EEF	exo-erythrocytic form
EMP	erythrocyte membrane protein
ER	endoplasmatic reticulum
et al.	*et alia*
ETRAMP	early-transcribed membrane proteins
EXP	Exported protein
FACS	Fluorescence activated cell sorting
Fig.	Figure
FCS	Fetal calf serum
fwd	forward
g	gram
G	guanosine
GAP	Genetically attenuated parasites

GAP50	Glideosome associated protein
gDNA	genomic DNA
GFP	green fluorescent protein
GPI	Glycophosphatidylinositol
h	hour/s
hDHTR	human dihydrofolate reductase
hpi	hours post-infection
HSP	Heat shock protein
HSP70	Heat shock protein 70
Huh7	Hepato cellular carcinoma cells
IBIS	intra-erythrocytic *P. berghei*-induced structures
IFA	immunofluorescence assay
IFN-γ	Interferon gamma
IgG	Immunoglobulin G
IL	interleukin
iRBC	infected red blood cell
i.p.	intraperitoneal
i.v.	intravenously
kb	kilo bases
KHARP	knob-associated histidine-rich protein
kg	kilogram
KO	knockout
L	liter
LB	Lysogeny Broth
LISP	Liver specific protein
LS	Liver stage
M	molar
m	meter
MΦ	macrophage
mCh	mCherry
MgCl2	magnesium chloride
MHC	major histocompatibility complex
ml	milliliter
min	minutes
mm	millimeter
mRNA	messenger ribonucleic acid
n	number
NaCl	sodium chloride
N-terminal	amino-terminal
NF-κB	nuclear factor kappa-light-chain-enhancer of activated B cells
n.d.	not determinable
ng	nanogram
nm	nanometer
NMRI	Naval Medical Research Institute
ORF	open reading frame
P.	*Plasmodium*
p	p-value

p.i.	post infection
P36p	6-cysteine protein
P36	6-cysteine protein
PALM	*Plasmodium*-specific apicoplast protein important for liver merozoites formation
P. berghei/ P.b.	*Plasmodium berghei*
P. chabaudi	*Plasmodium chabaudi*
P. falciparum/ P.f.	*Plasmodium falciparum*
P. vivax	*Plasmodium vivax*
P. yoelii	*Plasmodium yoelii*
PBS	phosphate buffered saline
PCR	Polymerase chain reaction
PEXEL	*Plasmodium* export element
PFA	Paraformaldehyde
PM	Plasmepsin
PNEP	PEXEL-negative exported proteins
PPM	Parasite plasma membrane
PRR	pattern recognition receptor
PTEX	*Plasmodium* translocon of export proteins
PV	Parasitophorous vacuole
PVM	parasitophorous vacuole membrane
RAS	Radiation attenuated sporozoites
RBC	Red blood cells
rev	reverse
RFP	red fluorescent protein
RNA	Ribonucleic acid
rpm	revolutions per minute
RPMI	Roswell Park Memorial Institute medium
RT	room temperature
qRT-PCR	Real-time quantitative PCR
SLARP	Sporozoite and liver stage asparagine-rich protein
s	second/s
s. ch.	see chapter
SD	standard deviation
Taq	Thermus aquaticus
tKO	triple knockout
TMD	transmembrane domain
TNF-α	Tumor necrosis factor alpha
TRX	thioredoxin
TRAP	Thrombospondin-related anonymous protein
TVN	tubovesicular network
UIS	upregulated in infective sporozoites
UTR	untranslated region
WHO	World Health Organization
WT	wildtype

1 Introduction

1.1 Malaria: An introduction to the disease

Malaria remains the most important vector-borne infectious disease, affecting half of the world's population. Globally, >200 million infected individuals develop clinical symptoms, and >400,000 die because of severe malaria, primarily children in Sub-Saharan Africa (WHO, 2018). New strategies for malaria prevention and eradication are thus urgently required. The current malaria control programs target the causative agents, *Plasmodium falciparum*, *P. vivax*, and three other human-infecting *Plasmodium* parasites, at different life cycle stages, which together reduces morbidity and mortality in endemic regions. Attacking the parasite at its vector stage with long-lasting insecticide treated bed nets and insecticide-indoor residual spraying combined with access to rapid diagnosis and artemisinin-based combination therapy for clinical malaria episodes are recommended by the WHO (WHO, 2018)

Protozoan *Plasmodium* parasites belonging to the phylum of Apicomplexa, infect a diverse range of mammalian hosts. Five *Plasmodium* species are known to infect humans with *Plasmodium falciparum*, claiming most of the deadly cases. In contrast, *P. vivax* the most wide spread *Plasmodium* species forms dormant liver stages, so called hypnozoites, that can cause relapsing *Plasmodium* infections, thereby underestimating the impact of *P. vivax* on global malaria burden (Mueller *et al.*, 2009). Two other strains *P. ovale* (split in *curtisi* and *wallikeri*) and *P. malariae* contribute only to a small proportion of mild malaria infections, which are relatively short lived for *P. ovale* but can last a decade *P. malariae* (Faye *et al.*, 1998, Sutherland *et al.*, 2010, Ansari *et al.*, 2016). More recently, *P. knowlesi*, primarily a zoonosis, has been attributed to several human deaths in Southeast Asia. Human to human transmission has not been observed and its impact on the global malaria burden remains elusive (Ahmed & Cox-Singh, 2015).

Malaria burden in endemic regions is dependent on vector prevalence, transmission efficiency, asymptomatic carrier reservoirs, and *Plasmodium* strain and treatment availability. Primarily at risk are children under five years and pregnant women, since naturally acquired and placental immunity are absent in young patients and mothers carrying their first child, respectively. Symptomatic infections are caused by the blood stage of the parasites with symptoms including fever, headache and nausea. Complicated or severe malaria cases are described as cases causing hypoxia, anemia and cerebral malaria, which can lead to death in patients. Infections in adults are often asymptomatic, with mild symptomatic periods, and as a consequence fail to be treated. This reservoir of untreated infections propagates the cycle of malaria infections (Chen *et al.*, 2016).

Repeated exposure to *Plasmodium* transmission in malaria-endemic countries leads only to very slow acquisition of naturally acquired immunity that rapidly wanes. Development of protective immunity is likely hindered by blood infection, the exclusive cause of malaria-related morbidity and mortality. Therefore, the pre-erythrocytic phase of the *Plasmodium* life cycle in the mammalian host is particularly attractive as immunization agent since no clinical symptoms are associated with this first replication phase (Prudencio *et al.*, 2006, Silvie *et al.*, 2008, Matuschewski *et al.*, 2011). Prevention of disease by vaccination is an ideal addition to the portfolio of malaria intervention tools; however, it remains one of the greatest challenges in medical research.

1.2 *Plasmodium*: Shining a light on the parasite life cycle

Continuous stage conversion while evading the human immune system requires a constant change in parasitic protein repertoire. Determined by its life cycle parasites switch between intra- and extracellular stages leading to perpetual change in parasite morphology.

Upon an infectious mosquito bite, the parasite is injected into the dermis of the host with the saliva of the mosquito. The active parasite stage, termed sporozoite, travels in a gliding movement to the nearest blood vessel (**Fig. 1**). Hereby TRAP-like protein (TLP) plays a major role in parasite gliding ability and infectivity (Sultan *et al.*, 1997, Heiss *et al.*, 2008, Moreira *et al.*, 2008). Sporozoites remaining in the dermis contribute to antibody development against sporozoite surface antigens in the draining lymph nodes of the skin (Amino *et al.*, 2008). Particularly CSP (circumsporozoite protein) and TRAP (thrombospondin-related anonymous protein) are recognized as sporozoite antigens; however, many other surface proteins might play a role in this process (Yoshida *et al.*, 1980, Trieu *et al.*, 2011).

Once in the blood stream, parasites actively invade the liver through the sinusoidal barrier in a process termed traversal. Sporozoites traverse several hepatocytes before infecting a final one to mature into infective merozoites for red blood cell (RBC) infection (**Fig. 1**). Traversal requires expression of SPECT (Sporozoite microneme protein essential for traversal), SPECT2 (perforin-like protein 1, PLP1), CelTOS (cell traversal protein for ookinetes and sporozoites) and several other parasite proteins (Ishino *et al.*, 2004, Bhanot *et al.*, 2005, Risco-Castillo *et al.*, 2015), however, precise protein function in traversal remains to be elucidated. Infection of hepatocytes is mediated by sporozoites binding to hepatocyte surface proteins CD81 and scavenger receptor B1, inducing sporozoite invasion and formation of a parasitophorous vacuole (PV) (Rodrigues *et al.*, 2008, Manzoni *et al.*, 2017). PV establishment, remodeling and maintenance are vital for intra-hepatocytic development and rely on, amongst other processes, interaction of hepatocyte receptor EphA2 with parasite proteins *P36p* (P52) and *P36* (Kaushansky *et al.*, 2015). During

sporozoite maturation liver stage gene expression is tightly controlled by various mechanisms among them proteins e.g. SLARP and PUF2 controlling mRNA translation or internal sequences in ORFs of liver specific genes (Silvie *et al.*, 2008, Muller *et al.*, 2011). Incorporation of transcriptionally and translationally regulated sporozoite genes such as UIS3 and UIS4 (upregulated in infective sporozoites gene 3 and 4) remodel the PVM (Mueller *et al.*, 2005). Parasites eventually develop into liver stage trophozoites. Further maturation to liver stage schizonts induces elevated protein export facilitating PVM destruction and subsequent merosome release (Burda *et al.*, 2015, Burda *et al.*, 2017). Mature merosomes harboring thousands of merozoites bud off and attach to the host's lung blood capillaries from where they are released after 44 hours in the liver for *P. berghei* and 7-10 days in *P. falciparum* (Sturm *et al.*, 2006).

Within seconds, merozoites invade RBCs using a complex interplay of multiple parasite and host proteins to induce a patent blood stage infection. The parasite then rapidly matures in a PV from ring stages into trophozoites (**Fig. 1**). However, blood cells are deprived of most living cell components including a mechanism to acquire nutrients for cell growth or recognize non-self proteins to be displayed to cytotoxic T cells via the major histocompatibility complex (MHCI). Hence, the parasite uses a protein translocon termed PTEX to export parasitic proteins beyond the PV to remodel its host cell (Boddey & Cowman, 2013). Remodeling phases enable the parasite to acquire nutrients, dispose waste and establish knob like structures on the iRBC surface to sequester in the blood vessels to avoid splenic killing (Langreth & Peterson, 1985, Miller *et al.*, 2012). However, *Pf*EMP1 (erythrocyte membrane protein 1), the mediator of vascular sequestration, is also a target for the host immune system to recognize and eventually attack the otherwise hiding parasite. To avoid clearance parasite by the host's immune system use a system of 60 sequentially expressed *var* genes encoding EMP1 to undergo antigenic changes (Guizetti & Scherf, 2013).

After completing schizogony, schizonts rupture and release 16-32 mature merozoites to infect other RBCs (Cowman & Crabb, 2006). A few of the parasites are programmed to follow a different path in the next maturation phase developing into mature sexual stages, termed female or male gametocytes, in the bone marrow. During the next blood meal, mosquitoes take up mature gametocytes with the ingested blood into the midgut of the mosquito (**Fig. 1**). Exflagellating male gametocytes form zygotes with female gametocytes and sexually replicate into ookinetes, which travel across the midgut barrier to mature into oocysts. During oocyst maturation thousands of sporozoites are formed which are released after 17 days and travel to the salivary glands of the mosquito where they are then transmitted to the human host during the next infectious bite of a mosquito (Guttery *et al.*, 2015, Sinden, 2015).

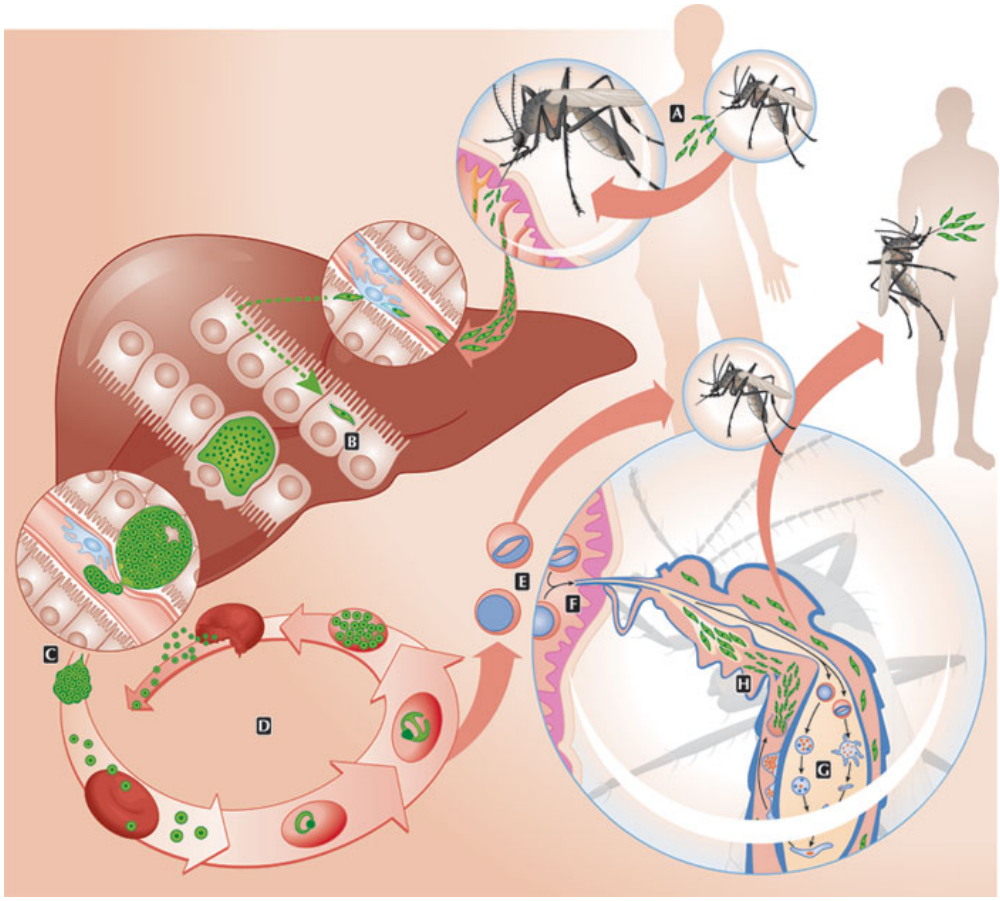

Figure 1 *Plasmodium* life cycle

Upon a bite of an infected mosquito, sporozoites glide through the dermis to reach the next blood vessel. When reaching the liver, sporozoites traverse across the sinusoidal barrier and several hepatocytes before infecting the one to asexually mature into mature merosomes. Merosomes harboring thousands of merozoites bud into the lung lumen where they release the merozoites. Free merozoites invade red blood cells where they mature from ring stages over trophozoites to merozoites, which break free to infect new red blood cells and complete the asexual cycle. Each cycle, a small proportion of parasites develop into sexual stage gametocytes. During the mosquito's next blood meal gametocytes are ingested to complete the life cycle in the mosquito by developing via ookinetes and oocyst to sporozoites (Portugal *et al.*, 2011).

1.3 The murine *Plasmodium* vaccine model

Rodent *Plasmodium* parasites were first discovered in the Democratic Republic of Congo in 1984 (Vincke & Lips, 1948). Studies of infected African thicket rats led to the discovery of four rodent species *P. berghei*, *P. yoelii*, *P. chabaudi* and *P. vinckei*, which were all transferred to rodent laboratory models. In the early 2000s, genome sequencing for *P. falciparum* and *P. berghei* opened up new possibilities for genetic manipulation of *Plasmodium* parasites. Conventional double homologous crossover of haploid asexual *Plasmodium* blood stages allowed investigation of the parasite's unique maturation. CRISPR-Cas9 and DiCre conditional knockout systems revolutionized indepth exploration of *P. falciparum* blood stage's genome and proteome (Collins *et al.*, 2013, Ghorbal *et al.*, 2014). However, the mosquito stages and the clinically silent liver stage remained poorly studied. Larger screens for sporozoites and liver stage-specific genes

identified essential stage-specific proteins. Established murine malaria models employing the rodent malaria parasites *P. berghei* and *P. yoelii* enable the exploration of stage-specific proteins and their importance for parasite survival. In recent years more than 120 candidate genes have been analyzed by reverse genetics (Janse *et al.*, 2011), data that is valuable for non-blood stage drug and vaccine studies.

To evaluate immunological host-parasite interactions and induce robust long-term immunity against challenge infections, it is important to identify the correct parasite/host combination from which to draw valid conclusions following pre-clinical immunization experiments (Matuschewski, 2013). The *P. berghei*-C57BL/6 combination remains the most robust vaccine model to date, whereas immunizations using *P. yoelii* mutants in BALB/c mice are only of modest predictive value, since protection is easily achieved in this model. Other combinations, such as *P. berghei* and BALB/c mice, are invalid because of refractoriness of particular combinations of mouse strains and infections with certain murine malaria sporozoites (Scheller *et al.*, 1994). One important immunological difference is that protection in the *P. yoelii*-BALB/c model largely depends on the immunodominant $CD8^+$ T cell epitope of CSP. In marked contrast, T cell responses in the *P. berghei*-C57BL/6 model are likely multifactorial (Hafalla *et al.*, 2011, Hafalla *et al.*, 2013), which closely mimics infections in human populations with a large range of MHCI haplotypes and only infrequent CSP–specific $CD8^+$ T cell responses (Offeddu *et al.*, 2012).

This observation raises the general questions as to which mouse model best mimics the potential outcome of an orthologous knockout vaccine in humans and how transferable data generated in a mouse model are for human application. Transferring these findings to the human malaria agent *P. falciparum* is a challenge since studies on human liver stages are difficult. Humanized mouse models and primary human hepatocytes give the first indication on liver developmental abortion and safety of vaccine candidates. Only very few vaccine candidates have been tested for their safety and protection in human volunteers, however an ultimate study is inevitable.

In conclusion, comparative studies on vaccine efficacy should include the *P. berghei*-C57BL/6 model (Friesen & Matuschewski, 2011), to better define long-term protection against re-challenges. The recent evaluation of *Grammomys dolichurus*, an Afrotropical arboreal rodent, which naturally harbors rodent *Plasmodium* infections, as a model to study pre-erythrocytic vaccine strategies will be an important addition for preclinical evaluation of safety and immunogenicity of GAP vaccines (Conteh *et al.*, 2017). In concordance with the data from murine *Plasmodium* models, the natural host is highly susceptible to *P. berghei* sporozoite induced infections and multiple high immunization doses are required for robust protection (Conteh *et al.*, 2017). Vaccines should be evaluated for vaccine safety and immunogenicity in a two-step preclinical process before advancing to human trials. First, comparative evaluation of

the candidate *P. berghei* and *P. yoelii* GAP lines in the respective mouse strains, C57BL/6 and BALB/c, will pre-select GAPs that are completely arrested upon high dose sporozoite inoculations and elicit long-lasting (>30 days) sterile immunity. Second, confirmation of safety and immunogenicity of the *P. berghei* GAP line in *G. dolichurus* immunization and challenge study provides an evidence-based rationale for translation to *P. falciparum* GAP trials.

1.4 Genetically attenuated parasites as vaccine candidates

Approaches to design a protective long-lasting malaria vaccine are wide-ranging, and some of them have already reached phase III clinical trials (WHO, 2016). Among these candidates is RTS,S/AS01, which is the first malaria vaccine to achieve licensure for administration in malaria endemic areas. RTS,S/AS01 is a hepatitis B-based subunit vaccine and contains a fragment of CSP (Stoute *et al.*, 1997). Recent phase III clinical trial results revealed an unfavorable protection level casting doubt on the impact of RTS,S/AS01 in malaria control efforts (Rts *et al.*, 2011, Olotu *et al.*, 2016).

A benchmark for a malaria vaccine has existed already for several decades, and this experimental vaccine with proven long-term protection is a whole sporozoite vaccine. Small immunization studies in mice, non-human primates, and humans demonstrated that radiation attenuated sporozoites (RAS) elicit sterile protection against *Plasmodium* challenge infections (Nussenzweig *et al.*, 1967, Nussenzweig *et al.*, 1969, Clyde *et al.*, 1973, Gwadz *et al.*, 1979) (Hoffman *et al.*, 2002). Irradiation induces DNA breakage in the parasites, which reduces the numbers of nuclear divisions and limits liver stage expansion to early schizonts (**Fig. 2**, Silvie *et al.*, 2002). Timing and radiation dosage are critical since over-irradiated sporozoites arrest early at the unicellular stage, thus decreasing protection in experimental cohorts (Friesen & Matuschewski, 2011). Successful hepatocyte invasion and initial intra-hepatic development of live, metabolically active sporozoites are required to elicit strong immunity, and, therefore, pose a substantial hurdle toward an affordable and undemanding sporozoite vaccine. The central importance of live and metabolically active sporozoites has been corroborated with heat-killed sporozoites, which elicit only very weak and short-term, antibody-mediated protection against subsequent *Plasmodium* sporozoite challenge infections (Hafalla *et al.*, 2006). On the other hand, suboptimal irradiation harbors the risk of breakthrough infections during vaccination — a considerable drawback concerning safety. RAS arrest early during liver stage development and express primarily sporozoite-derived antigens, including CSP and TRAP, which likely contribute to priming of T cell-mediated immunity.

Liver stage developmental arrest can also be achieved by an alternative approach, termed chemical attenuation of sporozoites (CAS), which is based on simultaneous administration of

normal sporozoites and anti-malarial drugs e.g. chloroquine, azithromycin (AZ) or pyrimethamine (**Fig. 2**, Belnoue *et al.*, 2004, Putrianti *et al.*, 2009, Roestenberg *et al.*, 2009, Friesen *et al.*, 2010, Bijker *et al.*, 2013). While these approaches offer interesting evaluations in small-scale exploratory clinical studies, they are critically reliant on continuous clinical supervision during drug administration and currently bear no translational perspective.

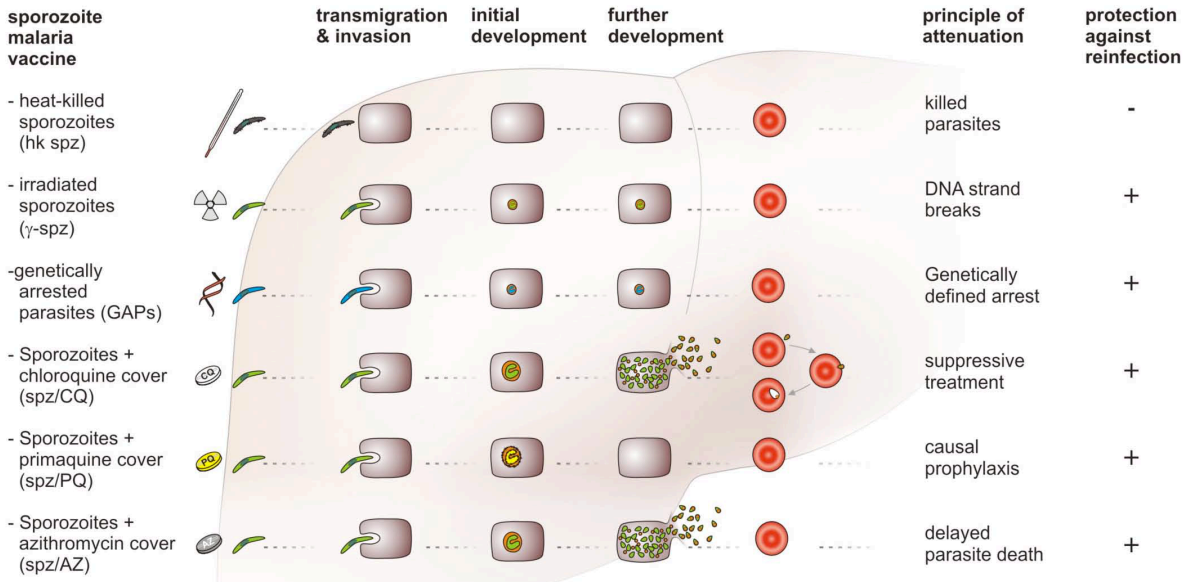

Figure 2 Malaria preventive vaccine strategies

The different pre-erythrocytic vaccine approaches tackle the parasite during its asymptomatic asexual replication in the liver. Immunizations with heat-killed sporozoites don not allow therefore, lack protection against follow-up infection. Irradiated sporozoites lead to early arrest of the parasite in the liver and therefore induce intermediate protection. Genetically attenuated parasites (GAPs) arrest, depending on the gene knockout, at early to late liver stage. Immunizations with GAPs elicit potent protection, but occasionally lead to breakthrough infections during immunization. Parasites under drug cover develop until early liver stages (PQ) or until the first replication cycle in blood stages (AZ or CQ) and immunizations elicit potent protection against follow-up infections (Matuschewski *et al.*, 2011).

The potential to induce lasting protection by live attenuated, metabolically active parasites led to the engineering of genetically attenuated parasites (GAPs) as tailored whole parasite vaccines against malaria infections (**Fig. 2**, Mueller *et al.*, 2005). Murine malaria models employing the rodent malaria parasites *P. berghei* and *P. yoelii* enable the exploration of liver stage-specific proteins function and their importance for parasite survival. In the past, over 120 genes have been targeted by experimental genetics and analyzed for defects during the *Plasmodium* life cycle in both vector and mammalian host (Janse *et al.*, 2011). Many gene knockouts resulted in normal parasite life cycle progression or refractoriness to targeted deletion, indicative of redundant functions during life cycle progression or vital roles for blood infection, respectively. Additionally, arrest of the parasite development in the mosquito midgut, prior to salivary gland colonization, or ahead of hepatocyte invasion was frequently observed. Accordingly, only very few candidate genes fulfill the criteria of potential GAP vaccine candidate lines.

1.4.1 First generation GAPs: Proof of principle studies

The first preclinical studies that showed successful generation of GAP lines and tested their efficacy in immunization protocols targeted *Plasmodium berghei* genes that represent members of the early transcribed membrane protein (ETRAMP) family (Mueller *et al.*, 2005, Mueller *et al.*, 2005). The selected genes, i.e., upregulated in infective sporozoites gene 3 (UIS3) and UIS4, fulfilled three principal criteria: (i) stage-specific gene expression in pre-erythrocytic stages, thereby allowing recombinant knockout strains to be selected during blood stage transfection; (ii) abundant expression in pre-erythrocytic stages, indicating likely vital roles during this phase of the life cycle; and (iii) genes that are unique to *Plasmodium* and related haemosporidian parasites, which all share the hallmark of the first obligate population expansion phase in the host liver (Matuschewski *et al.*, 2002). *In vitro* studies in cultured hepatoma cells revealed that *P. berghei* as well as *P. yoelii ΔUIS3* and *ΔUIS4* parasite lines arrest early during liver stage development after completion of sporozoite transformation to liver stages, but before onset of parasite replication (**Fig. 3**, Mueller *et al.*, 2005, Mueller *et al.*, 2005, Tarun *et al.*, 2007).

Immunization studies with one prime and two booster vaccinations showed complete long-term protection with *P. berghei* and *P. yoelii ΔUIS3* and *ΔUIS4* GAPs in C57BL/6 and BALB/cJ mice, respectively (Mueller *et al.*, 2005, Mueller *et al.*, 2005, Tarun *et al.*, 2007). The study on *P. berghei ΔUIS4* GAPs established frequent occurrence of breakthrough infections, i.e., a proportion of animals developed blood infections during the immunization procedure (Mueller *et al.*, 2005). This safety concern needs careful examination before progression of *P. falciparum* GAPs to human testing can take place (Matuschewski, 2013). Notably, the identification of orthologous genes for UIS3 and UIS4 in *P. falciparum* has so far remained elusive, although various ETRAMPs emerge as potential candidates (Spielmann *et al.*, 2012).

Another first generation GAP line in *P. berghei* and *P. yoelii* are parasites that lack *P36p* (also termed P52), a member of the *Plasmodium*-specific 6-Cysteine protein family (van Dijk *et al.*, 2005). Parasites lacking *P36p* (P52) or its paralogue, *P36*, arrest again early during liver stage development after completion of sporozoite transformation (**Fig. 3**, Ishino *et al.*, 2005, van Dijk *et al.*, 2005). *ΔP36p* sporozoites transmigrate and invade hepatocytes, wherein they initiate the formation of a parasitophorous vacuole (PV). Although they start to mature into liver stage trophozoites, *ΔP36p* parasites suddenly abort this development, most likely because maintenance and maturation of the PVM are critically impaired (van Dijk *et al.*, 2005).

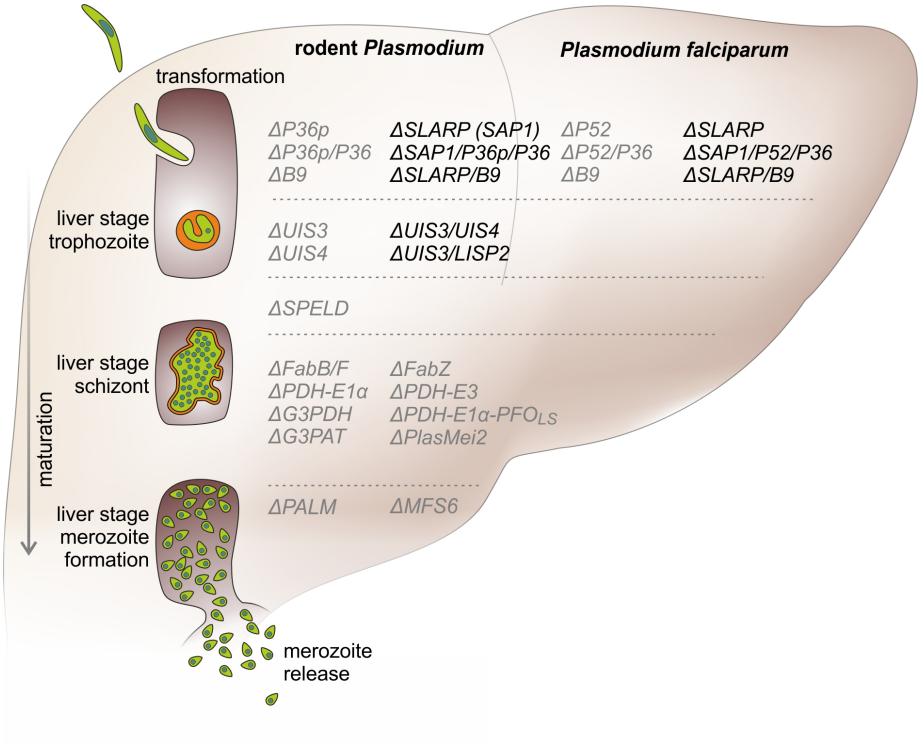

Figure 3 Precision developmental arrests during *Plasmodium* liver stage maturation by genetically arrested parasites (GAPs)

A sporozoite (green) invades a suitable hepatocyte under simultaneous formation of a replication-competent intracellular organelle, termed parasitophorous vacuole (orange). After intracellular transformation to round early liver stages, the parasite expands to a single-cell liver stage trophozoite. Early arresting GAPs, e.g., *ΔUIS3*, *ΔSLARP*,*ΔP36p*, stop cell division at this stage. Next, the trophozoite grows in size and replicates and eventually forms a schizont that exceeds the size of the original host cell. Many GAP lines, such as deletions of the FASII biosynthesis pathway or other apicoplast functions, e.g., *ΔPALM*, arrest after full liver stage maturation. In the last phase of pre-erythrocytic development, the first generation of erythrocyte-invading stages, termed merozoites are formed and released from the infected hepatocytes into the blood stream. This step marks the transition from the clinically and diagnostically silent liver phase to the blood infection, which is responsible for all malaria-related symptoms and pathology. GAPs (right) are listed next to the phase of liver stage development (left) according to their life cycle arrest. Safe and unsafe GAPs are depicted in black and gray, respectively. Knockouts of the murine and human *Plasmodium* species are shown on the left and right side, respectively (Kreutzfeld *et al.*, 2017).

Once more, occasional breakthrough infections in mice inoculated with *ΔP36p* sporozoites were observed (van Dijk *et al.*, 2005). Interestingly, in the *ΔP36p/P36* double knockout, parasite expression of the signature merozoite surface protein 1 (MSP1) could not be detected, and the mechanism of breakthrough infections remains unsolved (Ploemen *et al.*, 2012). Targeted gene deletion of a second member of the 6-Cys family, termed B9, led to a similar early arrest and occasional breakthrough infections (Annoura *et al.*, 2014).

Together, the first generation GAPs established that precise developmental arrests during the first clinically silent, intrahepatic *Plasmodium* expansion phase can be engineered by tailored removal of individual vital genes from the entire *Plasmodium* genome. These uniform, genetically defined parasites consistently elicit lasting protection against sporozoite challenge infections in vaccination protocols with three consecutive GAP sporozoite inoculations.

1.4.2 GAPs targeting liver stage differentiation: Safety first

The observations of breakthrough blood infections during the immunization protocol in a proportion of animals (Mueller et al., 2005b; van Dijk et al., 2005) initiated the search for candidate *Plasmodium* genes that are key developmental factors, for instance transcription factors at the nexus of sporozoite to liver stage transformation. Such a factor was identified during the analysis of sporozoite-specific (S) genes (Kaiser *et al.*, 2004). Targeted gene deletion of this factor, termed *S22* or sporozoite and liver stage asparagine-rich protein (*SLARP* or *SAP1*) (Aly *et al.*, 2008, Silvie *et al.*, 2008), resulted in a complete arrest of the parasite at early liver stage development prior to nuclear division (**Fig. 3**). A novel hallmark of *ΔSLARP* parasites was the differential down-regulation of many liver stage-specific mRNAs and their corresponding proteins, including PVM resident proteins such as UIS3 and UIS4 (Aly *et al.*, 2008, Silvie *et al.*, 2008), suggesting pleiotropic defects as a result of the absence of a major transcriptional or post-transcriptional regulator of liver stage differentiation.

Most importantly, *ΔSLARP* parasites are the first and only GAPs reported to fulfill all criteria of safe arrest (Aly *et al.*, 2008, Silvie *et al.*, 2008). Accordingly, after the safety failure of PfP52/*P36*, all PfGAPs developed for clinical testing in humans include the corresponding *PfSLARP* knockout (Mikolajczak *et al.*, 2014, van Schaijk *et al.*, 2014, Kublin *et al.*, 2017). However, immunization studies showed a reduction in long-term protection in animals immunized with *P. berghei ΔSLARP* parasites, where only 40% of all animals were protected 3.5 months after immunization (Silvie *et al.*, 2008). It is conceivable that *ΔSLARP* parasites display a smaller array of antigens, but this has to be experimentally tested employing systems immunology approaches.

In conclusion, immunization data together with the demonstration of a very early, complete arrest indicate that *ΔSLARP* parasites are comparable to RAS, with the important distinctions of a precision life cycle arrest in humans (Kublin *et al.*, 2017) and safe handling of *ΔSLARP*.

1.4.3 Late arresting GAPs: Improved immunogenicity but lack of safety

Studies employing co-administration of normal sporozoites and anti-malarial drugs have consistently shown superior immunity of late liver stage and/or early blood cycle arrest in murine malaria models (Belnoue *et al.*, 2004, Friesen *et al.*, 2010, Friesen & Matuschewski, 2011) and small scale human trials (Roestenberg *et al.*, 2009, Bijker *et al.*, 2013), suggesting that a late liver stage arrest offers multiple advantages, perhaps including broader antigen presentation (Borrmann & Matuschewski, 2011). Unexpectedly, antibiotic-induced arrest at the transition from late liver stages to blood infection leads to better protection than a later arrest, after a few rounds of blood stage replication, induced by chloroquine treatment (Friesen and Matuschewski, 2011). This indicates an immune-modulatory effect by infected red blood cells and potential

benefits of a complete arrest at the liver stage.

Therefore, tailored arrest toward the end of liver stage maturation was an important third step in GAP vaccine design. A CAS-based arrest using the antibiotic azithromycin showed that specifically targeting the *Plasmodium* apicoplast, a relict non-photosynthetic plastid organelle, resulted in late arrest after complete liver stage maturation (Friesen *et al.*, 2010). Accordingly, two complementary approaches targeting key factors in the *Plasmodium* apicoplast led to generation of late-arrested GAPs and their testing in vaccine studies (**Fig. 3**), namely deletion of a fatty acid biosynthesis enzyme (Butler et al., 2011) and a *Plasmodium*-specific protein of unknown function (Haussig *et al.*, 2011). In both cases potent protection against reinfection was reported and superior protection correlated with extended liver stage maturation. However, safety concerns were reported for *ΔPALM* whereas safety of fatty acid synthesis II (FASII) enzyme knockout was promising in *P. yoelii* (Vaughan *et al.*, 2009, Pei *et al.*, 2010, Butler *et al.*, 2011, Haussig *et al.*, 2011, Lindner *et al.*, 2014) but failed to be confirmed in *P. berghei,* thereby limiting the use of these vaccines candidates (Yu *et al.*, 2008, Annoura *et al.*, 2012, Shears *et al.*, 2017). The additional, unexpected finding of aborted parasite development in mosquitos infected with the corresponding *P. falciparum* knockouts (Cobbold *et al.*, 2013, van Schaijk *et al.*, 2014) essentially eliminated the possibility to develop GAP vaccines by targeted deletion of the FASII pathway. Together, these results also raise the important question of which prerequisites have to be fulfilled to transfer discoveries from murine models to PfGAP vaccines However, these examples illustrate that a tight late liver stage arrested parasite might be achieved once a suitable *P. falciparum* liver stage-specific gene at the nexus of stage conversion is identified.

1.5 Immune mechanisms in *Plasmodium* infections and immunizations

1.5.1 Fighting the disease: Host immune responses and parasite's hiding mechanism

Natural immunity is only slowly acquired after several rounds of infection and wanes quickly upon lack of constant exposure to parasites. Immunity is most likely a consequence of antigenic responses to erythrocytic stages either by exposure to a vast amount of *P. falciparum* isolates or cross-protection by shared antigenic targets. However, full immunity is never achieved as residents of malaria endemic countries only acquire immunity against symptomatic infections; yearly reinfections with asymptomatic outcome are seen on a regular basis. This serves as a constant reservoir for circulation of malaria infections. Studies on host-parasite interaction in particular on host immune responses to the parasite and *Plasmodium*'s mechanism of hiding are essential for development of a safe and efficacious vaccine.

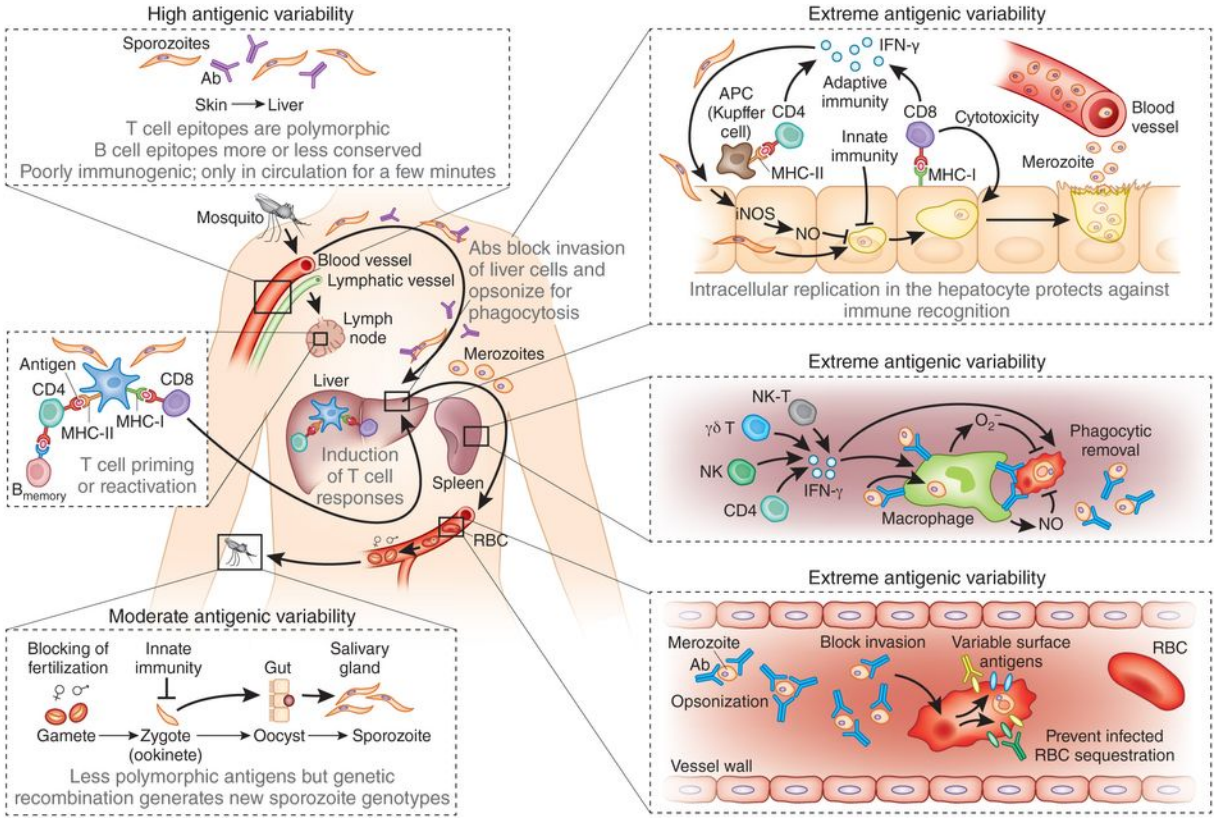

Figure 4 Host immune responses to malaria infections

Sporozoites, injected by a bite of an infected mosquito, elicit the first host immune responses during a *Plasmodium* infection. Primarily antibodies are generated against sporozoite surface antigens in the skin and skin-draining lymph nodes. During liver stage development an interplay of parasite peptide presentation by MHCI of hepatocytes and by MHCII of antigen presenting cells (APCs) prime $CD8^+$ T cells for reinfections. Innate immune responses tackle the parasite via nitric oxide (NO), which is triggered by a cascade of cytokine release by immune cells. Certainly, the spleen and draining lymph nodes play a major role in forming an adaptive immune response against reinfections. In blood stages antibodies are primed against parasitic proteins sitting on the remodeled erythrocyte (Riley & Stewart, 2013).

Once sporozoites enter the host they are detected by the host's immune system. Thus, sporozoites move quickly to the next stage and limit protein discharge to avoid recognition by the host. However, motility is based on an actomyosin motor mediated by TRAP-like proteins, which enable parasites to glide and transmigrate through the dermis, blood stream and sinusoidal barrier (Sultan *et al.*, 1997, Menard, 2001). Sporozoites defective for gliding are rapidly targeted and removed by $CD11b^+$ phagocytic cells. A percentage of parasites remains in the dermis and can be taken up by the lymphatic system where they are eventually targeted by $CD11c^+$ dendritic cells (**Fig. 4**). Furthermore, a subset of sporozoites that escaped the first wave of host immune response manage to form exo-erythrocytic forms (EEF), potentially displaying an unknown set of additional parasite antigens (Amino *et al.*, 2008). Sporozoite specific antibodies, generated during sporozoite migration, help to block sporozoite gliding and hepatocyte infection in subsequent infections. Although TRAP has been demonstrated to be the major ligand for hepatocyte entry, antibody-mediated blockage of TRAP led to normal infection

rates (Gantt *et al.*, 2000). CSP is most likely the pre-dominant contributor to antibody responses, but other antigens might also play a role since whole sporozoite antibody responses have been reported.

Pre-erythrocytic contribution to natural acquired immunity is only limited and most likely dampened by blood stage infections as parasite/DC interaction mediates cytokine secretion suppressing liver stage protective effector $CD8^+$ T cells (Ocana-Morgner *et al.*, 2003, Ocana-Morgner *et al.*, 2007). Parasites crossing the sinusoidal barrier encounter Kupfer cells, specialized liver MΦ (Frevert *et al.*, 2006, Frevert *et al.*, 2008). KCs might act as an actual "barrier" as depletion of KCs led to an enhanced infection rate in *P. yoelii* parasites (Baer *et al.*, 2007). Subsequent parasite migration through hepatocytes induces MyD88 (Torgler *et al.*, 2008), which leads to NF-κB activation and in return to expression of the inducible nitric oxide synthase (iNOS) interfering with EEF development (**Fig. 4**, Nussler *et al.*, 1993, Seguin *et al.*, 1994). Pre-dominant responses to parasitic CSP are seen at early stages, as it is highly expressed in sporozoites and very early liver stage development. Discharge of CSP might redirect NF-κB responses to traversed and not infected cells (Singh *et al.*, 2007). Upon liver infection, parasites develop in a PV to shield themselves from host recognition. In contrast to blood stage infections, parasites keep host cell remodeling to a minimum as antigen discharge and protein export can lead to antigen presentation via MHCI for priming of naïve $CD8^+$ T cells. Other antigen presenting cells (APCs) play a minor role however, it is believed that long persisting parasites induce further responses by DC opsonization and secondary MHCII presentation (Plebanski *et al.*, 2005). However, damaging inflammation in this vital organ is kept to a minimum (Crispe *et al.*, 2006), thereby limiting priming and recruitment of immune cells. Interestingly, merosomes are directly released into the lung circulation where they attach to release merozoites, evading discharge of merozoites close to phagocytic KCs. This notion was confirmed *in vitro* where MΦs failed to phagocytose merosomes (Sturm *et al.*, 2006, Baer *et al.*, 2007).

Natural acquired immunity is predominantly based on B-cell mediated antibody responses to parasite blood stage infection, corroborated by a study reporting that gamma globulins from adults in highly endemic areas where able to protect children against high parasitic infections (Cohen *et al.*, 1961). Two mechanisms are most likely contributing to blood stage protection i) inhibition of merozoites invasion and ii) antibody response to infected RBCs (**Fig. 4**, Langhorne *et al.*, 2008). The latter is an interplay between parasite hiding and efficient replication. Upon RBC infection the parasite replicates in a PV avoiding recognition by the host immune system. Moreover, erythrocytes lack the MHCI presentation pathway and are therefore not targeted by conventional T cells. However, the parasite needs to remodel its "empty" host cell to provide nutrients and dispose waste for maturation. It exports a vast amount of proteins to establish a

well-structured network for cell function. A drawback is recognition by the spleen, as iRBCs, deformed by parasite infections, are cleared. To avoid splenic killing trophozoites and schizonts expose a protein termed EMP1 at the RBC surface to mediate vascular endothelial cell adhesion. Sequestration of trophozoites and schizonts is a major contributor to mortality and morbidity; particularly, cerebral malaria is associated with parasite sequestration to microcapillaries in the brain causing vascular occlusion leading to local hypoxia and inflammation (Cunnington *et al.*, 2013). Sequestration is enhanced in a feedback loop by pathogenic immune responses. Upregulation of major EMP1 binding receptors such as ICAM-1 (cell-adhesion molecule-1) and VCAM-1 (vascular cell adhesion molecule-1) and many more is triggered by overproduction of TNF-α and IFN-γ (Berendt *et al.*, 1989, Lennartz *et al.*, 2017, Mahamar *et al.*, 2017). Blocking cytoadhesion enhances splenic killing of iRBCs, as demonstrated in a study, where severe malaria outcome was avoided by antibody responses to iRBCs surface. EMP1 was verified to be the major target for protective antibodies in individuals from high transmission areas (Bull *et al.*, 1998). To avoid population limiting immune responses the parasite harbors a family of 60 *var* genes encoding different EMP1 surface proteins, a major factor for slow acquisition of immunity. Thus, humoral responses to *Plasmodium* infection are critically timed and determine disease outcome.

Additionally, overwhelming the reticuloendothelial system with parasite biomass in the form of hemozoin can hamper macrophage and dendritic cell antigen presentation and lead to the release of large amounts of cytokines such as TNF-α, IL-1 and IFN-γ. Cytokine storms are a major factor of malaria pathology (Clark & Vissel, 2017). Expression of anti-inflammatory cytokines as TGFβ and IL-10 counterbalances cytokine storms and has a major impact on disease outcome (Stevenson & Riley, 2004). Subsets of $CD4^+$ T cells, Th1, have been shown to control blood stage infection in humans and rodents by expression of IFN-γ and IL-10 (Su & Stevenson, 2000, Jagannathan *et al.*, 2014).

1.5.2 Primary immune responses: The role of IgG-antibody in sporozoite infections

Natural infection with sporozoites induces little inflammation, as pattern recognition receptors (PRRs) are unable to detect sporozoite innate immune ligands e.g. CSP. This notion was corroborated with *P. yoelii* irradiated sporozoites inducing inflammation whereas viable *P. yoelii* sporozoites reduced inflammation in BALB/c mice (Khan & Vanderberg, 1992, Vanderberg *et al.*, 1993). However, the major antigen CSP seems to be immunogenic as long as it is presented in an inflammatory context, as RTS,S vaccine induces a 20-fold higher antibody expression compared to natural infections (Polhemus *et al.*, 2009). Immunization with irradiated sporozoites in rodents revealed presence of anti-CSP antibodies (Kumar *et al.*, 2006), which was confirmed in naturally *P. vivax* exposed individuals carrying detectable levels of anti-CSP antibodies (Wipasa *et al.*, 2010). High antibody titers are essential for impeding hepatocyte entry and neutralizing

sporozoites, as low antibody-titers are associated with enhanced infection (Nudelman *et al.*, 1989). However, an array of studies raised the question whether CSP-mediated antibodies are dispensable for sporozoite-induced protection (Kumar *et al.*, 2006, Gruner *et al.*, 2007, Mauduit *et al.*, 2009). Sporozoite immunization enabled exposure to the whole parasite surface antigenic repertoire, which led to the discovery of two other sporozoite surface antigens TRAP and LSA-1 (liver stage antigen type 1) (Guerin-Marchand *et al.*, 1987, Robson *et al.*, 1988).

Induction of high antibody titers is also dependent on an interplay between B cells with $CD4^+$ cells triggered by MHCII antigen presentation (**Fig. 4**). IFN-γ producing $CD4^+$ T cells from RAS-immunized individuals lyse B-cells pulsed with CSP epitopes *in vitro* (Frevert *et al.*, 2009). Similarly, IFN-γ producing $CD4^+$ T cells have been linked to reinfection resistance (Reece *et al.*, 2004). $CD4^+$ T cells are essential for development of CSP-specific $CD8^+$ T cells, which are primed by DCs in the draining lymph node (Carvalho *et al.*, 2002, Morrot *et al.*, 2005, Chakravarty *et al.*, 2007). CSP-specific $CD8^+$ T cells make their way to the liver to recognize parasite antigens presented by infected liver cells via MHCI and eliminate them (Chakravarty *et al.*, 2008).

1.5.3 Immune mechanisms of GAPs: The central role of effector memory $CD8^+$ T cells in liver stage immunity

IFN-γ producing $CD8^+$ T cells were identified to be the key mediator of pre-erythrocytic induced protection in RAS immunized rodents (Schofield *et al.*, 1987, Weiss *et al.*, 1988, Romero *et al.*, 1989). Immunizations with low dose *P. yoelii* RAS led to immunity in mice (Chattopadhyay *et al.*, 2009), whereas in endemic areas repeated exposure failed to induce a robust $CD8^+$ T cell response (Overstreet *et al.*, 2008). It remains to be determined which factors contribute to robust sterile protection, but patent blood stage infections seem to play a central role in efficiency of pre-erythrocytic immunity (White *et al.*, 2015).

$CD8^+$ T cells remain the primary target cells for induced immunity as immunization in β2-microglobulin knockout mice, deficient of $CD8^+$ T cell responses, failed to induce sterile immunity after wildtype (WT) challenge (White *et al.*, 1996). Infected hepatocytes display parasite antigens via MHCI to cytolytic $CD8^+$ T cells, which leads in return to hepatocyte destruction (**Fig. 5**, Schofield (Mellouk *et al.*, 1987, Schofield *et al.*, 1987, Malik *et al.*, 1991, Sano *et al.*, 2001). This was confirmed by CSP-T cell clones recognizing hepatocytes expressing the matching haplotype on their cell surface (Balam *et al.*, 2012). Destruction of hepatocytes is mediated mainly by IFN-γ, as neutralizing studies revealed (Ferreira *et al.*, 1986, Schofield *et al.*, 1987, Hafalla *et al.*, 2006). IFN-γ production is upregulated in a positive feedback loop by subsequent IL-12 release, which in turn triggers NK-cells to release IFN-γ (**Fig. 5**, Tsuji *et al.*, 1995, Hafalla *et al.*, 2011).

CD4⁺ T cells are generally a major contributor to mount an effective T cell response whether this is true for liver stage immunity still needs to be determined. Importance of CD8⁺ T cells in immunity to infections, but neither of CD4⁺ T cells nor antibodies, was confirmed by immunization studies with *P. berghei ΔUIS3* parasites in B-cell deficient mice or C57BL/6 mice depleted of an additional adoptive transfer with CD4⁺ or CD8⁺ cells (Mueller *et al.*, 2007). These findings were supported in another study where immunization with *P. yoelii ΔUIS3* and *ΔUIS4* of CD8⁺ T cell deficient mice abrogated vaccine efficacy (Tarun *et al.*, 2007).

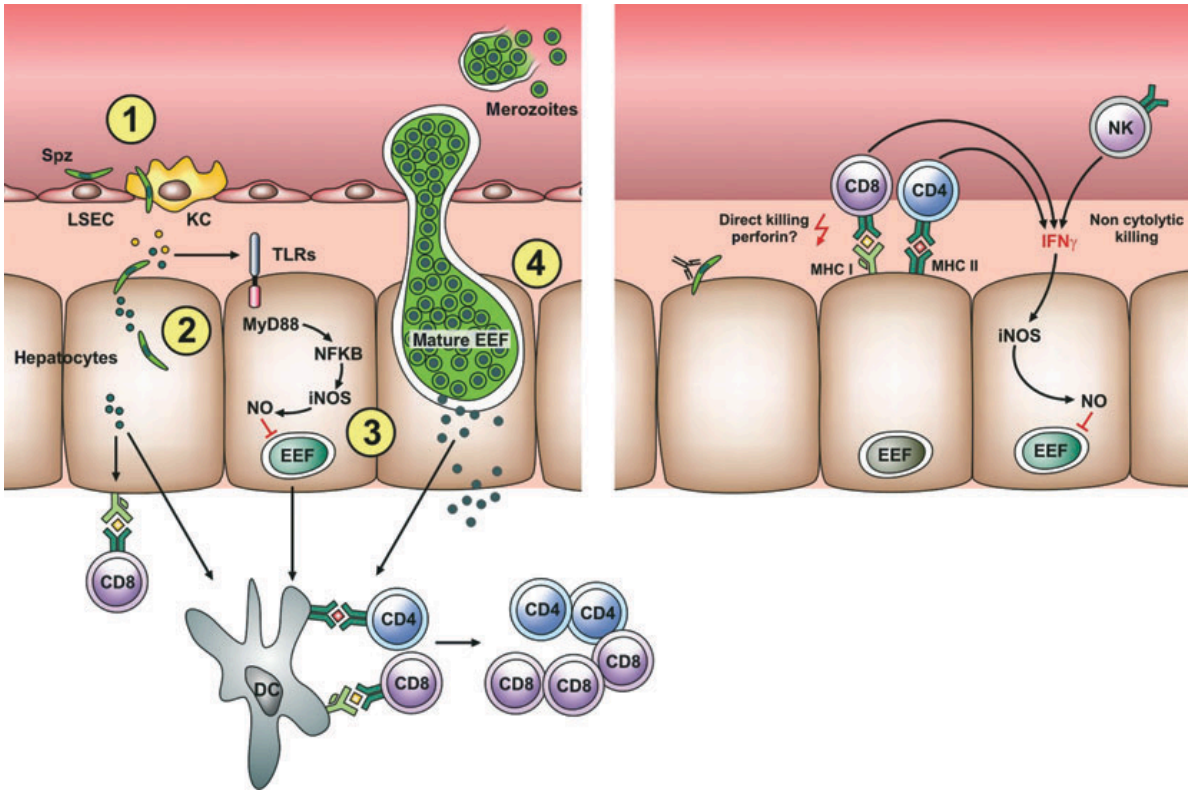

Figure 5 CD8⁺ T cell priming and effector mechanisms

Once sporozoites reached the liver they cross the sinusoidal barrier (1) and traverse through several hepatocytes (2) before infecting a final one to mature into exo-eryhtrocytic forms (EEF) (3). Mature liver stages, merosomes, bud into the lung microcapillaries and release merozoites directly into the blood stream – the onset of symptomatic *Plasmodium* infections. Parasitic material derived from sporozoite traversal, EEF material and autophagy of EEF primes CD8⁺ by MHCI presentation of infected hepatocytes and CD8⁺ and CD4⁺ T cells through cross presentation by DCs. Upon reinfection adaptive immune responses can eliminate EEF by cytolysis or indirectly by IFN-γ secretion inducing a signaling cascade and EEF elimination by NO (Hafalla *et al.*, 2011).

Long-term protection is based on persistence of intra-hepatic metabolically active parasites (Scheller & Azad, 1995). Comparison studies with GAP-based and RAS vaccines corroborated this notion as GAP immunized animals revealed higher levels of IFN-γ producing T cells (Jobe *et al.*, 2007). Furthermore, increased CD8⁺ T cell responses were detected in mice immunized with late arresting GAPs (Butler *et al.*, 2011). Expansion of short-lived CD11a^{hi}, CD62^{lo}, CD44^{hi} CD8b⁺ cells was observed in late arresting GAP immunized mice. Upon restimulation of infected

hepatocytes these effector cells release IFN-γ, TNF-α and IL-2 for subsequent hepatocyte destruction (Cooney *et al.*, 2013).

$CD8^+$ T cell priming is still poorly understood and is probably based on a large set of target antigens that are displayed by infected hepatocytes (Hafalla *et al.*, 2013). An interplay of cross-presentation by DCs in different organs e.g. spleen, liver and skin-draining lymph nodes is certainly required for sufficient immunity (Sano *et al.*, 2001, Chakravarty *et al.*, 2007, Balam *et al.*, 2012). Whether late arresting GAPs present an array of additional antigens leading to the observed superior immunity remains elusive.

1.6 Advanced GAP research: An approach to enhanced immunity and safety

1.6.1 GAPs with multiple gene deletion: Synergetic or antagonistic

Development of parasite lines that harbor multiple gene deletions is likely to increase safety; however, whether synergistic or antagonistic effects modulate immunogenicity is less straightforward to predict and likely depends on the selected knockout combination. Soon after the first proof-of-principle studies, a GAP parasite line that harbors two consecutive gene deletions, namely *ΔUIS3* and *ΔUIS4*, was engineered in *P. berghei* (Jobe *et al.*, 2007). As expected, *ΔUIS3*/*UIS4* parasites displayed a complete arrest in early liver stages, indicating that vaccine strains harboring multiple independent gene deletions perform safer than single knockout GAPs. Importantly, long-term protection against a high-dose sporozoite challenge infection was induced.

In marked contrast, when a double knockout was performed for the *P. berghei* paralogs *P36p* (P52) and *P36*, which are neighboring genes and likely arose through gene duplication, safety was not improved (Annoura *et al.*, 2012), strongly suggesting that independent genes need to be targeted in multiple gene knockout strategies. Since *ΔSLARP* GAPs lead to a complete termination of liver stage development (Aly *et al.*, 2008, Silvie *et al.*, 2008), they constituted the obvious platform for combinations with other arresting single knockouts of the 6-Cys gene family (**Fig. 3**)(Mikolajczak *et al.*, 2014, van Schaijk *et al.*, 2014, Kublin *et al.*, 2017). However, it remains to be shown whether addition of B9, *P36*, and/or *P36p* (P52) knockout provides any additional benefit beyond perception of additional gene deletions. An important investigation with combinatorial knockouts will be the systematic expression profiling of liver stage-specific genes, as was previously done for *ΔSLARP* parasites (Silvie *et al.*, 2008). Such an analysis will provide first insights into the expected antigenic repertoire displayed by the respective GAPs. Instead of adding additional gene deletions, which might not add significantly to vaccine efficacy, the combination of a gene deletion with transgene expression of additional factors could amplify antigen presentation during pre-erythrocytic development. However, a principal concern in

gain-of-function mutants is that parasites containing mutations in the transgene promoter and other regulatory elements, which lead to a reduced transgene expression, will be swiftly selected. Therefore, GAPs that express additional *Plasmodium* antigens in order to broaden the immunogenic repertoire without further reducing parasite fitness might be a particularly rewarding research direction.

1.6.2 Immunogenicity vs. safety: Taking a closer look at two promising vaccine candidates

Promising induction of immune responses by GAP vaccines were first received with *ΔP36p,* the paralogue gene *ΔP36* immunization or a combined *ΔP36p/P36* parasite line (van Dijk *et al.*, 2005). These two genes belong to the *Plasmodium*-specific-6-Cys gene family and are likely contributing to the selective CD81-independent hepatoma cell entry in *P. berghei* (Manzoni *et al.*, 2017). A potential, albeit untested, advantage of 6-Cysteine protein based GAPs is enhanced antigen presentation via MHCI on infected hepatocytes, since maintenance of the parasitophorous vacuole is impaired (**Table 1**). Perhaps even more importantly, the propensity to increase apoptosis in *ΔP36p*-infected hepatocytes (van Dijk *et al.*, 2005) might enhance cross priming by dendritic cells (DCs) that phagocytose apoptotic bodies (Leiriao *et al.*, 2005), although this conjecture remains controversial (Renia *et al.*, 2006).

Unfortunately, despite favorable immune responses, as seen in *ΔUIS4/UIS3* parasites, occasional breakthrough infections limit the vaccine potential of this parasite line (**Table 1**, van Dijk *et al.*, 2005). However, only the knockout of one candidate transcript of the sporozoites containing a targeted deletion of a master regulator of liver stage development *SLARP*, Sporozoite and liver stage Asparagine-Rich Protein, has so far been proven to arrest fully in liver stages in both animal models and humans (Aly *et al.*, 2008, Silvie *et al.*, 2008). The drawback of the early arrest of *ΔSLARP* parasites lies within a decreased potent immunity against follow-up infections (**Table 1**, Silvie *et al.*, 2008). To improve GAP safety and efficacy, several double and triple knockout GAPs have been engineered in *P. yoelii* and *P. falciparum* (Mikolajczak *et al.*, 2014, van Schaijk *et al.*, 2014, Kublin *et al.*, 2017).

Table 1 Features of *ΔSLARP* and *ΔP36p* vaccine candidates

	ΔSLARP	***ΔP36p***
Attenuation (safety)	complete	breakthrough infections
PVM (establishment, remodeling and maintenance)	establishment but no remodeling	no PVM
Protection after immunization	partial	sterile

The first human clinical phase I trial was recently conducted with a *P. falciparum* 3KO GAPs missing the paralog genes *P52* (*P36p*) and *P36* and in addition *SLARP* (Kublin *et al.*, 2017). The study showed complete arrest of the 3KO GAP in humans (<10) and mice in the CSP-response dominated BALB/c *P. yoelii* model (<30). Immunization/challenge studies in BALB/cJ mice revealed complete protection after 7, 30 and 180 days post immunization (Kublin *et al.*, 2017). However, sufficient pre-clinical data of this 3KO GAP remains elusive. In particular, studies using the *P. berghei* C57BL/6 model that mimics the human MHCI epitope situation of a combination of epitope specific $CD8^+$ T cell responses for protection. GAPs are not only eliciting antibody responses against sporozoites and intra-hepatic stages but also contribute to $CD8^+$ T cell mediated protection against liver stages (Kreutzfeld *et al.*, 2017). It is critical for a sufficient long-term potent immunity to take the $CD8^+$ T cell mediated response into consideration. Studies of $CD8^+$ T cells responses in humans are difficult; therefore, to study $CD8^+$ T cells responses, pre-clinical studies in mice are unavoidable. By generating a triple genetically attenuated parasite line in *P. berghei* potent immunity mediated by antibody and $CD8^+$ T cell responses as well as safety could be studied.

1.7 Protein export in *Plasmodium*: Remodeling the host cell from inside out

1.7.1 *Plasmodium*'s export machinery

Asexual development inside a parasitophorous vacuole in intra-erythrocytic as well as intra-hepatic stages requires the parasite to remodel its host cell for survival and rapid replication. Insertion of pores into the PVM to uptake nutrients and dispose waste is key for parasite survival, especially in intra-erythrocytic development where the parasite is required to remodel its host cell as essential cell mechanisms in nucleated cells are missing. Therefore, the parasite exports a large set of proteins to remodel the host cell for its purposes. The exportome of *Plasmodium* is believed to be 10% of its whole proteome (Spielmann & Gilberger, 2015).

To export proteins across two membranes, plasma membrane and parasitophorous vacuole membrane, a tight processing pathway is required. Proteins destined for export travel from the endoplasmic reticulum (ER) to the PV in a poorly understood manner (**Fig. 6**). *Plasmodium* export element (PEXEL) comprising of a RxLxE/Q/D sequence located downstream of the ER signal sequence, was determined to be the key export label in proteins sequences (Hiller *et al.*, 2004, Marti *et al.*, 2004). Early studies with *Pf*KHARP (knob-associated histidine-rich protein) GFP chimaeras confirmed the notion that an amino-terminal signal sequence is required for ER entry, suggesting that a further downstream sequence is required for PVM translocation (Wickham *et al.*, 2001). Interestingly, studies revealed that a change in amino acid residues from arginine or leucine to alanine trapped the export protein in the ER or PV (Marti *et al.*, 2004).

Upon ER entry the PEXEL motif is cleaved downstream of the leucine residue by Plasmepsin V, an aspartyl protease, as the new N-terminus is acetylated (Chang *et al.*, 2008, Boddey *et al.*, 2009, Boddey *et al.*, 2010, Russo *et al.*, 2010, Marapana *et al.*, 2018). Recently, Marpana et al. reported that Plasmepsin V binds several proteins forming a unique complex to enable ER entry of cargo proteins destined for export, which is distinct from secretory pathway (Marapana *et al.*, 2018). It remains unclear how exported proteins can thereafter be recognized as distinct export signals are missing after cleavage. However, a class of exported proteins does not harbor a PEXEL motif, termed PEXEL independent export proteins (PNEPs), but rather uses an internal transmembrane segment as ER entry signal (Spielmann & Gilberger, 2010, Kulzer *et al.*, 2012, Boddey *et al.*, 2013). Surprisingly, REX2 (ring export protein 2), a PNEP protein, was shown to be N-terminally processed independent of Plasmepsin V, suggesting that the sequence right downstream of PEXEL might also play an important role in targeted export (Haase *et al.*, 2009, Gruring *et al.*, 2012). Processed proteins are believed to be loaded into secretory vesicles to be transported and released into the PV.

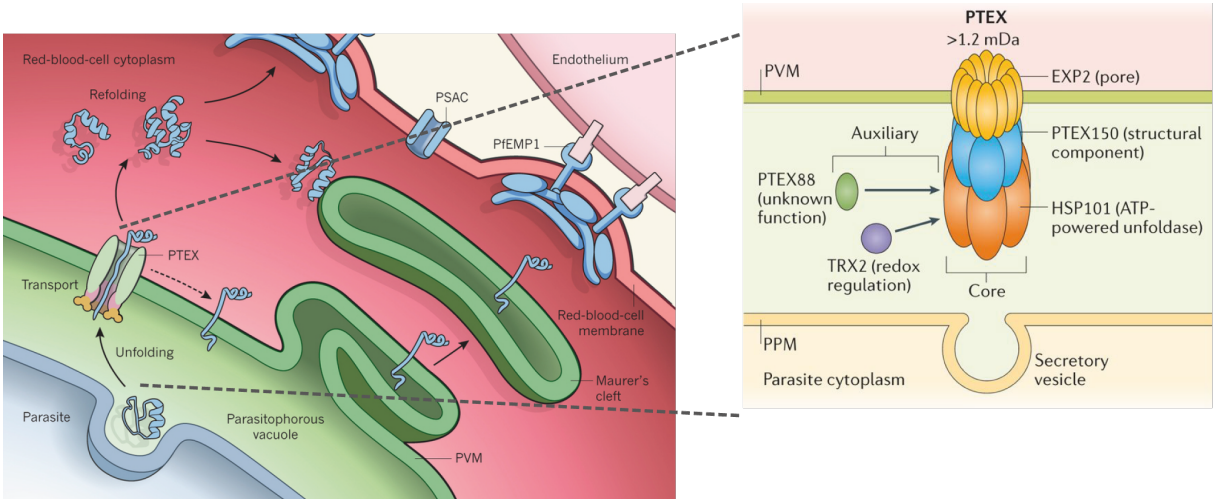

Figure 6 PTEX-dependent export in blood stages and the PTEX export machinery

Host cell remodeling requires export of parasite proteins eg. knob-associated proteins for knob assembly and cell adherence via the *Pf*EMP1 complex. Proteins destined for export are processed in the ER, deposited in export zones in the PV and translocated into the host cell cytoplasm by a protein translocon termed PTEX. Refolding of proteins is possibly taking place in parasitic compartments of the iRBC (J dots). PTEX is composed of three core components EXP2, PTEX150 and HSP101. EXP2 is the membrane spanning protein, PTEX150 has a structural component linking EXP2 and HSP101 and HSP101 is a AAA^+ ATPase unfolding and translocating proteins across the PVM. Two other auxiliary proteins TRX2 and PTEX88 are involved in protein unfolding and help to transport specialized subsets of cargo, respectively (modified from Desai & Miller, 2014, de Koning-Ward *et al.*, 2016).

Once in the PV, proteins need to cross the PVM to reach the host's cells cytoplasm. As erythrocytes are deficient of translocons and can therefore not be scavenged by the parasites, a parasitic PVM translocon (PTEX) was identified (**Fig. 6**, de Koning-Ward *et al.*, 2009). Studies in human and rodent *Plasmodium* revealed that the complex is comprised of five proteins of which three are core proteins (EXP2, HSP101, PTEX150) and two are non-essential (PTEX88, TRX2)

(de Koning-Ward *et al.*, 2009, Matthews *et al.*, 2013, Matz *et al.*, 2013). These proteins seem to be *Plasmodium* specific with very little structural evidence of orthologs in other Apicomplexa (Ho *et al.*, 2018). HSP101, the motor of the complex, is a Cl1 AAA^{+}-ATPase harboring a cargo-binding pore loop at the N-terminal end and is most likely responsible for protein unfolding and active translocation through the complex (**Fig. 6**, de Koning-Ward *et al.*, 2009, Beck *et al.*, 2014, Ho *et al.*, 2018). In contrast, EXP2 plays a central role as a membrane-spanning component, but simultaneously acts as nutrient channel in a PTEX-independent manner (**Fig. 6**, Garten *et al.*, 2018). There is little evidence of functional domain in PTEX150, however, recent studies confirmed early assumptions that PTEX150 plays a structural role linking EXP2 and HSP101 (**Fig. 6**, Bullen *et al.*, 2012, Elsworth *et al.*, 2014, Garten *et al.*, 2018). Knockout studies of all core components in human and rodent *Plasmodium* species corroborated the importance of these proteins for parasite blood stage survival (Matthews *et al.*, 2013, Matz *et al.*, 2013, Beck *et al.*, 2014, Elsworth *et al.*, 2014). The roles of Trx2 and PTEX88 in protein translocation are poorly understood, however, knockout of Trx2 led to a prolonged cell cycle and reduced parasitic surface proteins on iRBCs indicating that Trx2 might help unfolding cargo proteins by reduction and oxidation of disulfide bonds (Matthews *et al.*, 2013, Matz *et al.*, 2013, Elsworth *et al.*, 2014). PTEX88 knockout resulted in normal life cycle progression but reduced experimental cerebral malaria cases and cytoadherens was observed in knockout parasites, thus possibly helping HSP101 in specific protein translocation important for virulence of the parasite (Matz *et al.*, 2015, Chisholm *et al.*, 2016, Chisholm *et al.*, 2018). Protein translocation seems to be an interplay of many proteins, further transient protein involvement has been predicted for PV1 (parasitophorous vacuolar protein 1) as a dense granule protein facilitating export of specific cargos and Pf113 to define export zones in the PV. Whether HSP70-x a heat-shock-protein helps to pull proteins through the PTEX complex remains controversial (Elsworth *et al.*, 2016, Cobb *et al.*, 2017, Matz & Matuschewski, 2018, Morita *et al.*, 2018).

1.7.2 Export in blood stages

Plasmodium is among very few parasites which have evolved to replicate in a non-nucleated cell. To modulate the cell to its purposes specific exported proteins are required which are particularly important for cell rigidity and virulence. It is believed that 25% of the exportome are essential for parasite survival in blood stages (Maier *et al.*, 2008).

PTEX components are stored in granules, which are released upon merozoite invasion of RBCs and immediately initiate PTEX formation. Exported proteins have three distinct destinations in the host cell i) the Maurer's clefts ii) soluble proteins the cytoplasm or iii) the membrane cytoskeleton. Upon translocation proteins might be transported in a vesicle-independent manner through the erythrocytes' cytoplasm as chaperon-associated transport complexes (Knuepfer *et*

al., 2005, Knuepfer *et al.*, 2005). How exported proteins are refolded still remains elusive, however, there is strong evidence that parasitic chaperons in cytoplasmic J-dot structures, with the help of host chaperons, mediate this process (Kulzer *et al.*, 2010). Of particular interest are the so-called knob structures at the erythrocytic membrane, which mediate sequestration of the parasite to vascular endothelial cells to avoid splenic macrophage killing (**Fig. 6**). These knob-like protrusions are assemblies of the KAHRP protein linked to the host cell cytoskeleton (Watermeyer *et al.*, 2016) where EMP1, a PEXEL-independently exported protein, is inserted into the blood cell membrane to mediate cell adherence (Kriek *et al.*, 2003). Parasites deficient of knobs reveal a decreased cytoadherence, which can be potentially mediated by blocking PEXEL-dependent KHARP export (Crabb *et al.*, 1997, Glenister *et al.*, 2002).

1.7.3 Export in liver stages

Most of our knowledge on protein export is derived from the intra-erythrocytic stage and liver stage export remains largely elusive. As metabolically active cells, hepatocytes enable the parasite to exploit the host cell limiting the need for intensive remodeling and thus directing energy into extensive growth (Prudencio *et al.*, 2006). Moreover, hepatocytes harbor an active MHCI pathway with the potential to present parasitic antigens to the host's immune cells (Chakravarty *et al.*, 2007). To avoid recognition by the host, the parasite might keep protein translocation during early to mid liver stage development to a minimum. To date only peptides of sporozoite origin could be identified on MHCI expressing cells (Bongfen *et al.*, 2007, Hafalla *et al.*, 2013, Muller *et al.*, 2017). Recently the first liver stage specific peptide Kb-17 was identified but its influence on protection remains to be determined (Pichugin *et al.*, 2018).

Only two proteins are reported to translocate during liver stage growth: CSP and LISP2 (Singh *et al.*, 2007, Orito *et al.*, 2013). CSP export remains controversial, while Singh *et al.* suggested that CSP is localizing to and around the host nucleus 2-6 hours post infection (p.i.) (Singh *et al.*, 2007), Cockburn *et al.* could not confirm these observations 6 hours p. i. (Cockburn *et al.*, 2011). As a major surface antigen of sporozoites, CSP might be already released into the host's cytoplasm during sporozoite entry. Corroborating this notion, studies demonstrated that CSP is constantly shed during sporozoite transmigration and released into traversed cells where it localizes to the host's nucleus to redirect host immune responses to traversed but not infected cells. In contrast, LISP2 is the only liver stage protein exported during liver stage development. Immunofluorescence assays with LISP2 antibodies demonstrated onset of export at 24 hours post infection. However, parasites harboring a C-terminal mCherry tagged LISP2 failed to export the tagged protein to the hepatocyte cytoplasm (Orito *et al.*, 2013), possibly due to C-terminal processing of LISP2. Sequence analysis revealed that LISP2 harbors a PEXEL motive and is additionally cleaved on both sides, confirming the observations made by Orito *et al.* (personal

communication Melanie Shears, John Hopkins School of Medicine). It will be of great interest whether the potential liver stage exportome is processed differently to blood stages exported proteins.

Further experimental genetics revealed similar restrictions in liver stage export. Fusion of the CSP PEXEL motif to truncated OVA (ovalbumin) and infection with these transgenic parasites increased $CD8^+$ T cell proliferation but failed to induce export (Montagna *et al.*, 2014). Similarly, mCherry fused to *CS-PEXEL* or *IBIS-PEXEL* under the control of liver stage promoters *IBIS* or *UIS4* remained in the PV during liver stage development *in vitro* (Josephine Grützke, MPIIB, PhD thesis 2015).

Strikingly, during liver stage maturation, HSP101 is not expressed until 48 hours post infection, whereas all other PTEX components are present (Matz *et al.*, 2015), offering a potential explanation why liver stage export seems to be restricted or is limited to yet unidentified proteins. Unraveling processes involved in pre-erythrocytic protein translocation or potential substitution of HSP101 would significantly impact our current knowledge of liver stage export. Of interest would be whether increasing export in early liver stages would lead to increased parasite-recognition by presentation of parasite-derived epitopes via MHCI and consequently upscaling immune responses.

1.8 Aim of the study

Immunity against malaria infections can be achieved by various whole sporozoite vaccine approaches, which have previously been shown to be effective in non-human primates, humans and rodents. Targeted deletion of liver stage genes enables specific liver stage arrest of parasites, which can serve as metabolic active live attenuated vaccines. These genetically attenuated parasite (GAP) vaccines enable development of pre-erythrocytic immunity and therefore hinder the onset of symptomatic blood stage infections after sporozoite challenge. Considerable numbers of GAP-based candidates have been successfully tested, however, drawbacks in safety or efficacy kept the search going for the "one" perfect GAP-based vaccine candidate.

Two GAPs displaying different required vaccine features are of particular interest. *ΔSLARP* parasites were the first and remain the only GAPs to induce complete arrest of liver stages, probably induced by down regulation of important liver stage genes, making it a perfect vaccine candidate. However, sterile protection was absent in immunized mice a sign of inferior vaccine efficacy. On the other side of the spectrum are *ΔP36p/P36* parasites, a double knockout of two neighboring paralog genes required for PVM establishment, which elicit sterile protection, but occasional blood stage breakthrough infections limit the use as potential vaccine candidate. By combining these two knockouts, I hoped to increase safety and efficacy of GAP-based vaccine candidates. To determines whether triple knockout (tKO) GAPs are superior to other GAP candidates, the following questions were asked, whether:

i) safety requirements are fulfilled in tKO GAPs
ii) immunizations with tKO GAPs confer sterile protection against *Plasmodium* challenge
iii) underlying immune mechanism can be deciphered and correlated with protection

It still needs to be determined, whether late arresting parasites confer better protection. It is hypothesized that better induction of immune responses in later liver stages is among other factors realized by an increased parasitic antigenic display via MHCI to the host's immune system. Parasites harbor an export complex, termed PTEX, responsible for targeted protein export in blood and late liver stages. Expression of a core component; HSP101, is absent in early liver stages, perhaps limiting protein export during this stage of the life cycle. Whether this is a way for the parasite to hide from the host's immune system remains elusive. The prospect of restoring protein export in early liver stages by overexpressing HSP101, might lead to increased protein export and in consequence antigen presentation by infected liver cells, which in turn

could promote immune cell priming and subsequent protection against sporozoite challenge (**Fig. 7**). The aim of the study was to determine whether HSP101:

i) overexpression interferes with *Plasmodium* life cycle

ii) is the limiting factor for liver stage protein export

iii) liver stage overexpression and concomitant PTEX reconstruction leads to increased immunity against re-infections

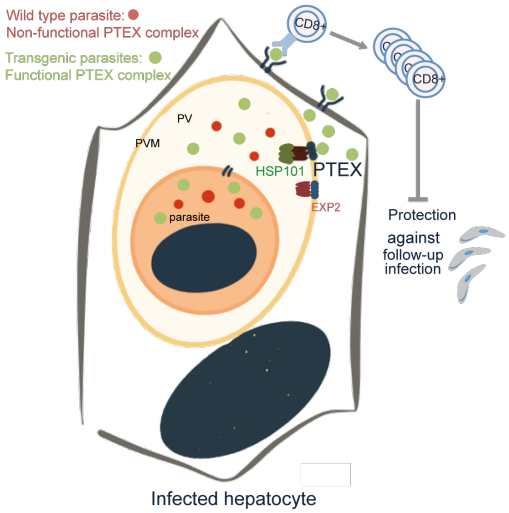

Figure 7 Hypothesis of early liver stage export

Protein export in early liver stages is absent in *P. berghei* parasites (red). Proteins destined for export (red dots) cannot cross the PVM. A transgenic parasite overexpressing HSP101 (green) could restore the complex and onset protein export (green dots). Parasitic protein could be processed and peptide presented to $CD8^+$ T cells in an MHCI dependent manner. This could potentially lead to increased protection against follow-up infections.

Exploring two different approaches on increasing pre-erythrocytic immunity by GAP-based vaccination might give a novel insight into pre-erythrocytic host-parasite interplay and underlying immune mechanisms to sterile protection.

2 Material and Methods

2.1 Materials

The laboratory work was conducted at the Max Planck Institute of Infection Biology, Berlin and Humboldt University, Berlin. The following is a combined collection of materials used in both laboratories.

2.1.1 Biological resources

Animals / cells	**Source**
Mus musculus Naval Medical Research Institute (NMRI) mice	Charles River Laboratories, Germany
Mus musculus C57BL/6	Charles River Laboratories, Germany Janvier LABS, Germany
Anopheles stephensi	Nijmegen, Netherlands (Janse *et al.*, 2006)
Plasmodium berghei ANKA-GFP507 cl	Nijmegen, Netherlands (Janse *et al.*, 2006a)
Plasmodium berghei ANKA	Nijmegen, Netherlands (Janse *et al.*, 2006a)
Plasmodium berghei ANKA *bergreen*	Nijmegen, Netherlands (Janse *et al.*, 2006a, Kooij *et al.*, 2012)
Huh7 human hepatoma cells	
Escherichia coli XL-1 Blue	Stratagene, Germany
Escherichia coli XL-10-Gold	Stratagene, Germany

2.1.2 Laboratory equipment

Instruments	**Company**
Agarose Gel Casting System	Horizon 11-14 Biometra, Germany Owe Scientific Inc.
Electrophoresis power supply	Amersham Pharmacia Biotech, UK
Agarose gel EPS 200, power supply	Pharmacia Biotech
Gel documentation system Gel Doc 2000	Bio-Rad, Germany
Magnetic stirrer, Yellow MAG MS7	IKA laboratory equipment, Germany
Amaxa Electroporator	Amaxa, Germany
Bench top centrifuge 5424	Eppendorf, Germany
5415R Refirgerated Centrifuge	Eppendorf, Germany
Megafuge 1.OR, Thermo Scientific	Heraeus, Germany
Multifuge X1, Thermo Scientific	Heraeus, Germany
Mini centrifuge	Heathrow Scientific
Fridge 4°C	Liebherr, Germany
Freezer -20°C	Liebherr, Germany
Freezer -80°C	Heraeus, Germany
Ice machine AF 200	Scotsman ICe Systems, USA
Nitrogen cavitation chamber	Parr Instrument Company, USA
Heating Block, Thermo Scientific	Eppendorf, Germany

Incubator for cell culture	Heraeus, Germany
Incubator *P. berghei* cultures	Mytrom, Germany
Incubator *E.coli*	Heraeus, Germany
Incubator and shaker for liquid *E.coli* cultures (Innova 4000)	New Brunswick Scientific
Mice facility incubator	Ehret, Germany
Vortex-Genie2	Scientific Industries, USA
Rocking platform, Rotamax 120	Heidolph Instruments, Germany
Shaker DRS-12	Heraeus, Germany
Micropipettes (Gilson)	Abimed, Germany
Pipetus®	Hirschmann Laborgeräte, Germany
Mosquito cages	BioQuip Products Inc, USA
Mice cages	Ehret, Germany
Nanodrop ND 1000	peQLab, Germany
Hemocytometer	Marienfeld, Germany
PCR Thermocycler, MJ-mini	Bio-Rad, Germany
pH-meter	Mettler Toledo, Germany
Sterile bench, Herasafe KS12	Heraeus, Germany
Scale MXX-212 and SI-64	Denver Instrument, USA
Balances	Sartorius, Germany
Binocular, M80, MZ10F	Leica, Germany
BX50 fluorescence microscope	Olympus, Germany
DM LS microscope	Leica, Germany
EOS700D camera	Canon, Japan
Leica DM2500 brightfield microscope	Leica, Germany
Axio Observer Z1 inverted fluorescence microscope with AxioCam MRm	Zeiss, Germany
AnxiioCam MRm	Zeiss, Germany
Axio Observer Z2	Zeiss, Germany
Microscope (cell culture) DMIL LED	Leica, Germany
Vortex-Genie 2	Scientific industries
HERAsafe KS12 KS Sterile hood	Thermo Scientific
Water bath	GFL, Germany
PCR machine, MJ Mini™	Bio-Rad, Germany
Thermal cycler, MJ Mini, Gradient	Bio-Rad, Germany
MACSQuant® benchtop Flowcytometer	Miltenyi Biotec, Germany
BD FACS –CantoII Flowcytometer	BD Bioscience, Germany
BD FACS – Aria cell sorter	BD Bioscience, Germany

2.1.3 Laboratory materials

Consumables	**Company**
6-well plate	Greiner Bio-One, Germany Sarstedt, Germany
24-well plate	Greiner Bio-One, Germany Sarstedt, Germany
48-well plate	Greiner Bio-One, Germany Sarstedt, Germany
Cell culture flask (T-25 and T-75)	Greiner Bio-One, Germany
Microplate 96-well, µ-clear (U-bottom)	Greiner Bio-One, Germany
Microplate 96-well, µ-clear (V-bottom)	Greiner Bio-One, Germany
8-well glas bottom chamber slides, LabTek	Nunc, Thermo Fischer, Germany
8-well plastic bottom chamber slides,	Nunc, Thermo Fischer, Germany

LabTek	
µ-slide, 8-well	ibidi Germany
Round glas cover slips	Roth, Germany
Petri dishes	Greiner Bio-One, Germany
Cover slips	Roth, Germany
	Corning BioCoat Cellware, USA
Cryo-freezing tubes	Greiner Bio-One, Germany
Electroporation cuvettes	Amaxa, Germany
Eppendorf tubes, 1.5 ml	Eppendorf, Germany
	Sarstedt, Germany
Eppendorf tubes, 2 ml	Eppendorf, Germany
	Sarstedt, Germany
PCR tubes	Greiner Bio-One, Germany
	Sarstedt, Germany
FACS tube	Sarstedt, Germany
Falcon blue cap tubes (50 mL and 15 mL)	Greiner Bio-One, Germany
Forceps	Neolab, Germany
	FST by DUMONT
Glass slides, clear	Menzel, Germany
Microscope oil	Zeiss, Germany
Needles, sterile (0,4 x 20 mm)	Braun, Germany
Needles, sterile (0,6 x 25 mm)	Henke-Sass Wolf, Germany
Omnifix ®-F Syringes 1ml	Braun, Germany
Inject ® Syringes 5 ml	Braun, Germany
Syringes, insulin	Braun, Germany
Serological pipettes (5, 10 and 25 mL)	Greiner Bio-One, Germany
Sterile filter (0.2 and 0.4 mm)	Millipore, Ireland
Sterile filtration units (500 mL)	NALGENE®, USA
Filtration bottle Rapid Flow	Thermo Scientific, USA
Pipette tips	Brand GMBH, Germany
	Sarstedt, Germany
Pasteur pipettes	Roth, Germany
Cell strainer	BD Bioscience, USA
Bel Nature cotton	Hartmann, Germany

2.1.4 Chemicals

Reagents	**Company**
1 kb DNA-Ladder	MBI Fermentas, Thermo Fischer, USA
GeneRuler 1kb Plus DNA Ladder	MBI Fermentas, Thermo Fischer, USA
6 x DNA loading dye	MBI Fermentas, Thermo Fischer, USA
Agarose	Invitrogen, Germany
Alsever's solution	Sigma-Aldrich, Germany
Ammonium persulfate (APS)	Roth, Germany
Albumin fraction	Roth, Germany
Ampicillin	Roth, Germany
LB-Agar powder (Lennox L Agar)	Invitrogen, Germany
Cellulose (Carboxymethyl)	Sigma-Aldrich, Germany
Cutsmart Restriction Enzyme Buffer	New England BioLabs, USA
SYBR Safe DNA Gel stain	Invitrogen, Germany
Dulbecco's modifiec Eagle Medium (DMEM)	GibcoBRL, Germany
DMSO (Dimethyl sulphoxide)	Merck, Germany
dNTP-mix	MBI Fermentas, Germany

FCS (Fetal Calf Serum), certified (USA)	Gibco Invitrogen, Germany
FCS Gibco	Invitrogen, Germany
	PAN-biotech, Germany
Fluoromount G	Southern Biotec, USA
Fibrous Cellulose Powder	Whatman, United Kingdom
	Sigma-Aldrich Germany
Formaldehyde	Merck, Darmstadt Germany
Formaldehyde 16%, MeOH-free	Polyscience Germany
Gentamycin	Invitrogen, Germany
	Gibco, Life Technologies Germany
Giemsa stain	VWR Germany
Glass beads, unwashed	Sigma-Aldrich, Germany
Glucose	Merck, Germany
Glycerol	Roth, Germany
Heparin	Ratiopharm, Germany
HEPES	Merck/Calbiochem, Germany
HCl	Roth, Germany
Immersion oil	Roth, Germany
Isoflurane	Baxter, Germany
Methanol	Thermo Scientific
NaOH	Merck, Germany
Nycodenz density gradient medium	Axis Shield, Norway
Phalloidin 1:50	Molecular Probes, Netherlands
Paraformaldehyde powder	Merck, Germany
Percoll	GE Healthcare, USA
PBS, sterile solution	Gibco Invitrogen, Germany
PBS, tablets	Gibco Invitrogen, Germany
Penicillin-Streptomycin, liquid	Invitrogen, Germany
Pyrimethame	Sigma, Germany
RPMI 1640-medium	GibcoBRL, Germany
Saponin	Sigma, Germany
Sodium chloride	Roth, Germany
Sodium acetate	Roth, Germany
	Ambion, Germany
Sodium hydrogencabonate	Roth, Germany
SYBR Safe DNA Gel stain	Invitrogen, Germany
SOC Outgrowth Medium	New England Biolabs
Tris (hydoxymethyl)aminomethane (TRIS)	Roth, Germany
Trypsin-EDTA	Invitrogen, Germany
Triton X-100	Roth, Germany
Tween 20	Roth, Germany
ß-Mercaptoethanol	Sigma-Aldrich, Germany
L-Glutamine	Gibco, Life technologies, Germany
Anti-Anti	Gibco, Life technologies, Germany
Glycine	Roth, Germany
Ethanol, absolute	AppliChem, Germany
Hoechst 33342	Invitrogen, Germany
Nocodazole	Calbiochem, Merck, Germany
Brefeldin A (1:1,000)	AppliChem, Germany
Glutaraldehyde	Sigma-Aldrich, Germany
2-Propanol Rotipuran	Roth, Germany
BD Wash	BD Bioscience, Germany
Trizol	Invitrogen, Germany
Perm-Wash Buffer	BD Bioscience, Germany

2.1.5 Commercial kits

Kits	Company
Human T Cell Nucleofector Kit	Lonza, Germany
QIAprep Spin Miniprep Kit	QIAGEN, Germany
QIAprep Spin Midiprep Kit Q	QIAGEN, Germany
QIAamp DNA-Blood Mini Kit	QIAGEN, Germany
QIAquick PCR Purification Kit	QIAGEN, Germany
QIAquick Gel Extraction Kit	QIAGEN, Germany
Rapid DNA Dephos & Ligation Kit	Roche, Switzerland
Rapid DNA Ligation Kit	Roche, Switzerland
Taq PCR Kit	Thermo Scientific, Germany

2.1.6 Antibodies and peptides

IFA antibodies	Company
Anti-mCherry (rat) 1:500	Chromotek, Germany
Anti-c-Myc (clone 9E10) (mouse) 1:500	Santa Cruz Biotechnology, Germany
Anti- *P. b.* HSP70 (mouse) 1:500	Tsuji, M; NYU
Anti- *P. b.* UIS4 (1165) (rabbit) 1:500	(Muller *et al.*, 2011)
Anti-GFP (chicken) 1:1,000	Abcam, Germany
Anti-MSP1 (mouse) 1:500	Prof. Dr. A. Holder, National Institute for Medical Research, London,UK
Anti- *P. b.* CSP 1:500	(Yoshida *et al.*, 1981)
Anti-sporozoite surface antigens (polyclonal) 1:300	2x WT immunized mice
Anti-LC3 1:100	Nanotools
Anti mouse/rabbit/rat/chicken Alexa 546-, Alexa 594-, Alexa 488- or Alexa-633-conjugated secondary antibodies 1:1,000	Invitrogen, Germany
Hoechst 33342 1:5,000	Invitrogen, Germany

FACS antibodies	Company
CD3 (500A2) – PerCP-Cy7	eBioscience, Germany
CD8 (53.-6.7) – PerCP-Cy5.5	eBioscience, Germany
CD8 (53.-6.7) – PO	eBioscience, Germany
CD11a (M17/4) – e450	eBioscience, Germany
IFN-γ (XMG1.2) – APC	eBioscience, Germany
IFN-γ (XMG1.2) – PE	eBioscience, Germany
TNF-α (MP6-XT22) – FITC	eBioscience, Germany
FITC-Dextran	Invitrogen, Germany

Peptides	Sequence	Company
*Pb*TRAP$_{130-138}$	SALLNVDNL	Peptides & Elephants, Germany
*Pb*S20$_{318-326}$	VNYSFLYFL	Peptides & Elephants, Germany
OVA$_{257-264}$	SIINFEKL	Peptides & Elephants, Germany

2.1.7 Enzymes

Enzymes	Company
Restriction endonucleases	New England Biolabs, Fermentas
T4-DNA-Ligase	Fermentas, Germany
Taq DNA Polymerase	Fermentas, Germany
Platinum Taq DNA Polymerase (HF)	Invitrogen, Germany
Dream Taq	Thermo Fisher, Germany

2.1.8 Stocks and working solutions

Nycodenz stock (autoclaved, protected from light):
KCl 3 mM (250 mM stock)
EDTA 0.3 mM (0.5 M stock)
Tris pH 7.5, 5 µM
Nycodenz 110.4 g
ddH_2O to 400 ml
Solution stored at 4°C

Lysogeny Broth (LB) medium (pH 7.5):
Bacto-tryptone 10 g
Bacto-yeast extract 5 g
NaCl 5 g
ddH_2O to 1,000 ml
Medium stored at RT

LB-Agar:
LB-Medium 1,000 ml
Bacto-Agar 15 g
Solution stored at 4°C

Transfection Medium:
RPMI1640 160 ml
FCS (origin USA) 40 ml
Gentamycin 50-60 µl
Solution stored at 4°C

Pyrimethamine H2O (pH 3.5 - 4.5):
Pyrimethamine 0.35 g
DMSO 50 ml
H_2O add 5 L
Solution stored at RT (in the dark)

Heparin/PB**S:**
Heparin 40 µl
PBS 960 µl
Solution stored at 4°C

Ketamine/Xylazine hydrochloride:
Ketamine (100 mg/ml) 1 ml
2 % Rompun (Xylazine) 150 µl
1x PBS 2.85 ml
Solution stored at 4°C

4% Paraformaldehyde (pH 7.2)
Paraformaldehyde powder 20 g
NaOH 2M 10 µl (clear solution)
10x PBS 50 ml pH 7.2
ddH_2O add 100 ml (55-60°C)
Solution stored at -20°C (long-term)/4°C (short term)

50x TAE-buffer (pH 7.8)
Tris 2 M
Sodium acetate 250 mM
EDTA 0.5 mM
Solution stored at RT

Freezing solution
Alsever's Solution 90 ml
Glycerol 10 ml
Solution stored at 4°C

Percoll solution
RPMI complete (37°C) 27.1 ml
Percoll (37°C) 14.2 ml
10x PBS (autoclaved, 37°C) 1.6 ml

2.1.9 DNA oligonucleotides

2.1.9.1 Cloning primers

Number	Purpose	Restriction site	Sequence
1	5' *UIS4* fwd	*Bss*HII	CATGAGCGCGCCTTTATGTTTTTTGAAAGATTTAAC
2	5' *UIS4* rev	*Xba*I	GCTCATCTAGATTCAGACGTAATAATTATGTGCTG
3	*HSP101* ORF fwd	*Xba*I	CATCTAGAATGGTACGGAACATTGCTAAAAATTATTTATTTG
4	*HSP101* ORF rev	*Age*I	GCCCTTGCTCACACCGGTTGACAATGAAAGGTTAATAACAATGTTG
5	5' EF1a fwd	*Bss*HII	CATGAGCGCGCGATTTACATGGCGTTTTATGTTTATATG
6	5' EF1a rev	*Xba*I	GCTCATCTAGATTTTATAAAATTTTTATTTTATTTATAAGCAAATATA
7	linker fwd		CGAGTGGCCACGTGGCCACCAGAACCACCACCGGTTCATG
8	linker rev		CATGAACCGGTGGTGGTTCTGGTGGCCACGTGGCCACTCG

2.1.9.2 Genotyping primers

Number	Purpose	Locus /Plasmid	Sequence
9	5' integration rev	*HSP101*+++ (Myc)	GCTCATCTAGATTCAGACGTAATAAT TATGTGCTG
10[a]	WT fwd	Silent 6 locus	GACAGCGCATATGATGGATG
11[a]	WT rev	Silent 6 locus	TTTGAGAAATTGCGTATTCGTA
12[c]	3 integration fwd	*HSP101*+/ +++ (Myc)	ATGAAATACCGCTCCATTTTTCC
13	5' integration rev	*HSP101*+ (Myc)	CATCTAGATTTTATAAAATTTTTATTT ATTTATAAGCAAATATA
14	3' integration fwd	*HSP101*++	GACTGAGGTTGTGTGATGGC
15	3' integration rev	*HSP101*++	GAGCCAAATTGTTCAATGTTTAAT
16	5' integration fwd	*HSP101*++	CTATAAATTTAGTAGAAATGGTACGG AAC
17	5' integration rev	*HSP101*++	GACACTTATATATTTATACTAAGTTCG
18[b]	5' Integration	*SLARP* locus	CGCTACATTATACAATGAACTTTTCC
19[c,f]	5' Integration		CAATTTGTTGTACATAAAATAGGCAG
20[c,g]	3' Integration		ATGAAATACCGCTCCATTTTTCC
21[c]	3' Integration		CCAGCTTTTATTTTCCATAATATCC
22[c]	WT fwd		GAGACATATCAAATAATTACTACATA CCACC
23[c]	WT rev		GGGGTTCATAATTATATTTTCATTAGG GTCC
24[b]	5' Integration	*P36p/P36* locus	AAATGTTTGTATGTTTGGAATATCAG G
25[c]	5' Integration		TAATAATTGAGTCTTTAGTAACGAATT GCC
26[c]	3' Integration		GATGGAAGCGTTCAACTAGCAGACC
27[b]	3' Integration		ATTCGCGTTTAATCTTTTAATTATACC
28[c]	WT fwd		GCCTAATGCAAAATATTATCCCGATTT AG
29[c]	WT rev		GCTAGTCCTTTGTTCCCATTATATG
30[d]	5' UTR fwd	*UIS4* locus	CAAATAATTGTGTATGTAATATTTAAG TGTAGAATGGAAT
31[e]	ORF rev	*UIS4* locus	TAAATCATTCGGCCCATACATA
32[d]	3' UTR rev	*UIS4* locus	CTCTATAACATTATTTTTCCTTTTCTC TTACTT

[a] kindly provided by Prof. Dr. Taco Kooij, Radboud Institute for Molecular Life Sciences, Netherlands.
[b] kindly provided by Dr. Sanketha Kentirapalan.
[c] kindly provided by Dr. Katja Müller, Hu Berlin.
[d] kindly provided by Dr. Josephine Grützke.
[e] kindly provided by Dr. Alyssa Ingmundson, Hu Berlin
[f] P2 was also used as fwd primer for validating 5' Integration in the *ΔP36p/P36* parasite line.
[g] P3 was also used as fwd primer for validating 3' Integration in the *ΔP36p/P36* parasite line.

2.1.9.3 qRT-PCR primers

Number	Purpose	Sequence
33[a]	*HSP70* fwd	GCTAACGCAAAAGCAAAGC
34[a]	*HSP70* rev	TCGGTAAAAGCTACATAGGATG
35[b]	*UIS4* fwd	CCCATTGATGAGACAAACGATTCAAAACC
36[b]	*UIS4* rev	TCCATGTTATAAACGTTATTTCCTTCACCC
37[b]	*EF1α* fwd	GAAATTGAGATGGAAGGATTAACTTG
38[b]	*EF1α* rev	CAATCCTCATCACTTAATCCCAC
39[c]	*HSP101* fwd	TTTGTTATTGTCTGTGCTCAAGG
40[c]	*HSP101* rev	GCAAAGGTTTTAATTGGTTATGACC
41[c]	*PTEX150* fwd	CCAAAGTTTTAGCTATTACCGC
42[c]	*PTEX150* rev	TTATTTGTGTTGCCATTGTTGCC
43[c]	*EXP2* fwd	CAACAAATATTGTAAAATGTGACGC
44[c]	*EXP2* rev	TGACTAATAATATCCACCACATACG
45[c]	*PTEX88* fwd	GAATACTTGATGAACTTCCCGG
46[c]	*PTEX88* rev	TAATCCATTATTAGCAGCCATTCC
47[c]	*TRX2* fwd	CAAGATTGGAACAAAGCAGC
48[c]	*TRX2* rev	TTGTAACAAAATGCTCATTTTTTGC
49[a]	*Pb18* fwd	AAGCATTAAATAAAGCGAATACATCCTTAC
50[a]	*Pb*18 rev	GGAGATTGGTTTTGACGTTTATGTG
51[a]	mGAPDH fwd	CGTCCCGTAGACAAAATGGT
52[a]	mGAPDH rev	TTGATGGCAACAATCTCCAC
53[a]	*GFP* fwd	GATGGAAGCGTTCAACTAGCAGACC
54[a]	*GFP* rev	AGCTGTTACAAACTCAAGAAGGACC

[a] kindly provided by Dr. Katja Müller, HU Berlin.
[b] kindly provided by Prof. Dr. Olivier Silvie, Centre Hospitalier Universitaire Pitié-Salpêtrière, Paris, France.
[c] kindly provided by Dr. Joachim Matz, HU Berlin.

2.1.10 Database and software

2.1.10.1 Online

PlasmoDB
NCBI PubMed
NCBI Blast
GeneDB

2.1.10.2 Software

4Peaks
Adobe Illustrator CS6
ImageJ / Fiji
Image Lab
FlowJo 8.7.3
GraphPad Prism 6
Microsoft Office 2011
Microsoft EndNote X7
RStudio
Serial Cloner 2-6-1
SnapGene

2.2 Methods

2.2.1 Molecular- and microbiological methods

2.2.1.1 Plasmid design for *P. berghei* transfection

2.2.1.1.1 Generation of *P. berghei ΔSLARP, ΔP36p/P36, ΔSLARP/P36p/P36* knockouts

Parasite lines were generated in *P.b. ANKA* clone 507 (for *ΔP36p/P36*) and clone 15cyl (for *ΔSLARP*, *ΔSLARP/P36p/P36*) by double homologous recombination.

sKO parasites: Marker-free *ΔSLARP* and *ΔP36p/P36* parasites were kindly provided by Olivier Silvie (Manzoni *et al.*, 2014, Manzoni *et al.*, 2017). For generation of *ΔSLARP*, the GOMO plasmid comprising of 5' and 3' homologous sites flanking the *SLARP* ORF, hDHFR, as a selection marker and mCherry (mCh) as well as GFP as indications for positive integration of the plasmid was used as described (Manzoni *et al.*, 2014). Recycled, marker free, *P.b.* ANKA *ΔSLARP* parasites served as recipient strain for the tKO parasite line. *ΔP36p/P36* plasmids were designed using the pBART vector (Kooij *et al.*, 2012) including *P36p* 5' and 3' UTR regions, a GFP cassette and a *Toxoplasma gondii* pyrimethamine selection cassette (kindly provided by Sanketha Kentirapalan).

tKO parasites: Plasmids were linearized up- and downstream of 5' and 3' UTR homologous regions and integrated into *ΔSLARP* parasites using homologous recombination. Josephine Scholz performed transfection and cloning of *ΔSLARP/P36p/P36* parasites.

2.2.1.1.2 Generation of *P.berghei HSP101+, HSP101++, HSP101+++* plasmids for *HSP101* overexpression

HSP101+/HSP101+++: Plasmids were design using the pBART-SIL6 vector (Kooij *et al.*, 2012) harboring drug selectable hDHFR-yFcu cassette for positive/negative clone selection, a GFP under the *PbHSP70* promoter for parasite life cycle analysis, a mCherry/triple c-Myc (3xMyc) Tag sequence for protein tagging, 3'*Pb*PPPK-DHPS as 3' UTR as well as two sequences for stable integration into the silent 6 locus. *HSP101* ORF (*Pb*ANKA_0931200), generated with primers 3 und 4, was inserted with *Xba*I and *Age*I in front of the mCherry/3xMyc tag. For *HSP101+* a constitutively low expression promoter 5' EF1α (*Pb*ANKA_113330), generated with primers 5 und 6, an for *HSP101+++* liver stage specific strong expression *UIS4* (*Pb*ANKA_0501200), generated with primers 1 und 2, were integrated with *Bss*HII and *Xba*I in front of *HSP101* ORF. mCherry was excised in *HSP101+ Myc and HSP101+++ Myc* plasmids and replaced by a sequence, generated with primers 7 und 8, linking *HSP101* ORF and 3xMyc.
HSP101++: endogenous promoter swap plasmids were kindly provided by Joachim Matz.

2.2.1.2 Polymerase chain reaction (PCR)

To amplify *P. berghei* gene of interest (GOI) or untranslated region of interest (UROI) for subsequent molecular cloning, a polymerase chain reaction (PCR) was performed. Specific primers (s. ch. 2.1.9.1) were designed for GOIs and UROIs. GOIs were amplified using Platinum® *Taq* Polymerase High Fidelity, which comprises a proof reading enzyme for higher fidelity.

Reagents	**Concentration**
10x HiFi PCR Buffer	1x
50 mM $MgSO_4$	2.0 mM
2 mM dNTP Mix	0.2 mM
10 µM fwd primer	0.2 µM
10 µM rev primer	0.2 µM
P. berghei ANKA DNA	<400 ng
Platinum® *Taq* Polymerase High Fidelity (5U/µl)	1U/rxn
ddH_20	final volume to 50 µl

Reagents for each reaction were briefly mixed, spun down and amplified using the following conditions:

Step		**Temperature (°C)**	**Time**
Initial Denaturation		94	2 min
30 cycles	Denaturation	94	30 s
	Annealing	55	30 s
	Extension	60	1.2 min/kb
Final Extension		60	15 min
Hold		4	∞

Amplification of UROIs was performed with Dream Taq DNA Polymerase according to manufacturer's protocol.

Reagents	**Concentration**
10x Dream Taq Buffer	1x
2 mM dNTP Mix	0.2 mM
10 µM fwd primer	0.2 µM
10 µM rev primer	0.2 µM
P. berghei ANKA DNA	<400 ng
Dream® *Taq* Polymerase High Fidelity (5U/µl)	1.25 U
ddH_20	final volume to 50 µl

Samples were briefly mixed and amplified under the following conditions:

Step		Temperature (°C)	Time
Initial Denaturation		95	5 min
30 cycles	Denaturation	95	30 s
	Annealing	55	30 s
	Extension	64	1.2 min/kb
Final Extension		64	15 min
Hold		4	∞

Samples were subsequently purified with Qiagen PCR Purification kit according to manufacturer's protocol.

2.2.1.3 Agarose gel electrophoresis

To determine whether amplification of GOI and UROI was successful, PCR products were separated according to bp length with agarose gel electrophoresis. Efficiency of all PCRs was examined on 1% agarose TAE gels (agarose, 1x TAE) run at 100 V for 40 minutes with 0.1% SYBR Safe, for DNA visualization, and documented with a gel documentation system.

2.2.1.4 *Enzymatic* DNA restriction digest

In order to generate customized plasmids for *P. berghei* transfection, PCR products and plasmid vectors were incubated with specific restriction enzymes to generate compatible 3' or 5' overhangs for subsequent plasmid ligation and transformation. Purified PCR products (inserts) and vectors were digested as follows:

Reagents	Concentration
10x NEB Buffer	1x
Insert/vector	<800 ng
NEB restriction enzyme	1.25 U
ddH_20	final volume to 30 µl

Digestion of insert and vector DNA was performed at 37°C/50°C degrees depending on respective enzyme digestion conditions for 2-6 hours. Heat inactivation at >60°C for 20 seconds was used to terminate the enzymatic reaction. Digested samples were purified with Qiagen PCR Purification Kit according to manufacturer's protocol.

2.2.1.5 Ligation

To generate plasmids of interest, the digested, purified vectors and inserts were ligated guided by newly formed compatible ends using Rapid DNA Ligation Kit according to manufacturer's protocol. In brief:

Steps	Reagents	Concentration
1	5x DNA dilution buffer	1x
	Vector	100 ng
	Insert	1:3 (Vector/Insert ratio)
	distilled H_20	Final volume 10 µl
2	2x T4 Ligation buffer	1x
3	T4 Ligase	0.01 U/µl

Reaction was incubated at room temperature (RT) for 5 minutes.

2.2.1.6 Transformation of competent *E. coli* bacteria

Ligated plasmids were inserted into *E. coli* bacteria for growth and selection. Chemically competent *E. coli* bacteria were thawed on ice, mixed with 24 mM (final concentration) β-mercaptoethanol and 5 µl ligation reaction and incubated for 30 minutes on ice. The bacterial solution was heat-shocked for 45s at 42°C and subsequently placed on ice for 2 minutes. After addition of 200 µl LB-medium, transformed bacteria were plated on an agarose plate (1% ampicillin) under sterile conditions and grown over night at 37°C. Positive bacterial clones harboring the desired plasmid were selected by colony PCR.

2.2.1.7 Culturing of *E. coli*

To upscale plasmid yield, plasmid harboring bacterial clones were grown over night in liquid cultures. Mini (5ml) or Midi (250ml) LB-cultures, were inoculated with a small amount of bacteria harboring the desired plasmid and grown over night at 37°C in an incubator and shaker for liquid *E. coli* cultures. Plasmids were extracted with the Qiagen Mini- or Midi Plasmid Extraction Kit according to manufacturer's protocol. Subsequent restriction digest was used to confirm plasmid clone and the desired sequence changes were analyzed by Sanger sequencing.

2.2.1.8 Overnight enzymatic plasmid digest

For the transfection of *P. berghei* parasites plasmid DNA was linearized to produce free 5' and 3' homologous ends. Plasmids were digested over night on a shaker at 37°C.

Reagents	Concentration
10x NEB Buffer	1x
Final plasmid	30 µg
NEB restriction enzyme (ApaLI or PvuI)	9 µl
ddH_20	final volume to 500 µl

1 µl of enzyme was added the next day and the digest was incubated for another hour.

2.2.1.9 DNA ethanol precipitation

In order to obtain clean plasmid DNA for subsequent transfection of *P. berghei* parasites, plasmids underwent an ethanol precipitation step. The digested plasmid was incubated at -80°C for 30 minutes with 2.5x volume of 100% ethanol and 10% (of digested plasmid solution) 3M natriumacetate (pH 4.8) (NaOAc). The mixture was centrifuged at 4°C for 30 minutes and the pellet washed with 70% ethanol. After another centrifugation the pellet was air dried and resolved in 10-30 µl distilled H_2O to a concentration of 1 µg/µl.

2.2.1.10 RNA isolation

For analyzing *P. berghei* stage specific gene expression, parasite mRNA was extracted, serving as a template for subsequent cDNA amplification and qRT-PCR analysis. Parasite samples from different life cycle stages were mixed with 500 µl TRIzol, incubated at RT for 5 minutes, mixed with 200 µl Chloroform and incubated for 3 minutes at RT. After centrifugation the upper layer was transferred to a new eppendorf tube and mixed with 250 µl isopropanol, 60 µl 5M ammonium acetate (pH 7) and 1.5 µl glycogen and incubated at –20°C for 20 minutes to precipitate RNA. Pelleted samples were washed with ice-cold 70% ethanol and the air-dried pellet resuspended in 30 µl RNase/DNase-free water. RNA samples are subsequently treated with DNase to removal traces of DNA.

2.2.1.11 Complementary DNA (cDNA) synthesis

mRNA samples were reverse-transcribed into cDNA for quantitative real-time PCR analysis. cDNA was synthesized with Ambion RETRO Script kit according to manufacturer's protocol using 5 µl RNA template. Samples were incubated at 42°C for 60 minutes followed by 10 minutes at 90°C.

2.2.1.12 Quantitative real-time PCR (qRT-PCR)

Rapid real time quantification of parasite specific gene expression was used to determine parasite burden in liver and stage specific gene expression in transgenic and WT parasites. qRT-PCRs were performed in optical 96-well plates in triplicates.

Reagents	Concentration
SYBR GREEN I Master Mix	6.25 µl
cDNA sample (dilution 1:30)	5 µl
100 µM fwd primer	0.025 µl
100 µM rev primer	0.025 µl
distilled H_20	0.75 µl

Gene specific primer combinations (s. ch. 2.1.9.3) were used to amplify ~100-200 bp fragments for target gene ORFs. Simultaneous amplification of a house-keeping gene (e.g. *PbHSP70*, *mGAPDH*) enabled determination of ΔCT for relative (m)RNA expression. An additional sample without cDNA was used as a negative control. Samples were processed as follows:

Step		Temperature (°C)	Time
Initial Denaturation		95	15 min
40 cycles	Denaturing	95	15 s
	Annealing	55	15 s
	Extending	65	45 s
Final extension		64	15
Denaturation	Melt curve	95	15 s
Annealing		60	1 min
Melting		95	15 s

Data was analyzed with Excel 2011. Quantity was calculated by using ΔΔCt method comparing nr of cDNA copies of GOI compared to endogenous cDNA.

$$\Delta\Delta Ct = 2^{-\Delta Ct\ housekeeping\ gene - \Delta Ct\ target\ gene}$$

2.2.1.13 DNA isolation

Parasite DNA was extracted from blood stage cultures for genotyping transgenic parasite lines and for amplification of parasite specific GOIs and UROIs from WT genomic DNA. Infected blood was retrieved by tail vein puncture or heart puncture and washed once with 1x PBS. To rupture the red blood cells the sample was incubated with 0.2 Saponin and centrifuged at 2800 rpm for 8 minutes. The pellet was washed until the color of the supernatant was clear and resuspended in 200 µl 1x PBS. Parasite DNA was extracted using Qiagen Blood DNA Kit according to manufacturer's protocol. DNA was eluted in 80 µl distilled H_2O.

2.2.2 Plasmodium berghei analysis

2.2.2.1 Animal statement

Animal experiments were performed according to rules of the German "Tierschutzgesetz in der Fassung vom 18. Mai 2006 (BGB1, IS. 1207)" with implements the directive 2010/6 3/EU from the European Union with the experimental number G0249/15.

Transgenic parasites were generated and the life cycle was maintained in NMRI mice obtained from Charles River. Immunization experiments and immunoprofiling were performed with C57BL/6 mice purchased from Janvier and Charles River. All mice were bred in house.

Anopheles stephensi mosquitoes were reared at 80% humidity and 28°C and infected by a blood meal on parasitized mice.

2.2.2.2 Infection of mice

In order to culture blood stage *P. berghei* parasites, mice were infected with 100 µl thawed cryopreserved blood stage parasites intravenously or 200 µl peritoneal or by transferring a desired amount of fresh parasitized blood. Parasitemia was monitored with Giemsa-stained thin blood smears.

2.2.2.3 Molecular genetics in *P. berghei*

To study the function e.g. by C-or N-terminal tagging, knockouts or overexpression of *Plasmodium* genes of interest, parasites can be genetically manipulated by conventional homologous crossover. Parasites are haploid during asexual blood stage development, thus hold perfect conditions for straightforward genetic manipulation. Recent advances in molecular genetics have advanced the filed in particular for *P. falciparum* (de Koning-Ward *et al.*, 2015). Nevertheless, double homologous crossover in *P. berghei* is relatively efficient and remains the major technique for parasite genetic manipulation. *P. berghei* molecular genetics are performed *in vivo* as parasites are maintained in mice. To yield mature schizonts for transfection, insertion of linearized plasmids harboring *Plasmodium* genes for desired genetic crossover, ring stages and trophozoites are cultured over night *in vitro*. Transfected schizonts are injected into mice where double or single homologous crossover can take place (van Dijk *et al.*, 1995, Janse *et al.*, 2006).

2.2.2.3.1 Overnight *P. berghei* schizont culture

For genome editing of *P. berghei* ANKA, transfections were performed in late blood stage parasites (schizonts). Since schizonts sequester on blood vessel walls of infected mice, ring stages and trophozoites are grown into schizonts *in vitro*. *P. berghei* schizonts do not rupture *in vitro*. NMRI mice were infected with *P. berghei* ANKA and parasites were grown until a parasitemia of ~3-5%. One ml of whole blood was collected by heart puncture, carefully mixed with transfection medium (sterile filtered: RPMI, 10% FCS USA, 1% Gentamycin) supplemented with 0.0225 U Heparin (37°C) and centrifuged at 1500 rpm for 10 minutes without brake. The pellet was resuspended in a small amount of transfection medium and underlayered with transfection medium in an Erlenmeyer flask (pre-warmed under culture conditions). The Erlenmeyer flask was incubated for 18-22 hours at 37°C and 5%CO_2, 80% N_2 and 60% humidity. Schizont development was confirmed by Giemsa-stained blood smears.

2.2.2.3.2 Purification of *P. berghei* schizonts

To obtain purified schizonts, 35 ml of the culture was placed in a 50 ml flacon and underlayered with 55% Nycodenz (37°C). Flacon tubes were centrifuged for 20 minutes at 1500 rpm and RT without brake and with accurate balance to obtain schizonts between the gradient layers.

Schizonts accumulating in a brown ring on top of the Nycodenz were carefully transferred to a new 50 ml tube using a pasteur pipette. For washing, the falcon tube was filled up to 30 ml with transfection medium to remove any remains of Nycodenz and centrifuged for 10 minutes at 1500 rpm. The schizont pellet was resuspended in adequate amount (1-10 ml dependent on number of desired transfections) of transfection medium and split into eppendorf tubes (ca. 4 transfections per infected mouse) and centrifuged at full speed for 15 seconds to pellet schizonts.

2.2.2.3.3 Transfection of *P. berghei* schizonts

5-10 µg linearized DNA was mixed with 100 µl T cell nucleofactor solution. Schizont pellets were mixed with DNA solution, transferred to an electroporation cuvette and electroporated using AMAXA Nucleofector device (program U33). Electroporated parasites were mixed with additional 50 µl transfection medium and intravenously injected into NMRI mice.

Selection of transgenic parasites: Transgenic parasites harbor an hDHFR cassette enabling resistance against pyrimethamine. Parasites grew under pyrimethamine (70 mg/L) selection administered to the mice in the drinking water starting day one post transfection, for approximately 6-8 days post infection.

2.2.2.4 Genotyping of parasite lines

The clonal and isogenic transgenic parasite lines were genotyped using 5' and 3' integration and WT specific primer combinations (s. ch. 2.9.1.2). Thus, parasite blood was collected and parasite gDNA was extracted followed by a PCR using Dream Taq according to 2.2.1.2.

2.2.2.5 Generation of an isogenic parasite line (by FACS cloning) or a clonal parasite line (by limiting dilution)

Flowcytometric (FACS) clonal selection: Expression of GFP or mCherry in transgenic parasites during blood stage development allowed selection of isogenic clonal populations. Once transgenic parasites grew to a parasitemia of 0.1-0.8% in NMRI mice one drop of blood was mixed with 1 ml Alsever's solution and filtered into a FACS tube. 100 GFP or mCherry positive parasites were sorted into RPMI/20% FCS USA and intravenously injected into one or two mice. Isogenic parasite populations were grown under pyrimethamine selection until a parasitemia of ~1-3%, parasitized blood was isolated by heart puncture was and stored in 100 µl aliquots in freezing solution (45% Alsever's solution, 55% Glycerin) at -80°C or liquid nitrogen. The residual blood was used for gDNA isolation and subsequent genotyping.

Conventional clonal selection: Once parasitemia reached ~0.1-1% parasites were cloned were subjected to of limiting dilution. Giemsa-smears were used to determine parasitemia (counting 3 independent areas) and used to calculate one parasite/100 µl.

$$7\ x\ 10^6\ \left(Nr\ of\ \frac{RBC}{1} ml\ blood\right) x\ parasitemia\ x\ 10^{-2}\ parasites$$
$$=\ Nr.of\ parasitized\ RBC\ per\ \mu l\ blood$$

Ten mice were infected with one clone each. Transgenic parasites were selected by providing pyrimethamine in the drinking water and growth rate was monitored by Giemsa-stained thin blood smears. Parasite populations were grown until a parasitemia of ~1-3% and stored in 100 µl aliquots in freezing solution (45% Alsever's solution, 55% Glycerin) at -80°C or liquid nitrogen. The residual blood was used for gDNA isolation and subsequent genotyping.

2.2.2.6 Crossing of two transgenic *P. berghei* parasites

For sexually crossing two parasite lines in the mosquito, female NMRI mice were intravenously infected intravenously (i.v.) with 100 µl thawed transgenic parasite stabilates (stabilate/mouse). On day 4, parasitemia was determined and five million parasites of each line were intravenously injected into one naïve female NMRI mice for subsequent mosquito infection.

2.2.2.7 Infection of mosquitoes

In order to analyze parasite development in mosquitoes *in vivo* with subsequent retrieval of sporozoite for mouse infection, mosquitoes were infected with WT and transgenic parasites. Three days prior to feeding female NMRI mice were infected with 10 million iRBCs. Exflagellation of male gametes was examined by counting exflagellation centers per field. A drop of blood from a tail vein puncture of infected mice was placed on a glass slide with a cover slip and incubated at 20°C (RT) for 10 minutes before analyzing exflagellation with 400x magnification of the light microscope. Mosquitoes were starved three hours prior to infection. Infected mice were anaesthetized with 56 µl Ketamine/Xanthoxin/g (mouse weight) and mosquitoes were able to take a blood meal for one hour at RT.

2.2.2.8 Oocyst, midgut and salivary gland sporozoite infectivity

Oocyst production and midgut sporozoites formation were analyzed on day 10 and day 14 and compared to WT parasites. Midguts of infected female mosquitoes were harvested and percentage of infected mosquitoes per 10 mosquitoes was determined. Salivary gland invasion by sporozoites was analyzed at day 17 post infection by extracting salivary glands of infected female mosquitoes. Sporozoite load per infected mosquito were compared to WT parasite infected mosquitoes.

2.2.2.9 Isolation of salivary gland and haemocoel sporozoites

In order to obtain salivary gland sporozoites, infected mosquitoes were dissected in RPMI complete medium (RPMI, 10% FCS, 1% Penicillin/Streptomycin), for *in vivo* infection of mice. For *in vitro* infections of cultured hepatoma cells, sporozoites were dissected in DMEM complete medium (DMEM, 10% FCS, 1% Penicillin/Streptomycin). Salivary glands were grinded with a pestle and centrifuged at 4°C for 3 minutes at 10,000 rpm, resuspended in medium and diluted 1:10 to be counted in a Neubauer chamber.

To retrieve haemocoel sporozoites mosquitoes were dissected alive on ice to reduce motility. After removal of legs and wings, one third of (V-VII abdominal segment) the abdominal tip was cut off and the tip of a 1 ml BD Micro Fine syringe filled with pure RPMI was placed between the forelegs and hind legs. Roughly 50-100 µl (one drop) was inserted and collected on parafilm. The medium with the haemocoel sporozoites was transferred to an eppendorf tube while measuring the volume to calculate the numbers of sporozoites in the total volume. Sporozoites were counted in a Neubauer chamber.

$$\frac{Total\ sporozoites}{Nr.of\ dissected\ mosquitoes} = Nr.sporozoites/mosquito$$

2.2.2.10 Analysis of live sporozoites and immunofluorescence assay (IFA)

Live analysis of sporozoites: Sporozoites were incubated for 10 minutes with 1:50 Phalloidin to reduce gliding motility during live imaging and 1:5,000 Hoechst 33342 for nuclear staining. 8-well glass slides were coated with 10 µl sporozoite solution and covered with a cover slip. Sporozoite protein (GFP, mCherry) expression was analyzed with an Axio vision fluorescent microscope with 400x or 630x magnification.

Immunofluorescence assays (IFA) of sporozoites: Specific protein expression in sporozoites was analyzed via immunofluorescence assays. 8-well glass slides were precoated with 3% BSA (in RPMI) for 10 minutes at 37° in a humid chamber. $1x10^4$ isolated salivary gland sporozoites/ well were incubated at 37°C in a humid chamber for 15 minutes for sporozoite settling. Slides were fixed with 4% paraformaldehyde (PFA) for 15 minutes at RT, permeabilized with 0.2% TritonX-100 and blocked with 3% BSA for 15 minutes at RT. Primary antibodies were added for one hour at 37°C followed by three washing steps and one hour incubation at 37°C in a humid chamber with fluorophore-linked secondary antibody and 1:5,000 Hoechst 33342 for nuclear staining. Both staining steps were performed in RPMI containing 2% TritonX-100 and 3% BSA. Slides were mounted with Fluoromount G and analyzed with Axio vision observer fluorescence microscope. Images were obtained at 630x magnification.

2.2.2.11 Sporozoite motility assay

Gliding ability of sporozoites is essential for liver stage infection. To access whether transgenic sporozoites are able to glide, sporozoite motility assays were performed. 8-well glass slides were precoated with 3% BSA (in RPMI) for 30 minutes at 37° in a humid chamber. $1x10^4$ isolated salivary gland sporozoites/ well were incubated at 37°C in a humid chamber for 20 minutes for sporozoite settling and gliding. Sporozoites display circular movement on two-dimensional glass surface, shedding surface proteins such as TRAP and CSP. Primary α-sporozoite surface polyclonal antibody was added for 1 hour at 37°C followed by three 1x PBS washing steps and one hour incubation at 37°C in a humid chamber with the secondary antibody goat α-mouse Alexa-Fluoro 488 and Hoechst 33342 for nuclear staining. All stainings were performed in RPMI containing 3% BSA. Slides were mounted with Fluoromount G and analyzed with Axio vision observer fluorescent microscope. Percentages of gliding vs. non-gliding sporozoites were determined for each well.

2.2.2.12 Ratio of intra- vs. extracellular sporozoites

To determine sporozoites' ability to attach or enter hepatocytes, cultured Huh7 hepatoma cells were infected with sporozoites *in vitro* and analyzed for cell attachment or intracellular development. One day prior to the experiment $3x10^4$ Huh7 cells/well were plated in an 8-well Labtek glass slide. Next day, sporozoites were isolated from infected mosquitoes' salivary glands and cells were infected with $1x10^4$ sporozoites/well (~100µl DMEM complete) in triplicates, centrifuged at 1500 rpm for 5 minutes without brake at RT and incubated for two hours at 37°C and 5%CO_2. Infected cells were washed three times, fixed with 4% PFA for 10 minutes at RT, washed and blocked with 3%BSA (in PBS) for 1 hour at 37°C. After blocking, cells were incubated with the primary α-CSP antibody, staining extracellular parasites, in 3%BSA (in PBS) for one hour at 37°C. Cells were washed prior to adding the secondary antibody goat α-mouse Alexa-Fluoro 546 (1:1,000) for one hour at 37°C. Subsequently, cells were washed intensively to remove assess of secondary antibody and permeabilized with 3% BSA, 0.2% Triton-X forone1 hour at 37°C. Primary α-CSP antibody was applied again to cells for one hour at 37°C, cells were washed and incubated with secondary antibody goat α-mouse Alexa-Fluoro 488 (1:1,000) staining intra- and extracellular parasites and Hoechst 33342 (1:5,000) staining host cell and parasite nucleus for one hour at 37°C. After additional washing steps cells were mounted with Fluoromount G and analyzed with the Axio vision fluorescence microscope. Based on stainings, ratios of both red and green extracellular parasites / only green intracellular parasites were counted per well.

2.2.2.13 C57BL/6 *P. berghei* sporozoite infection

In order to analyze infectivity and liver stage development *in vivo*, mice were infected with *Plasmodium* sporozoites. Sporozoites were diluted in 200µl pure RPMI and $1x10^4$ or $1x10^5$ each were intravenously injected in C57BL/6 mouse.

Bite back assays were used to resemble natural mosquito infections. 15 infected mosquitoes were kept in a separate container allowing targeted blood meal on one C57BL/6 mouse. Mice were anesthetized with 60 µl Ketamine/Xanthoxin intraperitoneal (i.p.) and mosquitoes were allowed to feed for 15 minutes. Mosquitoes were analyzed for successful feeding by examining blood uptake in the mosquito midgut.

2.2.2.14 Blood stage parasite detection: Giemsa-stained thin blood smears

Tail vein punctures for blood smears were performed day 3-14 post sporozoite infection. After fixation in methanol, smears were stained with a 10% Giemsa solution and analyzed for presence of blood stage parasites. Parasitemia was determined as followed:

$$Parasitemia\ (\%) = \frac{Parasites/counted\ fields}{RBC/field\ x\ counted\ fields}\ x100$$

2.2.2.15 Pre-patency analysis

In order to determine whether transgenic as well as WT parasites are able to develop in the liver and infect RBCs, mice were infected with sporozoites (s. ch. 2.2.2.2) and blood stage parasite development was analyzed as described in 2.2.2.14. Infected mice were monitored from day 3-14 post infection for parasite development. Results of pre-patency analysis were plotted Kaplan-Meyer-curves using Graphpad Prism.

2.2.2.16 Determining experimental cerebral malaria (ECM)

Cerebral malaria is a complication of severe malaria. C57BL/6 mice infected with WT sporozoites develop ECM approximately 7 days post infection. Animals infected with sporozoites were monitored for up to 10 days for ECM development. Ruffled fur, hunching, wobbly gait, limb paralysis, convulsions and coma are signs of ECM (Riley *et al.*, 2010, Haque *et al.*, 2011). Animals that had ≥4 of those symptoms were determine as severe ECM cases and sacrificed with neck fracture.

2.2.2.17 *P. berghei* blood stage IFA

Parasite blood stage protein expression was determined in immunofluorescence assays (IFA). Infected RBC were retrieved by tail vein punctures of infected mice, mixed with 1x PBS and placed on a poly-L-lysine covered 12 mm ø cover slips in a 24-well plate to settle for 60 minutes.

Cells were fixed with 4% PFA / 0.0075% fresh glutaraldehyde (GA) at RT. After three washing steps cells were permeabilized with 0.2% TritionX-100 (in PBS) for 20 minutes at RT. Cells were washed and blocked with 3% BSA, 0.2% TritonX-100 (in PBS) for 30 minutes at RT on a shaker. Primary antibody was added in blocking solution for one hour at RT, shaking, followed by three washing steps and incubation with fluorophore labeled secondary antibody and Hoechst 33342 in blocking solution for one hour at RT, shaking. Additional washing steps removed remaining secondary antibody before cells were mounted with Fluoromount G on a glass slide. Cells were analyzed with Zeiss Axio Observer immunofluorescence microscope and images were taken at 640x magnification.

2.2.2.18 Parasite burden in mouse livers

Prime/boost immunized animals were challenged with freshly dissected sporozoites five months post immunization and the livers were harvested at 42 or 48 hours post challenge infection. (Half of the liver was taken for $CD8^+$ T cell analysis the other half for parasite load analysis). Mice livers were homogenized in TRIzol and subsequently total RNA was extracted from the cells. cDNA was generated by reverse transcription with the RETRO Script Kit. Quantitative real-time PCR (qRT-PCR) analysis was performed with primers specific for *Pb*18s rRNA and mouse GAPH for normalization (Table S1). Relative liver parasite levels were determined with the ΔΔCt method.

2.2.3 Cell biological methods

2.2.3.1 Maintenance of hepatoma cells

Cell lines were kept according to standard cell culture conditions for human hepatoma cell lines Huh7 and HuhB3H. In brief: Huh7 cells were thawed at 37°C and cultured in DMEM complete (DMEM, 10% FCS, 1% Penicillin-Streptomycin) in T25 or T75 flasks at 37°C and 5% CO_2. HuhB3B cells were cultured in RPMI supplemented with 5% FCS, 10 mM HEPES, 1x MEM non-essential amino acids and 2 mM L-Glutamine in T25 or T75 flasks at 37°C and 5% CO_2. Passaging of cells was performed every three days, splitting 1:10 of a confluent culture. Cells were incubated with 1 ml (T25) or 3 ml (T75) trypsin for 3 minutes, spun down at 1200 rpm for 2 minutes and resuspended in an adequate amount of culture medium. Cells remained in culture for up to 15 passages. Both cell types were stored in freezing solution (10% DMSO, 20% FCS, 70% culture medium) in a freezing container at -80°C for 24 hours and then transferred to liquid nitrogen (for long term storage) or -80°C (for short time storage).

2.2.3.2 Infection of hepatoma cells

Hepatoma cells were infected as described in 1.2.2.12. Infected cells were incubated at 37°C and 5% CO_2 for 4h, 16h, 24h, 48h and 72h. Cells were washed at two hours post infection to remove non-invaded sporozoites and then medium was changed daily. Growth was terminated by fixation with 4% PFA for 10 minutes at RT.

2.2.3.3 Live imaging of infected hepatoma cells

For protein export analysis of infected Huh7 cells with crossed transgenic parasite lines, live imaging of parasites was performed. Infected cells in Ibidi slides were washed once with 1x PBS and remained in PBS solution for the time of imaging. Live imaging was performed with a Zeiss Axio Observer immunofluorescence microscope with 1,000x lens. Duration of analysis was kept at a minimum to ensure cell survival.

2.2.3.4 Immunofluorescence assays (IFAs) of infected hepatoma cells

Infected cells were blocked with PBS/10%FCS and permeabilized with 0.2% Triton for 1h at 37°C. Primary antibodies (α-GFP, α-USI4, α-MSP1, α-mCherry, α-Myc, α-CSP or α-LC3, for dilutions s. ch. 2.1.6) were applied for one hour at 37°C. After washing, cells were incubated with the respective fluorescently labeled secondary antibody (α-chicken Alexa Fluor 488, α-mouse Alexa Fluor 546, α-mouse Alexa Fluor 488, α-rat Alexa Fluor 546 α-rat Alexa Fluor 488, α-rabbit Alexa Fluor 546, α-rabbit Alexa Fluor 488, for dilutions s. ch. 2.1.6) and Hoechst 33342 for one hour at 37°C. Subsequently, cells were washed and mounted with Fluoromount G.

2.2.3.5 Microscopical analysis of exo-erythrocytic forms (EEFs) IFAs

Stained and fixed cells were analyzed with a Zeiss Axio Observer immunofluorescence microscope. Pictures of parasites were taken with 630x magnification for immunofluorescence pictures and 10-20 pictures of infected cells per well were taken for size analysis of the parasite. Pictures were analyzed with Fiji using a previously coded macro. Parasite size was determined for all strains at 24h, 48h and 72h post infection.

Each well of duplicates/ triplicates of all time points (24h, 48h and 72h) was completely screened to determine the amount of infected host cells per well.

2.2.3.6 Transmigration assay

Upon arrival at the liver, sporozoites transmigrate through several hepatocytes before infecting a final cell to undergo maturation into thousands of merozoites. During the process of transmigration, sporozoites create holes in hepatoma cell membrane. Transmigration assays take

advantage of this process, with help of a normally non cell-permeable dye, in order to analyze whether transgenic sporozoites are able to transmigrate through hepatoma cells.

One day prior to infection $1x10^6$ Huh7 cells per well were seeded in a 24-well plate and kept in 1 ml DMEM complete at 37°C and 5% CO_2. The next day, salivary gland sporozoites were isolated from infected mosquitoes and incubated with 0.5 mg/ml FITC-dextran. Huh7 cells were subsequently infected in duplicate or triplicates with 75.000 sporozoites/well (~280µl/well). Additionally, two wells received parasites(-)/dextran(+) medium to account for natural dextran uptake of uninfected cells and a further two wells received parasites(-)/dextran(-) medium as a negative control. Infected cells, were centrifuged at 1800 g for 5 minutes without brake and incubated for two hours at 37°C and 5% CO_2. After washing (three to five x) with PBS, cells were trypsinized with 200 µl/well and collected in an eppendorf tube. Additional five to seven washing steps with medium removed excess of dextran. For subsequent FACS analysis cells were resuspended in 200µl 1% PFA/PBS and stored at 4°C in the dark until analysis. Cells were transferred to FACS tubes through a cell strainer and analyzed with MACSquant (Channel FSC/FITC) for amount of dextran positive cells/sample. Parasites(-)/dextran(-) cells were used to set the 0% threshold and parasite(-)/dextran(+) cells were used to set threshold for natural dextran influx. All were analyzed with MACSQuant gating for FFC/FITC. Results were subsequently analyzed with FlowJo.

2.2.3.7 RNA isolation of infected hepatoma cells

To determine expression of liver stage specific genes, relative mRNA levels were determined in WT and transgenic parasites. 3 $x10^5$ Huh7 cells/well were plated in a 24-well plate. Next day, salivary gland sporozoites were isolated from infected mosquitoes and Huh7 cells were infected with 100.000 sporozoites/well (in 200 µl DMEM complete). For parasite sedimentation plates were centrifuged for 10 minutes at 3000 rpm, no brake, and incubated at 37°C and 5%CO_2. Two hours post infection, cells were washed once to remove extracellular sporozoites. After 16h, 24h, 48h or 72h cells were trypsinized with 200 µl for 3 minutes at 37°C, and carefully resuspended in DMEM. Cells were transferred to 50 ml falcon tubes and washed with additional 20 ml DMEM. After 5 minutes centrifugation at 1200 rpm with brake, the pellet was resuspended in 500 µl TRIzol and RNA was extracted for subsequent cDNA synthesis and qPCR analysis as described in chapter 1.2.1.10.

2.2.4 Immunological analysis

2.2.4.1 Immunization of C75BL/6 mice

Immunizations of C57BL/6 mice were performed with $1x10^4$ sporozoites intravenously in a prime/boost regimen (day 0 and day 7 or day 10). For γ-sporozoites, parasites were irradiated for 2h at $1.2x10^4$ cGy to induce DNA damage resulting in liver stage attenuation. For attenuation with AZ, mice were given 4,8 mg/mouse AZ in 200 µl sodium chloride (NaCl) i.p. Immunized animals were challenged with $1x10^4$ WT sporozoites injected intravenously 37, 67, 97 or 120 days post immunization. Daily thin blood smears were performed day 3-14 and stained with Giemsa to analyze blood stage parasitemia.

2.2.4.2 Dissection of mouse livers and spleens

ΔSLARP/P36p/P36: For the analysis of IFN-γ producing effector-memory $CD8^+$ T cells after one and two months post boost immunization. Animals immunized and challenged for protection experiments were, if blood stage positive, treated with pyrimethamine in the drinking water for 10 consecutive days to clear blood stages from circulation. One month post challenge (one and two months challenge) spleens and livers were excised. For the dataset generated five months post immunization, animals were immunized in a prime/boost regime, challenged after five months and spleens were excised after 42h after the challenge.

Retrieval of splenic and hepatic lymphocytes: Animals were perfused with PBS and liver and spleen harvested. For retrieval of splenic lymphocytes, the spleen of each animal was homogenized with the help of a 40 µm cell strainer in complete RPMI (RPMI, 10% FCS, 2% Penicillin/Streptomycin). The cell suspension was centrifuged 1800 rpm for 3 minutes and red blood cells were lysed with 1 ml 1x BD PharmLyse buffer for 10 minutes at RT. Lysis was stopped by adding 4 ml complete RMPI and after centrifugation the pellet was resolved in 1 ml complete RPMI for further analysis. For the retrieval of liver cells, the liver of each mouse was homogenized by passing the livers through a 70 µm cell strainer in complete RMPI. Cell suspension was centrifuged for 10 minutes at 4 °C at 1200 rpm. The pellet was resuspended in a 40% percoll solution (37°C) and centrifuged for 20 minutes at 2000 rpm at RT without brake. Pellet was resuspended and lysed as described for splenic cells. Pellets were resuspended in a final volume of 150 µl RPMI complete for further analysis.

2.2.4.3 Restimulation of lymphocytes

In order to activate TNF-α and IFN-γ production, cells (~2 million cells/well or $1-2x10^5$ hepatic lymphocytes) were plated in a 96 well flat bottom plate and restimulated with 10µg/ml (1:1,000) TRAP-SALLNVDNL, S20-VNYSFLYLE or OVA-SIINFEKL (as a negative control) MHCI-H2

K^b/D^6 CD8-peptides and Brefeldine A (1:1,000) for inhibition of retrograde ER-transport. Plates were incubated for 5-6 hours at 37°C and 5% CO_2 and subsequently at 4°C overnight. All centrifugation steps were performed in PBS/1% FCS for 3 minutes at 1800 rpm. Next, cells were washed and extracellular stained with fluorescently labeled antibodies (CD11a (M17/4), CD8 (53-6.7), CD3 (500A2)) was performed in PBS/1%FCS for one hour at 4°C in the dark, followed by fixation with 4% PFA for 15 minutes at RT (dark). After two subsequent washing steps with PERM-wash buffer, the extracellular stain IFN-γ (XMG1.2) and TNF-α (MP6-XT22)) was applied for 1h at 4°C (dark) in PERM-wash buffer. Cells were washed and resuspended in 150 µl PBS/1% FCS buffer for subsequent FACS analysis with the MACSquant. Cells were gated to exclude doubles and lymphocyte population was determined using FSC/SSC. Data was collected from the whole restimulated sample or 1 million events for the lymphocyte population. Computational analysis was performed with FlowJo.

2.2.4.4 Antibody titers

Serum of prime/boost-immunized animals was retrieved one, two or five months post boost immunization. Approximately 50 µl blood was taken from the tail vein of animals with a heparinized capillary. Blood was centrifuged at 1800 rpm for 10 minutes to separate serum from the red blood cells, which was stored at 80°C for further analysis. Air-dried sporozoites were prepared with 5-10,000 WT sporozoites in PBS/well of epoxy covered eight well glass-slides for antibody staining. After fixation in Aceton (ice-cold), slides were rehydrated with PBS and blocked with PBS/3%BSA solution for 30 minutes at 37°C. Serum of each immunized or naïve animal was diluted in serial dilutions of 1:10,000, 1:33,000, 1:100,000, 1:33,0000 and sporozoite slides were incubated with the serum for 1h at 37°C. After several washing steps, slides were incubated with fluorescently labeled secondary antibody (goat α-mouse Alexa-Fluor 488) for one hour at 37°C. Nuclei were stained with Hoechst 33342. Slides were mounted with Fluoromount G (Southern Biotech) and analyzed for the lowest dilution with detectable sporozoites staining with help of a Zeiss Axio vision fluorescence microscope.

2.2.5 Statistical analysis

Data was analyzed with Excel, FlowJo V8.7, GraphPad Prism V5.0c. Statistical significance was analyzed by non-parametrical Whitney-U test for non-normally distributed data (infected hepatoma cells) and one-way ANOVA for normally distributed data (antibody titers). Log rank (Mantel-Cox) test was applied for Kaplan-Meyer-curves and slope of parasite growth curves was analyzed using R Studio.

3 Results

3.1 Pre-clinical analysis of a triple genetically attenuated parasite (tKO GAP) vaccine candidate

Attacking and eliminating *Plasmodium* parasites in the liver prior to the symptomatic blood infection is one of the most promising malaria vaccine strategies. In the case of malaria, experimental immunizations with genetically arrested liver stages (GAPs) have proven safe and efficacious against challenge infections in mice, primates, and humans. Thus far, only one GAP-vaccine candidate, parasite harboring a targeted deletion of the master regulator of liver stage development *SLARP,* provides complete life cycle arrest *in vivo* and *in vitro,* but fails to induce sterile protection. In contrast, *ΔP36p/P36* parasites elicit potent immunity but cause occasional breakthrough infections. To decipher whether transgenic parasites harboring a triple gene deletion *ΔSLARP/P36p/P36* (tKO GAP) perform better in safety and efficacy compared to their single knockout counterparts, pre-clinical immunization and challenge studies were conducted. Comparative immune profiling of mice immunized with tKO and single GAPs as well as irradiated WT (γ-WT) parasites were done prior to and after challenge infections in spleens, livers and peripheral blood to capture pathogen-specific host responses. To examine synergistic or antagonistic effects of combining gene knockouts with different liver stage developmental defects, the following questions were asked i) are vaccine safety requirements fulfilled in this tKO GAP, ii) can immunizations with tKO GAPs confer sterile protection against *Plasmodium* challenge infections and iii) can underlying immune mechanisms be deciphered and correlated to increased or reduced immunity. Comparing the tKO to the original KO GAPs is critical to fully evaluate the advantages of a multiple KO GAP.

3.1.1 Generation of a *ΔSLARP/P36p/P36* parasites

To investigate the vaccine potential of a triple genetically attenuated parasite, a single and a double knockout parasite were combined by sequential deletion of *SLARP* and *P36p/p36* using the GOMO- followed by pBART-strategy and subsequent FACS-based isolation of isogenic parasites (**Fig. 8A**) (Manzoni *et al.*, 2014)(kindly provided by Josephine Scholz, Master thesis 2015). Diagnostic PCR confirmed successful deletions of *SLARP* and *P36p/P36* in the triple knockout parasites (**Fig. 8B**).

As expected from observations of *ΔSLARP* and *ΔP36p/P36* phenotypes (van Dijk *et al.*, 2005, Silvie *et al.*, 2008), blood infection, comprising asexual replication and differentiation into sexual stages, was indistinguishable between *ΔSLARP/P36p/P36* and WT parasites (data not shown).

Similarly, development in the *Anopheles* vector, including colonization of the mosquito midgut, sporogony, and maturation of sporozoites was normal (**Table S1**). Accordingly, preclinical testing of safety and immunogenicity of these triple knockout parasites in a murine malaria vaccine model could be performed.

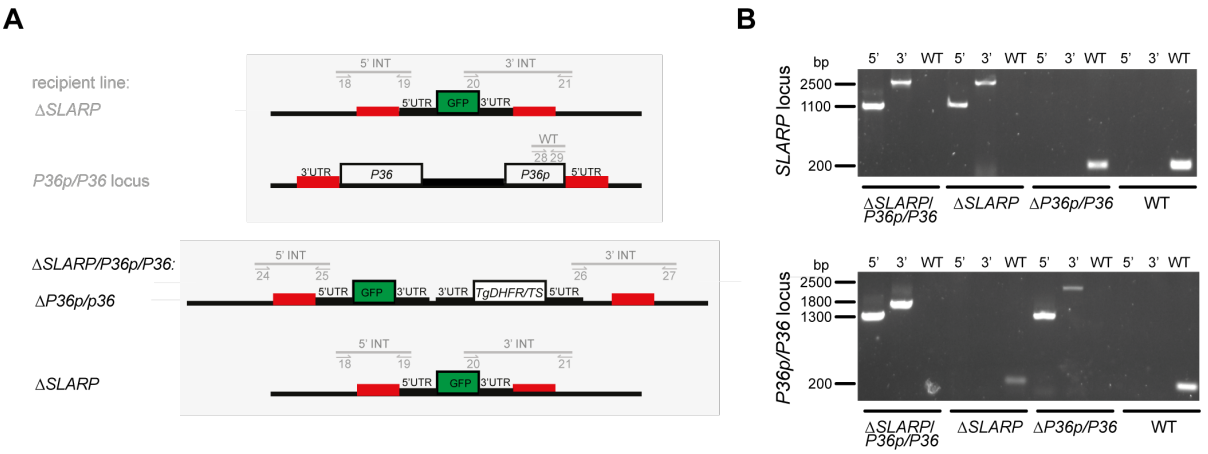

Figure 8 Generation of *ΔSLARP/P36p/P36* parasites

A Schematic representation of the *SLARP* and *P36p/P36* loci of the original *ΔSLARP* (upper grey box) and the generated *ΔSLARP/P36p/P36* (lower grey box) parasites. *ΔSLARP* parasites harbor a modified *SLARP* locus, where *SLARP* is replaced by *GFP* (green) and an intact P36p/P36 locus of which P36 3' UTR and P36p 5' UTR (red) were used for generating *ΔSLARP/P36p/P36* by double homologous recombination. While eliminating P36p and P36, a GFP reporter sequence (green, for parasite life cycle analysis) and TgDHFR/Ts resistant cassette (for positive selection with pyrimethamine) are incorporated. Grey lines indicate regions used for genotyping recombined parasites and the numbers refer to integration (INT) and WT specific primer combinations. **B** Genotyping PCR of *ΔSLARP/P36p/P36* parasites. 5' and 3' integration and WT specific primer combinations (A) verified successful recombination events. Absence of WT signal for *SLARP* and *P36p/P36* loci from *ΔSLARP/P36p/P36* confirmed their isogenic purity. *ΔSLARP*, *ΔP36p/P36* and *P.b.* ANKA WT gDNA were used as a control.

3.1.2 Complete arrest but inferior protection in *ΔSLARP/P36p/P36*-immunized animals

To analyze the safety profile of *ΔSLARP/P36p/P36* in comparison to *ΔSLARP* and *ΔP36p/P36* sporozoites, the most susceptible mouse strain for *P. berghei*, C57BL/6 mice (Scheller *et al.*, 1994), was infected by i.v. injection of $1x10^4$ sporozoites (**Table 2**). Daily monitoring of blood infection revealed complete pre-erythrocytic life cycle arrests in mice infected with *ΔSLARP/P36p/P36* and *ΔSLARP* sporozoites. As described previously (van Dijk *et al.*, 2005), infections with *ΔP36p/P36* sporozoites resulted in occasional breakthrough infections, which develop into fulminant blood infections. Together, *ΔSLARP/P36p/P36* parasites arrest fully in the liver and are as safe as *ΔSLARP* sporozoites for GAP immunization.

.

Table 2 Safety of genetically attenuated *P. berghei* lines.

Parasite strain	Blood stage-positive mice[a]	Prepatent period[b]
ΔSLARP/P36p/P36	0/34 (0%)	-
ΔSLARP	0/34 (0%)	-
ΔP36p/P36	4/34 (12%)	(>6 days)
WT	10/10 (100%)	3 days

[a] Mice were inoculated by i.v. injection of $1x10^4$ sporozoites. Shown are numbers and respective percentage of infected to total animals.
[b] The prepatent period is defined as time to detection of first blood stage parasites.

Animals were immunized twice in a seven day interval with $1x10^4$ *ΔSLARP/P36p/P36, ΔSLARP*, *ΔP36p/P36,* and γ-WT sporozoites. Challenge of immunized mice and naïve control animals by intravenous injection of $1x10^4$ normal sporozoites was performed 37 days after the immunization. This prime/boost/challenge protocol typically leads to intermediate protection, permitting the identification of superior and inferior vaccine candidate effects (**Fig. 9**). Pre-patency analysis after challenge revealed that mice immunized with *ΔSLARP/P36p/P36* were least protected in comparison to mice immunized with the cognate single knockout sporozoites.

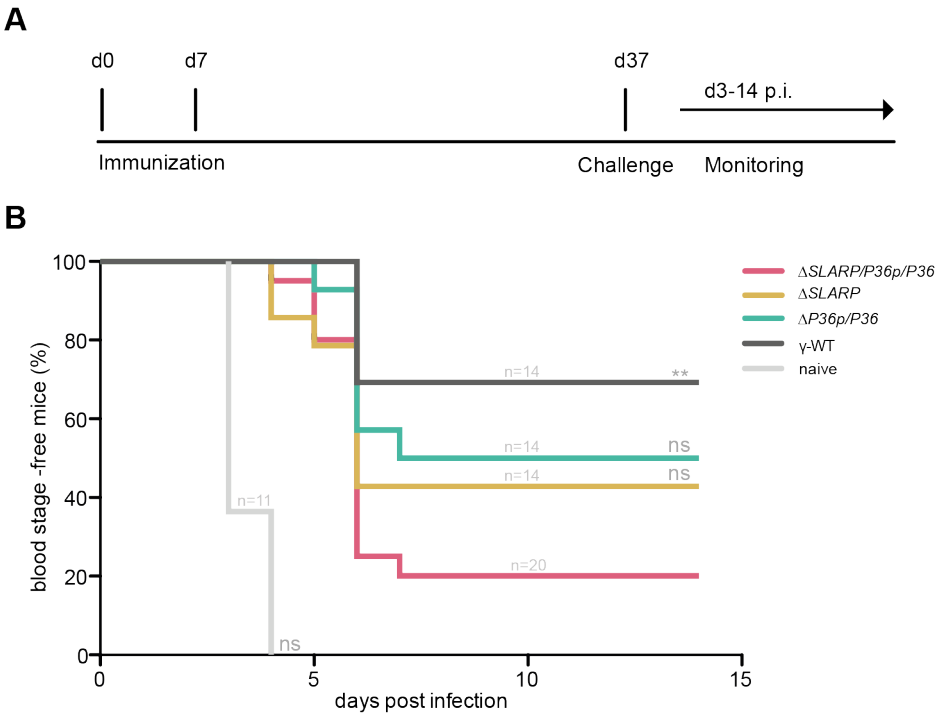

Figure 9 Inferior protection in *ΔSLARP/P36p/P36* sporozoite immunizations.

A Schematic representation of the immunization procedure. C57BL/6 mice were immunized and boosted at a 7-day interval with $1x10^4$ sporozoites i.v., challenged with $1x10^4$ WT sporozoites i.v. at 36 days post 1st immunization and blood infection was monitored by daily microscopic examination of Giemsa-stained blood films. **B** Kaplan-Meier analysis of time to pre-patency after sporozoite challenge reveals inferior protection in *ΔSLARP/P36p/P36*-immunized animals. Mice were immunized with *ΔSLARP/P36p/P36* (pink), *ΔSLARP* (yellow), *ΔP36p/P36* (turquoise), or γ-WT (dark grey) sporozoites. WT sporozoite challenge was performed 36 days post immunization and non-immunized control animals (naïve, light grey) confirmed sporozoite infectivity by patent blood stage infection 3 days post inoculation. Infected animals were treated orally with pyrimethamine in the drinking water to clear parasitemia. Statistical analysis: Log rank (Mantel-Cox) test n.s., non-significant; **, $p< 0.01$

In comparison, γ-WT sporozoites protected best against follow-up infection. As expected, WT challenge two months post prime/boost *ΔSLARP/P36p/P36* and γ-WT immunizations reduced protection against follow-up infections in all cohorts, eliminating all protective effects in *ΔSLARP/P36p/P36* immunized mice (Josephine Scholz, Master thesis 2015). In comparison, three immunizations elicited complete protection in all animals immunized with *ΔSLARP*, *ΔP36p/P36* or γ-WT sporozoites (Josephine Scholz, Master thesis 2015). Together, these challenge data suggest an antagonistic effect of the two gene knockouts in GAP-induced protection.

3.1.3 High liver parasite load in tKO immunized cohorts after WT challenge

To estimate whether parasite load in the liver after challenge in prime/boost immunized cohorts correlates with the protection profile, tKO, single KO and γ-WT-immunized animals (0/7) received a high dose of WT sporozoites five months post immunization, followed by liver excision after 42 hours and *Pb*18s mRNA levels assessment relative to the mouse GAPDH levels (**Fig. 10**). As expected, *ΔP36p/P36*-immunized animals had a ~100-fold reduction in parasite load compared to non-immunized animals (naïve). Challenged mice that were immunized with *ΔSLARP* parasites revealed slightly higher parasite loads than *ΔP36p/P36*-immunized animals indicating reduced protection. Both original KO immunized cohorts had lower parasite loads in the liver compared to tKO immunized animals which is in concordance with reduced protection against follow-up infections. However, tKO immunized and challenged animals still had a ~10-fold reduction in parasite load compared to non-immunized animals. Corroborating this notion, γ-WT-immunized animals had the lowest liver parasite burden correlating with good protection. Taken together, reduced liver load in tKO immunized animals was observed. However *ΔSLARP* and *ΔP36p/P36*-immunized cohorts revealed even higher reduction in parasite load confirming the results seen in the immunization profile.

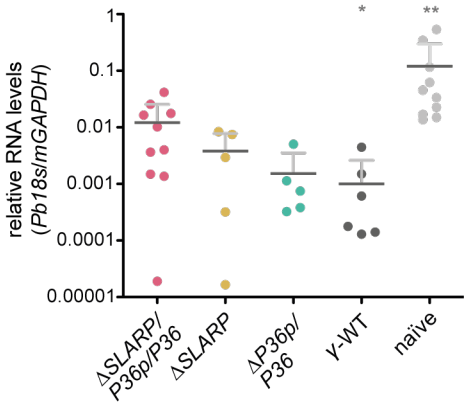

Figure 10 Elevated parasite load in livers of *ΔSLARP/P36p/P36*-immunized and challenged mice

Quantitative RT-PCR analysis of relative parasite rRNA levels in immunized and challenged cohorts. C57BL/6 mice were immunized twice in a 7-day interval with 1x10^4 ΔSLARP/P36p/P36 (pink), ΔSLARP (yellow), ΔP36p/P36 (turquoise), or γ-WT sporozoites (dark grey). 30 days later immunized animals and naïve control (light grey) were inoculated with 1x10^4 WT sporozoites. The livers were excised 42h post challenge, RNA was extracted and cDNA amplified. ΔΔCT *Pb*18s rRNA levels normalized to the murine

GAPDH mRNA levels are depicted showing relative parasite load in the liver of individual immunized and challenged animals (dots) of two independent experiments, as well as the general mean ±SD. Only significant differences are shown. **, p<0.01

3.1.4 Immunization with tKO induces high antibody titers

Antibodies against *Plasmodium* sporozoites hamper attachment to and invasion of hepatocytes. As a first measure of protection, antibodies bind to surface proteins of sporozoites, a mechanism exploited by subunit vaccine RTS,S (Stoute *et al.*, 1997). GAPs do not only induce production of antibodies against one target protein, but rather induce production of an array of antigens against all sporozoites surface proteins (Offeddu *et al.*, 2012). Measuring antibody titers of tKO, single KO and γ-WT-immunized animals determines antigen exposure and induction of antibody production by (t)KOs. Serum of prime/boost immunized animals one, two and five months post immunization were taken and measured in a dilution series staining air-dried sporozoites. High antibody titers were observed one month post infection for tKO and control groups (**Fig. 11A**). Antibody titers dropped after two-thirds two months post infection in all groups. However, overall antibody titers did not decline further after 5 months post infection in all groups (**Fig. 11B**). However, *ΔSLARP*-immunized animals had significant lower antibody titers compared to the other immunized cohorts one and two months post infection. Concluding, high antibody titers were observed in all of the immunized animals with a steady decrease after the first months post immunization, questioning overall contribution of antibodies to GAP-induced protection.

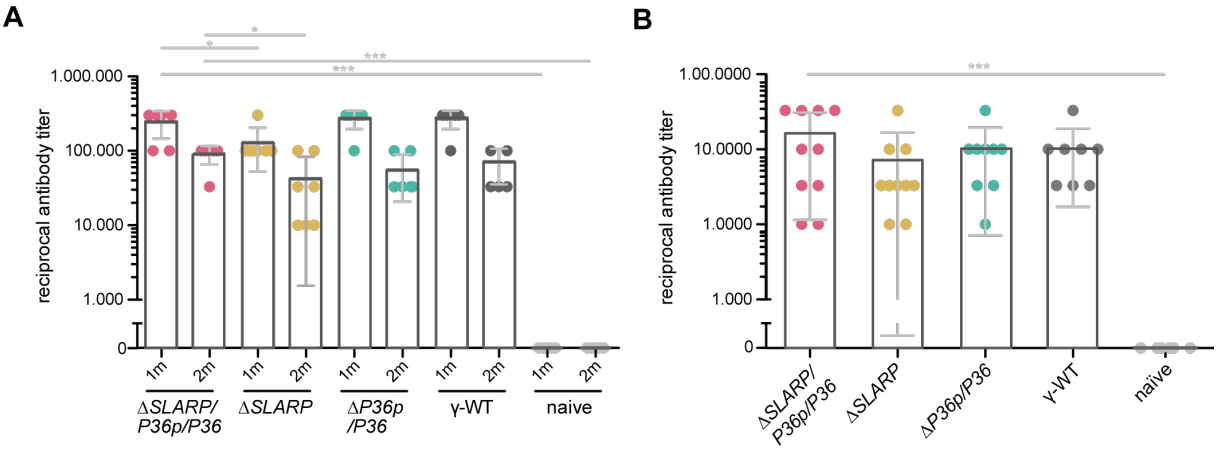

Figure 11 High antibody titers after *ΔSLARP/P36p/P36* immunization

Reciprocal antibody titers of *ΔSLARP/P36p/P36* (pink), *ΔSLARP* (yellow), *ΔP36p/P36* (turquoise), or γ-WT (dark grey) immunized animal cohorts. Serum was taken from C57BL/6 immunized/boosted animals at 30, 60 or 150 days post immunization. Air dried WT sporozoites were exposed to the serum in a dilution series of 1: 10,000, 1: 33,000, 1: 100,00, 1: 330,000 and visualized by α-mouse Alexa-fluor 488 secondary antibody. Titers were compared to stainings with serum of naïve mice (light grey). Each dot presents serum dilution of an individual mouse. Depicted are only significant statistical differences of cohorts compared to *ΔSLARP/P36p/P36*-immunized mice. *, $p<0.05$,***, $p<0.001$. **A** Reciprocal antibody titers of immunized animal cohorts one and two months post immunization. **B** Reciprocal antibody titers of immunized animal cohorts five months post immunization.

3.1.5 Exo-erythrocytic development is attenuated in tKO *in vitro*

Another factor contributing to GAP vaccine-induced immunity is thought to be the developmental status and persistence of arrested liver stages inducing protective $CD8^+$ T cells. Developmental arrest at late liver stages, as shown for parasites under drug cover, is believed to induce superior protective immunity (Borrmann & Matuschewski, 2011). Furthermore, parasites that arrest early, but persist longer in the liver, have shown to induce protective $CD8^+$ T cell production (Putrianti *et al.*, 2009). To determine whether reduced tKO GAP vaccine efficacy can be explained by limited or impaired parasite liver stage development, hepatoma cells were infected *in vitro* with tKO, single KO GAPs and WT parasites and growth and infectivity of these sporozoites were analyzed (**Fig. 12**). The approximate time point of tKO liver stage arrest was determined by comparing the size of tKO, single KO and WT parasites at 24, 48 and 72 hours post infection, as *P. berghei* liver stage development is completed after 72 hours (**Fig. 12A**). tKO size of ~8µm was similar to single GAPs at 24 hours p.i. whereas WT parasites were significantly larger in size (~32µm). Size difference at 48 hours post infection between GAPs and WT increased significantly by ~10-fold, due to WT parasite growth and GAPs developmental arrest.

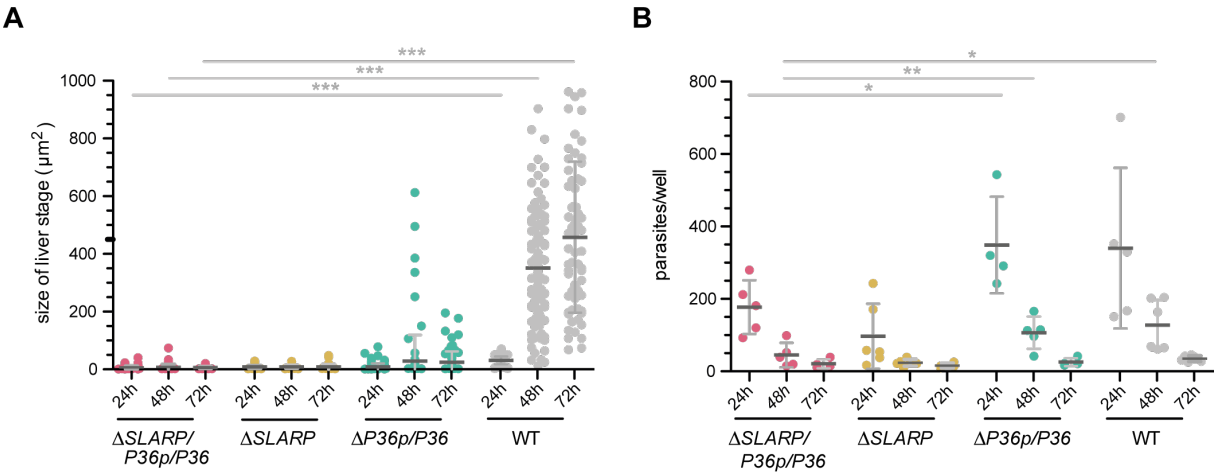

Figure 12 Reduced size and number of *ΔSLARP/P36p/P36* exo-erythrocitic stages *in vitro*

$3x10^4$ hepatoma (Huh7) cells were infected with $1x10^4$ *ΔSLARP/P36p/P36* (pink), *ΔSLARP* (yellow), *ΔP36p/P36* (turquoise), and WT (light grey) sporozoites per well in two independent experiments with three technical replicates each. **A** EEF sizes of *ΔSLARP/P36p/P36, ΔSLARP, ΔP36p/P36* or WT *P.b.* parasites. 20 parasites per technical replicate per time point were measured by immunofluorescence microscopy and analyzed with Fiji for determining the size (µm) of the parasite. Depicted are individual parasites per time point (dots) and the mean ±SD. Statistical analysis was performed on the means of the replicates: Mann-Whitney-U test, only significant differences to tKO parasites at each time point are shown. ***, $p<0.001$. **B** EEF numbers in *ΔSLARP/P36p/P36, ΔSLARP, ΔP36p/P36* or WT *P.b.* infected Huh7 cells measured by immunofluorescence microscopy. Numbers of EEF per well were counted in all replicates per time point. Depicted are the numbers of each replicate and the combined mean ±SD. Statistical analysis: Mann-Whitney-U-test. Only significant differences to tKO parasites at each time point are shown. *, $p<0.05$,**, $p<0.01$

Liver stage arrest around 12-18 hours post infection in KO GAPs has been reported previously and, as expected, tKO parasites arrest at a similar time point. The arrest in *ΔSLARP* is most likely due to the downregulation of PVM resident proteins, UIS and other important liver stage genes, whereas *ΔP36p/P36* parasites seem to lose their ability to build and maintain the PVM by absence of the 6-cysteine domain protein (van Dijk *et al.*, 2005, Aly *et al.*, 2008, Silvie *et al.*, 2008). Sporadic larger parasites in the *ΔP36p/P36* line indicate a potential reason for the occasional breakthrough infections observed in this GAP parasite line. Determining parasite infection rates *in vitro* can give insight into sporozoite infectivity and parasite persistence in the liver. To estimate whether reduced infectivity and persistence of tKO parasites could be an explanation for lower vaccine efficacy, 30,000 Huh7 cells were infected with $1x10^4$ tKO sporozoites and compared to original KOs and WT infections (**Fig. 12B**). Numbers of *ΔSLARP/P36p/P36* parasites were similar to *ΔSLARP* parasites revealing a significant 50% reduced infection rate compared to *ΔP36p/P36* and WT. Induction of long-lasting protective $CD8^+$ T cells is important for an effective vaccine candidate. Small-scale studies reported high induction of $CD8^+$ T cells by persistent liver stage parasites under drug cover (Scheller & Azad, 1995, Mueller *et al.*, 2007, Putrianti *et al.*, 2009). Rapidly decreasing parasite numbers between 24 and 48 hours post infection indicate lack of persistence and death of parasites. Persistence of parasites was similar in all transgenic parasites, however larger numbers of persisting parasites in *ΔP36p/P36* and WT are likely contributing to the superior protection in immunized animals.

Immunofluorescence images of tKO and original KOs display absence of UIS4, a PVM resident protein (**Fig. 13**). *ΔP36p/P36* parasites showed no sign of UIS4 expression, an indicator for (post)-transcriptional downregulation of gene expression, as shown for SLARP (Silvie *et al.*, 2008) or absence of a PVM. In contrast, WT parasites expressed UIS4 at 24h and 48h post infection as well as lower presence of UIS4 at 72h post infection (**Fig. 13C**). Since UIS4 is not an indicator for PVM presence, as it could be absent from an otherwise excitant PVM, staining for recruitment of host cell LC3, an autophagy marker, to the parasitophorous vacuole of early liver stage parasites was performed (Prado *et al.*, 2015, Thieleke-Matos *et al.*, 2016) (**Fig. 13A**). As expected, *ΔP36p/P36* parasites were not labeled with LC3, since LC3 recruitment requires an intact PVM, which is absent in *ΔP36p/P36* parasites (Labaied *et al.*, 2007, Wacker *et al.*, 2017). Similar results were observed for *ΔSLARP/P36p/P36* suggesting inability to establish a PVM. Surprisingly, LC3 recruitment was not present in *ΔSLARP* parasites, likely due to insufficient PVM remodeling after invasion, as an intact PVM is required for proper LC3 recruitment (Prado *et al.*, 2015). In contrast, WT parasites were labeled with LC3 at 24h post infection. To examine parasite development into mature liver stage schizonts, transgenic parasites were stained with the merozoite surface antigen MSP1 (**Fig. 13B**). As expected, all transgenic parasite lines were

lacking MSP1 staining as developmental arrest occurred before maturing into late liver stages. In contrast, WT parasites showed MSP1 presence in mature liver stages and schizonts (**Fig. 13C**).

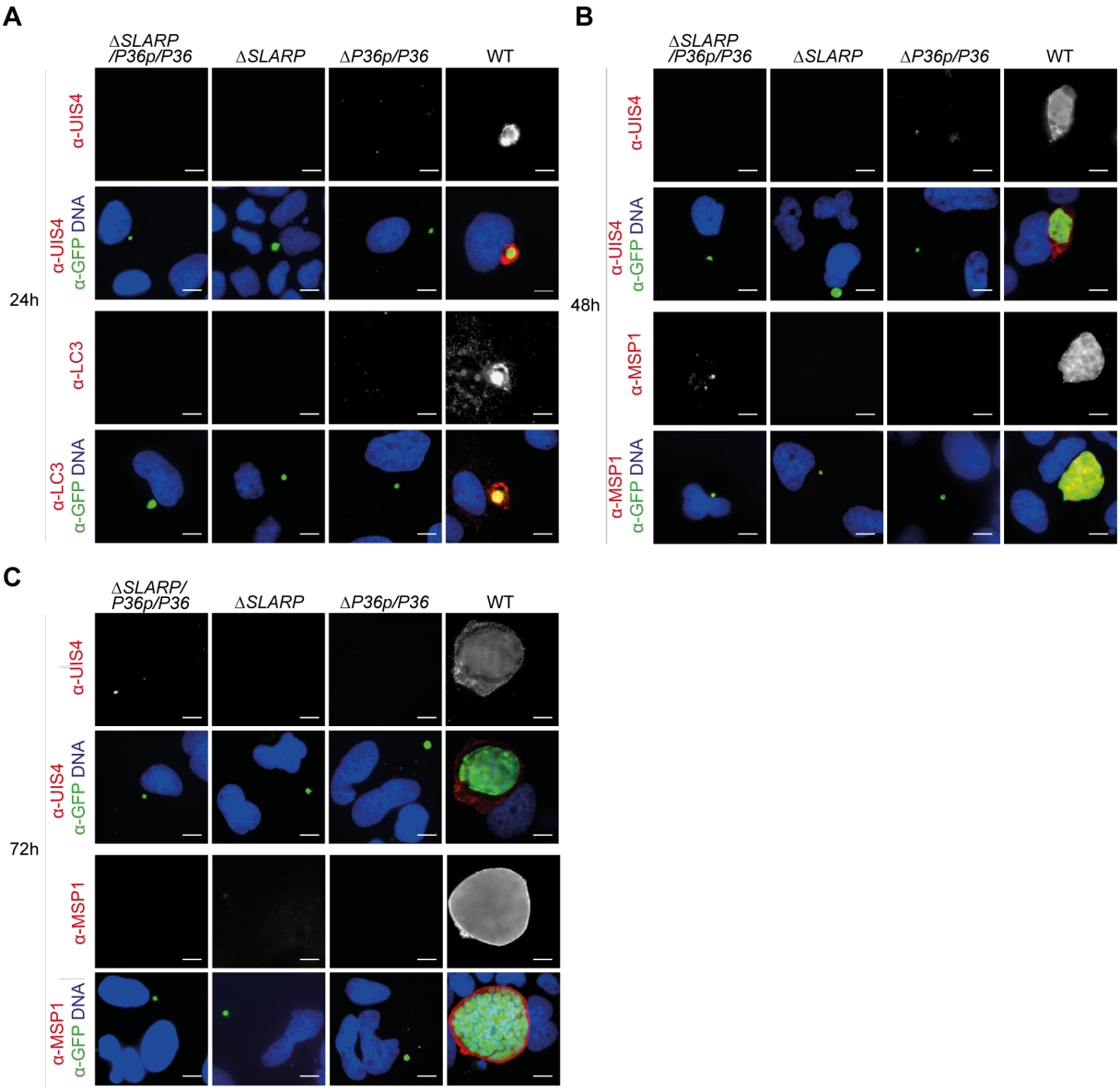

Figure 13 *ΔSLARP/P36p/P36* exo-erythrocytic stages do not harbor a parasitophorous vacuole

A Immunofluorescence microscopy analysis (IFA) of α-UIS4 (red) or α-LC3 (red) and α-GFP (green) *ΔSLARP/P36p/P36*, *ΔSLARP*, *ΔP36p/P36* and WT *P.b.* parasites at 24 hours post hepatoma cell (Huh7) infection shows absence of UIS4 in and recruitment of host LC3 to GAP parasites. Nuclear staining was performed with Hoechst 33342 (blue). Upper panel is showing α-UIS4 (red) or α-LC3 (red) staining only, lower panel is displaying the merged image. (Scale bar 10 µm) **B** Representative immunofluorescence images of α-UIS4 (red) or α-MSP1 (red) localization in *ΔSLARP/P36p/P36*, *ΔSLARP*, *ΔP36p/P36* and WT *P.b.* parasites in infected Huh7 cells at 48 hours p.i.. Upper panel is showing α-UIS4 (red) or α-MSP1 (red) staining only, lower panel is displaying the merged image with α-GFP (green) and nuclear staining with Hoechst 33342 (blue). (Scale bar 10 µm) **C** IFA of α-UIS4 (red) or α-MSP1 (red) and α-GFP (green) stained *ΔSLARP/P36p/P36*, *ΔSLARP*, *ΔP36p/P36* and WT *P.b.* parasites at 72 hours post Huh7 infection reveals absence of UIS4 and MSP1 in GAP parasites. Nuclear staining is displayed with Hoechst 33342 (blue). Upper panel is showing α-UIS4 (red) or α-MSP1 (red) staining only, lower panel is displaying the merged image. (Scale bar 10 µm)

In vitro studies indicated an early arrest of tKO parasites, absence or insufficient remodeling of a PVM, decreased hepatocyte infection rate and reduced persistence of arrested parasites in the liver, a prerequisite for sufficient $CD8^+$ T cell priming, providing an explanation for lower protection in tKO immunized animals.

3.1.6 $CD8^+$ T cells in tKO animals decline after two months post infection

$CD8^+$ T cells have been shown to play a major role in protection against malaria infections. As seen for immunizations with parasites under drug cover, eliciting high $CD8^+$ T cell titers contributes to a significant increase in protection (Borrmann & Matuschewski, 2011). In contrast, immunization with heat killed sporozoites, which fail to attach, transmigrate and invade hepatocytes, establish only low $CD8^+$ T cell titers along with protection of these whole parasite vaccines (Hafalla *et al.*, 2006). To investigate whether $CD8^+$ T cells are induced by tKO, single KO and γ-WT-immunized animals and if this in turn can explain the difference in protection, amounts of IFN-γ producing effector memory $CD8^+$ T cell titers were determined in the spleen and liver of prime/boost immunized animals one month post WT challenge (**Fig. 14**). Animals were immunized with tKO, single/double KO or γ-WT (d0/7) and challenged one, two or five months post immunization. Spleens and livers of challenged animals were excised one month post challenge (one and two months challenges) or 42h post challenge (five months challenge). Animals that developed a blood stage infection were cured with pyrimethamine in the drinking water for two weeks. Spleens and livers of immunized animals were processed and restimulated with brefeldin A and sporozoite specific $CD8^+$ T cell peptide epitopes $TRAP_{130\text{-}138}$ and $S20_{318\text{-}326}$, and $OVA_{257\text{-}264}$ as a negative control not recognized in H2-K^b restricted C57BL/6 mice. Furthermore, control naïve animals were included that have not been in contact with any parasites. Restimulated spleen and liver cells were stained with α-CD3 and α-CD8 antibodies to determine $CD3^+CD8^+$ positive lymphocytes and α-CD11a antibody for activated T cells as well as intracellular α-IFN-γ and α-TNF-α antibodies for detection of parasite specific cytokine production of activated $CD8^+$ T cells and measured with FACS (**Fig. 14A**).

Despite decreased EEF numbers for tKO and *ΔSLARP*, immunized and challenge animals displayed similar robust numbers (~0.2%) of IFN-γ producing $CD8^+$ T cells amongst all GAP and control groups for lymphocytes stimulated with TRAP after one month post challenge (**Fig. 14B+C**). Cells from naïve animals as well as cells stimulated with the control peptide OVA showed no induction of IFN-γ producing $CD8^+$ T cells. Surprisingly, $CD8^+$ T cell numbers dropped significantly to 0.08% two months post immunization in *ΔSLARP/P36p/P36*-vaccinated animals, whereas in single/double KO and γ-WT vaccinated mice $CD8^+$ T cell numbers were similar to or even higher than one month post infection.

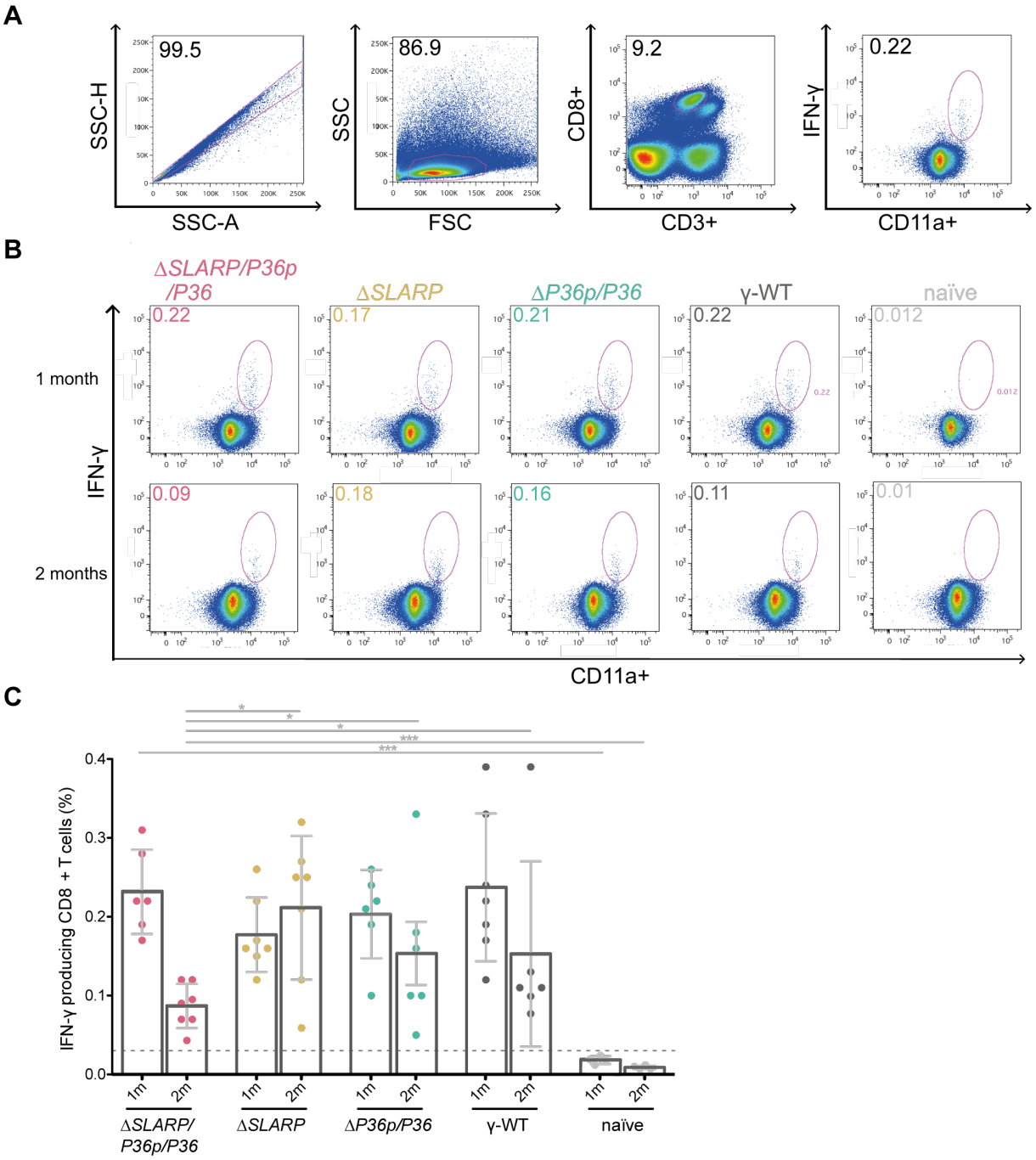

Figure 14 Reduced longevity of CD8⁺ T cells in *ΔSLARP/P36p/P36*-immunized mice

Analysis of CD8⁺ T cells elicited in immunized cohorts. C57BL/6 mice were immunized in a prime/boost regimen (7 days apart), challenged one or two months post immunization and treated with pyrimethamine water before excision of spleen one month post challenge. Splenic cells were restimulated with CD8⁺ TRAP peptide epitopes and stained with fluorescently labeled antibodies for analysis with MACSQuant. **A** Depicted is the gating strategy used for FACS analysis one and two months p.i.. Doublets were excluded, before gating for lymphocytes. CD8⁺/CD3⁺ positive cells were analyzed for activation with CD11a⁺ for IFN-γ secretion. **B** Examples of mean IFN-γ secretion by CD8⁺ T cells in immunized cohorts one and two months post immunization compared to naïve controls. **C** Percentage of IFN-γ secreting CD8⁺ T cell in immunized cohorts. Depicted are IFN-γ producing CD8⁺ T cells of individual mice (dots), as well as the mean of each group ± SD. Only significant statistical differences of each group compared to *ΔSLARP/P36p/P36* immunized mice are shown. *, $p<0.05$,***, $p<0.001$. The baseline represents mean naive +2xSD.

As expected, numbers of IFN-γ secreting $CD8^+$ T cell decreased further in all cohorts five months post immunization with *ΔSLARP/P36p/P36* still harboring the lowest numbers of IFN-γ producing $CD8^+$ T cells (**Fig. S1A**). Similar trends could be seen for spleens stimulated with S20 (**Fig. S1B**) and TNF-α producing $CD8^+$ T cells stimulated with TRAP (**Fig. S2A**) and S20 (**Fig. S2B**). Splenic cells restimulated with OVA did not show elevated $CD8^+$ T cell presence (**Fig. S1EC** and **Fig. S2C**).

3.2 Inducing PTEX-dependent export in liver stages for an improved malaria vaccine candidate

Host cell remodeling is critical for successful *Plasmodium* replication inside erythrocytes and achieved by targeted export of parasite-encoded proteins into the host cell cytoplasm. In contrast, during liver infection, the malarial parasite appears to avoid protein export, perhaps to limit exposure of parasite antigens by infected liver cells via MHCI. Matz *et al.* have previously shown that the ATPase of the protein translocon of exported proteins (PTEX), termed HSP101, is not expressed during early to mid liver infection (Matz *et al.*, 2015). Thus, hypothesizing that this protein might be a limiting factor explaining the absence of liver stage PTEX-dependent export.

To clarify PTEX component expression during the *Plasmodium* life cycle and in particular in liver stages, relative mRNA levels (to *PbHSP70*) of all PTEX components were determined in mixed blood stages, oocysts, sporozoites and liver stages (at 24, 48 and 72 hours post infection). Expectedly, core components (*PTEX150, EXP2* and *HSP101*) were highly expressed in mixed blood stages as well as the auxiliary component PTEX88. Surprisingly, expression of the potential cargo unfolding helper protein TRX2 was low in blood stages. Similarly, expression of all components was decreased in sporozoites indicating that PTEX is dispensable for the motile transmission stage. Interestingly, mid liver stages revealed expression of all core components with very low expression for *HSP101*. In contrast to previous findings from Matz *et al.*, *HSP101* mRNA levels decreased up to 48 hours post infection before meeting EXP2 like levels at 7 hours post infection (**Fig. 15**).

Thus, *HSP101* mRNA is highly expressed in all life cycle stages except for liver stages, demonstrating that HSP101 might be the limiting factor for successful early liver stage export. I therefore asked the questions 1) whether HSP101 can be overexpressed in liver stages, 2) how transgenic HSP101 expression influences the parasite's life cycle, 3) if HSP101 is the limiting factor for liver stage export and 4) whether PTEX reconstitution in early liver stages leads to increased protection in immunized cohorts.

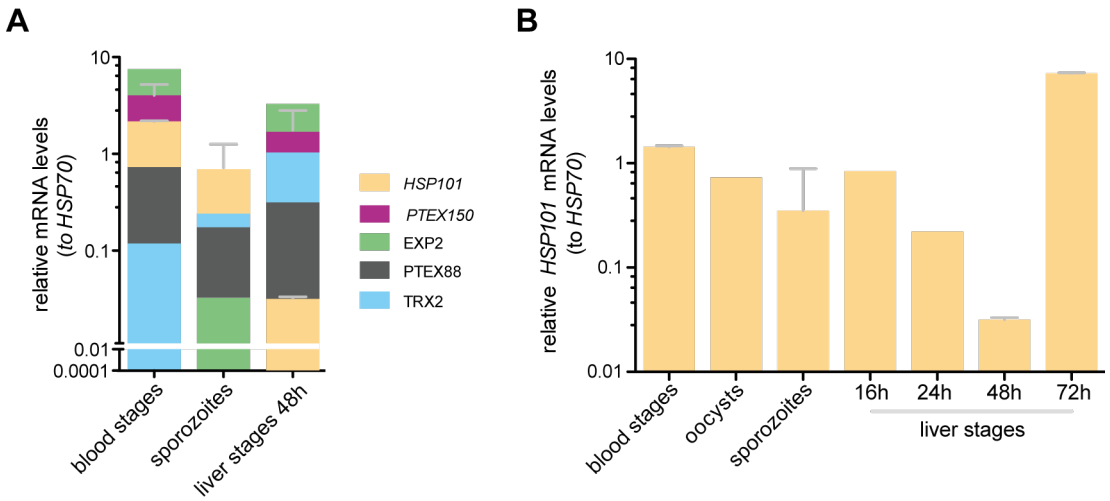

Figure 15 Relative mRNA levels of PTEX components during *P. berghei* life cycle

Quantitative RT-PCR analysis of parasite gene expression in infected Huh7 cells. **A** ΔΔCT mRNA levels of *HSP101*, *EXP2*, *PTEX150*, *PTEX88* and *TRX2* in blood stages, sporozoites and 48h p.i. in liver stages normalized to *PbHSP70*. Data is displayed as mean of two to five independent experiments with three replicates each for *HSP101* and *PTEX150* and as mean of three technical replicates of one independent experiment for *EXP2*, *TRX2* and *PTEX150* ±SD. **B** ΔΔCT mRNA levels of *HSP101* normalized to *PbHSP70* in blood stages (BS), oocysts (O), sporozoites (S) and 16h, 24h, 48h and 72h p.i. in liver stages (LS). Data is displayed as mean of two to four independent experiments with three replicates each for BS, S, LS 48h and 72h p.i. and mean of three technical replicates of one independent experiments for O, LS 16h and 24h p.i. ±SD.

3.2.1 Normal life cycle development of parasites with constitutively weak to moderate HSP101 overexpression

3.2.1.1 Generation of HSP101 overexpression parasites

To characterize induced PEXEL-dependent protein export in early *P. berghei* liver stages, transgenic parasite lines overexpressing HSP101 were generated. This strategy would allow PTEX reconstitution, since other major PTEX components (PTEX150, EXP2, TRX2 and PTEX88) are expressed during liver development. Reconstitution of the PTEX export machinery can facilitate protein export in early liver stages, thus may promote presentation to and recognition of parasites by the host immune system.

First, transgenic parasites were generated using two different overexpression strategies: 1) by endogenous promoter swap, 2) by insertion of a *HSP101* copy under the control of a constitutively active promoter into the silent 6 locus. Plasmids for *P. berghei* transfection were assembled using the pBART-SIl6 vector (Kooij *et al.*, 2012) harboring drug selectable hDHFR-yFcu cassette for positive/negative clone selection, a GFP under the control of the *PbHSP70* promoter for facilitating parasite life cycle analysis or for acquiring isogenic lines by FACS cloning. In addition, a mCherry/triple c-Myc (3xMyc) tag sequence for protein tagging, 3'*Pb*PPPK-DHPS as 3' UTR as well as two sequences for stable integration into the silent 6 locus. For the *HSP101* extra copy overexpression plasmid pHSP101+ or pHSP101+Myc, *HSP101* ORF

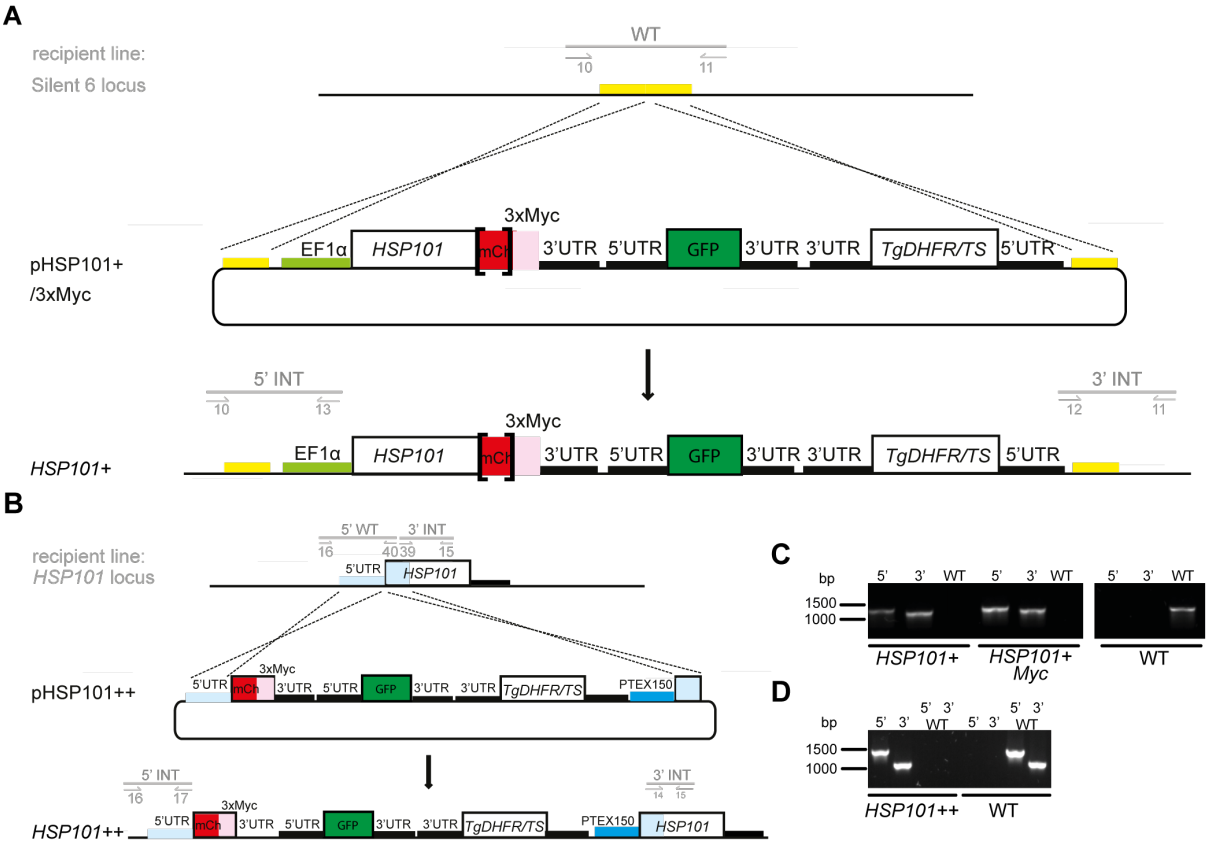

Figure 16 Stable integration of pHSP101+/Myc and pHSP101++

A Schematic representation of integration of linearized pHSP101+/Myc into the silent locus on chromosome 6 of *P.b.* ANKA parasites. The pHSP101+/Myc illustrates the plasmids used to generate *HSP101+/HSP101*+Myc parasites. Two sequences (yellow) homologous to the silent 6 locus were used for recombination. By double homologous recombination, an additional copy of *HSP101* under the control of *EF1α* promoter (light green), a *GFP* reporter sequence (green, for parasite life cycle analysis) and TgDHFR/Ts resistant cassette (for positive selection with pyrimethamine) were incorporated. Shown is the double homologous crossover of plasmid and silent 6 locus and the final recombined silent 6 locus in *HSP101+/HSP101+Myc* parasites. Grey lines indicate regions used for genotyping recombinant parasites and the numbers refer to integration and WT specific primer combinations. **B** Schematic representation of integration of linearized pHSP101++ into the *HSP101* locus on chromosome 9 of *P.b.* ANKA parasites. The pHSP101++ illustrates the plasmid used to generate *HSP101++* parasites. Two sequences of *HSP101* 5' UTR and N-terminal ORF (light blue) homologous to the sequence in the *HSP101* locus allow double homologous recombination, thereby inserting a new promoter PTEX150 (blue) for *HSP101* expression, a GFP reporter sequence (green, for parasite life cycle analysis) and TgDHFR/Ts resistance cassette (for positive selection with pyrimethamine) and an mCherry/3xMyc sequence, which is not expressed due to a missing start codon. Depicted is the double homologues crossover of plasmid and *HSP101* locus leading to the final recombined *HSP101* locus in *HSP101++* parasites. Grey lines indicate regions used for genotyping recombined parasites and the numbers refer to integration (INT) and WT specific primer combinations. **C+D** Genotyping PCR of *HSP101+* and *HSP101++* parasites. 5' and 3' integration and WT specific primer combinations (A+B) verified successful recombination events. Absence of WT signal from *HSP101+*/Myc and *HSP101++* confirmed their isogenic purity. *P.b.* ANKA WT gDNA was used as a control.

(*Pb*ANKA_0931200) was inserted into the *Xba*I-*Age*I restriction site in frame with the mCherry/3xMyc tag. Upstream of HSP101 a constitutively low expressing promoter *EF1α* (*Pb*ANKA_113330) was inserted into the *Bss*HII-*Xba*I restriction site (**Fig. S3A**). mCherry was excised in pHSP101+Myc plasmids and replaced by a small sequence (TGGTGGTTCTGGTG-

GCC) linking *HSP101* ORF and 3xMyc (**Fig. S3B**). pHSP101++ endogenous promoter swap plasmids were kindly provided by Joachim Matz (**Fig. S3C**). In brief, 5' UTR of *HSP101* was inserted into the *Nae*I-*Age*I restriction site in the pBART vector (Kooij *et al.*, 2012). Additionally, N-terminal *HSP101* ORF was integrated under the control of PTEX150 promoter. 5'UTR and N-terminal *HSP101* served as homologous recombination sites.

In order to generate stable transgenic parasite lines, *P.b.* ANKA parasites were transfected with *Apa*LI linearized plasmids creating free homologous ends using Amaxa electroporation enabling double homologous recombination (**Fig. 16**). For *HSP101+/Myc,* pHSP101+ or pHSP101+Myc linearized plasmids integrated in the silent locus in chromosome 6 and positive recombination events were selected with pyrimethamine in the mice drinking water followed by FACS cloning of GFP-positive iRBCs to generate isogenic transgenic parasite lines (**Fig. 16A**). For *HSP101++* transgenic parasites, pHSP101++ integrated between the endogenous *HSP101* 5'UTR and ORF inducing a new constitutively active promoter for *HSP101* expression (**Fig. 16B**). Similarly, *HSP101++* positive clones were selected by pyrimethamine and a stable isogenic line was established by FACS cloning. To verify successful integration, transgenic parasites were genotyped using oligonucleotides specific for 5' and 3' integration as well as for the WT locus (s. ch. 2.1.9.2). As expected, pHSP101+ or pHSP101+Myc as well as pHSP101++ integrated at the desired sites as shown by 5' and 3' integration specific amplification and isogenic lines could be confirmed by absence of WT specific amplifications (**Fig. 16C+D**).

Taken together, stable isogenic HSP101 overexpressing *P.b.* ANKA parasite lines were generated, showing that constitutive low overexpression of HSP101 does not interfere with parasite blood stage development. These parasite lines enable further characterization of the life cycle progression with constant HSP101 overexpression and eventually liver stage export analysis.

3.2.1.2 Normal life cycle progression of *HSP101+* and *HSP101++* parasites

To examine the phenotype of *HSP101+/Myc* and *HSP101++,* parasite development was analyzed throughout the parasite life cycle. Phenotypic analysis can provide answers to whether low to moderate overexpression of HSP101 leads to developmental delay and/or arrest. Normal life cycle progression of *HSP101+* and *HSP101++* line is key to successful liver stage export evaluation.

Successful generation of stable isogenic lines confirmed that low to moderate overexpression of HSP101 does not interfere with blood stage development. To demonstrate that HSP101 is expressed in blood stages, a blood stage immunofluorescence assay was performed with *HSP101+/Myc* parasites. Weak expression of HSP101, depicted in red for mCherry tag, was observed in *HSP101+* blood stages (**Fig. 17B**). Notably, in gametocytes HSP101-mCherry

localized to the PVM, where PTEX complex assembles. Similarly, normal blood stage development was observed for *HSP101+Myc* parasites (**Fig. S4B**).

To further investigate transgenic parasite development during sexual reproduction in the mosquito vector, female *Anopheles stephensi* mosquitoes were allowed to feed on mice infected with *HSP101+* or *HSP101++* parasites. Successful development in the mosquito was determined at day 10 for oocyst, day 14 for midgut sporozoites and day 17 for salivary gland sporozoite formation and results were compared to *P. berghei* WT parasites (*P. bergreen*) (Matz *et al.*, 2013), also expressing GFP under the control of *HSP70* promoter to account for any potential developmental delays due to GFP expression. Similar to WT, *HSP101+* showed oocysts development on the outside of mosquito midguts and WT-like numbers of midgut sporozoites on day 14 post infection (**Fig. 17A**). Midgut infectivity and numbers of salivary gland sporozoite in *HSP101+* and *HSP101++* revealed no differences to WT (**Table S2**). HSP101 was moderately expressed in *HSP101+* oocysts and sporozoites (**Fig. 17A**).

Thus, development of transgenic parasite lines *HSP101+/Myc* and *HSP101++* in the mosquito vector showed no significant difference to WT parasite and can be further analyzed for exo-erythrocytic growth and liver stage export.

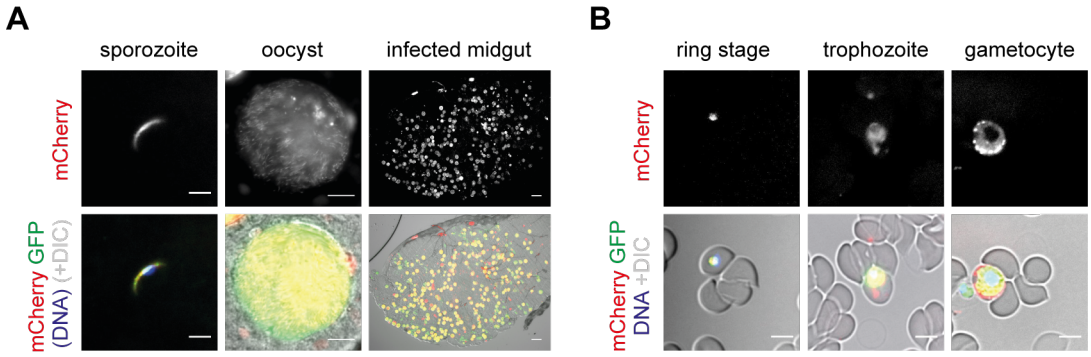

Figure 17 Normal *HSP101+* oocyst and sporozoite development

A+B Live imaging of sporozoites (nuclear staining with Hoechst 33342 1:5,000 and motility inhibition with 1:50 Phalloidin, scale bar: 5 µm), oocyst at day 14 post mosquito infection harboring midgut sporozoites (scale bar: 10 µm) and infected mosquito midguts at day 10 p.i. harboring *Plasmodium* oocysts (scale bar: 100 µm). Expression of HSP101-mCh is displayed in red and transgenic parasite marker GFP staining the parasite's cytoplasm in green. B Live imaging of asexual blood stages throughout the replication cycle: ring stages, trophozoites and gametocytes. Cells were stained with Hoechst 33342 1:5,000 for nuclear staining. Expression of HSP101-mCh is displayed in red was observed in the PVM. Transgenic parasite marker GFP staining the parasite's cytoplasm is shown in green. Scale bar: 5 µm.

Parasite liver stage development is key to establish a symptomatic blood stage infection. Upon a bite of an infected mosquito, sporozoites travel to the liver where they grow from one sporozoite into thousands of liver-merozoites, which subsequently infect red blood cells (RBC). To examine whether *HSP101+* and *HSP101++* parasites are able to complete exo-erythrocytic development and establish a patent blood stage infection, cohorts of C57BL/6 mice were intravenously infected

with a high dose of *HSP101*+ and *HSP101*++ sporozoites and monitored for blood stage pre-patency, parasite growth and experimental cerebral malaria (ECM) development (**Fig. 18**).

To evaluate whether parasites are able to undergo normal liver stage development and initiation of blood stage infection, parasite blood stage development was monitored with the help of Giemsa-stained thin blood smears starting 3 days post infection. Intra-hepatic development in C57BL/6 mice takes up to 50-60 hours post infection enabling asexual blood stage parasite detection 3 days post infection (Khan & Vanderberg, 1991). Interestingly, a one day delay in pre-patency was observed in mice infected with *HSP101*+ parasites as compared to WT, which developed a patent blood stage infection 3 days post infection (**Fig. 18A**). Similar results were observed for *HSP101+Myc* sporozoite i.v. injection whereas bites of 15 infected mosquitoes reversed the delays seen in pre-patency (**Fig. S4A**). Furthermore, these findings were confirmed by quantifying relative parasite RNA levels in mice livers 48 hours post infection. To determine parasite load in the liver of infected animals, livers were excised, parasite and host RNA extracted and a qRT-PCR conducted on RNA derived cDNA measuring ΔΔCT levels of parasite *Pb*18s to mouse GAPDH. As expected, no significant difference was observed in *HSP101*+ parasite burden in the liver compared to parasite burden in WT infected mice (**Fig. 18G**). Notably, *HSP101*+ RNA levels showed a trend of increased parasite load in the liver. In *in vivo* infection a proportion of exo-erythrocytic stages has fully matured at 44 hours post infection and starts to rupture to release merosomes to induce blood stage infections (Khan & Vanderberg, 1991). Since a delay in pre-patency was observed for *HSP101*+ parasites, the majority of parasites might still be present in the infected liver. Similar to *HSP101*+, pre-patency was determined for mice infected with *HSP101*++ parasites. Pre-patency analysis showed no significant difference to WT parasites, but a trend towards 0.5 days delay in blood stage development was observed (**Fig. 18B**). Thus, the results clearly demonstrate that transgenic parasites complete liver stage development but are found to have a delay in pre-patency by 0.5-1 day.

Based on observing a patent blood stage infection in *HSP101*+ and *HSP101*++ infected mice, it was investigated how and if HSP101 overexpression influences parasite growth and whether it determines disease outcome. To answer the first question, blood stage parasitemia of *HSP101*+ and *HSP101*++ infected mice was measured from day 3 to 7 using Giemsa-stained thin blood smears of individual mice. Parasite growth of *HSP101*+ was similar to WT except the one-day delay in patency (**Fig. 18C**). Similarly, there was no significant difference detected in *HSP101*++ parasite growth compared to WT (**Fig. 18D**).

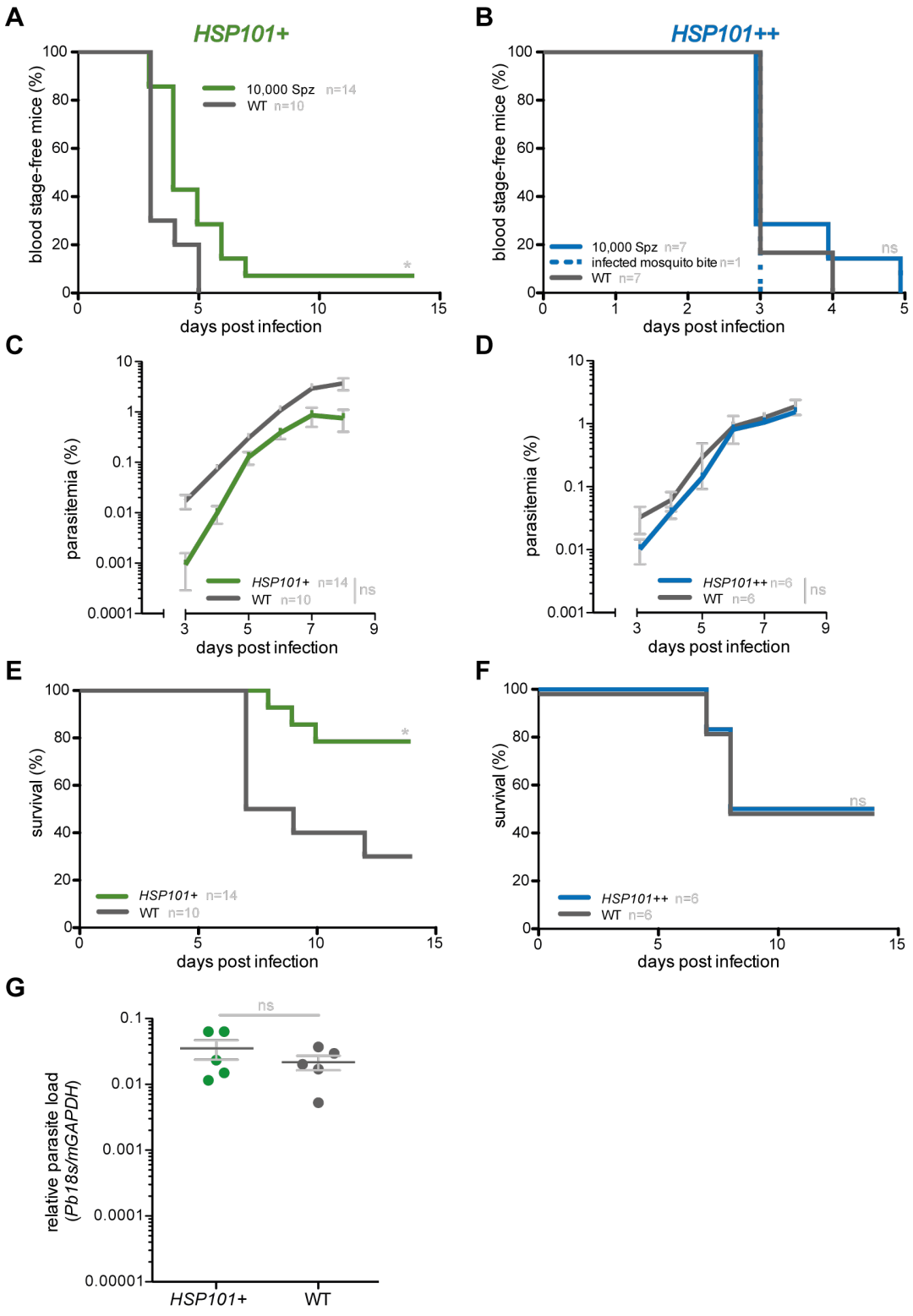

Figure 18 *HSP101*+ and *HSP101*++ liver stage development is slightly affected while remaining normal blood stage maturation

A+B Kaplan-Meier curve of blood infection over time after sporozoite infection. C57BL/6 mice were infected with 1x10^4 *HSP101*+ (green), *HSP101*++ (blue) or WT (dark grey) sporozoites or by bites of 15 *HSP101*++ infected mosquitoes and blood infection was monitored by daily microscopic examination of Giemsa-stained blood smears of three (for *HSP101*+) and two (for *HSP101*++) independent biological experiments. Statistical analysis: Log rank (Mantel-Cox) test, n.s., non-significant; *, p<0.05. **C+D** Blood stage growth (parasitemia %) 3-8 days post sporozoite infection is unaffected in comparison to WT infections. Giemsa-stained thin blood smears from pre-patency analysis were additionally used for

quantifying parasitemia of three (for *HSP101*+) and two (for *HSP101*++) independent biological experiments. Shown is the mean of all experiments ±SD. Statistical analysis: growth slope difference n.s., non-significant. **E+F** Kaplan-Meier curve depicts survival of mice over time after sporozoite infection. Experimental cerebral malaria (ECM) in *HSP101*+ (green), *HSP101*++ (blue) and WT (dark grey) infected C57BL/6 mice was monitored 6-12 days post sporozoite infection of three (for *HSP101*+) and two (for *HSP101*++) independent biological experiments. Statistical analysis: Log rank (Mantel-Cox) test n.s., non-significant; *, $p<0.05$. **G** Relative parasite rRNA levels 48 hours post sporozoite infection are unaffected in *HSP101*+ infected mice. C57BL/6 mice were infected with $1x10^4$ *HSP101*+ (green) or WT (dark grey) sporozoites. The livers were excised 48h post challenge, RNA extracted and cDNA amplified. Quantitative real-time PCR on *Pb*18s rRNA against the murine GAPDH mRNA is depicted showing relative parasite load in the liver of individual infected animals (dots), as well as the general mean ±SD. Only significant differences are shown. Statistical analysis: Mann-Whitney-U-test n.s., non-significant;

In order to analyze pathology of blood stage infections, mice were monitored for ECM development within 6-8 days post sporozoite inoculation. ECM is a severe form of malaria, where parasites are able to cross the blood-brain barrier. C57BL/6 mice frequently develop ECM under laboratory conditions and it is used as a marker for disease progression and severity. Interestingly, *HSP101*+ and *HSP101*++ mice developed ECM despite the 0.5-1 day delay in pre-patency. However, only 20% of animals developed ECM if infected with *HSP101*+ compared to 70% of WT infected mice (**Fig. 18E**). In contrast, only 50% of *HSP101*++ infected animals developed ECM (**Fig. 18F**), however this was consistent with ECM development in WT infected mice in this experiment.

Taken together, the results show that pre-patency is minimally affected in *HSP101*+ and *HSP101*++ infected mice, but does not interfere with subsequent parasite growth. However, delay in pre-patency in *HSP101*+ infected mice heavily influences disease outcome as compared to WT and *HSP101*++ infections. These results demonstrate that neither pre-patency nor parasite growth but disease progression is severely affected by low to moderate overexpression of *HSP101*.

3.2.1.3 HSP101 overexpression does not interfere with exo-erythrocytic development of *HSP101*+ and *HSP101*++ parasites *in vitro*

Having found the before mentioned 0.5-1 day delay in pre-patency, reasoned in depth studies of *HSP101*+ and *HSP101*++ liver development, asking whether HSP101 is expressed in *HSP101*+ and *HSP101*++ liver stages, how it influences sporozoite infectivity and exo-erythrocytic development and if other liver stage signature proteins are affected by HSP101 overexpression.

In order to answer these questions, hepatoma cells were infected *in vitro* with a constant number of infective transgenic and WT control sporozoites and EEF growth and HSP101 expression were monitored and sizes as well as numbers of infected cells were quantified. Figure 20 presents transgenic parasite growth *in vitro*. In *HSP101*+, parasites overexpression of HSP101 and localization to the PV could be detected at 24, 48 and 72 hours post infection by staining the red mCherry tag as well as the HSP70 as parasite cytoplasm marker and Hoechst for nuclear staining

(**Fig. 20A**). To verify PVM presence and maintenance, *HSP101*+ parasites were stained with antibodies against the PVM resident protein UIS4 (red). USI4 staining was detected in the PV and TVN at 24, 48 and 72 hours post infection. For *HSP101*++ parasite growth was monitored with the help of antibody staining against HSP70 (green) or GFP (green) and UIS4 (red) or LC3 (red), an early host cell autophagy marker labeling the PVM from the host cell side, to indicate parasite growth and PVM presence and maintenance, respectively. *HSP101*++ EEF growth rates were similar to WT and UIS4 expression was detected in the PV and TVN at 24, 48 and 72h post infection (**Fig. 20B**). Similarly, LC3 was observed at 16 hours post infection (**Fig. 20C**). In contrast to *HSP101*+, HSP101 expression in *HSP101*++ could not be verified with immunofluorescence assay (IFA), as a tag to visualize HSP101 was not included in these transgenic parasites. Therefore, liver stage mRNA levels of *HSP101* at 16, 24, 48 and 72 hours post infection were quantified to estimate protein overexpression (**Fig. 19**). As expected, *HSP101* mRNA levels were markedly elevated at 24 and 48 hours in *HSP101*++ compared to weak expression in WT (**Fig. 19**). Thus, it was shown for both *HSP101*+ and *HSP101*++ that HSP101 could be overexpressed in low levels without interfering with the parasite's liver development or expression of PVM proteins indicating full maintenance of PVM throughout the liver stage.

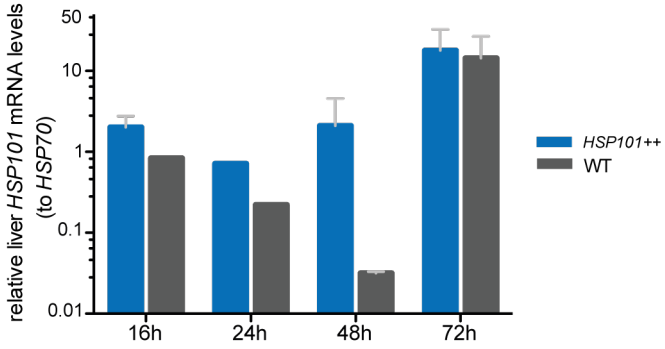

Figure 19 Elevated liver stage *HSP101* mRNA levels in *HSP101*++ parasites

Relative liver stage *HSP101* mRNA levels in *HSP101*++ parasites. Total RNA was extracted from *HSP101*++ or *WT P.b.* infected Huh7 cells at 16, 24, 48 and 72 hours p.i., followed by a qRT-PCR on RNA derived cDNA. ΔΔCT of *HSP101* mRNA levels were normalized to *HSP70* mRNA levels. Depicted is the mean of two (one for 24 hours) independent experiments ±SD.

Taken together, *HSP101*+ and *HSP101*++ parasites revealed WT-like infection, development and persistence of parasites in infected cells with consistent HSP101 and signature PVM protein expression, demonstrating that HSP101 overexpression is possible without interfering with parasite infectivity and growth.

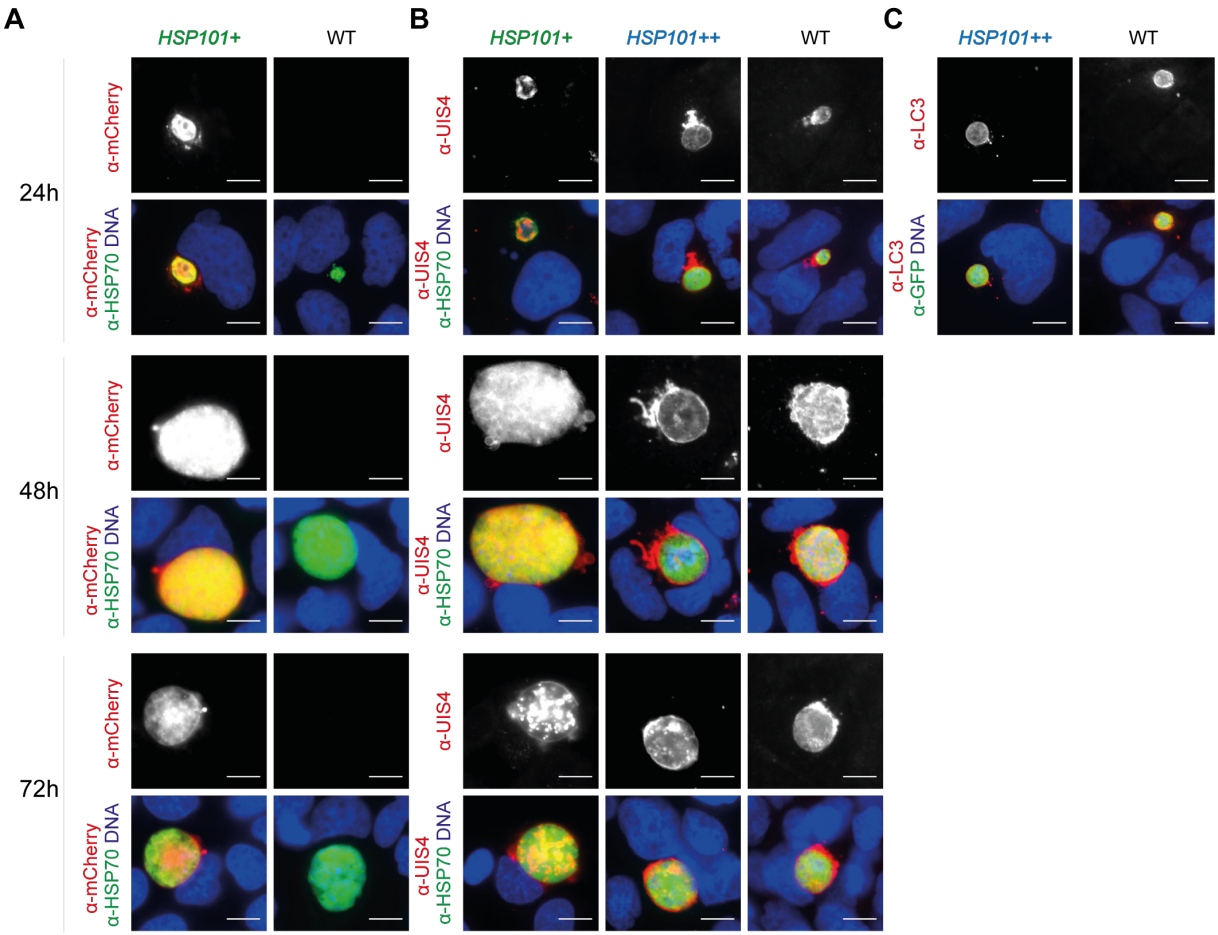

Figure 20 *HSP101* is overexpressed in exo-erythrocytic stages of *HSP101*+ and *HSP101*++ and localizes to the parasite's PV

A Immunofluorescence microscopy analysis (IFA) of α-mCherry (HSP101, red) and α-HSP70 (green) stained *HSP101*+ and WT *P.b.* parasites at 24, 48 and 72 hours post hepatoma cell (Huh7) infection shows localization of HSP101 to the parasite's PV. Nuclear staining was performed with Hoechst 33342 (blue). Upper panel is showing mCherry (HSP101) staining only and lower panel is displaying the merged image. (Scale bar 10 µm) **B** Localization of UIS4 by IFA in *HSP101*+, *HSP101*++ and WT *P.b.* parasite infected Huh7 cells at 24, 48 and 72 hours p.i.. Upper panel is showing α-UIS4 (red) staining only, lower panel is depicting the merged image with α-HSP70 (green) and nuclear staining with Hoechst 33342 (blue). (Scale bar 10 µm) **C** IFA of α-LC3 (red) and α-GFP (green) stained *HSP101*++ and WT *P.b.* parasites at 24 hours post Huh7 infection reveals LC3, a host autophagy marker, localization to the parasite's PVM. Nuclear staining is displayed with Hoechst 33342 (blue). Upper panel is showing α-LC3 (red) staining only, lower panel is displaying the merged image. (Scale bar 10 µm)

3.2.1.4 Reduced protection in *HSP101*+ and *HSP101*++-immunized cohorts

Immunization with late liver stage arresting parasites e.g. Δ*PALM* and Δ*MFS6* have shown to induce superior protection compared to immunization with early arresting irradiated sporozoites (Haussig *et al.*, 2011, Kenthirapalan *et al.*, 2016). One reason apart from increased persistence and parasite biomass is the expansion of parasite antigens possibly increasing parasite recognition by the host's immune system by late liver stage protein export. To define the role of protein export in protection efficacy in *HSP101*+ and *HSP101*++ potentially PTEX reconstituted parasites, immunization experiments were carried out in C57BL/6 mice. Cohorts of C57BL/6 received a prime/boost vaccination within 10 days, with either a $1x10^4$ of *HSP101*+, *HSP101*++ or

WT sporozoites that were chemically attenuated with azithromycin (AZ) and were challenged with 1x10^4 of WT sporozoites 3 months later (**Fig. 21A**). AZ treatment leads to a delayed death phenotype, resulting in merozoite release and first round of blood stage replication before death. This model was chosen to enable comparison of the influence of protein export in transgenic parasites and natural late liver stages. Additionally, mice only received two immunizations as three immunizations have shown to fully protect from subsequent infection.

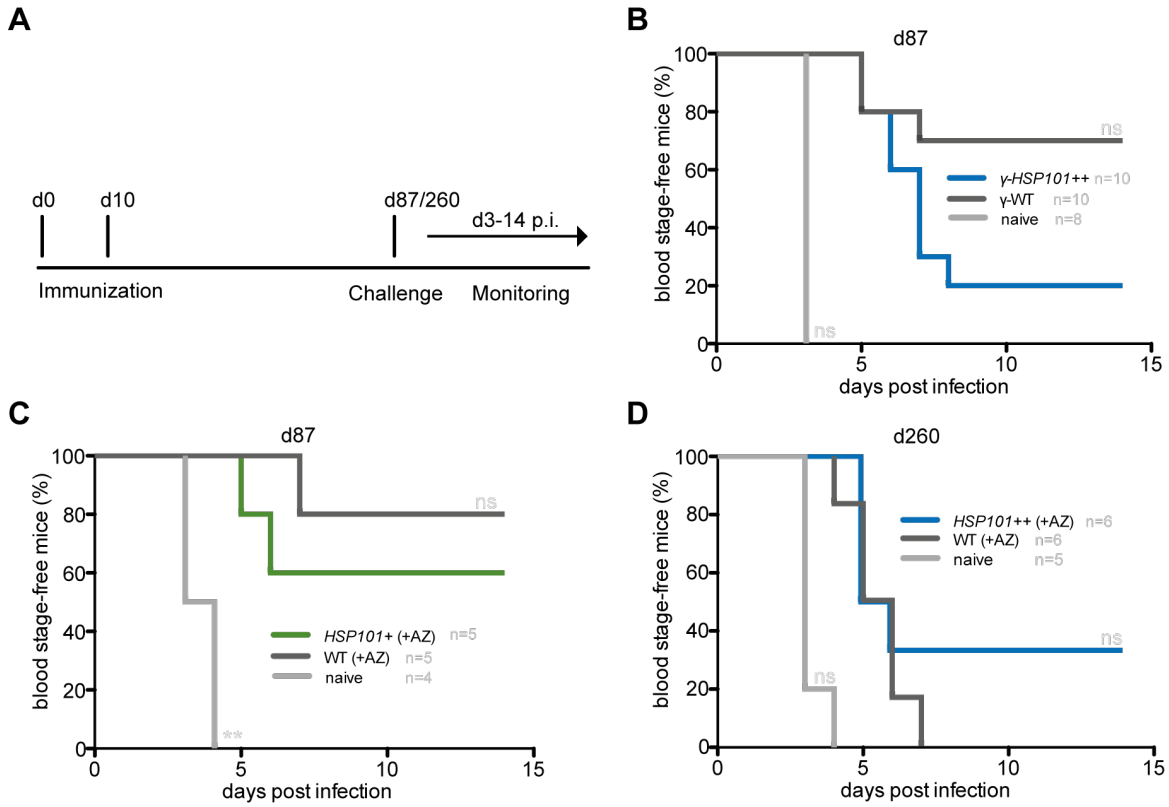

Figure 21 Inferior protection in *HSP101+* and *HSP101++*-immunized animals

Kaplan-Meier analysis of blood infection over time after sporozoite challenge reveals inferior protection in *HSP101+* and *HSP101++*-immunized animals. **A** Schematic representation of immunization procedure. C57BL/6 mice were immunized and boosted at a 10-day interval with 1x10^4 sporozoites i.v., challenged with 1x10^4 WT *P.b.* sporozoites i.v. 87 or 260 days post 1st immunization and blood infection was monitored by daily microscopic examination of Giemsa-stained blood films. (modified pictures from Smart, servier medical art) **B** Protection of mice immunized with irradiated *HSP101++* (γ-*HSP101++*, blue) and γ-WT (dark grey) sporozoites. WT *P.b.* sporozoite challenge was performed 87 days post immunization and non-immunized control animals (naïve, light grey) confirmed sporozoite infectivity by patent blood stage infection 3 days post inoculation. Statistical analysis: Log rank (Mantel-Cox) test **, $p<$ 0.01, ***, $p<$ 0.001 **C** Protection of mice immunized with *HSP101+* (green) and WT (dark grey) sporozoites under AZ drug cover. Challenge with WT *P.b.* sporozoites was performed 87 days post immunization and non-immunized control animals (naïve, light grey) confirmed sporozoite infectivity by patent blood stage infection 3 days post inoculation. Statistical analysis: Log rank (Mantel-Cox) test n.s., non-significant. **D** Protection of mice immunized with irradiated *HSP101++* and γ-WT sporozoites under AZ drug cover against WT *P.b.* sporozoite challenge 260 days p.i.. Blood stage development was monitored and WT *P.b.* sporozoites infectivity was confirmed in non-immunized animals (naïve, light grey) by patent blood stage infection 3 days post inoculation using Giemsa-stained thin blood smears. Statistical analysis: Log rank (Mantel-Cox) test n.s., non-significant.

To decipher differences in potent protection of the transgenic vaccine, a semi-protective two immunizations scheme was chosen. Only 60% of *HSP101*+ immunized animals were protected against WT infection after 3 months, however, protection in cohorts immunized with WT were not significantly higher (80% protection). Naive mice that received a challenge infection of $1x10^4$ WT sporozoites to determine WT sporozoite infectivity developed a patent blood stage infection 3-4 days post infection (**Fig. 21C**). Unexpectedly, only 20% of irradiated *HSP101*++ immunized mice were protected compared to 70% of γ-WT sporozoite immunized mice against challenge infections. Control mice were again blood stage positive three days post infection confirming normal WT sporozoite infectivity (**Fig. 21B**). Protection in *HSP101*++ under AZ drug cover immunized animals vanished completely when challenged at 260 days post immunization (**Fig. 21D**).

Collectively, slightly lower protection was observed in *HSP101*+ and *HSP101*++-immunized mice as compared to mice immunized with WT sporozoites, both under AZ drug cover or after irradiation of sporozoites. This indicates that HSP101 overexpression leading to potential early liver stage export does not lead to superior protection in immunized cohorts but tends to lower efficacy.

3.2.2 Absence of PEXEL-dependent export in *HSP101*+ and *HSP101*++ liver stages

Reduced protection levels in mice immunized with HSP101 overexpressing parasites hints towards the absence of early liver stage export in these parasites. Based on observing reduced protection in *HSP101*+ and *HSP101*++ immunized mice, I asked whether *HSP101*+ and *HSP101*++ parasites actually export proteins during early liver development, whether different PEXEL sequences influence export efficiency and when export commences in early liver stages.

To answer these questions, crossing of transgenic parasites with different reporter lines were performed to analyze PEXEL-dependent export in liver stages (**Table 3**). In order to confirm export in *HSP101+Myc* and *HSP101*++, transgenic parasites were crossed by co-infection of mosquitoes with export reporter lines. These reporter lines contain *CS-PEXEL* or *IBIS-PEXEL* fused in frame to mCherry for subsequent export analysis using IFA. The PEXEL constructs are under the control of *IBIS* promoter, which is active in several life cycle stages, or *UIS4* promoter, that is liver stage specific. Transgenic and reporter lines were sexually crossed in mosquitoes feeding on a double infected mouse and subsequently mixed cultures of sporozoites were isolated to infect Huh7 cells *in vitro* (**Fig. 22A**). 25% of the mixed sporozoite cultures carry one chromosome each with the desired genetic modification as visualized by fluorescent tags (GFP in HSP101 overexpression parasites and mCherry in reporter constructs). The other 75% are a mixture of WT, HSP101 overexpression parasites (only green) or reporter parasites (only red)

sporozoites. To evaluate export in exo-erythrocytic stages, infected Huh7 were imaged live as well as after antibody staining. Strikingly, the reporter construct *UIS4::CS-PEXEL-mCh* stayed confined to the PV of *HSP101+Myc* as seen for reporter constructs in WT parasites. *UIS4::CS-PEXEL-mCh* remained in the parasite PV 16, 40 and 48 hours post infections (**Fig. 22B**). Similar observations were made for further transgenic crossings with a list of different other reporter constructs (**Table 3**). CSP is among the only two proteins reported to translocate during early liver stage development, whether this is the case remains controversial (Singh *et al.*, 2007, Cockburn *et al.*, 2011). This notion was not confirmed in *HSP101+Myc* parasites as staining of endogenous CSP at 4 hours post infection revealed confinement of CSP to the PV (**Fig. 22C**).

Table 3 Export ability of reporter lines in *HSP101+Myc* or *HSP101++* parasites

Transgenic parasites	Reporter line	Export (Yes/No)
HSP101+Myc	*UIS4::CS-PEXEL-mCh*	N
	UIS4::IBIS-PEXEL-mCh	N
	IBIS::IBIS-PEXEL-mCh	N
	UIS4::CS-PEXEL-OVA	N
HSP101++	*UIS4::CS-PEXEL-mCh*	N
	UIS4::IBIS-PEXEL-mCh	N
	IBIS::IBIS-PEXEL-mCh	N
	UIS4::CS-PEXEL-OVA	N

Thus, protein export could not be confirmed in *HSP101+Myc* and *HSP101++* parasites neither by using a range of PEXEL sequences nor at different time points during liver stage maturation, demonstrating that low overexpression of HSP101 does not lead to PEXEL-dependent protein export.

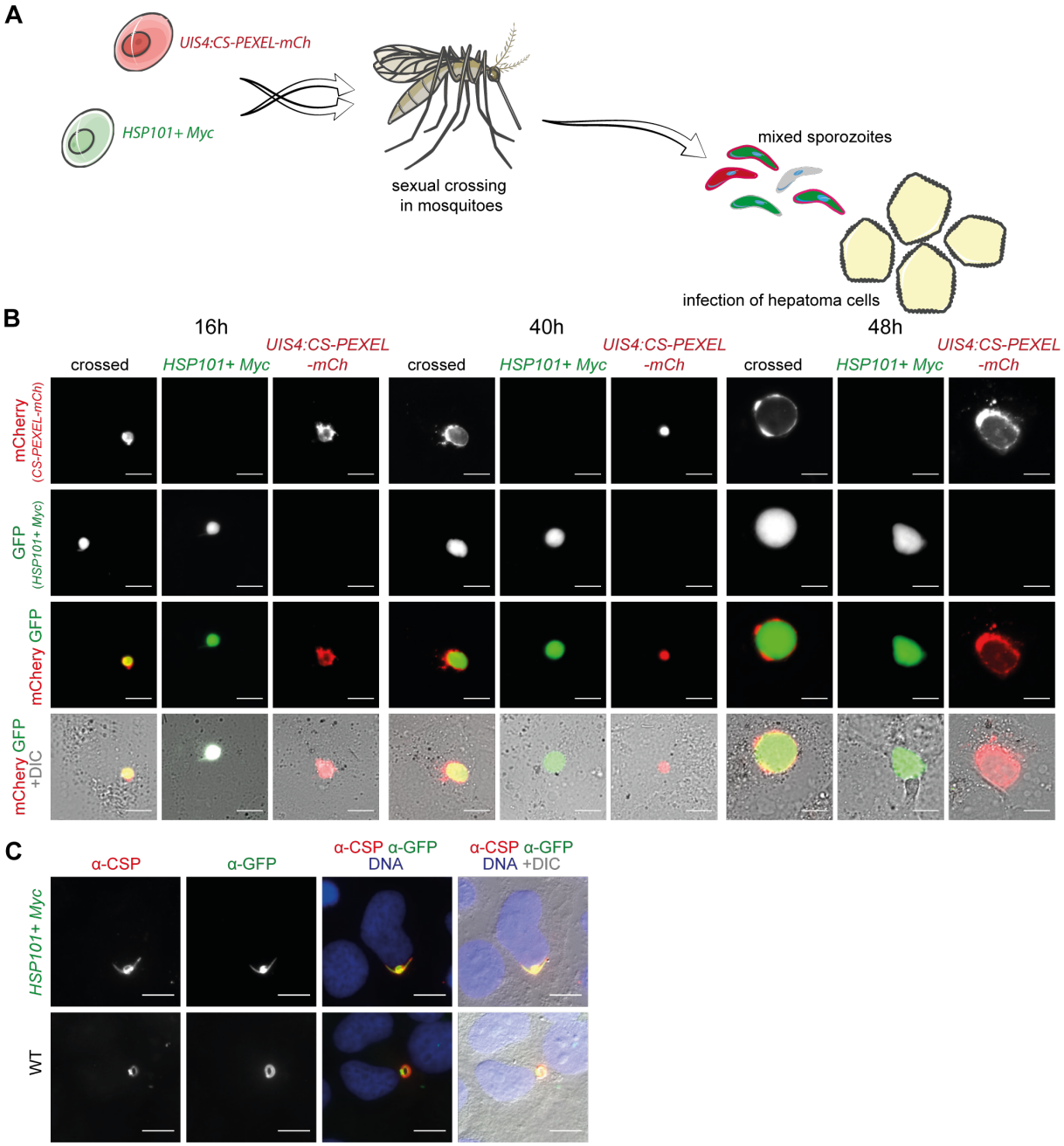

Figure 22 Export is blocked in *HSP101+* parasites

A Schematic representation of sexually crossing two *P.berghei* lines in the mosquito vector. Transgenic parasite *HSP101+Myc* (green) were co-infected with *UIS4::CS-PEXEL-mCh* (red) expressing parasites in NMRI mice and sexually crossed in mosquitoes. 25% of the mixed sporozoites carry one chromosome each with the desired genetic modification as visualized by fluorescent tags (GFP in HSP101 overexpression parasites and mCherry in reporter constructs, red and green). The other 75% are a mixture of 25% WT (grey), 25% HSP101 overexpression parasites (only green) or 25% reporter parasites (only red) sporozoites. Hepatoma cells were infected with genetically mixed sporozoites and export of reporter constructs was monitored. **B** Live imaging of of hepatoma cell infection at 16, 40 and 48 hours with mixed sporozoite, *HSP101+Myc*/*UIS4::CS-PEXEL-mCh* (termed crossed, red and green), *HSP101+Myc* (green), *UIS4::CS-PEXEL-mCh* (red). The mCherry (red) of the reporter construct remains confined to the PV in transgenic lines expressing GFP (green) at all time points p.i.. 1st panel is showing mCherry (*UIS4::CS-PEXEL-mCh)* only, 2nd panel is displaying GFP (HSP101+Myc) only, 3rd panel is showing the merged image and the last panel merge and DIC. (Scale bar: 10µm) **C** Immunofluorescence microscopy analysis (IFA) of α-CSP (red) and α-GFP (green) stained *HSP101+Myc* and WT *P.b.* parasites at 4 hours post hepatoma cell (Huh7) infection shows localization of CSP to the parasite's PV. Nuclear staining was performed with Hoechst 33342 (blue). (Scale bar 10 µm)

3.2.3 Abort of pre-erythrocytic development in strong HSP101 overexpressing parasites

3.2.3.1 Generation and *in vivo* life cycle analysis of *HSP101*+++ parasites reveals impaired pre-erythrocytic development

Protein export machineries are complex systems relying on constant adequate amounts of component expression, correct protein folding and complex assembly. The stoichiometric ratio of complex proteins can be an important factor for correct protein complex assembly. Having observed that HSP101 can be weakly overexpressed without interfering with the life cycle, but thereby failing to enable protein export, I asked whether high liver stage specific overexpression of HSP101 interferes with pre-erythrocytic development. Moreover, I raised the questions whether strong overexpression enables PTEX assembly, thereby commencing liver stage export and how this could have an effect on protection efficacy of the transgenic vaccine candidate.

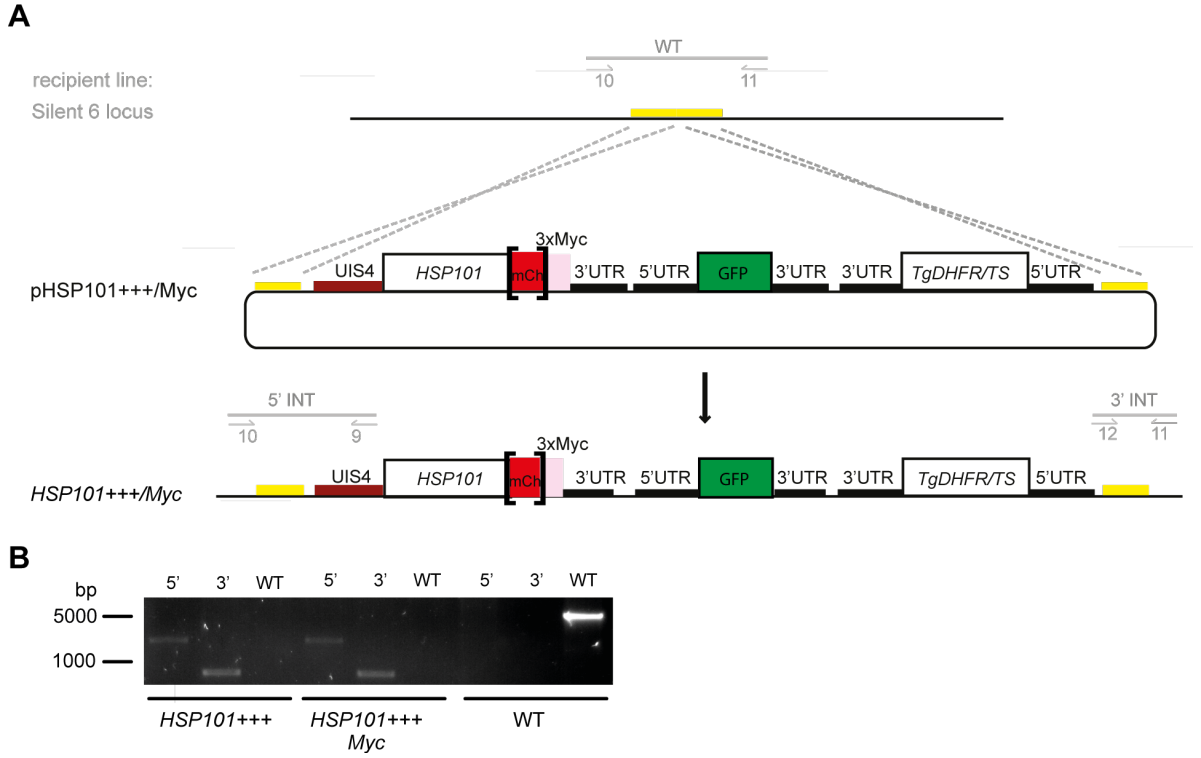

Figure 23 Stable integration of pHSP101+++/Myc

A Schematic representation of integration of linearized pHSP101+++/Myc into the silent locus on chromosome 6 of *P.b.* ANKA parasites. The pHSP101+++/Myc illustrates the plasmids used to generate *HSP101*+++/Myc parasites. By double homologous recombination an additional copy of *HSP101* under the control of *UIS4* promoter (dark red), a GFP reporter sequence (green, for parasite life cycle analysis) and TgDHFR/Ts resistance cassette (for positive selection with pyrimethamine) are incorporated. Shown is the double homologous crossover of the plasmid's two sequences (yellow) homologous to the silent 6 locus into the locus and the final recombined silent 6 locus in *HSP101*+++*/Myc* parasites. Grey lines indicate regions used for genotyping recombined parasites and the numbers refer to integration and WT specific primer combinations. **B** Genotyping PCR of *HSP101*+++ and *HSP101*+++*Myc* parasites. 5' and 3' integration and WT specific primer combinations (A) verified successful recombination events. Absence of WT signal from *HSP101*+++/Myc confirmed their isogenic purity. WT gDNA was used as a control.

In order to study the influence of strong HSP101 overexpression on liver stage development and export, parasites overexpressing HSP101 under the liver stage specific *UIS4* promoter were generated similarly as described in 3.2.1 for *HSP101*+ parasites. For *HSP101*+++ parasites *UIS4* 5' UTR was integrated in the *Bss*HII-*Age*I restriction site instead of the EF1α 5' UTR, upstream of *HSP101* ORF for acquiring pHSP101+++/3xMyc (**Fig. S5A**). mCherry was excised and replaced by a linker, to ensure correct Myc expression, in pHSP101+++Myc (**Fig. S5B**). Successful pHSP101+++ and pHSP101+++Myc integration into the silent 6 locus on chromosome 6 of *P.b.* ANKA with subsequent FACS cloning to receive isogenic lines was confirmed by genotyping PCR with specific primer pairs (s. ch. 2.1.9.2) for 5' and 3' integration and absence of WT locus amplification (**Fig. 23**).

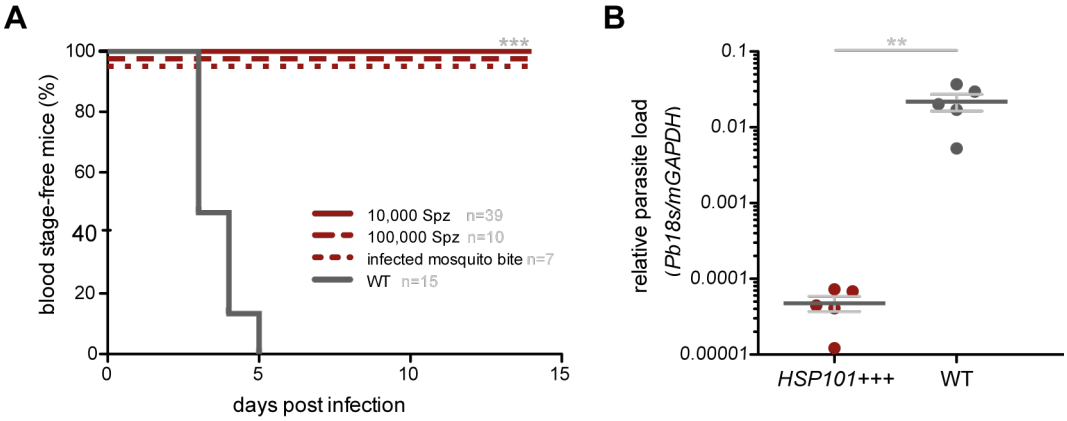

Figure 24 Complete arrest of pre-erythrocytic stages of *HSP101*+++ parasites *in vivo*

A Kaplan-Meier curve showing percentage of blood stage positive mice over time after infection with sporozoites. C57BL/6 mice were infected i.v. with $1x10^4$ or $1x10^5$ *HSP101*+++ (dark red) or WT (dark grey) sporozoites or natural transmission by exposure to 15 *HSP101*+++ (dark red) infected mosquitoes. Blood infection was monitored by daily microscopic examination of Giemsa-stained thin blood smears starting 3 days p.i.. Data is representative of eight independent experiments with five mice each for infections with $1x10^4$ *HSP101*+++ of which two were performed with a different isogenic parasite line. Experiments of infections with $1x10^5$ and natural infections were performed in two independent experiments. Statistical analysis: Log rank (Mantel-Cox) test, ***, $p<0.001$. **B** Relative parasite rRNA levels 48 hours post sporozoite infections are significantly reduced in *HSP101*+++ infected mice. C57BL/6 mice were infected with $1x10^4$ *HSP101*+++ (dark red) or WT (dark grey) sporozoites. The livers were excised 48h post challenge, RNA extracted and cDNA amplified. Quantitative real-time PCR on *Pb*18s rRNA against the murine GAPDH mRNA is depicted showing relative parasite load in the liver of individual infected animals (dots), as well as the general mean ±SD. Only significant differences are shown. Statistical analysis: Mann-Whitney-U-test , **$p<0.01$.

HSP101+++ and *HSP101*+++*Myc* developed normally in blood and mosquito stages (**Table S3**). To estimate whether strong overexpression interferes with parasite liver stage development, C57BL/6 mice were infected intravenously with a high dose of infective sporozoites and pre-patency was analyzed 3 to 10 days post infection. Surprisingly, mice remained blood stage negative compared to mice infected with WT sporozoites, which developed a patent blood stage infection 3 days post infection (**Fig. 24A** and **Table 4**). To rule out that sporozoites numbers influence disease outcome, mice were infected with a ten times higher dose of sporozoites,

however, strikingly infected mice remained blood stage negative. In addition, cohorts were exposed to bites of infectious mosquitoes to demonstrate the natural infection routes. Similarly to the previous infections no blood stage parasites were observed. Notably, *HSP101+++Myc* infected animals developed blood stages on day 5 post infection whereas in two experiments remained blood stage negative (**Fig. S6A**). To exclude that mCherry overexpression is the reason for the parasite's developmental arrest, mice were infected with *UIS4::mCh* (Silvie *et al.*, 2014) or *:::HSP101-mCh* (Matz *et al.*, 2015) sporozoites and parasite development was monitored 3 to 10 days post infection. In contrast to *HSP101+++*, mice developed a patent blood stage infection after 3 days similar to WT parasites (**Fig. S8A** and **Table 4**). To confirm the pre-patency observations, parasite load in the hosts' livers was determined. C57BL/6 mice were infected with a $1x10^4$ of sporozoites, liver excised 48h post infection and parasite and host RNA extracted. Relative parasite load was determined by comparing levels of parasite *Pb*18s RNA to host GAPDH RNA. Parasite liver load was over 1,000-fold reduced in *HSP101+++* infected animals compared to WT infected mice, indicating either a low infection rate or an early liver stage arrest (**Fig. 24B**).

Table 4 Pre-patency of HSP101 overexpressing *P. berghei* parasites

Parasite strain	Route of infection	Blood stage-positive mice[a]	Prepatent period[b]
HSP101+	i.v. $1x10^4$ spz	13/14 (92%)	>3 days (4)
HSP101+Myc	i.v. $1x10^4$ spz	1/1 (100%)	4 days
	infectious mosquito bite	2/2 (100%)	3 days
HSP101++	i.v. $1x10^4$ spz	7/7 (100%)	>3 days (3.5)
	infectious mosquito bite	1/1 (100%)	3 days
HSP101+++	i.v. $1x10^4$ spz	0/39 (0%)	-
	i.v. $1x10^5$ spz	0/10 (0%)	-
	infectious mosquito bite	0/7 (0%)	-
	i.v. $1x10^4$ haemocoel spz	0/5 (0%)	-
HSP101+++Myc	i.v. $1x10^4$ spz	8/20 (40%)	>5 days (5.5)
	infectious mosquito bite	7/7 (100%)	>4 days (6)
::HSP101-mCh	infectious mosquito bite	6/6 (100%)	>3 days (3)
UIS4::mCh	i.v. $1x10^4$ spz	5/5 (100%)	>3 days (3)
WT	i.v. $1x10^4$ spz	40/40 (100%)	>3 days (3)
	i.v. $1x10^5$ spz	1/1 (100%)	3 days
	infectious mosquito bite	4/4 (100%)	3 days
	i.v. $1x10^4$ haemocoel spz	1/1 (100%)	3 days

[a] Shown are numbers and respective percentage (in brackets) of infected to total animals.
[b] The prepatent period is defined as time to detection of first blood stage parasites after sporozoite infection. Shown are the day of commencing blood stage infection and in brackets the average start of the prepatent period.

Taken together, parasites strongly overexpressing HSP101 can be generated but high HSP101 expression leads to full abortion of liver stage development and a low relative parasite load in the liver, demonstrating that HSP101 expression and potentially PTEX assembly is tightly regulated in *Plasmodium* parasites.

3.2.3.2 Gliding is impaired in *HSP101*+++ sporozoites

Based on the before mentioned reduced parasite load in the liver, I speculated that sporozoite motility and in consequence sporozoite infectivity is impaired in *HSP101*+++ parasites. This raises the questions whether HSP101 is overexpressed in sporozoites and if overexpression interferes with sporozoite motility and infectivity.

To answer the first question, live imaging of salivary gland sporozoites was conducted. Strong expression of mCherry was observed in *HSP101*+++ sporozoites in sharp contrast to *HSP101*+ overexpression (**Fig. 25A**). The difference in overexpression between the two parasite lines can clearly be explained by the difference in promoter activity, which was measured by qRT-PCR by comparing relative mRNA levels of WT *P.b. PTEX150*, endogenous *HSP101*, *UIS4* and *GFP*, under the control of *EF1a* promoter, expression relative to *PbHSP70* (**Fig. 24B**). This notion was confirmed by qRT-PCR analysis of *HSP101*+++ compared to WT *P.b. HSP101* transcript levels normalized to *PbHSP70* (**Fig. 24C**). Moreover, overexpressed HSP101 localized in vesicle-like compartments throughout the whole sporozoite in contrast to endogenously tagged HSP101, which was reported to localize to the apical end of the sporozoite (**Fig. 24A**, Matz *et al.*, 2015).

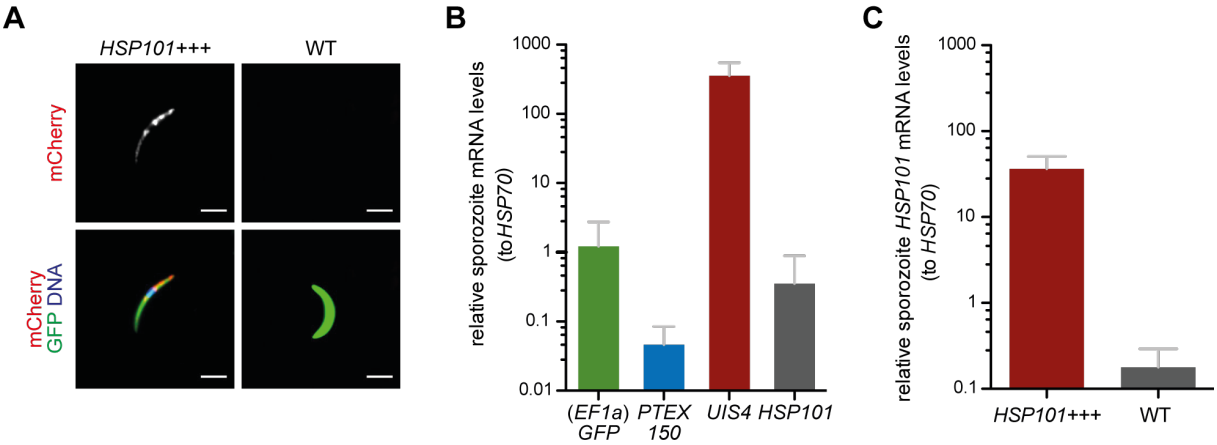

Figure 25 Strong vesicular overexpression of HSP101 in *HSP101*+++ sporozoites

A Live imaging of *HSP101*+++ and WT *P.b.* salivary gland sporozoites at day 17 post mosquito infection. Expression of HSP101-mCh is displayed in red and transgenic parasite marker GFP, staining the parasite's cytoplasm, in green. Nuclear staining was performed with Hoechst 33342 1:5,000 and motility inhibition with 1:50 Phalloidin (Scale bar: 5 µm). **B** Quantitative RT-PCR analysis of sporozoite gene expression. ΔΔCT mRNA levels of *PTEX150*, *UIS4*, *HSP101* and *GFP,* under the control of *EF1α* promoter, in sporozoites normalized to *PbHSP70*. Data is displayed as mean of two to four independent experiments with three replicates each ±SD. **C** Quantitative RT-PCR analysis of sporozoite gene expression reveals increased *HSP101* levels in *HSP101*+++ sporozoites. ΔΔCT *HSP101* mRNA levels of *HSP101*+++

compared to WT *P.b.* sporozoites were normalized to *PbHSP70*. Data is displayed as mean of two independent experiments with three replicates each ±SD.

Having found divergent HSP101 expression levels and localization in *HSP101*+++ compared to WT sporozoites, I asked whether this influences sporozoite motility and infectivity. To examine sporozoite motility, gliding assays were performed. Once sporozoites are injected during an infectious mosquito bite, they travel through the dermis to reach the next blood vessel in which they travel to the liver where they infect hepatocytes and undergo liver stage development. Sporozoite gliding ability was analyzed *in vitro* by staining and counting gliding trails (CSP protein trails which are deposited by sporozoites). Strikingly, the gliding ability of *HSP101*+++ was significantly reduced by 40% as compared to WT (**Fig. 26A**). To rule out overuse of ATP by increased HSP101 levels, a triple ATPase, sporozoite gliding was also examined with sporozoites incubated with ATP and glucose. *HSP101*+++ sporozoites were able to restore motility, however, subsequent *in vitro* sporozoite infection of hepatoma cells resulted in liver stage developmental arrest (**Fig. S9C**). Similarly, to exclude that mCherry expression in sporozoites accounts for the defect in gliding and exo-erythrocytic growth, haemocoel sporozoites, where *UIS4* promoter is not active, were used for subsequent *in vitro* and *in vivo* infections. Despite the enhanced sporozoite motility, *in vitro* hepatoma cell infections led to a complete developmental arrest and *in vivo* infections of C57BL/6 mice did not result in patent blood stage infections (**Fig. S9**). Once sporozoites reach the liver they transmigrate through several hepatocytes before infecting a final one where they mature into merozoites. The observed gliding defect let to the question whether the 20% of sporozoites that were able to glide were also able to transmigrate through hepatoma cells before infecting a final hepatoma cell for initiating liver stage growth. During transmigration sporozoites create holes in the hepatocyte membranes (Mota *et al.*, 2001). To determine transmigration ability, Huh7 cells were infected with sporozoites in dextran containing medium. Dextran is a membrane non-permeable dye. Sporozoites created holes during migration where dextran could enter the cells and percentage of dextran influx was measured with FACS. Transmigration was significantly reduced by 30% in *HSP101*+++ parasites (**Fig. 26B**). Natural non–sporozoite induced dextran influx was accounted for by a negative control of dextran and cells only.

Taken together, strong overexpression was detected in *HSP101*+++ sporozoites and gliding and transmigration ability were strongly inhibited, demonstrating that strong HSP101 overexpression has influence on sporozoite motility.

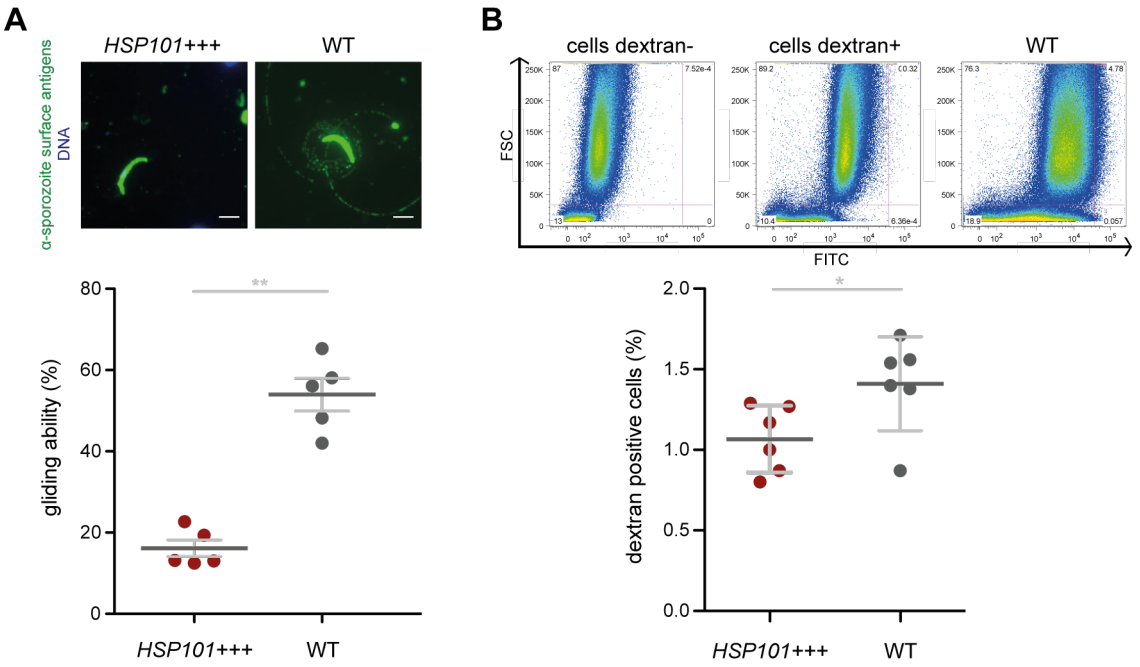

Figure 26 Gliding and transmigration are impaired in *HSP101*+++ sporozoites

A Impaired sporozoite gliding motility of *HSP101*+++. Salivary gland *HSP101*+++ sporozoites were excised at day 17 and left to settle and subsequently glide on a BSA-covered 2-dimensional glass slide. Sporozoite surface protein trails shed by gliding sporozoites were stained with α-sporozoite surface antibody and Hoechst 33342 for nuclear staining. Shown is a representative immunofluorescence image of *HSP101*+++ and WT *P.b.* salivary gland sporozoites (Scale bar: 5 µm). Three independent experiments (dots) were used to determine the percentage of gliding sporozoites. Depicted are the mean ±SD. Statistical analysis: Mann-Whitney-U-test **, $p<0.01$ **B** Impaired transmigration of *HSP101*+++ sporozoites. Shown is the FACS quantification of dextran-positive hepatoma cells after two hours post sporozoite infection. $1x10^6$ Huh7 cells were infected with $7.5x10^4$ *HSP101*+++ or WT *P.b.* sporozoites or dextran+/sporozoites- (as a control for dextran influx without sporozoite infection) and analyzed with FACS for dextran influx using MACSquant. Upper panel: Examples of gating strategy: FITC (dextran) is blotted against FFC for dextran-/sporozoite-, dextran+/sporozoite- and dextran+/sporozoite+ (WT) cells. Lower panel: Depicted are individual percentages of dextran positive cells of each replicate of three independent experiments (with three replicates each) ±SD. Statistical analysis: Mann-Whitney-U-test *, $p<0.05$,

3.2.3.3 Liver stage development is arrested in *HSP101*+++ parasites *in vitro*

HSP101+++ sporozoites are strongly impaired in their gliding ability, however, the 20% that are able to glide are also able to transmigrate through hepatoma cells, demonstrating that a second defect during hepatocyte entry or development prevents patent blood stage infections. Therefore, I was prompted to analyze *HSP101*+++ infectivity and liver stage development *in vitro*. To define the role of strong HSP101 overexpression for sporozoite infectivity, hepatoma cells were infected with *HSP101*+++ sporozoites and percentage of intra- and extracellular sporozoite were quantified two hours post infections. Unexpectedly, similar numbers of intracellular parasites were detected after hepatoma cell infection with *HSP101*+++ and WT parasites. Notably, a trend towards lower infection rate was observed in *HSP101*+++ infected cells (**Fig. 27A**). *HSP101*+++ sporozoites showed no sign of decreased *in vitro* infectivity, hence, suggesting that a second defect in liver stage development might account for the lack of patent blood stage infection.

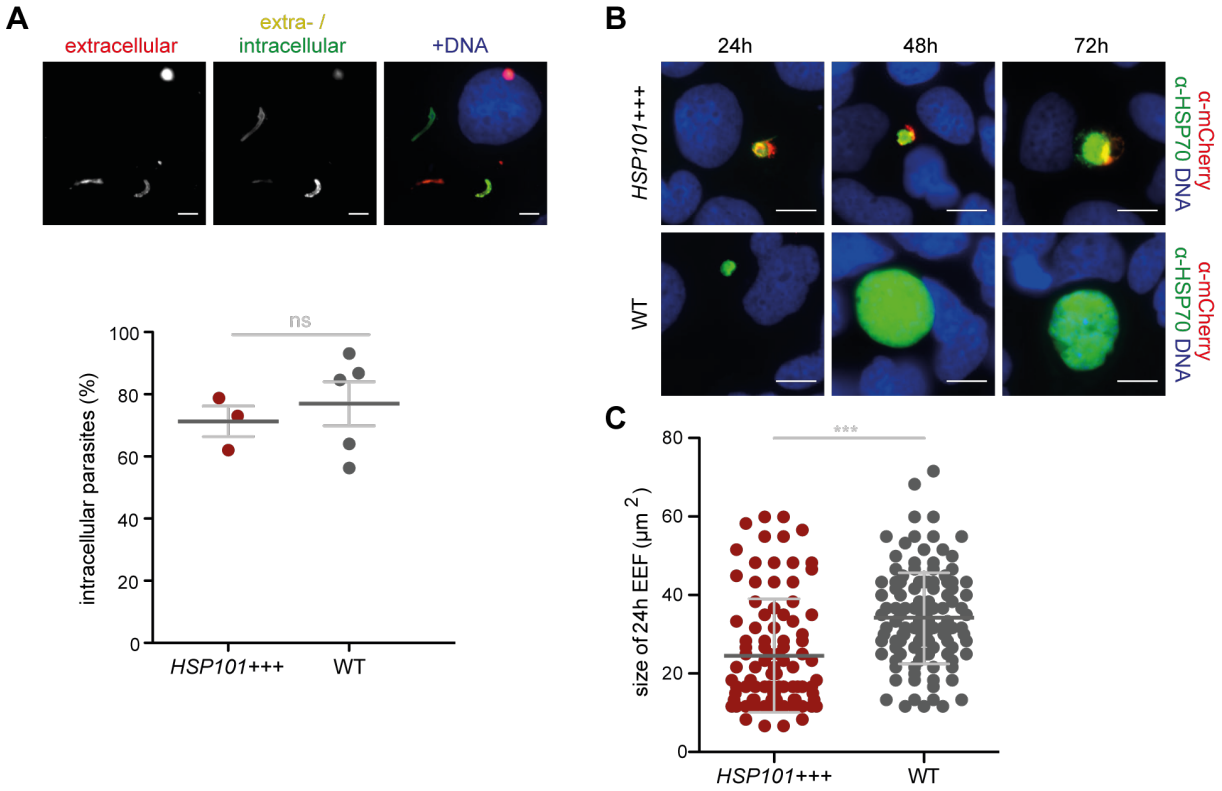

Figure 27 *HSP101*+++ arrests during liver stage development

3x10^4 hepatoma (Huh7) cells were infected with 1x10^4 *HSP101*+(dark red) and WT (dark grey) sporozoites per well. **A** Normal invasion of *HSP101*+++ sporozoites. Hepatoma cells were infected with *HSP101*+++ or WT *P.b.* sporozoites. After fixation, extracellular sporozoites were stained with α-CSP antibody and α-mouse Alexa546 (red) and after a permeabilization step stained again with α-CSP antibody and α-mouse Alexa488 (green) for intra- and extracellular parasites. This allows differentiation of attached (red and green) and invaded (green) sporozoites. Representative immunofluorescence image shows one attached (red, green) and one invaded (green) sporozoite. Nuclear staining was performed with Hoechst 33342. Intracellular sporozoites were quantified by determining attachment versus invasion per 100 parasites per replicate. Results represent the mean of replicates of three independent experiments and the overall mean ±SD. Statistical analysis: Mann-Whitney-U-test, ns, not significant. **B** Representative immunofluorescence microscopy images of α-mCherry (HSP101, red) and α-HSP70 (staining the parasite's cytoplasm in green) stained *HSP101*+++ and WT *P.b.* parasites at 24, 48 and 72 hours post hepatoma cell (Huh7). Nuclear staining was performed with Hoechst 33342 (blue) (Scale bar: 10 µm). **C** EEF sizes of HSP101+++ and WT *P.b.* parasites at 24 hours. 20 parasites per technical replicate of two independent experiments were measured by immunofluorescence microscopy and analyzed with Fiji for determining the size (µm) of the parasite. Depicted are individual parasites per time point (dots) and the mean ±SD. Statistical analysis was performed on the means of three replicates: Mann-Whitney-U test, ***, $p<0.001$.

Liver stage development goes hand in hand with parasite expansion from ~5 µm^2 to 800 µm^2 and can be used as an estimate for parasite maturation in the liver. In order to confirm liver stage arrest, EEF size at 24 hours post infection was measured. EEF sizes were significantly reduced in *HSP101*+++ parasites with only ~ 25 µm^2 in size compared to ~35 µm^2 in WT parasites at 24 hours post infection (**Fig. 27C**). Moreover, developmental arrest is clearly visualized in images of antibody stained EEFs, where *HSP101*+++ EEFs remain smaller in size at 24 hours post infection (**Fig. 27B**). Notably, HSP101-mCh signal localized to the whole parasite and was not confined to the PV of the parasite (**Fig. 28**). As *HSP101*+++ parasites revealed a similar phenotype as

described for *ΔUIS4* (Mueller *et al.*, 2005), experiments confirming presence of UIS4 and other PVM residual proteins were conducted to rule out false integration into and destruction of *UIS4* locus. To exclude the possibility of accidental *ΔUIS4* parasite generation, the *UIS4* locus of *HSP101*+++ was characterized by genotyping using WT *UIS4* locus specific primer pairs and relative mRNA levels of *UIS4* were determined in *HSP101*+++ sporozoites. Genotyping revealed the presence of an intact *UIS4* locus and relative *UIS4* mRNA levels in *HSP101*+++ were similar to mRNA levels of WT parasites (**Fig. S10**).

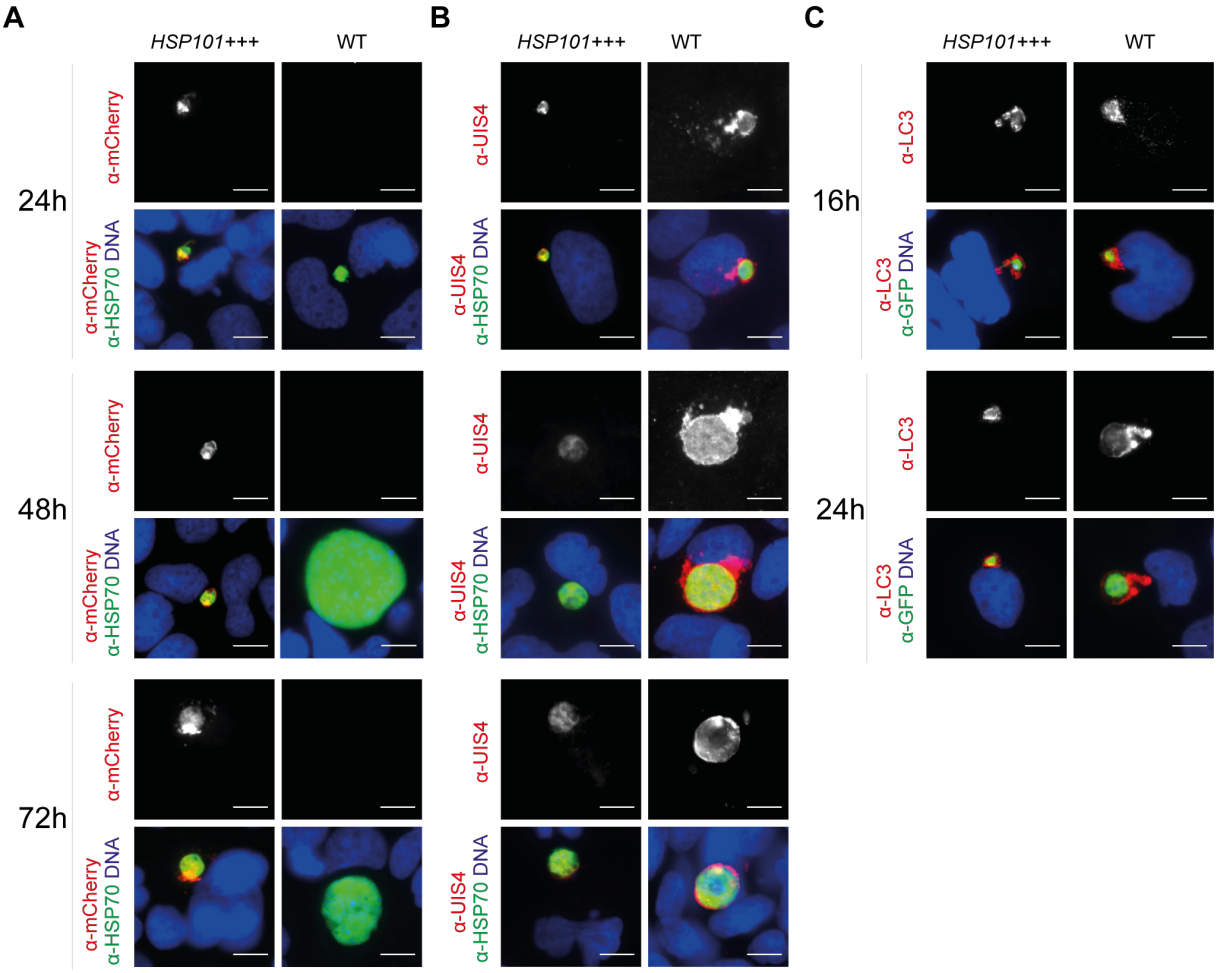

Figure 28 *HSP101*+++ exo-erythrocytic stages establish and maintain a PVM

A Immunofluorescence microscopy analysis (IFA) of α-mCherry (HSP101, red) and α-HSP70 (staining the parasite's cytoplasm in green) stained *HSP101*+++ and WT *P.b.* parasites at 24, 48 and 72 hours post hepatoma cell (Huh7) infection shows distorted localization of HSP101. Nuclear staining was performed with Hoechst 33342 (blue). Upper panel is showing mCherry (HSP101) staining only, lower panel is displaying the merged image. (Scale bar 10 µm) **B** Localization of UIS4 by IFA in *HSP101*+++ and WT *P.b.* parasites infected Huh7 cells at 24, 48 and 72 hours p.i.. Upper panel is showing α-UIS4 (red) staining only, lower panel is depicting the merged image with α-HSP70 (green) and nuclear staining with Hoechst 33342 (blue). (Scale bar 10 µm) **C** IFA of α-LC3 (red) and α-GFP (green) stained *HSP101*+++ and WT *P.b.* parasites at 16 and 24 hours post Huh7 infection reveals LC3, a host autophagy marker, localization to the parasite's PVM. Nuclear staining is displayed with Hoechst 33342 (blue). Upper panel is showing α-LC3 (red) staining only, lower panel is displaying the merged image (Scale bar 10 µm).

Furthermore, EEF were stained for presence of UIS4, a PVM resident protein, and LC3, a host cell autophagy marker. The presence of UIS4 could be confirmed in *HSP101*+++ parasites at 24, 48 and 72 hours post infection, regardless of the developmental arrest before 24 hours post infection. Presence of LC3 at 16 and 24 hours post infection confirmed an intact PVM of *HSP101*+++ parasites (**Fig. 28B**). Notably, the minority of *HSP101*+++*Myc* parasites that develop beyond 24 hours post infection revealed HSP101 and UIS4 expression in the parasite's PV and recruitment of LC3 16 and 24 hours post *in vitro* hepatoma cell infection (**Fig. S7**)

Taken together, successful invasion of hepatoma cells was not impaired in *HSP101*+++ sporozoites, however liver stage arrest was observed at 24 hours post infection even though parasites were able to build and maintain an intact PVM, demonstrating that strong overexpression of HSP101 leads to pleiotropic defects: an impaired sporozoite motility and a liver stage developmental arrest.

3.2.3.4 *HSP101*+++ parasites elicit weak protection against follow-up infection

Complete liver stage arrest is a prerequisite for a safe GAP-based vaccine candidate. *ΔSLARP* parasites are so far the only known GAP-based vaccine candidate to fully arrest during liver stage development. However, efficacy of *ΔSLARP* parasites has shown to be low compared to other GAP-based vaccines (Kreutzfeld *et al.*, 2017). Here, we generated a new fully arresting GAP vaccine candidate with the potential to induce better protection by increased visibility of the parasite to the immune system due to regulated protein export into the hepatocyte cytoplasm.

Table 5 Protection after immunization with HSP101 overexpressing *P. berghei* sporozoite

Parasite strain	Immunization/ Challenge shedule[a]	Blood stage-positive mice[b]	Prepatent Period[c]
HSP101+ (+AZ)	0/10 (87)	3/5 (60%)	(>5 days)
γ-*HSP101++*	0/10 (87)	8/10 (80%)	(>5 days)
HSP101++ (+AZ)	0/10 (260)	4/6 (70%)	(>4 days)
HSP101+++	0/10 (87)	15/17 (88%)	(>3 days)
	0/10 (260)	4/4 (100%)	>3 days
HSP101+++Myc	0/10 (87)	10/10 (100%)	>4 days
WT +AZ	0/10 (87)	13/30 (40%)	>5 days
	0/10 (260)	8/8 (100%)	>4 days
γ-WT	0/10 (87)	3/10 (30%)	
naive	-	22/22 (100%)	>3 days

[a] Mice were inoculated by i.v. injection of $1x10^4$ sporozoites. Shown are immunization days and challenge post immunization in brackets.
[b]Shown are numbers and respective percentage of infected to total animals.
[c] The prepatent period is defined as time to detection of first blood stage parasites after sporozoite infection.

To define the impact of strong HSP101 overexpression on vaccine efficacy, C57BL/6 mice were immunized in a prime/boost regime with a 10 days interval, challenged three months later with WT sporozoites and monitored for blood stage infection 3-10 days post challenge (**Fig. 29A**). Interestingly, the majority of *HSP101*+++-immunized animals became blood stage positive 4-6 days post infection in contrast to immunizations with AZ attenuated WT sporozoites, which lead to 55% of animals being protected against subsequent sporozoite challenge. Sporozoite infectivity was confirmed by challenging naïve mice, which developed a patent blood stage infection 3-4 days later (**Fig. 29B** and **Table 5**). A challenge of immunized cohorts 260 days post immunization completely eliminated all protective effects (**Fig. 29C**).

Conclusively, *HSP101*+++ fulfills whole sporozoite vaccine safety requirements, but fails to protected against challenge infections, demonstrating that early liver stage arrest and reduced liver load of *HSP101*+++ does not lead to superior immunity in immunized cohorts.

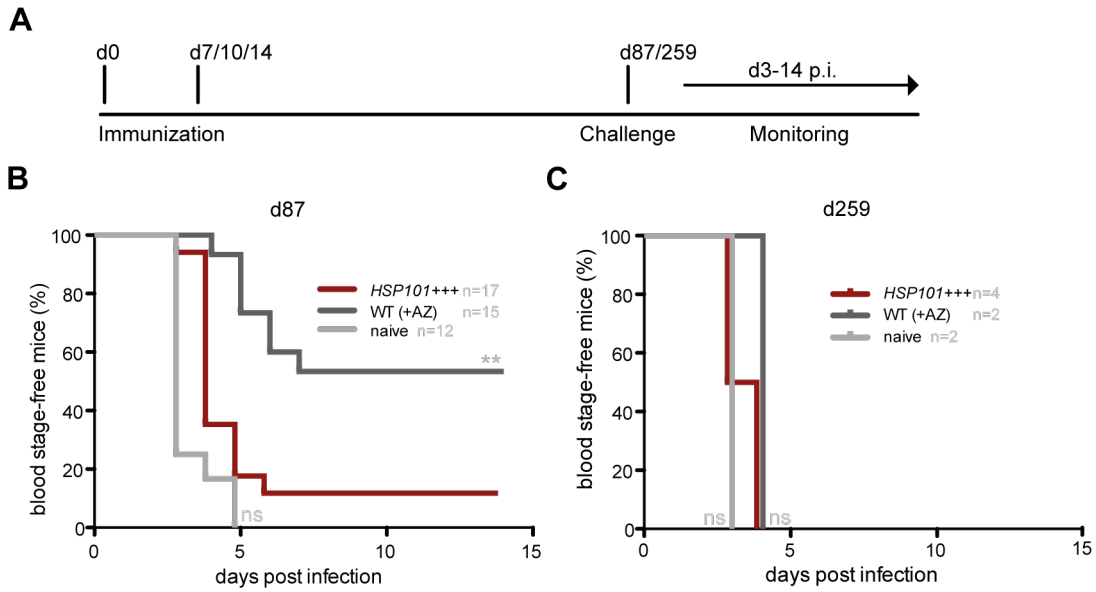

Figure 29 Inferior protection in *HSP101*+++-immunized mice

Kaplan-Meier analysis of percentage of blood stage infected mice over time after sporozoite challenge reveals inferior protection in *HSP101*+++-immunized animals. **A** Schematic representation of immunization procedure. C57BL/6 mice were immunized and boosted at a 10-day interval with $1x10^4$ sporozoites i.v., challenged with $1x10^4$ WT *P.b.* sporozoites i.v. 87 or 260 days post 1st immunization and blood infection was monitored by daily microscopic examination of Giemsa-stained blood films. **B** Protection of mice immunized with *HSP101*+++ sporozoites (dark red) and WT sporozoites attenuated by co-administration of AZ (dark grey). WT *P.b.* sporozoite challenge was performed 87 days post immunization and non-immunized control animals (naïve, light grey) confirmed sporozoite infectivity by patent blood stage infection 3 days post inoculation. Statistical analysis: Log rank (Mantel-Cox) test n.s., non-significant, **, $p< 0.01$ **C** Protection of mice immunized with *HSP101*+++ sporozoites (dark red) and WT sporozoites under AZ drug (dark grey). Challenge with WT *P.b.* sporozoites was performed 260 days post immunization and non-immunized control animals (naïve, light grey) confirmed sporozoite infectivity by patent blood stage infection 3 days post inoculation. Statistical analysis: Log rank (Mantel-Cox) test n.s., non-significant

4 Discussion

4.1 Pre-clinical analysis of a triple genetically attenuated parasite (tKO GAP) vaccine candidate

Many GAP-based vaccines for immunization against *Plasmodium* have been explored in the last decade, promoting the idea of whole sporozoites vaccines. However, drawbacks for all candidates in safety or protection limit their vaccine potential. This study describes for the first time a side-by-side preclinical study of a triple KO (*ΔSLARP/P36p/P36*) malaria vaccine candidate compared to its single and double KO counterparts (*ΔSLARP*, *ΔP36p/P36*). Surprisingly, even though similar infection and exo-erythrocytic growth rates were observed *in vitro* for the tKO parasites and for the original KO parasites, inferior vaccine efficacy was observed already one month after immunization with tKO parasites. Thus, it can be hypothesized that the combination of two knockout lines has an antagonistic effect on the protective capacity, potentially caused by deficient antigen presentation and failure to induce long-lasting $CD8^+$ T cell responses in the spleen, leading to a decreased vaccine efficacy of *ΔSLARP/P36p/P36*.

4.1.1 Complete arrest but inferior protection in *ΔSLARP/P36p/P36*-immunized animals

Full arrest of GAP-based vaccine candidates in the liver before onset of the symptomatic blood stage infection is a prerequisite for a safe vaccine candidate. My results demonstrate that the tKO parasites undergo normal blood and mosquito stage development, as described for *ΔP36p* and *ΔSLARP* (van Dijk *et al.*, 2005, Silvie *et al.*, 2008), a necessary prerequisite for sporozoite based vaccine candidates. Parasite lines lacking *SLARP* have been shown to fully arrest in the liver (van Dijk *et al.*, 2005, Aly *et al.*, 2008, Silvie *et al.*, 2008, van Schaijk *et al.*, 2014, Kublin *et al.*, 2017), whereas parasites lacking either *P36p* or both *P36p/P36* reveal occasional breakthrough infections (van Dijk *et al.*, 2005, Labaied *et al.*, 2007). To ensure complete arrest of tKO parasites, C57BL/6 mice were infected with a high dose ($1x10^4$) of sporozoites and monitored for blood stage infection for at least 14 days. The results demonstrate, as described previously by Silvie *et al.*, that parasites lacking *SLARP* fully arrest in the liver without any breakthrough infections (**Table 2**). Corroborating, blood stage infection with *ΔSLARP* parasites is very unlikely as previous studies showed no sign of blood stage pre-patency if mice were infected with 10-fold higher dose of sporozoites (Silvie *et al.*, 2008). This side-by-side study revealed for the first time breakthrough infections of *P. berghei ΔP36p/P36* parasites, as described for *P. yoelii* (Labaied *et*

al., 2007). Similar breakthrough levels were observed in infections with the *P. berghei ΔP36p* single knockout (van Dijk *et al.*, 2005)

Results of the current study revealed that *ΔSLARP/P36p/P36*-immunized animals were less protected compared to single KO and γ-WT-immunized animals (**Fig. 9**). Only ~20% of the mice were protected from infectious WT sporozoites when challenged one month after the last immunization.

This is surprising as original KOs performed better compared to the tKO in prime/boost vaccine trials. To my knowledge previous studies only looked at prime and two booster immunizations. In a comparative study, three immunizations with either *ΔP36p/P36*, *ΔSLARP* or γ-WT sporozoites led to full protection against a patent blood stage infection (Josephine Scholz, MPIIB, Master thesis 2015). This finding confirms the complete protection observed with *ΔP36p/P36* parasites (Labaied *et al.*, 2007). In contrast, *ΔSLARP* parasites were reported not to be fully protective with 75% of the immunized mice developing delayed pre-patency (Silvie *et al.*, 2008). In this work-declined protection levels were observed in all immunized cohorts, likely being a result of only two immunizations (**Fig. 9**). Thus, protection seems to decline quickly, as tKO immunized mice were not protected against sporozoite challenge two months after the last immunization (Josephine Scholz, MPIIB, Master thesis 2015), indicating that long-term protection can be hardly achieved by immunizations with *ΔSLARP/P36p/P36* sporozoites.

Quantification of relative liver parasite loads by quantitative qRT-PCR can be used as an alternative to determine the protective efficacy of immunizations. In good agreement with the findings from the pre-patency study after sporozoite challenge, ~100-fold to 1,000-fold reduction of liver parasites in *ΔSLARP/P36p/P36, ΔSLARP, ΔP36p/P36* and γ-WT-immunized animals was detected (**Fig. 10**). Similar reductions were observed for *ΔP36p* (Friesen & Matuschewski, 2011). To my knowledge this is the first time a study reports liver load levels after immunization for *ΔSLARP*. Of note, individual values of immunized animals varied strongly, ranging over several orders of magnitude, indicative of a high degree of individual variation. To explain the differences in protection observed in *ΔSLARP/P36p/P36* parasites to its original counterparts, further phenotypical and immunological characterization of the tKO parasites is required to identify the reason for the antagonistic effects.

4.1.2 Exo-erythrocytic development is attenuated in tKO *in vitro*

A hallmark of GAPs is the life cycle arrest during liver stage development. The absence of *in vitro* growth in *ΔSLARP/P36p/P36* indicates early liver stage arrest. In concordance with the phenotypes observed for *ΔSLARP* and *ΔP36p* parasites (van Dijk *et al.*, 2005, Aly *et al.*, 2008, Silvie *et al.*, 2008). Developmentally more advanced liver stage parasites, as reported for *ΔP36p*

*(*van Dijk *et al., 2005)*, were not observed for *ΔSLARP/P36p/P36* (**Fig. 12**) Thus, Δ*SLAP/P36p/P36* parasites closely resemble *ΔSLARP* parasites in liver stage growth and arrest *in vitro* and pose a first indication for the absence of breakthrough infections. However, arrest at a very early stage in liver development might represent a considerable disadvantage in terms of protection. Silvie *et al.* already noticed a limited capacity to induce sterilizing immune responses in immunizations with *ΔSLARP* parasites most likely due to the early arrest, which substantially limits the antigenic repertoire (Silvie *et al.*, 2008). A short development phase significantly reduces the amount of antigens, which can be presented on the surface of infected hepatocytes (Kreutzfeld *et al.*, 2017). In support of this hypothesis, immunizations with late-arresting GAP, like Δ*FabB/F* and *ΔPALM* parasites, mount superior immunity and enhance protection against reinfections (Butler *et al.*, 2011, Haussig *et al.*, 2011, Butler *et al.*, 2012). Δ*FabB/F* GAP immunizations induce larger populations of antigen specific $CD8^+$ T cells, perhaps due to the presence of additional and multistage-expressed antigens (Butler *et al.*, 2011). Whether the limited potential of early arresting GAPs to amplify biomass or to differentiate plays a role in decreased protection remains unclear (Butler *et al.*, 2012). Similarly, tKO sporozoites infectivity and liver stage expansion resemble *ΔSLARP* parasites. As infectivity plays a major role in vaccine efficacy, the significant decrease observed in *in vitro* hepatoma cell infections might explain the observed lowered protection in *ΔSLARP/P36p/P36* and *ΔSLARP*-immunized mice (**Fig. 12**). In contrast, *ΔP36p/P36* revealed hepatoma cell infection rates similar to WT strengthening the hypothesis that good protection might be achieved by adequate hepatocyte infections. In order to maintain long-term protection, parasite persistence as metabolically active intra-hepatic stages is required (Scheller & Azad, 1995). *ΔSLARRP/P36p/P36* and *ΔSLARP* persistence rates, determined by steady numbers of liver stage parasites over time, are similar to those of *ΔP36p/P36,* however the overall reduced infection rate of hepatoma cells might be too low to induce elevated immune responses. Possible solutions to low infection rates in vaccine candidates could imply upscaling of immunization doses to achieve similar parasite loads as observed for γ-WT infections in the liver and thus, overall protection.

Protection from host defense and autophagy mechanisms is achieved by an intact and remodeled PVM (Prado *et al.*, 2015, Wacker *et al.*, 2017). *ΔP36p* and *ΔSLARP* have been reported to either be deficient of PVM establishment and maintenance or PVM remodeling after initial PVM acquisition, respectively (van Dijk *et al.*, 2005, Silvie *et al.*, 2008). *In vitro* studies of tKO infected hepatoma cells suggest that *ΔSLARP/P36p/P36* parasites are deficient of a PVM, as staining of a PVM resident protein USI4 and the host's autophagy protein LC3, which is recruited to a functional parasite PVM, was absent in and around *ΔSLARP/P36p/P36* parasites (**Fig. 13A**). UIS4 is incorporated into the PVM during remodeling of the initial vesicular membrane, which is established upon hepatocyte invasion (Mueller *et al.*, 2005). Labaied *et al.* reported non-typical

UIS4 staining for several early arresting *ΔP36p/P36* parasites (Labaied *et al.*, 2007). This phenotype was even more pronounced in my study, where UIS4 staining was absent in *ΔP36p/P36* parasites. In contrast, *ΔSLARP* parasites down regulate important liver stage proteins including UIS4 (Silvie *et al.*, 2008). However, integration of PVM proteins is required for remodeling of the early liver stage PVM to be intact and functional. Thus, *ΔSLARP* parasites initiate but fail to remodel the PVM and incorporate UIS4, resulting in absent UIS4 staining in *ΔSLARP* parasites. To ensure absence of the PVM in *ΔSLARP/P36p/P36* parasites, additional staining for a host cell autophagy marker termed LC3 was performed. LC3 is recruited and incorporated into early fully functional PVMs (Kabeya *et al.*, 2000, Prado *et al.*, 2015, Thieleke-Matos *et al.*, 2016). To my knowledge this is the first time the original KOs were stained for LC3 recruitment in early liver stages. As expected, *ΔSLARP/P36p/P36* and *ΔP36p/P36* lacked LC3 staining, however, LC3 recruitment was also absent in *ΔSLARP* parasites. It is postulated that LC3 is only incorporated in mature existing PVMs and not in newly formed double membranes, hence, *ΔSLARP* likely fails to recruit LC3 due to the absence of PVM remodeling (Kabeya *et al.*, 2000). Concluding, *ΔSLARP/P36p/P36* parasites closely resemble *ΔSLARP* and *ΔP36p/P36* during *in vitro* liver stage development, thereby aborting liver stage maturation and failing to establish and maintain a functional PVM during intra-hepatic infection.

4.1.3 High antibody titers but reduced longevity CD8$^+$ T cells in tKO immunization mice

Immunizations with all parasite strains induce profound IgG-antibody titers. In *ΔSLARP/P36p/P36*, *ΔP36p* and γ-WT-immunized mice the antibody titers were significantly higher than in *ΔSLARP*-immunized animals (**Fig. 11**). It has been argued that IgG-antibody responses to sporozoite proteins reflect former exposure (Offeddu *et al.*, 2012). Specific antibody titers can be used to predict vaccine intake and can serve as a biomarker. Hence, my results prove that IgG-antibodies only partially contribute to the overall protection in GAP-based vaccines. Corroborating this notion, CD8$^+$ T cell depleted but not CD4$^+$ or IgG1 antibodies depleted BALB/c mice abolished *P. yoelii* GAP-based vaccine induced protection (Tarun *et al.*, 2007). Although CD4$^+$ T cells and antibodies partially contribute to sterile protection, vaccine-induced and liver-stage directed CD8$^+$ T cells are the major effector cell populations to elicit sterilizing immunity in different rodent models (Schmidt *et al.* 2010, Nganou-Makamdop *et al.*, 2012). Cytolytic CD8$^+$ T cells secreting interferon gamma (IFN-γ) were identified as the mediators of protection in a RAS-based immunization study (Schofield *et al.*, 1987, Weiss *et al.*, 1988, Romero *et al.*, 1989). Accordingly, my study focused on the analysis of CD8$^+$ T cell responses after immunization with *ΔSLARP/P36p/P36, ΔSLARP, ΔP36p/P36* and irradiated sporozoites. High parasite-specific IFN-γ *ex vivo* responses were detected, when stimulated with two different CD8$^+$

T cell epitopes (S20/TRAP). The level of IFN-γ secretion was slightly higher in *ΔSLARP/P36p/P36* and γ-WT-immunized mice compared to *ΔSLARP* and *ΔP36p/P36*. However, *ΔSLARP/P36p/P36* failed to induce long-lasting $CD8^+$ T cell responses as numbers dropped sharply two months post infection, postulating that reduction in CD8+ T cells contributes to reduced efficacy of the *ΔSLARP/P36p/P36* vaccine (**Fig. 14**). Elevated levels of IFN-γ-secreting lymphocytes can be found in livers compared to spleens, indicating that cellular immune responses occur to a higher extent in the sporozoite target organ (Nganou-Makamdop *et al.*, 2012, Haussig *et al.*, 2014). It should be noted that vaccine-induced memory $CD8^+$ T cells are required but not sufficient to induce sterile protection (Schmidt *et al.*, 2010). Several studies observed that efficient priming is a complex interplay between immune cells and different immune dominant organs. It is likely that cross-presentation by dendritic cells (DCs) in spleen and liver plays a major role in sufficient priming against hepatic infections. However, details of underlying immune processes to eliminate infective parasites remain elusive. Further studies need to clarify which immune processes contribute to reduced efficacy of this triple KO GAP-based vaccine.

Concluding, *ΔSLARP/P36p/P36* is a safe vaccine candidate but fails to induce sterile protection likely due to decreased hepatocyte infections, failure in growth, maintenance of intra-hepatic stages and insufficient maintenance of long-term IFN-γ producing $CD8^+$ T cells. Based on inferior protection in *ΔSLARP/P36p/P36*-immunized cohorts, I conclude that an immunization with *ΔSLARP* parasites only provides similar results as immunization with *ΔSLARP/P36p/P36*, hence, knocking out *P36p/P36* does not contribute to vaccine efficacy. My results underscore the importance of pre-clinical studies in the robust *P. berghei*/C75BL/6 vaccine model before translation to human clinical trials.

4.1.4 Conclusion and Outlook

GAP-based vaccines offer a tremendous potential for exploration of controlled stage arrest and immune responses. Whole sporozoite approaches enable antibody and T cell responses to a wide range of antigens compared to subunit vaccines, a prerequisite for potent immunity. Cellular responses are crucial for pathogen recognition, however, early arresting parasites do not trigger substantial immune responses. Establishing a robust cellular immune response might be the first step to develop an efficacious vaccine. Investigating tKO sporozoite infectivity and liver stage persistence *in vivo* by quantifying parasite burden in the liver of infected mice by qRT-PCR can provide an explanation for the paucity of protection in the tKO GAP vaccine. Further immune profiling of the tKO GAP in comparison to a late arresting GAP by examining liver stage specific peptide epitopes e.g. KB17, thereby exploring liver stage specific immune responses, might give insights into failure of this tKO GAP.

Parasites maturing into late liver stages are likely to induce greater quantity and breadth of antigen exposure and protect against sporozoite challenge. Generating further double or triple GAPs with a robust late stage arrest might increase sterile immunity in immunization/challenge studies. Potential candidates have been investigated, however it remains to be determined whether combination of two late arresting KO parasites would lead to complete liver stage arrest. A recent study tested a double KO of two late liver stage arresting parasite corroborating the notion that complete arrest can be achieved in the *P. yoelii*/BALB/c model, a parasite host combination where a complete arrest is easily achieved (Vaughan *et al.*, 2018). Further studies in the *P. berghei*/C57BL/6 model need to confirm this finding. Additionally, genetically engineering the parasite to enhanced parasite recognition by the host's immune system and in turn increase $CD8^+$ T cell priming in early liver stages is another promising strategy.

In conclusion, transition of suitable vaccine candidates from the established mouse models *P. berghei* and *P. yoelii* to the human strain *P. falciparum* remains challenging. My work demonstrates that small scale pre-clinical studies can evaluate vaccine safety and efficacy, thereby deciphering underlying immune mechanisms for inducing sterile long-term protection. Ultimately, pre-clinical evaluations can warrant evidence-based design of a *P. falciparum* GAP vaccine before translation to extensive and expensive human clinical trials.

4.2 Inducing PTEX-dependent export in liver stages for an improved malaria vaccine candidate

Plasmodium switches between intra- and extracellular developmental stages thereby avoiding host immune recognition. To impede pathogen recognition, parasites replicate inside a PV for intracellular maturation. However, shielding themselves from their host cell leads to nutrient depletion, waste acquisition and splenic iRBC killing, thus parasites remodel their host cells to ensure efficient replication. As larger parasitic proteins are unable to cross nutrient channels in the PVM, a protein translocon (PTEX) is enabling protein export. Export is especially important and well understood during intra-erythrocytic maturation, enabling the parasite to avoid splenic killing by vascular sequestration of mature blood stage parasites. Surprisingly, during early intra-hepatic development one of the PTEX core components, the AAA^+ ATPase HSP101, is not expressed, raising the question whether protein export is feasible in early liver stages (Matz *et al.*, 2015). To determine whether HSP101 is the limiting factor for liver stage protein export, transgenic parasites constitutively or pre-erythrocytically overexpressing HSP101 were generated. Subsequent analysis of transgenic parasite life cycle progression and co-expression with PEXEL-reporter constructs gave insights into whether HSP101 overexpression interferes with parasites' life cycle, how HSP101 contributes to liver stage export and if immunizations with

parasites potentially harboring a functional liver stage PTEX-dependent export machinery leads to protective immune responses due to increased parasite recognition.

4.2.1 Normal life cycle development of parasites with constitutively weak to moderate HSP101 overexpression

This study provides compelling evidence that constitutive low overexpression of HSP101 does not interfere with *P. berghei* life cycle progression. Analysis of *HSP101+*, a transgenic line constitutively overexpressing *HSP101* under the control of *EF1α* promoter, revealed HSP101 expression in oocysts, sporozoites and asexual blood stages. Endogenous HSP101 localizes to the PVM during blood stage development to form a protein translocon (PTEX). Live imaging of immunofluorescencely tagged transgenic HSP101 in gametocytes confirmed localization to the parasite's PV, whereas localization in rings and trophozoites were observed throughout the whole parasites. One plausible explanation is that EF1α promoter activity peaks in trophozoites (Otto *et al.*, 2014), enabling translation of HSP101 for later stages. Thus, these findings suggest no interference of transgenic HSP101 in pre-hepatic stages, hence, enabling WT-like life cycle progression.

To characterize intra-hepatic development, mice were infected with transgenic sporozoites. *In vivo* infections demonstrated one day delay in pre-patency for *HSP101+* and half a day delay for *HSP101++*, parasites expressing HSP101 under the regulation of PTEX150 promoter. Similarly, subsequent blood stage growth started delayed and therefore parasitemia remained lower, however slope analysis demonstrated no significant differences in growth rate. Thus, it can be postulated that intra-hepatic growth is minorly affected whereas blood stage development remains unaffected by HSP101 overexpression (**Fig. 18**). This notion was strengthened by parasite loads of infected mouse livers, which were slightly higher at 48 hours post infection in *HSP101+* than WT infected cohorts. As budding of merozoite-filled merosomes initiates as early as 48 hours post infection in WT parasites (Khan & Vanderberg, 1991), slightly higher parasite load in *HSP101+* infected mice could indicate a delay in maturation and budding of merosomes leading to the observed delay in pre-patency. Notably, the delay in pre-patency influences disease outcome as *HSP101+* animals had a reduced risk of ECM development. In contrast, *HSP101++* infected animals harbored the same risk of acquiring ECM as WT infected mice. Pinpointing the cause of severe and cerebral malaria has been challenging (Cunnington *et al.*, 2013) and animal models fail to mimic human severe malaria cases (Craig *et al.*, 2012). However, high parasite biomass is predicted to be the dominant cause of severe malaria. High biomass is caused by parasite replication and sequestration, a vicious cycle increasing parasite vascular adherence. In the brain this can lead to microvascular obstruction and endothelial dysfunction, which in turn

increases the risk of CM development (Cunnington *et al.*, 2013). Taken together, these findings suggest an effect of HSP101 overexpression on efficient intra-hepatic development, thereby influencing severity of disease outcome. Whether this is actually caused by HSP101 overexpression itself or subsequent up- or downregulation or obstruction of other liver stage proteins remains to be determined.

In vivo data of *HSP101*+ and *HSP101*++ demonstrated that HSP101 overexpression plays a critical role during intra-hepatic development. To examine liver stage maturation and exo-erythrocytic *HSP101* overexpression, *in vitro HSP101*+ and *HSP101*++ hepatoma cell infections were analyzed. WT-like liver stage development was observed for *HSP101*+ and *HSP101*++ (**Fig. 20**), postulating that liver stage maturation is not affected *in vitro*. *HSP101*+ parasites revealed HSP101 expression, however, the mCherry tag signal in the PV was weak (**Fig. 20A**), questioning if reconstruction of the machinery is feasible. As *HSP101*++ parasites lack a tagged version of HSP101, mRNA levels confirmed increased liver *HSP101* transcription (**Fig. 19**), however, whether HSP101 localizes to the PV remains to be determined. Liver stage maturation is tightly linked to PVM establishment, remodeling and maintenance. Parasites lacking P36p/P36, proteins important for PVM formation, or UIS4, protein important for PVM remodeling, arrest early during liver stage development (Mueller *et al.*, 2005, van Dijk *et al.*, 2005). To exclude obstruction of PVM establishment, immunofluorescence assays were used to determine UIS4 expression in *HSP101*+ and *HSP101*++ parasites. UIS4 was observed in the PV of *HSP101*+ and *HSP101*++ parasites throughout liver maturation, thereby suggesting presence of a remodeled PVM. Collectively, transgenic parasites display UIS4 and HSP101 expression in liver stages with localization to the PV, thereby ruling out developmental delays due to lack of PV formation and promising PTEX reconstruction feasibility, respectively.

Taking advantage of pathogen stage conversion for immunization strategies is one way to attack the parasite at its developmental bottleneck. Studies have shown that superior immunity can be achieved by a developmental arrest shortly before liver-to-blood stage conversion, as a bigger and broader array of antigens is presented compared to early arresting GAPs. Induction of memory $CD8^+$ T cells is increased by antigen presentation via the hepatocyte MHCI pathway and parasite antigen release is increased in later liver stages (Butler *et al.*, 2011). Therefore, pre-clinical immunization and challenge studies were performed to answer the question whether transgenic parasites overexpressing HSP101 can elicit stronger host immune responses due to increased parasite recognition. Prime/boost immunizations with *HSP101*+ and *HSP101*++ parasites attenuated with AZ elicited decreased protection to WT sporozoite challenges 87 and 260 days post immunization compared to standard γ-WT or WT under AZ cover immunized control mice (**Fig. 21** and **Fig. 30**). In contrast, prime and two booster immunizations with a late arresting

overexpression GAP *pdh_E1_PFO$_{LS}$*, deficient of pyruvate dehydrogenase E1 alpha subunit, thus arresting late, while simultaneously expressing the pore forming bacterial toxin cholesterol-dependent cytolysin perfringolysin O, elicited complete long term protection in C57BL/6 mice (Nagel *et al.*, 2013). Perfringolysin O expression induced premature PVM rupture roughly 30 hours post infection (Nagel *et al.*, 2013) allowing parasite antigen exposure to the host cell cytoplasm, arguing for an increased $CD8^+$ T cell response. While it cannot be excluded that three immunization doses lead to better protection, it remains elusive why *HSP101+* and *HSP101++* fail to induce potent protection. An intriguing possibility could be the failure to reconstruct a functional protein translocon.

4.2.2 Absence of PEXEL-dependent export in *HSP101+* and *HSP101++* liver stages

To investigate the export potential of these transgenic parasite lines, the expression of a PEXEL-mCherry reporter protein under the control of liver (*UIS4*) and liver/blood (*IBIS*) stage promoters (Josephine Grützke. MPIIB, PhD Thesis 2015) in *HSP101+* and *HSP101++* was analyzed. Live imaging of liver stage maturation in parasites overexpressing both, HSP101 and mCherry-PEXEL, *in vitro* revealed confined mCherry signal in the parasite PV and absence of mCherry in the host cell cytoplasm, concluding that transgenic parasites were not able to restore the PEXEL-dependent export machinery in liver stages (**Fig. 30**). Four possible reasons could contribute to absence of efficient export upon HSP101 expression.

First, signatures of export-determined proteins, except of the apparent PEXEL, remain poorly understood (Spielmann & Gilberger, 2015). Indeed, it is not clear whether blood stage PEXEL sequences efficiently label proteins for liver stage export. Grützke *et al.* showed blood stage export of reporter constructs used in this study, but failed to demonstrate mCherry export in WT liver stage parasites (Josephine Grützke, MPIIB, PhD Thesis 2015). This raises the question whether PEXEL sequences of blood stage proteins, as seen in *IBIS-PEXEL*, are efficient in liver stage export. To clarify this notion, an unconventional PEXEL sequence of CSP, a sporozoite surface antigen, linked to mCherry was analyzed for its liver stage export potential, however CS-PEXEL-mCh remained confined to the PV of the parasite (**Fig. 22B**). Similarly, endogenous CSP was not detected in the host cell cytoplasm at 4 hours post *HSP101+* infection (**Fig. 22C**). These findings vary from results observed by Singh *et al.* where CSP was exported to the host's cytoplasm and nucleus 2-6 hours post infection (Singh *et al.*, 2007). However, these findings remain controversial, as CSP might be already released during sporozoite entry and not through protein export, which is corroborated by the notion that CSP is constantly shed during sporozoite transmigration (Singh *et al.*, 2007, Cockburn *et al.*, 2011). It remains to be determined whether CSP PEXEL induces export in a PEXEL-dependent manner. As of now, LISP2 remains the only liver stage protein reported to translocate during early (~36 hours p.i.) liver stage

development. In contrast to other PEXEL-proteins, C-terminal mCherry tagging of LISP2 lead to accumulation of mCherry in the PV, suggesting C-terminal processing of LISP2 (Orito *et al.*, 2013). Recent sequence analysis revealed two PEXEL motives one at the N-terminal and another at the C-terminal end confirming earlier findings of dual processing of LISP2 by Orito *et al.* (personal communication Melanie Shears, John Hopkins School of Medicine, Baltimore). In perspective, discovery of liver stage export signals might help to define the liver stage exportome.

Second, in other infectious organisms, protein translocons fail to export larger stably folded proteins, therefore limiting translocation. Bacterial type III secretion system fail to translocate stably folded fluorescent proteins (Akeda & Galan, 2005). In this study reporter constructs harbored a PEXEL linked to mCherry (**Table 3**), which is a stably folded and large tag, potentially limiting export of the reporter constructs. Arguing against this hypothesis is an observation made by Grützke *et al.* where reporter constructs were translocated during blood stage development (Josephine Grützke, MPIIB, PhD Thesis 2015). Moreover, accumulation of *CS-PEXEL-OVA*, a smaller protein, in liver stage PVs was observed in *HSP101+* and WT parasites (**Table 3**) (Montagna *et al.*, 2014), Collectively, these findings could indicate absence of a functional PTEX translocon in general and enough quantity of PV resident transgenic HSP101 in particular, as decreased HSP101 levels blocked export and led to vascular accumulation of proteins in blood stages (Beck *et al.*, 2014, Elsworth *et al.*, 2014).

Third, PV and PVM make-up could play an essential role in protein export. Previous studies have established a model of regional PV export protein storage (Bullen *et al.*, 2012). These export areas localise to bulgy PV regions, which are defined by PTEX assembly which in turn might be initiated by host cell determined EXP2 localization (Meibalan *et al.*, 2015, de Koning-Ward *et al.*, 2016). Results of the current study demonstrate accumulation of mCherry signal in bulgy liver PV compartments (**Fig. 22B**), whether these are defined export areas remains to be determined. Corroborating this notion, proteins resistant to unfolding get trapped in loop-like PVM extensions in blood stages and unblocking the unfolding capacity only partially recovers protein export, as cargo remains spatially segregated from the export machinery (Charnaud *et al.*, 2018). Although PV localization of cargo proteins was observed in the current study, previously mentioned studies propose that proteins need to remain in defined export zones for efficient translocation, which might be determined by yet unknown proteins. Whether this complex system relies on further helper proteins, thereby raising the question whether these proteins are present in liver stages, remains to be determined.

Finally, PTEX assembly itself plays a major role in effective protein export. For example, C-terminal truncation of PTEX150, the linker between the pore spanning EXP2 and the AAA^+ ATPase HSP101, led to decrease in quantity of other PTEX components (Elsworth *et al.*, 2016),

suggesting complex destabilization. In comparison, in this study HSP101 was either C-terminally tagged by mCherry together with 3xMyc or 3xMyc alone (**Fig. 16A**), possibly interfering with correct protein folding. Indeed, recent structural analysis of PTEX complex assembly revealed stable binding of EXP2 protomer to the C-terminal ends of the HSP101 protomer, thereby placing the HSP101 cargo tunnel directly on top of the EXP2-PTEX150 pore (Ho *et al.*, 2018). This suggests that interfering with the HSP101 C-terminus and in consequence with correct protein folding may prevent PTEX assembly, as incomplete or unstable complex assembly has been proposed to inhibit protein translocon activity (de Koning-Ward *et al.*, 2016, Gilson *et al.*, 2017). Combined with the proposed paucity of a functional PTEX assembly, it remains unclear if further proteins are essential in export and whether these proteins are present in liver stages. Parasites lacking TRX2 or PTEX88 were able to undergo cell cycle progression, suggesting only a minor role in protein export (Matz *et al.*, 2013). Similarly, host cell chaperons are postulated to play a role in active protein translocation (Gilson *et al.*, 2017). Further studies will need to confirm the role of host cell proteins in export and whether they are present in liver stages. Although HSP101 expression was achieved in *HSP101*+ and *HSP101*++ parasites (**Fig. 20**), *EF1α* and *PTEX150* are only weak promoters during liver stage development, hence, limiting HSP101 availability for PTEX formation. Ho *et al.* indicate that six HSP101 protomers are required for each complex and that a stoichiometry of 6:7:7 (HSP101-PTEX150-EXP2) is a prerequisite for functional PTEX assembly (Ho *et al.*, 2018). This suggests that HSP101 might not be expressed in the right stoichiometric ratios in *HSP101*+ and *HSP101*++ parasites to form the complex at the liver stage PVM.

Concluding, *HSP101*+ and *HSP101*++ fail to translocate proteins in liver stages either due to deficiencies in reporter constructs or correct complex assembly in defined export areas. Learning from other infectious agents is difficult, but orthologues of EXP2 can be found in other Apicomplexa and HSP101 belongs to the well-studied 1 Clp/AAA$^+$ ATPases, with a conserved role in unfolding proteins (Ho *et al.*, 2018). However, as PTEX150 is unique to *Plasmodium* the PTEX export machinery remains unique to *Plasmodium* species as well. These results warrant further work to identify potential liver stage export signals, define involvement of PTEX in liver stage export and characterize the liver stage exportome by proteomic approaches.

4.2.3 Abort of pre-erythrocytic development in strong HSP101 overexpressing parasites

So far, it cannot be ascertained whether HSP101 is the limiting factor in liver stage export. Based on the poor export potential of low HSP101 overexpression lines, another HSP101 high overexpression parasite, *HSP101*+++, was generated, which expresses HSP101 under the control

of the pre-erythrocytic specific *UIS4* promoter. In contrast to *HSP101*+ and *HSP101*++, *HSP101*+++ fully arrests during liver stage development *in vivo* and *in vitro* (**Fig. 24A** and **Fig. 27A**). This notion was confirmed in dramatically reduced parasite loads in mouse livers 48 hours post infection, which in turn indicates poor sporozoite infectivity or early arrest of parasite liver development. However, pre-patency of *HSP101*+++*Myc* was not in line with the mCherry tagged *HSP101*+++ as blood stage infections were observed in 40% of the infected animals. It should be considered that larger and smaller protein tags might influence HSP101 folding and in turn can influence PTEX assembly. As mentioned earlier, folded cargo blocks export and nutrient channels if not deposited into tubular extensions of the PV (Charnaud *et al.*, 2018). This argues against mCherry as a functional tag for HSP101. However, endogenously mCherry tagged HSP101 maintained protein translocon activity in blood stages. As HSP101 is essential in blood stages and refractory to deletion (Matz *et al.*, 2015), an endogenously mCherry tagged HSP101 would not have been doable if mCherry influences HSP101 folding. This discrepancy in successful exo-eryhtrocytic development between low and high overexpression indicates that HSP101 expression is tightly controlled in pre-erythrocytic stages to ensure parasite development.

Reduced parasite burden in mouse livers is associated with reduced liver infection, suggesting reduced biomass per parasite, an indicator of early liver stage arrest, or poor sporozoite infectivity. Quantitative analysis of *P. yoelii* versus *P. berghei* infectivity confirmed superior infectivity of *P. yoelii* sporozoites in C57BL/6, leading to increased intra-hepatic development and a higher detected parasite biomass (Briones *et al.*, 1996). The reduced parasite burden in the *HSP101*+++ infected liver points towards decreased sporozoite infectivity. Upon sporozoite injection during an infectious mosquito bite, sporozoites glide through the dermis to reach the closest blood vessel. Efficient gliding is essential for reaching the liver and crossing the sinusoidal barrier (Frevert *et al.*, 2006). *HSP101*+++ and *HSP101*+++ *Myc* sporozoite gliding was drastically impaired (**Fig. 26** and **Fig. 30**). UIS4 expression is tightly controlled by cis-regulatory elements in its ORF, repressing protein synthesis until hepatocyte invasion. However, promoter activity peaks in salivary gland sporozoites enabling transcription and translation of target protein if not under the control of *UIS4* ORF elements (Silvie *et al.*, 2014). Thus, *HSP101*+++ parasites expressed high amounts of HSP101-mCh, which have a granular staining, suggesting localization to dense granules and organelles of the secretory pathway in sporozoites. This finding was corroborated by high endogenous *UIS4* mRNA levels in WT sporozoites and increased *HSP101* mRNA levels in *HSP101*+++ sporozoites (**Fig. 25B+C**.). On the one hand, large amounts of bulky proteins in dense granules could block the micronemal pathway. Indeed, obstruction of microneme secretion by cysteine protease inhibitors in *Toxoplasma gondii* impaired invasion and gliding motility of the parasite (Teo *et al.*, 2007). Conversely, localization of mCherry in

UIS4::mCh, parasites expressing similar amounts of mCherry compared to *HSP101*+++, was observed throughout the whole sporozoite without any granular pattern (**Fig. S8B**). In addition, haemocoel sporozoites, not expressing HSP101 as *UIS4* promoter only starts in salivary gland sporozoites, were motile, but *in vivo* infections with *HSP101*+++ haemocoel sporozoites failed to induce patent blood stage infections whereas infections with *USI4::mCh* lead to WT-like blood stage pre-patency (**Fig. S8** and **Fig. S9**). These results demonstrate that overexpression of mCherry is not the cause for impaired motility. Gliding experiments of *HSP101*+++ with addition of ATP and glutamine, to compensate potential overuse of ATP by the triple ATP HSP101, reversed gliding ability of *HSP101*+++ sporozoites, but still arrested during liver stage development *in vitro* (**Fig. S9**). Based on these observations HSP101 overexpression must account for the gliding defect. On the other hand, mislocalization of HSP101 might be the key mediator of gliding disability. Tagging of endogenous HSP101 revealed localization to the sporozoite's apical end (Matz *et al.*, 2015). One characteristic of gliding motility is the discharge of micronemes from the apical end of the parasite. Micronemal proteins can in turn be driven towards the parasite's exterior end where these proteins act on the actomyosin system (Stewart & Vanderberg, 1991, Gantt *et al.*, 2000, Ono *et al.*, 2008, Tardieux & Baum, 2016). Indeed, parasites deficient of adenylyl cyclase, an enzyme driving cAMP synthesis which in turn mediates microneme discharge, showed an bisected infectivity (Ono *et al.*, 2008). In particular, the well-described sporozoite surface proteins CSP and TRAP play a major role in hepatocyte adhesion and invasion (Mota & Rodriguez, 2002). These findings indicate the importance for controlled microneme discharge during sporozoite gliding. Whether HSP101 localization to the apical end of the sporozoite is essential for gliding, thereby pinpointing the defect seen in *HSP101*+++ parasites, remains elusive.

To test whether the defect in motility correlates with reduced transmigration and infectivity of hepatoma cells, *in vitro* transmigration, cell invasion and liver growth was analyzed. Transmigration efficiency was reduced in *HSP101*+++ parasites, but in contrast to gliding only a quarter of sporozoites were affected. Similarly, sporozoite infectivity, measured by percentage of extra- and intracellular parasites two hours post infections, revealed only a trend towards fewer numbers of intracellular parasites (**Fig. 30**). One plausible explanation is that *in vitro* observations of transmigration and sporozoite infection can differ from results obtained from *in vivo* experiments. *In vivo* to *in vitro* comparison of parasites deficient of *HSP20*, a small heat shock protein that plays a role in *Plasmodium* motility, supports this idea as only 50% of mice infected with *ΔHSP20* developed a blood stage infection, but *in vitro* EEF numbers remained similar to WT (Montagna *et al.*, 2012). Infected hepatoma cells are centrifuged to ensure sufficient sporozoite entry, as infection rate of hepatoma cells *in vitro* is generally below 10%. This could limit the observed motility defect in *HSP101*+++ to cell adhesion and entry in *in vitro*

hepatoma cell infection (**Fig. 26**). Nevertheless, failure to induce a potent blood stage infection *in vivo* raises the possibility of a second defect of *HSP101*+++ in liver development.

Parasite replication in hepatocytes is a prerequisite for onset of blood stage infection. In line with the *in vivo* results of an absent blood stage infection after *HSP101*+++ sporozoite infection, *in vitro* exo-erythrocytic growth beyond 24 hours post infection was not observed in *HSP101*+++ infected hepatoma cells (**Fig. 27** and **Fig. 30**). In line with the observed *in vivo* pre-patency of HSP101+++Myc, *in vitro* infections had a number of parasites that grew beyond 24 hours of infection. Whether these results correlate with *in vivo* data or confirm previous assumptions that *in vitro* out-scale *in vivo* infections needs to be determined. As rhoptry and micronemal release, a prerequisite for proper PVM formation (Counihan *et al.*, 2013), might be obstructed in *HSP101*+++, immunofluorescence assays were used to ensure presence of UIS4, a PVM residual protein, and LC3, a host autophagy marker labelling the PVM (Mueller *et al.*, 2005, Wacker *et al.*, 2017). UIS4 was observed in all stages during liver maturation and LC3 up to 24h post infection, thereby confirming presence of a remodeled PVM in *HSP101*+++ parasites. Additional analysis of an intact *UIS4* locus and WT-like mRNA levels ruled out accidental *ΔUIS4* parasite generation, as *HSP101*+++ parasites displayed a similar phenotype to *ΔUIS4* parasites (Mueller *et al.*, 2005). Transgenic HSP101 expression was confirmed by mCherry detection in IFAs of liver stage parasites, but localization to the PVM was only partially observed (**Fig. 28**). In particular, later stages displayed a "blown up" vacuole whith HSP101 localization to distinct areas. One possible reason for parasite arrest could be the excessive use of ATP due to overexpression of the ATPase HSP101. Assays with supplemented ATP and glutamine could not reverse the observed phenotype, ruling out overuse of ATP from the AAA^+ ATPase HSP101. Recent studies reported that proper assembly of PTEX is important for its functionality (Ho *et al.*, 2018). Corroborating this notion, absence of HSP101 in blood stages leads to cargo accumulation in the PV (Beck *et al.*, 2014), which in turn can impede parasites to pass cell cycle check points and lead to parasite growth arrest (de Koning-Ward *et al.*, 2016). Although not yet supported by data, it is tempting to speculate that misfolded mCherry-tagged HSP101 might bind incorrectly to EXP2 nutrient channels, thereby blocking nutrient uptake and waste disposal and in turn leading to toxification of the parasite.

The complete liver stage arrest of *HSP101*+++ warrants further studies on its potential as a GAP-based vaccine. Prime/boost immunizations with a high dose of *HSP101*+++ elicited weak protection against WT follow-up infections 87 or 260 days post immunizations (**Fig. 29** and **Table 5**). Several lines of evidence strongly support that sporozoite infectivity and liver stage growth and persistence are prerequisite for potent immunity (Scheller & Azad, 1995, Mueller *et al.*, 2007, Putrianti *et al.*, 2009). Consistent with these studies, *HSP101*+++ parasite burden in the

liver was extremely reduced and parasites arrested early during liver development, thereby limiting the priming phase of $CD8^+$ T cells and therefore, *HSP101+++* does not meet the prerequisites of a successful GAP vaccine candidate. Notably, *HSP101+++ Myc* immunizations elicited better protection in agreement with increased liver stage development. Thus, *HSP101+++* immunizations stretch one more time the importance of sporozoite infectivity and liver persistence for efficient immunity against *P. berghei* infections.

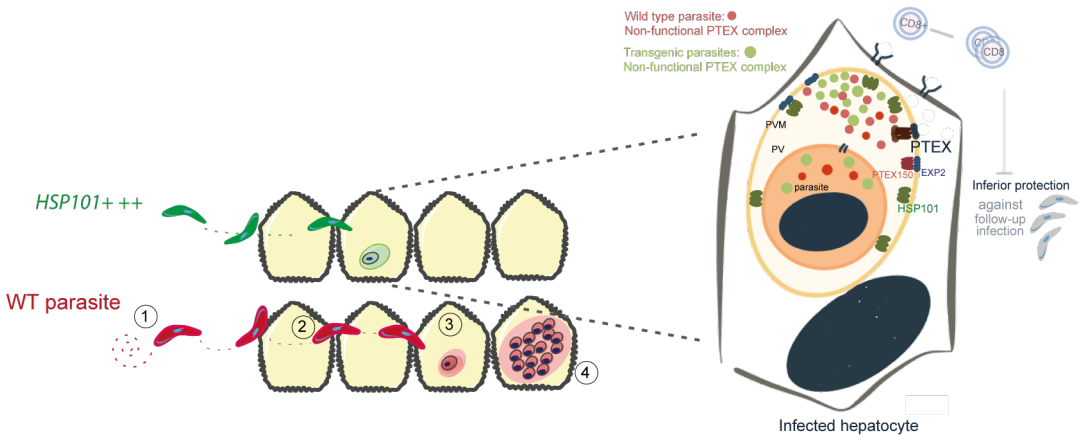

Figure 30 HSP101 overexpressing parasites abort pre-erythrocytic development and lack PTEX-dependent export in liver stages

Conclusion of the results observed in this study. Parasites (red) glide through the dermis to reach the next blood vessel (1). Parasites strongly overexpressing HSP101 (*HSP101+++*, green) are impaired in their gliding ability. Motile sporozoites (red) attach and transmigrate through liver cells (2) until they reach a final target cell to invade and mature (3) and mature into merosomes harboring thousands of merozoites (4). *HSP101+++* parasites (green) are affected in their attachment and gliding (2) ability and completely abort liver stage development right after hepatocyte infection (3). Depicted is an early hepatocyte infection with a HSP101 overexpressing parasite. HSP101 is expressed and localizes to the PV but the export of proteins is absent, probably due to HSP101 misfolding, thereby obstructing proper PTEX assembly. Accumulation of export destined proteins in defined export areas and miss assembly of EXP2 and HSP101 might account for failure of PTEX-dependent export. Obstruction of parasite nutrient channels by cargo proteins and misfolded HSP101 blocking EXP2 might lead to the liver stage abort of *HSP101+++*. Therefore, parasite recognition is not increased in HSP101 overexpressing parasites and immunizations with these parasites lead to inferior protection (for *HSP101+* and *HSP101++*) and absence of protection (for *HSP101+++*). (several modified pictures from Smart, servier medical art)

In conclusion, my results demonstrate that strong overexpression interferes with the parasite life cycle at its pre-erythrocytic stage, thereby preventing patent blood stage infections. This study on efficient HSP101 overexpression in liver stages does not reveal reconstruction of PTEX and PEXEL-dependent export, suggesting that HSP101 is not the limiting factor for liver stage export. In line with these findings, immunizations with transgenic strong HSP101 overexpressing parasites fail to elicit potent immunity against *Plasmodium* infections, in contrast to late stage arresting GAPs that manage to induce potent protection due to increased antigen presentation. This suggests that parasites tightly control HSP101 expression in pre-erythrocytic stages to maintain life cycle progression and avoid parasite recognition by the host.

4.2.4 Conclusion and Outlook

HSP101+ and *HSP101*++ parasites are able to complete the *Plasmodium* life cycle with only minor delays in pre-patency. However, subsequent exploration of export potential led to reporter construct confinement in the parasites' PV. Of outmost importance is to confirm PTEX reconstruction. Co-localization experiments with EXP2 and PTEX150 antibodies would confirm presence of core components in distinct PV export areas. In particular, Immunoprecipitation (IP) assays with HSP101-mCh can identify liver protein complexes formed with HSP101. However, EEF material is scarce and would not be sufficient for IP analysis. Parasites lacking HSP101 are not viable in blood stages (Matz *et al.*, 2015). Excising endogenous HSP101 in recycled *HSP101*+ (*HSP101*+ *rec*) while simultaneously inserting *IBIS::PEXEL-GFP/Myc* or *IBIS::GFP/Myc* (**Table S4**), can give insights into functionality of transgenic HSP101. Survival of the *ΔHSP101/HSP101+/IBIS::(PEXEL)-GFP/Myc* parasites will indicate efficient rescue by assembly of the complex. Export of *PEXEL-GFP/Myc* compared to the controls (GFP or Myc only) will serve as an indicator for a functional PTEX complex as well as the necessity of the PEXEL motive to target proteins for export.

Additionally, intermediate liver HSP101 overexpression, higher than *HSP101*++ and lower than *HSP101*+++, might circumvent stoichiometric complications of low levels or toxic effects of high levels of HSP101. Parasites with moderate HSP101 levels (*EXP2::HSP101*) were generated in a follow up study on this thesis and preliminary data suggest no phenotypic differences in life cycle progression (**Table S4).** Exploration of different promoters e.g. *HSP70* or *LISP2* or tags e.g. HA or FLAG for liver HSP101 expression (**Table S4**), might contribute to define mechanisms of tightly controlled HSP101 expression in liver stages.

The core components EXP2, PTEX150 and HSP101 are essential for PTEX assembly and parasite survival (de Koning-Ward *et al.*, 2009, Matz *et al.*, 2015). qRT-PCR revealed elevated mRNA levels of EXP2, but only intermediate levels for PTEX150 during liver maturation. Attempts to C-terminally tag PTEX150 in *P. berghei* and confirm protein presence remained unsuccessful. Despite successful C-terminal tagging of PTEX150 in *P. falciparum*, recent studies demonstrated that the C-terminus of PTEX150 extends in a claw-like structure to the ATPase and unfolding domain of HSP101 (Ho *et al.*, 2018), explaining loss of stable PTEX assembly upon PTEX150 C-terminal tagging. To confirm expression of PTEX150 in liver stages, N-terminal tagging with mCherry or HA can be applied to assure PV localization (**Table S4**). PTEX150 mRNA levels are reduced in intra-hepatic development compared to EXP2, whether this could have influence on stoichiometric 6:7:7 PTEX assembly needs to be determined. In case of translational repression of PTEX150, complex assembly would not be feasible by merely overexpressing HSP101. Following these assumptions, *HSP101* overexpression parasites can be modified to additionally overexpress

PTEX150 in liver stages (**Table S4**). Such parasites can provide a better understanding of liver stage protein export and identification of prerequisites for PTEX assembly.

mCherry accumulation, as seen in bacteria for type III secretion systems (Akeda & Galan, 2005), could obstruct additional liver stage protein export. Using smaller tags as FLAG or HA can circumvent protein accumulation in the PV. Potentially, this concept of reporter constructs does not allow protein detection in the cytoplasm as only limited amount of protein can be exported and might be degraded upon host cell arrival. Applying a GFP split in two spatially separated compartments and signal detection only upon concurrence, could enable detection of protein translocation (Cabantous *et al.*, 2005, Paulmurugan & Gambhir, 2005). Integration of one GFP half in hepatoma cells and the other half fused to PEXEL in parasites for targeted liver stage export, could enable detection of GFP signal only upon translocation of parasitic GFP half. LISP2 is the only reported liver protein to be exported around 36 hours post infection. In contrast to blood stage PEXEL proteins, it is additionally processed at the C-terminal end (Orito *et al.*, 2013). Designing a reporter construct with a tagged LISP2 could reveal whether *HSP101*+ and *HSP101*++ parasites export LISP2 at earlier time points during liver stage maturation. Additional antibodies against LISP2 would simplify this approach.

HSP101+++ parasites have an astonishing phenotype as HSP101 overexpression leads to a sporozoite gliding defect and liver stage developmental arrest. It can be hypothesized that localization to secretory organelles interferes with gliding motility. Co-localization with micronemal, rhoptry or dense granule proteins would confirm this notion. IPs with HSP101 could reveal protein-protein interactions and potentially answer whether obstruction of microneme release is induced by overexpression.

In order to gain a better immunological understanding of protective immune responses as opposed to parasite recognition, pre-clinical analysis and comparative immune profiling of *HSP101*+++ are currently performed as follow up work of this thesis. Sterile protection seems to be correlated to parasite development in the liver. *HSP101*+++, however, arrest early in liver stage development leading to the expected weaker protection. Markers of protection were identified, but are primarily sporozoite antigens (Hafalla *et al.*, 2011).

To investigate whether *HSP101*+ exports antigens into the hepatocyte cytoplasm *in vivo* and just simply lacks detection *in vitro*, thereby inducing an even stronger immune response, *HSP101*+ parasites can be crossed with parasites expressing OVA or TRAP linked to PEXEL in liver stages (**Table S4**). The CD8 epitopes of these two proteins are known to elicit strong immune responses in the host. Similarly, immunization studies can be performed with these parasite lines and liver load and T cell priming of infected animals can be analyzed. The OVA epitope will allow the use and analysis of $OVA_{SIINFEKL}$ recognising OT-1 transgenic $CD8^+$ T cells.

Concluding, PTEX cannot be reconstructed solely by overexpressing HSP101, but rather leads to obstruction of parasite life cycle progression and reduced parasite recognition. My work demonstrates that liver stage pathogen-host interaction remains relatively poorly understood and that parasites tightly control protein export, potentially to remain undetected during liver development. Ultimately, deciphering important factors for parasite replication and host-parasite interaction during liver maturation can give novel ideas for preventive vaccine candidates.

References

Ahmed MA & Cox-Singh J (2015) *Plasmodium knowlesi* - an emerging pathogen. *ISBT science series* **10**: 134-140.

Akeda Y & Galan JE (2005) Chaperone release and unfolding of substrates in type III secretion. *Nature* **437**: 911-915.

Aly AS, Mikolajczak SA, Rivera HS, Camargo N, Jacobs-Lorena V, Labaied M, Coppens I & Kappe SH (2008) Targeted deletion of SAP1 abolishes the expression of infectivity factors necessary for successful malaria parasite liver infection. *Molecular microbiology* **69**: 152-163.

Amino R, Giovannini D, Thiberge S, Gueirard P, Boisson B, Dubremetz JF, Prevost MC, Ishino T, Yuda M & Menard R (2008) Host cell traversal is important for progression of the malaria parasite through the dermis to the liver. *Cell host & microbe* **3**: 88-96.

Annoura T, Ploemen IH, van Schaijk BC*, et al.* (2012) Assessing the adequacy of attenuation of genetically modified malaria parasite vaccine candidates. *Vaccine* **30**: 2662-2670.

Annoura T, van Schaijk BC, Ploemen IH*, et al.* (2014) Two *Plasmodium* 6-Cys family-related proteins have distinct and critical roles in liver-stage development. *FASEB journal : official publication of the Federation of American Societies for Experimental Biology* **28**: 2158-2170.

Ansari HR, Templeton TJ, Subudhi AK*, et al.* (2016) Genome-scale comparison of expanded gene families in *Plasmodium* ovale wallikeri and *Plasmodium* ovale curtisi with *Plasmodium* malariae and with other *Plasmodium* species. *International journal for parasitology* **46**: 685-696.

Baer K, Roosevelt M, Clarkson AB, Jr., van Rooijen N, Schnieder T & Frevert U (2007) Kupffer cells are obligatory for *Plasmodium yoelii* sporozoite infection of the liver. *Cellular microbiology* **9**: 397-412.

Balam S, Romero JF, Bongfen SE, Guillaume P & Corradin G (2012) CSP--a model for in vivo presentation of *Plasmodium berghei* sporozoite antigens by hepatocytes. *PloS one* **7**: e51875.

Beck JR, Muralidharan V, Oksman A & Goldberg DE (2014) PTEX component HSP101 mediates export of diverse malaria effectors into host erythrocytes. *Nature* **511**: 592-595.

Belnoue E, Costa FT, Frankenberg T, Vigario AM, Voza T, Leroy N, Rodrigues MM, Landau I, Snounou G & Renia L (2004) Protective T cell immunity against malaria liver stage after vaccination with live sporozoites under chloroquine treatment. *Journal of immunology* **172**: 2487-2495.

Berendt AR, Simmons DL, Tansey J, Newbold CI & Marsh K (1989) Intercellular adhesion molecule-1 is an endothelial cell adhesion receptor for *Plasmodium* falciparum. *Nature* **341**: 57-59.

Bhanot P, Schauer K, Coppens I & Nussenzweig V (2005) A surface phospholipase is involved in the migration of *Plasmodium* sporozoites through cells. *The Journal of biological chemistry* **280**: 6752-6760.

Bijker EM, Bastiaens GJ, Teirlinck AC, *et al.* (2013) Protection against malaria after immunization by chloroquine prophylaxis and sporozoites is mediated by preerythrocytic immunity. *Proceedings of the National Academy of Sciences of the United States of America* **110**: 7862-7867.

Boddey JA & Cowman AF (2013) *Plasmodium* nesting: remaking the erythrocyte from the inside out. *Annual review of microbiology* **67**: 243-269.

Boddey JA, Moritz RL, Simpson RJ & Cowman AF (2009) Role of the *Plasmodium* export element in trafficking parasite proteins to the infected erythrocyte. *Traffic* **10**: 285-299.

Boddey JA, Carvalho TG, Hodder AN, Sargeant TJ, Sleebs BE, Marapana D, Lopaticki S, Nebl T & Cowman AF (2013) Role of plasmepsin V in export of diverse protein families from the *Plasmodium falciparum* exportome. *Traffic* **14**: 532-550.

Boddey JA, Hodder AN, Gunther S, *et al.* (2010) An aspartyl protease directs malaria effector proteins to the host cell. *Nature* **463**: 627-631.

Bongfen SE, Torgler R, Romero JF, Renia L & Corradin G (2007) *Plasmodium berghei*-infected primary hepatocytes process and present the circumsporozoite protein to specific CD8+ T cells in vitro. *Journal of immunology* **178**: 7054-7063.

Borrmann S & Matuschewski K (2011) Targeting *Plasmodium* liver stages: better late than never. *Trends in molecular medicine* **17**: 527-536.

Briones MR, Tsuji M & Nussenzweig V (1996) The large difference in infectivity for mice of *Plasmodium berghei* and *Plasmodium yoelii* sporozoites cannot be correlated with their ability to enter into hepatocytes. *Molecular and biochemical parasitology* **77**: 7-17.

Bull PC, Lowe BS, Kortok M, Molyneux CS, Newbold CI & Marsh K (1998) Parasite antigens on the infected red cell surface are targets for naturally acquired immunity to malaria. *Nature medicine* **4**: 358-360.

Bullen HE, Charnaud SC, Kalanon M, *et al.* (2012) Biosynthesis, localization, and macromolecular arrangement of the *Plasmodium falciparum* translocon of exported proteins (PTEX). *The Journal of biological chemistry* **287**: 7871-7884.

Burda PC, Caldelari R & Heussler VT (2017) Manipulation of the Host Cell Membrane during *Plasmodium* Liver Stage Egress. *mBio* **8**.

Burda PC, Roelli MA, Schaffner M, Khan SM, Janse CJ & Heussler VT (2015) A *Plasmodium* phospholipase is involved in disruption of the liver stage parasitophorous vacuole membrane. *PLoS pathogens* **11**: e1004760.

Butler NS, Vaughan AM, Harty JT & Kappe SH (2012) Whole parasite vaccination approaches for prevention of malaria infection. *Trends in immunology* **33**: 247-254.

Butler NS, Schmidt NW, Vaughan AM, Aly AS, Kappe SH & Harty JT (2011) Superior antimalarial immunity after vaccination with late liver stage-arresting genetically attenuated parasites. *Cell host & microbe* **9**: 451-462.

Cabantous S, Terwilliger TC & Waldo GS (2005) Protein tagging and detection with engineered self-assembling fragments of green fluorescent protein. *Nature biotechnology* **23**: 102-107.

Carvalho LH, Sano G, Hafalla JC, Morrot A, Curotto de Lafaille MA & Zavala F (2002) IL-4-secreting CD4+ T cells are crucial to the development of CD8+ T-cell responses against malaria liver stages. *Nature medicine* **8**: 166-170.

Chakravarty S, Baldeviano GC, Overstreet MG & Zavala F (2008) Effector CD8+ T lymphocytes against liver stages of *Plasmodium yoelii* do not require gamma interferon for antiparasite activity. *Infection and immunity* **76**: 3628-3631.

Chakravarty S, Cockburn IA, Kuk S, Overstreet MG, Sacci JB & Zavala F (2007) CD8+ T lymphocytes protective against malaria liver stages are primed in skin-draining lymph nodes. *Nature medicine* **13**: 1035-1041.

Chang HH, Falick AM, Carlton PM, Sedat JW, DeRisi JL & Marletta MA (2008) N-terminal processing of proteins exported by malaria parasites. *Molecular and biochemical parasitology* **160**: 107-115.

Charnaud SC, Jonsdottir TK, Sanders PR, *et al.* (2018) Spatial organization of protein export in malaria parasite blood stages. *Traffic* **19**: 605-623.

Chattopadhyay R, Conteh S, Li M, James ER, Epstein JE & Hoffman SL (2009) The Effects of radiation on the safety and protective efficacy of an attenuated *Plasmodium yoelii* sporozoite malaria vaccine. *Vaccine* **27**: 3675-3680.

Chen I, Clarke SE, Gosling R, Hamainza B, Killeen G, Magill A, O'Meara W, Price RN & Riley EM (2016) "Asymptomatic" Malaria: A Chronic and Debilitating Infection That Should Be Treated. *PLoS medicine* **13**: e1001942.

Chisholm SA, Kalanon M, Nebl T, Sanders PR, Matthews KM, Dickerman BK, Gilson PR & de Koning-Ward TF (2018) The malaria PTEX component PTEX88 interacts most closely with HSP101 at the host-parasite interface. *The FEBS journal* **285**: 2037-2055.

Chisholm SA, McHugh E, Lundie R, Dixon MW, Ghosh S, O'Keefe M, Tilley L, Kalanon M & de Koning-Ward TF (2016) Contrasting Inducible Knockdown of the Auxiliary PTEX Component PTEX88 in *P. falciparum* and P. *berghei* Unmasks a Role in Parasite Virulence. *PloS one* **11**: e0149296.

Clark IA & Vissel B (2017) The meteorology of cytokine storms, and the clinical usefulness of this knowledge. *Seminars in immunopathology* **39**: 505-516.

Clyde DF, Most H, McCarthy VC & Vanderberg JP (1973) Immunization of man against sporozite-induced *falciparum* malaria. *The American journal of the medical sciences* **266**: 169-177.

Cobb DW, Florentin A, Fierro MA, Krakowiak M, Moore JM & Muralidharan V (2017) The Exported Chaperone PfHsp70x Is Dispensable for the *Plasmodium falciparum* Intraerythrocytic Life Cycle. *mSphere* **2**.

Cobbold SA, Vaughan AM, Lewis IA, *et al.* (2013) Kinetic flux profiling elucidates two independent acetyl-CoA biosynthetic pathways in *Plasmodium falciparum*. *The Journal of biological chemistry* **288**: 36338-36350.

Cockburn IA, Tse SW, Radtke AJ, Srinivasan P, Chen YC, Sinnis P & Zavala F (2011) Dendritic cells and hepatocytes use distinct pathways to process protective antigen from *Plasmodium* in vivo. *PLoS pathogens* **7**: e1001318.

Cohen S, Mc GI & Carrington S (1961) Gamma-globulin and acquired immunity to human malaria. *Nature* **192**: 733-737.

Collins CR, Das S, Wong EH, Andenmatten N, Stallmach R, Hackett F, Herman JP, Muller S, Meissner M & Blackman MJ (2013) Robust inducible Cre recombinase activity in the human malaria parasite *Plasmodium falciparum* enables efficient gene deletion within a single asexual erythrocytic growth cycle. *Molecular microbiology* **88**: 687-701.

Conteh S, Anderson C, Lambert L, *et al.* (2017) Grammomys surdaster, the Natural Host for *Plasmodium berghei* Parasites, as a Model to Study Whole-Organism Vaccines Against Malaria. *The American journal of tropical medicine and hygiene* **96**: 835-841.

Cooney LA, Gupta M, Thomas S, *et al.* (2013) Short-lived effector CD8 T cells induced by genetically attenuated malaria parasite vaccination express CD11c. *Infection and immunity* **81**: 4171-4181.

Counihan NA, Kalanon M, Coppel RL & de Koning-Ward TF (2013) *Plasmodium* rhoptry proteins: why order is important. *Trends in parasitology* **29**: 228-236.

Cowman AF & Crabb BS (2006) Invasion of red blood cells by malaria parasites. *Cell* **124**: 755-766.

Crabb BS, Cooke BM, Reeder JC, Waller RF, Caruana SR, Davern KM, Wickham ME, Brown GV, Coppel RL & Cowman AF (1997) Targeted gene disruption shows that knobs enable malaria-infected red cells to cytoadhere under physiological shear stress. *Cell* **89**: 287-296.

Craig AG, Grau GE, Janse C, Kazura JW, Milner D, Barnwell JW, Turner G, Langhorne J & participants of the Hinxton Retreat meeting on Animal Models for Research on Severe M (2012) The role of animal models for research on severe malaria. *PLoS pathogens* **8**: e1002401.

Crispe IN, Giannandrea M, Klein I, John B, Sampson B & Wuensch S (2006) Cellular and molecular mechanisms of liver tolerance. *Immunological reviews* **213**: 101-118.

Cunnington AJ, Walther M & Riley EM (2013) Piecing together the puzzle of severe malaria. *Science translational medicine* **5**: 211ps218.

de Koning-Ward TF, Gilson PR & Crabb BS (2015) Advances in molecular genetic systems in malaria. *Nature reviews Microbiology* **13**: 373-387.

de Koning-Ward TF, Dixon MW, Tilley L & Gilson PR (2016) *Plasmodium* species: master renovators of their host cells. *Nature reviews Microbiology* **14**: 494-507.

de Koning-Ward TF, Gilson PR, Boddey JA, *et al.* (2009) A newly discovered protein export machine in malaria parasites. *Nature* **459**: 945-949.

Desai SA & Miller LH (2014) Malaria: Protein-export pathway illuminated. *Nature* **511**: 541-542.

Elsworth B, Sanders PR, Nebl T, *et al.* (2016) Proteomic analysis reveals novel proteins associated with the *Plasmodium* protein exporter PTEX and a loss of complex stability upon truncation of the core PTEX component, PTEX150. *Cellular microbiology* **18**: 1551-1569.

Elsworth B, Matthews K, Nie CQ, *et al.* (2014) PTEX is an essential nexus for protein export in malaria parasites. *Nature* **511**: 587-591.

Faye FB, Konate L, Rogier C & Trape JF (1998) *Plasmodium* ovale in a highly malaria endemic area of Senegal. *Transactions of the Royal Society of Tropical Medicine and Hygiene* **92**: 522-525.

Ferreira A, Schofield L, Enea V, Schellekens H, van der Meide P, Collins WE, Nussenzweig RS & Nussenzweig V (1986) Inhibition of development of exoerythrocytic forms of malaria parasites by gamma-interferon. *Science* **232**: 881-884.

Frevert U, Usynin I, Baer K & Klotz C (2006) Nomadic or sessile: can Kupffer cells function as portals for malaria sporozoites to the liver? *Cellular microbiology* **8**: 1537-1546.

Frevert U, Usynin I, Baer K & Klotz C (2008) *Plasmodium* sporozoite passage across the sinusoidal cell layer. *Sub-cellular biochemistry* **47**: 182-197.

Frevert U, Moreno A, Calvo-Calle JM, Klotz C & Nardin E (2009) Imaging effector functions of human cytotoxic CD4+ T cells specific for *Plasmodium falciparum* circumsporozoite protein. *International journal for parasitology* **39**: 119-132.

Friesen J & Matuschewski K (2011) Comparative efficacy of pre-erythrocytic whole organism vaccine strategies against the malaria parasite. *Vaccine* **29**: 7002-7008.

Friesen J, Silvie O, Putrianti ED, Hafalla JC, Matuschewski K & Borrmann S (2010) Natural immunization against malaria: causal prophylaxis with antibiotics. *Science translational medicine* **2**: 40ra49.

Gantt S, Persson C, Rose K, Birkett AJ, Abagyan R & Nussenzweig V (2000) Antibodies against thrombospondin-related anonymous protein do not inhibit *Plasmodium* sporozoite infectivity in vivo. *Infection and immunity* **68**: 3667-3673.

Garten M, Nasamu AS, Niles JC, Zimmerberg J, Goldberg DE & Beck JR (2018) EXP2 is a nutrient-permeable channel in the vacuolar membrane of *Plasmodium* and is essential for protein export via PTEX. *Nature microbiology* **3**: 1090-1098.

Ghorbal M, Gorman M, Macpherson CR, Martins RM, Scherf A & Lopez-Rubio JJ (2014) Genome editing in the human malaria parasite *Plasmodium falciparum* using the CRISPR-Cas9 system. *Nature biotechnology* **32**: 819-821.

Gilson PR, Chisholm SA, Crabb BS & de Koning-Ward TF (2017) Host cell remodelling in malaria parasites: a new pool of potential drug targets. *International journal for parasitology* **47**: 119-127.

Glenister FK, Coppel RL, Cowman AF, Mohandas N & Cooke BM (2002) Contribution of parasite proteins to altered mechanical properties of malaria-infected red blood cells. *Blood* **99**: 1060-1063.

Gruner AC, Mauduit M, Tewari R, *et al.* (2007) Sterile protection against malaria is independent of immune responses to the circumsporozoite protein. *PloS one* **2**: e1371.

Gruring C, Heiber A, Kruse F, *et al.* (2012) Uncovering common principles in protein export of malaria parasites. *Cell host & microbe* **12**: 717-729.

Guerin-Marchand C, Druilhe P, Galey B, Londono A, Patarapotikul J, Beaudoin RL, Dubeaux C, Tartar A, Mercereau-Puijalon O & Langsley G (1987) A liver-stage-specific antigen of *Plasmodium falciparum* characterized by gene cloning. *Nature* **329**: 164-167.

Guizetti J & Scherf A (2013) Silence, activate, poise and switch! Mechanisms of antigenic variation in *Plasmodium falciparum*. *Cellular microbiology* **15**: 718-726.

Guttery DS, Roques M, Holder AA & Tewari R (2015) Commit and Transmit: Molecular Players in *Plasmodium* Sexual Development and Zygote Differentiation. *Trends in parasitology* **31**: 676-685.

Gwadz RW, Cochrane AH, Nussenzweig V & Nussenzweig RS (1979) Preliminary studies on vaccination of rhesus monkeys with irradiated sporozoites of *Plasmodium knowlesi* and characterization of surface antigens of these parasites. *Bulletin of the World Health Organization* **57 Suppl 1**: 165-173.

Haase S, Herrmann S, Gruring C*, et al.* (2009) Sequence requirements for the export of the *Plasmodium falciparum* Maurer's clefts protein REX2. *Molecular microbiology* **71**: 1003-1017.

Hafalla JC, Silvie O & Matuschewski K (2011) Cell biology and immunology of malaria. *Immunological reviews* **240**: 297-316.

Hafalla JC, Rai U, Morrot A, Bernal-Rubio D, Zavala F & Rodriguez A (2006) Priming of CD8+ T cell responses following immunization with heat-killed *Plasmodium* sporozoites. *European journal of immunology* **36**: 1179-1186.

Hafalla JC, Bauza K, Friesen J, Gonzalez-Aseguinolaza G, Hill AV & Matuschewski K (2013) Identification of targets of CD8(+) T cell responses to malaria liver stages by genome-wide epitope profiling. *PLoS pathogens* **9**: e1003303.

Haque A, Best SE, Unosson K, Amante FH, de Labastida F, Anstey NM, Karupiah G, Smyth MJ, Heath WR & Engwerda CR (2011) Granzyme B expression by CD8+ T cells is required for the development of experimental cerebral malaria. *Journal of immunology* **186**: 6148-6156.

Haussig JM, Matuschewski K & Kooij TW (2011) Inactivation of a *Plasmodium* apicoplast protein attenuates formation of liver merozoites. *Molecular microbiology* **81**: 1511-1525.

Haussig JM, Matuschewski K & Kooij TW (2014) Identification of vital and dispensable sulfur utilization factors in the *Plasmodium* apicoplast. *PloS one* **9**: e89718.

Heiss K, Nie H, Kumar S, Daly TM, Bergman LW & Matuschewski K (2008) Functional characterization of a redundant *Plasmodium* TRAP family invasin, TRAP-like protein, by aldolase binding and a genetic complementation test. *Eukaryotic cell* **7**: 1062-1070.

Hiller NL, Bhattacharjee S, van Ooij C, Liolios K, Harrison T, Lopez-Estrano C & Haldar K (2004) A host-targeting signal in virulence proteins reveals a secretome in malarial infection. *Science* **306**: 1934-1937.

Ho CM, Beck JR, Lai M, Cui Y, Goldberg DE, Egea PF & Zhou ZH (2018) Malaria parasite translocon structure and mechanism of effector export. *Nature* **561**: 70-75.

Hoffman SL, Goh LM, Luke TC*, et al.* (2002) Protection of humans against malaria by immunization with radiation-attenuated *Plasmodium falciparum* sporozoites. *The Journal of infectious diseases* **185**: 1155-1164.

Ishino T, Chinzei Y & Yuda M (2005) Two proteins with 6-cys motifs are required for malarial parasites to commit to infection of the hepatocyte. *Molecular microbiology* **58**: 1264-1275.

Ishino T, Yano K, Chinzei Y & Yuda M (2004) Cell-passage activity is required for the malarial parasite to cross the liver sinusoidal cell layer. *PLoS biology* **2**: E4.

Jagannathan P, Eccles-James I, Bowen K, *et al.* (2014) IFNgamma/IL-10 co-producing cells dominate the CD4 response to malaria in highly exposed children. *PLoS pathogens* **10**: e1003864.

Janse CJ, Franke-Fayard B & Waters AP (2006) Selection by flow-sorting of genetically transformed, GFP-expressing blood stages of the rodent malaria parasite, *Plasmodium berghei*. *Nature protocols* **1**: 614-623.

Janse CJ, Ramesar J & Waters AP (2006) High-efficiency transfection and drug selection of genetically transformed blood stages of the rodent malaria parasite *Plasmodium berghei*. *Nature protocols* **1**: 346-356.

Janse CJ, Kroeze H, van Wigcheren A, Mededovic S, Fonager J, Franke-Fayard B, Waters AP & Khan SM (2011) A genotype and phenotype database of genetically modified malaria-parasites. *Trends in parasitology* **27**: 31-39.

Jobe O, Lumsden J, Mueller AK, Williams J, Silva-Rivera H, Kappe SH, Schwenk RJ, Matuschewski K & Krzych U (2007) Genetically attenuated *Plasmodium berghei* liver stages induce sterile protracted protection that is mediated by major histocompatibility complex Class I-dependent interferon-gamma-producing CD8+ T cells. *The Journal of infectious diseases* **196**: 599-607.

Kabeya Y, Mizushima N, Ueno T, Yamamoto A, Kirisako T, Noda T, Kominami E, Ohsumi Y & Yoshimori T (2000) LC3, a mammalian homologue of yeast Apg8p, is localized in autophagosome membranes after processing. *The EMBO journal* **19**: 5720-5728.

Kaiser K, Matuschewski K, Camargo N, Ross J & Kappe SH (2004) Differential transcriptome profiling identifies *Plasmodium* genes encoding pre-erythrocytic stage-specific proteins. *Molecular microbiology* **51**: 1221-1232.

Kaushansky A, Douglass AN, Arang N, Vigdorovich V, Dambrauskas N, Kain HS, Austin LS, Sather DN & Kappe SH (2015) Malaria parasites target the hepatocyte receptor EphA2 for successful host infection. *Science* **350**: 1089-1092.

Kenthirapalan S, Waters AP, Matuschewski K & Kooij TW (2016) Functional profiles of orphan membrane transporters in the life cycle of the malaria parasite. *Nature communications* **7**: 10519.

Khan ZM & Vanderberg JP (1991) Role of host cellular response in differential susceptibility of nonimmunized BALB/c mice to *Plasmodium berghei* and *Plasmodium yoelii* sporozoites. *Infection and immunity* **59**: 2529-2534.

Khan ZM & Vanderberg JP (1992) Specific inflammatory cell infiltration of hepatic schizonts in BALB/c mice immunized with attenuated *Plasmodium yoelii* sporozoites. *International immunology* **4**: 711-718.

Knuepfer E, Rug M & Cowman AF (2005) Function of the *Plasmodium* export element can be blocked by green fluorescent protein. *Molecular and biochemical parasitology* **142**: 258-262.

Knuepfer E, Rug M, Klonis N, Tilley L & Cowman AF (2005) Trafficking determinants for PfEMP3 export and assembly under the *Plasmodium falciparum*-infected red blood cell membrane. *Molecular microbiology* **58**: 1039-1053.

Kooij TW, Rauch MM & Matuschewski K (2012) Expansion of experimental genetics approaches for *Plasmodium berghei* with versatile transfection vectors. *Molecular and biochemical parasitology* **185**: 19-26.

Kreutzfeld O, Muller K & Matuschewski K (2017) Engineering of Genetically Arrested Parasites (GAPs) For a Precision Malaria Vaccine. *Frontiers in cellular and infection microbiology* **7**: 198.

Kriek N, Tilley L, Horrocks P, Pinches R, Elford BC, Ferguson DJ, Lingelbach K & Newbold CI (2003) Characterization of the pathway for transport of the cytoadherence-mediating protein, PfEMP1, to the host cell surface in malaria parasite-infected erythrocytes. *Molecular microbiology* **50**: 1215-1227.

Kublin JG, Mikolajczak SA, Sack BK, *et al.* (2017) Complete attenuation of genetically engineered *Plasmodium falciparum* sporozoites in human subjects. *Science translational medicine* **9**.

Kulzer S, Rug M, Brinkmann K, Cannon P, Cowman A, Lingelbach K, Blatch GL, Maier AG & Przyborski JM (2010) Parasite-encoded Hsp40 proteins define novel mobile structures in the cytosol of the *P. falciparum*-infected erythrocyte. *Cellular microbiology* **12**: 1398-1420.

Kulzer S, Charnaud S, Dagan T, Riedel J, Mandal P, Pesce ER, Blatch GL, Crabb BS, Gilson PR & Przyborski JM (2012) *Plasmodium falciparum*-encoded exported hsp70/hsp40 chaperone/co-chaperone complexes within the host erythrocyte. *Cellular microbiology* **14**: 1784-1795.

Kumar KA, Sano G, Boscardin S, Nussenzweig RS, Nussenzweig MC, Zavala F & Nussenzweig V (2006) The circumsporozoite protein is an immunodominant protective antigen in irradiated sporozoites. *Nature* **444**: 937-940.

Labaied M, Harupa A, Dumpit RF, Coppens I, Mikolajczak SA & Kappe SH (2007) *Plasmodium yoelii* sporozoites with simultaneous deletion of P52 and P36 are completely attenuated and confer sterile immunity against infection. *Infection and immunity* **75**: 3758-3768.

Langhorne J, Ndungu FM, Sponaas AM & Marsh K (2008) Immunity to malaria: more questions than answers. *Nature immunology* **9**: 725-732.

Langreth SG & Peterson E (1985) Pathogenicity, stability, and immunogenicity of a knobless clone of *Plasmodium falciparum* in Colombian owl monkeys. *Infection and immunity* **47**: 760-766.

Leiriao P, Mota MM & Rodriguez A (2005) Apoptotic *Plasmodium*-infected hepatocytes provide antigens to liver dendritic cells. *The Journal of infectious diseases* **191**: 1576-1581.

Lennartz F, Adams Y, Bengtsson A, *et al.* (2017) Structure-Guided Identification of a Family of Dual Receptor-Binding PfEMP1 that Is Associated with Cerebral Malaria. *Cell host & microbe* **21**: 403-414.

Lindner SE, Sartain MJ, Hayes K, Harupa A, Moritz RL, Kappe SH & Vaughan AM (2014) Enzymes involved in plastid-targeted phosphatidic acid synthesis are essential for *Plasmodium yoelii* liver-stage development. *Molecular microbiology* **91**: 679-693.

Mahamar A, Attaher O, Swihart B, *et al.* (2017) Host factors that modify *Plasmodium falciparum* adhesion to endothelial receptors. *Scientific reports* **7**: 13872.

Maier AG, Rug M, O'Neill MT*, et al.* (2008) Exported proteins required for virulence and rigidity of *Plasmodium falciparum*-infected human erythrocytes. *Cell* **134**: 48-61.

Malik A, Egan JE, Houghten RA, Sadoff JC & Hoffman SL (1991) Human cytotoxic T lymphocytes against the *Plasmodium falciparum* circumsporozoite protein. *Proceedings of the National Academy of Sciences of the United States of America* **88**: 3300-3304.

Manzoni G, Briquet S, Risco-Castillo V, Gaultier C, Topcu S, Ivanescu ML, Franetich JF, Hoareau-Coudert B, Mazier D & Silvie O (2014) A rapid and robust selection procedure for generating drug-selectable marker-free recombinant malaria parasites. *Scientific reports* **4**: 4760.

Manzoni G, Marinach C, Topcu S*, et al.* (2017) *Plasmodium* P36 determines host cell receptor usage during sporozoite invasion. *eLife* **6**.

Marapana DS, Dagley LF, Sandow JJ*, et al.* (2018) Plasmepsin V cleaves malaria effector proteins in a distinct endoplasmic reticulum translocation interactome for export to the erythrocyte. *Nature microbiology* **3**: 1010-1022.

Marti M, Good RT, Rug M, Knuepfer E & Cowman AF (2004) Targeting malaria virulence and remodeling proteins to the host erythrocyte. *Science* **306**: 1930-1933.

Matthews K, Kalanon M, Chisholm SA*, et al.* (2013) The *Plasmodium* translocon of exported proteins (PTEX) component thioredoxin-2 is important for maintaining normal blood-stage growth. *Molecular microbiology* **89**: 1167-1186.

Matuschewski K (2013) Murine infection models for vaccine development: the malaria example. *Human vaccines & immunotherapeutics* **9**: 450-456.

Matuschewski K, Nunes AC, Nussenzweig V & Menard R (2002) *Plasmodium* sporozoite invasion into insect and mammalian cells is directed by the same dual binding system. *The EMBO journal* **21**: 1597-1606.

Matuschewski K, Hafalla JC, Borrmann S & Friesen J (2011) Arrested *Plasmodium* liver stages as experimental anti-malaria vaccines. *Human vaccines* **7 Suppl**: 16-21.

Matz JM & Matuschewski K (2018) An in silico down-scaling approach uncovers novel constituents of the *Plasmodium*-containing vacuole. *Scientific reports* **8**: 14055.

Matz JM, Matuschewski K & Kooij TW (2013) Two putative protein export regulators promote *Plasmodium* blood stage development in vivo. *Molecular and biochemical parasitology* **191**: 44-52.

Matz JM, Goosmann C, Brinkmann V, Grutzke J, Ingmundson A, Matuschewski K & Kooij TW (2015) The *Plasmodium berghei* translocon of exported proteins reveals spatiotemporal dynamics of tubular extensions. *Scientific reports* **5**: 12532.

Mauduit M, Gruner AC, Tewari R*, et al.* (2009) A role for immune responses against non-CS components in the cross-species protection induced by immunization with irradiated malaria sporozoites. *PloS one* **4**: e7717.

Meibalan E, Comunale MA, Lopez AM, Bergman LW, Mehta A, Vaidya AB & Burns JM, Jr. (2015) Host erythrocyte environment influences the localization of exported protein 2, an essential component of the *Plasmodium* translocon. *Eukaryotic cell* **14**: 371-384.

Mellouk S, Maheshwari RK, Rhodes-Feuillette A, *et al.* (1987) Inhibitory activity of interferons and interleukin 1 on the development of *Plasmodium falciparum* in human hepatocyte cultures. *Journal of immunology* **139**: 4192-4195.

Menard R (2001) Gliding motility and cell invasion by Apicomplexa: insights from the *Plasmodium* sporozoite. *Cellular microbiology* **3**: 63-73.

Mikolajczak SA, Lakshmanan V, Fishbaugher M, *et al.* (2014) A next-generation genetically attenuated *Plasmodium falciparum* parasite created by triple gene deletion. *Molecular therapy : the journal of the American Society of Gene Therapy* **22**: 1707-1715.

Miller JL, Harupa A, Kappe SH & Mikolajczak SA (2012) *Plasmodium yoelii* macrophage migration inhibitory factor is necessary for efficient liver-stage development. *Infection and immunity* **80**: 1399-1407.

Montagna GN, Beigier-Bompadre M, Becker M, Kroczek RA, Kaufmann SH & Matuschewski K (2014) Antigen export during liver infection of the malaria parasite augments protective immunity. *mBio* **5**: e01321-01314.

Montagna GN, Buscaglia CA, Munter S, Goosmann C, Frischknecht F, Brinkmann V & Matuschewski K (2012) Critical role for heat shock protein 20 (HSP20) in migration of malarial sporozoites. *The Journal of biological chemistry* **287**: 2410-2422.

Moreira CK, Templeton TJ, Lavazec C, Hayward RE, Hobbs CV, Kroeze H, Janse CJ, Waters AP, Sinnis P & Coppi A (2008) The *Plasmodium* TRAP/MIC2 family member, TRAP-Like Protein (TLP), is involved in tissue traversal by sporozoites. *Cellular microbiology* **10**: 1505-1516.

Morita M, Nagaoka H, Ntege EH, *et al.* (2018) PV1, a novel *Plasmodium falciparum* merozoite dense granule protein, interacts with exported protein in infected erythrocytes. *Scientific reports* **8**: 3696.

Morrot A, Hafalla JC, Cockburn IA, Carvalho LH & Zavala F (2005) IL-4 receptor expression on CD8+ T cells is required for the development of protective memory responses against liver stages of malaria parasites. *The Journal of experimental medicine* **202**: 551-560.

Mota MM & Rodriguez A (2002) Invasion of mammalian host cells by *Plasmodium* sporozoites. *BioEssays : news and reviews in molecular, cellular and developmental biology* **24**: 149-156.

Mota MM, Pradel G, Vanderberg JP, Hafalla JC, Frevert U, Nussenzweig RS, Nussenzweig V & Rodriguez A (2001) Migration of *Plasmodium* sporozoites through cells before infection. *Science* **291**: 141-144.

Mueller AK, Labaied M, Kappe SH & Matuschewski K (2005) Genetically modified *Plasmodium* parasites as a protective experimental malaria vaccine. *Nature* **433**: 164-167.

Mueller AK, Deckert M, Heiss K, Goetz K, Matuschewski K & Schluter D (2007) Genetically attenuated *Plasmodium berghei* liver stages persist and elicit sterile protection primarily via CD8 T cells. *The American journal of pathology* **171**: 107-115.

Mueller AK, Camargo N, Kaiser K, Andorfer C, Frevert U, Matuschewski K & Kappe SH (2005) *Plasmodium* liver stage developmental arrest by depletion of a protein at the parasite-host interface. *Proceedings of the National Academy of Sciences of the United States of America* **102**: 3022-3027.

Mueller I, Galinski MR, Baird JK, Carlton JM, Kochar DK, Alonso PL & del Portillo HA (2009) Key gaps in the knowledge of *Plasmodium* vivax, a neglected human malaria parasite. *The Lancet Infectious diseases* **9**: 555-566.

Muller K, Matuschewski K & Silvie O (2011) The Puf-family RNA-binding protein Puf2 controls sporozoite conversion to liver stages in the malaria parasite. *PloS one* **6**: e19860.

Muller K, Gibbins MP, Matuschewski K & Hafalla JCR (2017) Evidence of cross-stage CD8+ T cell epitopes in malaria pre-erythrocytic and blood stage infections. *Parasite immunology* **39**.

Nagel A, Prado M, Heitmann A, Tartz S, Jacobs T, Deschermeier C, Helm S, Stanway R & Heussler V (2013) A new approach to generate a safe double-attenuated *Plasmodium* liver stage vaccine. *International journal for parasitology* **43**: 503-514.

Nganou-Makamdop K, Ploemen I, Behet M, Van Gemert GJ, Hermsen C, Roestenberg M & Sauerwein RW (2012) Reduced *Plasmodium berghei* sporozoite liver load associates with low protective efficacy after intradermal immunization. *Parasite immunology* **34**: 562-569.

Nudelman S, Renia L, Charoenvit Y, Yuan L, Miltgen F, Beaudoin RL & Mazier D (1989) Dual action of anti-sporozoite antibodies in vitro. *Journal of immunology* **143**: 996-1000.

Nussenzweig RS, Vanderberg J, Most H & Orton C (1967) Protective immunity produced by the injection of x-irradiated sporozoites of *Plasmodium berghei*. *Nature* **216**: 160-162.

Nussenzweig RS, Vanderberg JP, Most H & Orton C (1969) Specificity of protective immunity produced by x-irradiated *Plasmodium berghei* sporozoites. *Nature* **222**: 488-489.

Nussler AK, Renia L, Pasquetto V, Miltgen F, Matile H & Mazier D (1993) In vivo induction of the nitric oxide pathway in hepatocytes after injection with irradiated malaria sporozoites, malaria blood parasites or adjuvants. *European journal of immunology* **23**: 882-887.

Ocana-Morgner C, Mota MM & Rodriguez A (2003) Malaria blood stage suppression of liver stage immunity by dendritic cells. *The Journal of experimental medicine* **197**: 143-151.

Ocana-Morgner C, Wong KA, Lega F, Dotor J, Borras-Cuesta F & Rodriguez A (2007) Role of TGF-beta and PGE2 in T cell responses during *Plasmodium yoelii* infection. *European journal of immunology* **37**: 1562-1574.

Offeddu V, Thathy V, Marsh K & Matuschewski K (2012) Naturally acquired immune responses against *Plasmodium falciparum* sporozoites and liver infection. *International journal for parasitology* **42**: 535-548.

Olotu A, Fegan G, Wambua J, Nyangweso G, Leach A, Lievens M, Kaslow DC, Njuguna P, Marsh K & Bejon P (2016) Seven-Year Efficacy of RTS,S/AS01 Malaria Vaccine among Young African Children. *The New England journal of medicine* **374**: 2519-2529.

Ono T, Cabrita-Santos L, Leitao R, *et al.* (2008) Adenylyl cyclase alpha and cAMP signaling mediate *Plasmodium* sporozoite apical regulated exocytosis and hepatocyte infection. *PLoS pathogens* **4**: e1000008.

Orito Y, Ishino T, Iwanaga S, Kaneko I, Kato T, Menard R, Chinzei Y & Yuda M (2013) Liver-specific protein 2: a *Plasmodium* protein exported to the hepatocyte cytoplasm and required for merozoite formation. *Molecular microbiology* **87**: 66-79.

Otto TD, Bohme U, Jackson AP, *et al.* (2014) A comprehensive evaluation of rodent malaria parasite genomes and gene expression. *BMC biology* **12**: 86.

Overstreet MG, Cockburn IA, Chen YC & Zavala F (2008) Protective CD8 T cells against *Plasmodium* liver stages: immunobiology of an 'unnatural' immune response. *Immunological reviews* **225**: 272-283.

Paulmurugan R & Gambhir SS (2005) Firefly luciferase enzyme fragment complementation for imaging in cells and living animals. *Analytical chemistry* **77**: 1295-1302.

Pei Y, Tarun AS, Vaughan AM, Herman RW, Soliman JM, Erickson-Wayman A & Kappe SH (2010) *Plasmodium* pyruvate dehydrogenase activity is only essential for the parasite's progression from liver infection to blood infection. *Molecular microbiology* **75**: 957-971.

Pichugin A, Zarling S, Perazzo L, Duffy PE, Ploegh HL & Krzych U (2018) Identification of a Novel CD8 T Cell Epitope Derived from *Plasmodium* berghei Protective Liver-Stage Antigen. *Frontiers in immunology* **9**: 91.

Plebanski M, Hannan CM, Behboudi S, Flanagan KL, Apostolopoulos V, Sinden RE & Hill AV (2005) Direct processing and presentation of antigen from malaria sporozoites by professional antigen-presenting cells in the induction of CD8 T-cell responses. *Immunology and cell biology* **83**: 307-312.

Ploemen IH, Croes HJ, van Gemert GJ, Wijers-Rouw M, Hermsen CC & Sauerwein RW (2012) *Plasmodium* berghei Deltap52&p36 parasites develop independent of a parasitophorous vacuole membrane in Huh-7 liver cells. *PloS one* **7**: e50772.

Polhemus ME, Remich SA, Ogutu BR, *et al.* (2009) Evaluation of RTS,S/AS02A and RTS,S/AS01B in adults in a high malaria transmission area. *PloS one* **4**: e6465.

Portugal S, Drakesmith H & Mota MM (2011) Superinfection in malaria: *Plasmodium* shows its iron will. *EMBO reports* **12**: 1233-1242.

Prado M, Eickel N, De Niz M, *et al.* (2015) Long-term live imaging reveals cytosolic immune responses of host hepatocytes against *Plasmodium* infection and parasite escape mechanisms. *Autophagy* **11**: 1561-1579.

Prudencio M, Rodriguez A & Mota MM (2006) The silent path to thousands of merozoites: the *Plasmodium* liver stage. *Nature reviews Microbiology* **4**: 849-856.

Putrianti ED, Silvie O, Kordes M, Borrmann S & Matuschewski K (2009) Vaccine-like immunity against malaria by repeated causal-prophylactic treatment of liver-stage *Plasmodium* parasites. *The Journal of infectious diseases* **199**: 899-903.

Reece WH, Pinder M, Gothard PK, *et al.* (2004) A CD4(+) T-cell immune response to a conserved epitope in the circumsporozoite protein correlates with protection from natural *Plasmodium falciparum* infection and disease. *Nature medicine* **10**: 406-410.

Renia L, Maranon C, Hosmalin A, Gruner AC, Silvie O & Snounou G (2006) Do apoptotic *Plasmodium*-infected hepatocytes initiate protective immune responses? *The Journal of infectious diseases* **193**: 163-164; author reply 164-165.

Riley EM & Stewart VA (2013) Immune mechanisms in malaria: new insights in vaccine development. *Nature medicine* **19**: 168-178.

Riley EM, Couper KN, Helmby H, Hafalla JC, de Souza JB, Langhorne J, Jarra WB & Zavala F (2010) Neuropathogenesis of human and murine malaria. *Trends in parasitology* **26**: 277-278.

Risco-Castillo V, Topcu S, Marinach C, Manzoni G, Bigorgne AE, Briquet S, Baudin X, Lebrun M, Dubremetz JF & Silvie O (2015) Malaria Sporozoites Traverse Host Cells within Transient Vacuoles. *Cell host & microbe* **18**: 593-603.

Robson KJ, Hall JR, Jennings MW, Harris TJ, Marsh K, Newbold CI, Tate VE & Weatherall DJ (1988) A highly conserved amino-acid sequence in thrombospondin, properdin and in proteins from sporozoites and blood stages of a human malaria parasite. *Nature* **335**: 79-82.

Rodrigues CD, Hannus M, Prudencio M, *et al.* (2008) Host scavenger receptor SR-BI plays a dual role in the establishment of malaria parasite liver infection. *Cell host & microbe* **4**: 271-282.

Roestenberg M, McCall M, Hopman J, *et al.* (2009) Protection against a malaria challenge by sporozoite inoculation. *The New England journal of medicine* **361**: 468-477.

Romero P, Maryanski JL, Corradin G, Nussenzweig RS, Nussenzweig V & Zavala F (1989) Cloned cytotoxic T cells recognize an epitope in the circumsporozoite protein and protect against malaria. *Nature* **341**: 323-326.

Rts SCTP & Agnandji ST & Lell B, *et al.* (2011) First results of phase 3 trial of RTS,S/AS01 malaria vaccine in African children. *The New England journal of medicine* **365**: 1863-1875.

Russo I, Babbitt S, Muralidharan V, Butler T, Oksman A & Goldberg DE (2010) Plasmepsin V licenses *Plasmodium* proteins for export into the host erythrocyte. *Nature* **463**: 632-636.

Sano G, Hafalla JC, Morrot A, Abe R, Lafaille JJ & Zavala F (2001) Swift development of protective effector functions in naive CD8(+) T cells against malaria liver stages. *The Journal of experimental medicine* **194**: 173-180.

Scheller LF & Azad AF (1995) Maintenance of protective immunity against malaria by persistent hepatic parasites derived from irradiated sporozoites. *Proceedings of the National Academy of Sciences of the United States of America* **92**: 4066-4068.

Scheller LF, Wirtz RA & Azad AF (1994) Susceptibility of different strains of mice to hepatic infection with *Plasmodium* berghei. *Infection and immunity* **62**: 4844-4847.

Schmidt NW, Butler NS, Badovinac VP & Harty JT (2010) Extreme CD8 T cell requirements for anti-malarial liver-stage immunity following immunization with radiation attenuated sporozoites. *PLoS pathogens* **6**: e1000998.

Schofield L, Ferreira A, Altszuler R, Nussenzweig V & Nussenzweig RS (1987) Interferon-gamma inhibits the intrahepatocytic development of malaria parasites in vitro. *Journal of immunology* **139**: 2020-2025.

Schofield L, Villaquiran J, Ferreira A, Schellekens H, Nussenzweig R & Nussenzweig V (1987) Gamma interferon, CD8+ T cells and antibodies required for immunity to malaria sporozoites. *Nature* **330**: 664-666.

Seguin MC, Klotz FW, Schneider I, Weir JP, Goodbary M, Slayter M, Raney JJ, Aniagolu JU & Green SJ (1994) Induction of nitric oxide synthase protects against malaria in mice exposed to irradiated *Plasmodium* berghei infected mosquitoes: involvement of interferon gamma and CD8+ T cells. *The Journal of experimental medicine* **180**: 353-358.

Shears MJ, MacRae JI, Mollard V, Goodman CD, Sturm A, Orchard LM, Llinas M, McConville MJ, Botte CY & McFadden GI (2017) Characterization of the *Plasmodium falciparum* and P. berghei glycerol 3-phosphate acyltransferase involved in FASII fatty acid utilization in the malaria parasite apicoplast. *Cellular microbiology* **19**.

Silvie O, Goetz K & Matuschewski K (2008) A sporozoite asparagine-rich protein controls initiation of *Plasmodium* liver stage development. *PLoS pathogens* **4**: e1000086.

Silvie O, Briquet S, Muller K, Manzoni G & Matuschewski K (2014) Post-transcriptional silencing of UIS4 in *Plasmodium* berghei sporozoites is important for host switch. *Molecular microbiology* **91**: 1200-1213.

Silvie O, Semblat JP, Franetich JF, Hannoun L, Eling W & Mazier D (2002) Effects of irradiation on *Plasmodium falciparum* sporozoite hepatic development: implications for the design of pre-erythrocytic malaria vaccines. *Parasite immunology* **24**: 221-223.

Sinden RE (2015) The cell biology of malaria infection of mosquito: advances and opportunities. *Cellular microbiology* **17**: 451-466.

Singh AP, Buscaglia CA, Wang Q, Levay A, Nussenzweig DR, Walker JR, Winzeler EA, Fujii H, Fontoura BM & Nussenzweig V (2007) *Plasmodium* circumsporozoite protein promotes the development of the liver stages of the parasite. *Cell* **131**: 492-504.

Spielmann T & Gilberger TW (2010) Protein export in malaria parasites: do multiple export motifs add up to multiple export pathways? *Trends in parasitology* **26**: 6-10.

Spielmann T & Gilberger TW (2015) Critical Steps in Protein Export of *Plasmodium falciparum* Blood Stages. *Trends in parasitology* **31**: 514-525.

Spielmann T, Montagna GN, Hecht L & Matuschewski K (2012) Molecular make-up of the *Plasmodium* parasitophorous vacuolar membrane. *International journal of medical microbiology : IJMM* **302**: 179-186.

Stevenson MM & Riley EM (2004) Innate immunity to malaria. *Nature reviews Immunology* **4**: 169-180.

Stewart MJ & Vanderberg JP (1991) Malaria sporozoites release circumsporozoite protein from their apical end and translocate it along their surface. *The Journal of protozoology* **38**: 411-421.

Stoute JA, Slaoui M, Heppner DG, Momin P, Kester KE, Desmons P, Wellde BT, Garcon N, Krzych U & Marchand M (1997) A preliminary evaluation of a recombinant circumsporozoite protein vaccine against *Plasmodium falciparum* malaria. RTS,S Malaria Vaccine Evaluation Group. *The New England journal of medicine* **336**: 86-91.

Sturm A, Amino R, van de Sand C, Regen T, Retzlaff S, Rennenberg A, Krueger A, Pollok JM, Menard R & Heussler VT (2006) Manipulation of host hepatocytes by the malaria parasite for delivery into liver sinusoids. *Science* **313**: 1287-1290.

Su Z & Stevenson MM (2000) Central role of endogenous gamma interferon in protective immunity against blood-stage *Plasmodium* chabaudi AS infection. *Infection and immunity* **68**: 4399-4406.

Sultan AA, Thathy V, Frevert U, Robson KJ, Crisanti A, Nussenzweig V, Nussenzweig RS & Menard R (1997) TRAP is necessary for gliding motility and infectivity of *Plasmodium* sporozoites. *Cell* **90**: 511-522.

Sutherland CJ, Tanomsing N, Nolder D, *et al.* (2010) Two nonrecombining sympatric forms of the human malaria parasite *Plasmodium* ovale occur globally. *The Journal of infectious diseases* **201**: 1544-1550.

Tardieux I & Baum J (2016) Reassessing the mechanics of parasite motility and host-cell invasion. *The Journal of cell biology* **214**: 507-515.

Tarun AS, Dumpit RF, Camargo N, Labaied M, Liu P, Takagi A, Wang R & Kappe SH (2007) Protracted sterile protection with *Plasmodium yoelii* pre-erythrocytic genetically attenuated parasite malaria vaccines is independent of significant liver-stage persistence and is mediated by CD8+ T cells. *The Journal of infectious diseases* **196**: 608-616.

Teo Teo CF, Zhou XW, Bogyo M & Carruthers VB (2007) Cysteine protease inhibitors block Toxoplasma gondii microneme secretion and cell invasion. *Antimicrob Agents Chemother* **51**: 679-88

Thieleke-Matos C, Lopes da Silva M, Cabrita-Santos L, *et al.* (2016) Host cell autophagy contributes to *Plasmodium* liver development. *Cellular microbiology* **18**: 437-450.

Torgler R, Bongfen SE, Romero JC, Tardivel A, Thome M & Corradin G (2008) Sporozoite-mediated hepatocyte wounding limits *Plasmodium* parasite development via MyD88-mediated NF-kappa B activation and inducible NO synthase expression. *Journal of immunology* **180**: 3990-3999.

Trieu A, Kayala MA, Burk C, Molina DM, Freilich DA, Richie TL, Baldi P, Felgner PL & Doolan DL (2011) Sterile protective immunity to malaria is associated with a panel of novel *P. falciparum* antigens. *Molecular & cellular proteomics : MCP* **10**: M111 007948.

Tsuji M, Miyahira Y, Nussenzweig RS, Aguet M, Reichel M & Zavala F (1995) Development of antimalaria immunity in mice lacking IFN-gamma receptor. *Journal of immunology* **154**: 5338-5344.

van Dijk MR, Waters AP & Janse CJ (1995) Stable transfection of malaria parasite blood stages. *Science* **268**: 1358-1362.

van Dijk MR, Douradinha B, Franke-Fayard B, *et al.* (2005) Genetically attenuated, P36p-deficient malarial sporozoites induce protective immunity and apoptosis of infected liver cells. *Proceedings of the National Academy of Sciences of the United States of America* **102**: 12194-12199.

van Schaijk BC, Ploemen IH, Annoura T, *et al.* (2014) A genetically attenuated malaria vaccine candidate based on *P. falciparum* b9/slarp gene-deficient sporozoites. *eLife* **3**.

van Schaijk BC, Kumar TR, Vos MW, *et al.* (2014) Type II fatty acid biosynthesis is essential for *Plasmodium falciparum* sporozoite development in the midgut of Anopheles mosquitoes. *Eukaryotic cell* **13**: 550-559.

Vanderberg JP, Khan ZM & Stewart MJ (1993) Induction of hepatic inflammatory response by *Plasmodium* berghei sporozoites protects BALB/c mice against challenge with *Plasmodium yoelii* sporozoites. *The Journal of parasitology* **79**: 763-767.

Vaughan AM, Sack BK, Dankwa D, Minkah N, Nguyen T, Cardamone H & Kappe SHI (2018) A *Plasmodium* Parasite with Complete Late Liver Stage Arrest Protects against Preerythrocytic and Erythrocytic Stage Infection in Mice. *Infection and immunity* **86**.

Vaughan AM, O'Neill MT, Tarun AS, Camargo N, Phuong TM, Aly AS, Cowman AF & Kappe SH (2009) Type II fatty acid synthesis is essential only for malaria parasite late liver stage development. *Cellular microbiology* **11**: 506-520.

Vincke IH & Lips M (1948) Un noveau *Plasmodium* d'un rongeur
suvage du Congo *Plasmodium* berghei n.sp. *Annales de la Societe belge de medecine tropicale* **28**: 97-104.

Wacker R, Eickel N, Schmuckli-Maurer J, Annoura T, Niklaus L, Khan SM, Guan JL & Heussler VT (2017) LC3-association with the parasitophorous vacuole membrane of *Plasmodium* berghei liver stages follows a noncanonical autophagy pathway. *Cellular microbiology* **19**.

Watermeyer JM, Hale VL, Hackett F, Clare DK, Cutts EE, Vakonakis I, Fleck RA, Blackman MJ & Saibil HR (2016) A spiral scaffold underlies cytoadherent knobs in *Plasmodium falciparum*-infected erythrocytes. *Blood* **127**: 343-351.

Weiss WR, Sedegah M, Beaudoin RL, Miller LH & Good MF (1988) CD8+ T cells (cytotoxic/suppressors) are required for protection in mice immunized with malaria sporozoites. *Proceedings of the National Academy of Sciences of the United States of America* **85**: 573-576.

White CE, Villarino NF, Sloan SS, Ganusov VV & Schmidt NW (2015) *Plasmodium* suppresses expansion of T cell responses to heterologous infections. *Journal of immunology* **194**: 697-708.

White KL, Snyder HL & Krzych U (1996) MHC class I-dependent presentation of exoerythrocytic antigens to CD8+ T lymphocytes is required for protective immunity against *Plasmodium* berghei. *Journal of immunology* **156**: 3374-3381.

WHO (2016) Tables of malaria vaccine projects globally: << The Rainbow Table >>. p.^pp. World Health Organization.

WHO (2018) World Malaria Report. Geneva: World Health Organization; 2018. Licence: CC BY-NC-SA 3.0 IGO.

Wickham ME, Rug M, Ralph SA, Klonis N, McFadden GI, Tilley L & Cowman AF (2001) Trafficking and assembly of the cytoadherence complex in *Plasmodium falciparum*-infected human erythrocytes. *The EMBO journal* **20**: 5636-5649.

Wipasa J, Suphavilai C, Okell LC, Cook J, Corran PH, Thaikla K, Liewsaree W, Riley EM & Hafalla JC (2010) Long-lived antibody and B Cell memory responses to the human malaria parasites, *Plasmodium falciparum* and *Plasmodium* vivax. *PLoS pathogens* **6**: e1000770.

Yoshida N, Potocnjak P, Nussenzweig V & Nussenzweig RS (1981) Biosynthesis of *Pb*44, the protective antigen of sporozoites of *Plasmodium* berghei. *The Journal of experimental medicine* **154**: 1225-1236.

Yoshida N, Nussenzweig RS, Potocnjak P, Nussenzweig V & Aikawa M (1980) Hybridoma produces protective antibodies directed against the sporozoite stage of malaria parasite. *Science* **207**: 71-73.

Yu M, Kumar TR, Nkrumah LJ, *et al.* (2008) The fatty acid biosynthesis enzyme FabI plays a key role in the development of liver-stage malarial parasites. *Cell host & microbe* **4**: 567-578.

Appendix

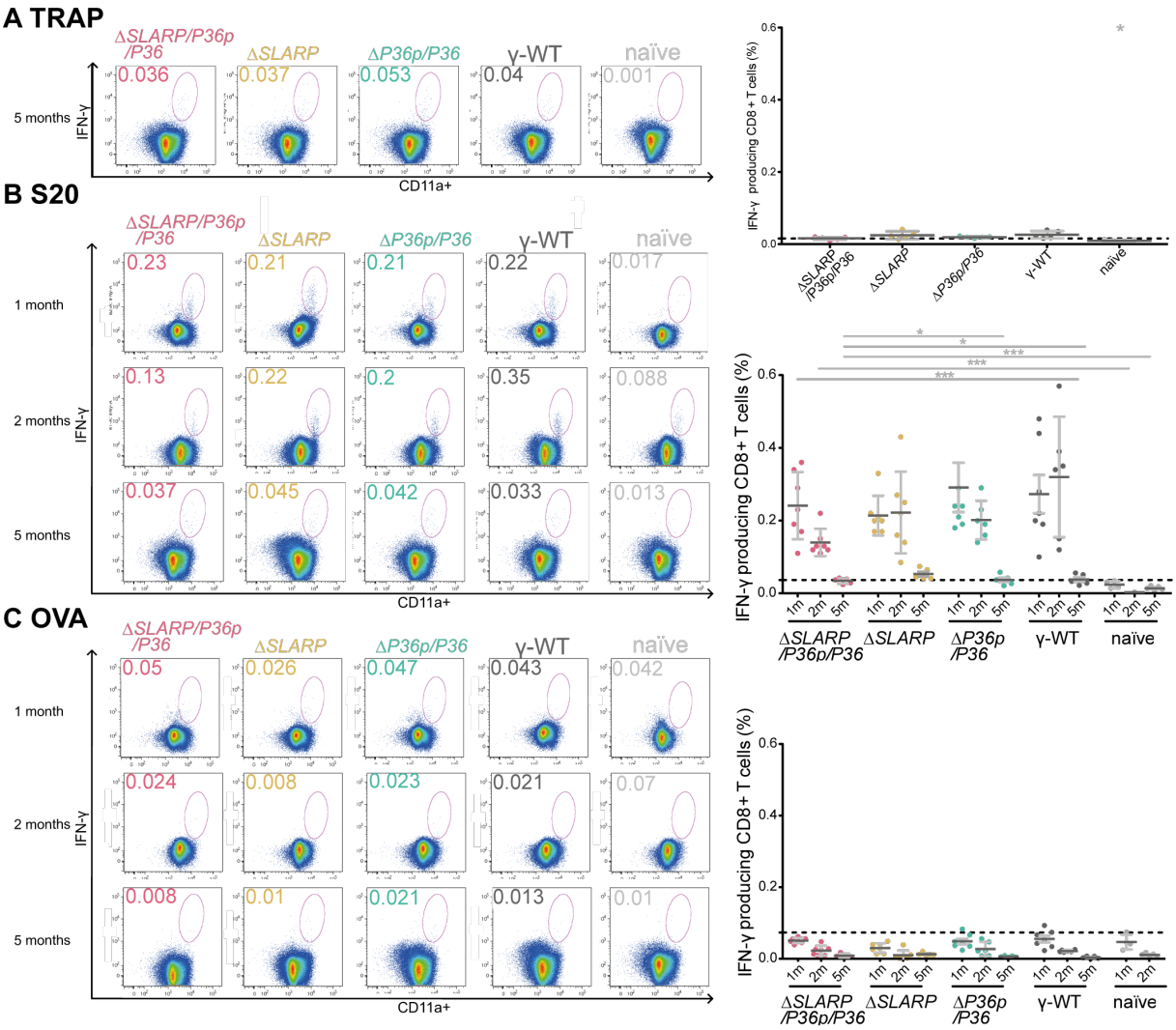

Supplementary Figure 1 IFN-γ secreting CD8⁺ T cells in spleen are reduced in *ΔSLARP/P36p/P36*-immunized animals

Analysis of CD8⁺ T cells elicited in immunized cohorts. C57BL/6 mice were immunized in a prime/boost regimen (7 days apart), challenged one or two months p.i. and treated with pyrimethamine in the drinking water before excision of spleens one month post challenge. For the excision of spleens from immunized mice 5 months p.i., animals were immunized in a prime/boost regimen (7 days apart) and challenged 5 months p.i.. Spleens were excised 42h post challenge. Splenic cells were restimulated with H2-K^b specific peptide epitopes (TRAP/S20) and a control OVA/H2-D^b and stained with fluorescently labeled antibodies for analysis with MACSQuant. FACS files were processed with FlowJo 8.7.3. **A** Examples of mean IFN-γ secreting CD8⁺ T cells after restimulation with TRAP peptide of immunized cohorts five months post immunization compared to naïve controls. Statistical analysis: Mann-Whitney-U test, *, $p<0.05$ **B** Examples of mean IFN-γ secreting CD8⁺ T cell restimulation with S20 peptide of immunized cohorts one, two and five months post immunization compared to naïve controls. Statistical analysis: Mann-Whitney-U test, *, $p<0.05$, ***, $p<0.001$**C** Examples of mean IFN-γ secreting CD8⁺ T cells restimulation with OVA peptide, as negative control, of immunized cohorts one, two and five months post immunization compared to naïve controls. Dot blot shows comparison of percentage of CD8⁺ T cell IFN-γ secretion in immunized cohorts. Depicted are IFN-γ producing CD8⁺ T cells of individual mice (dots), as well as the mean of the cohort ± SD. Only significant statistical differences of cohorts compared to *ΔSLARP/P36p/P36* immunized mice are shown. Statistical analysis: Mann-Whitney-U test.

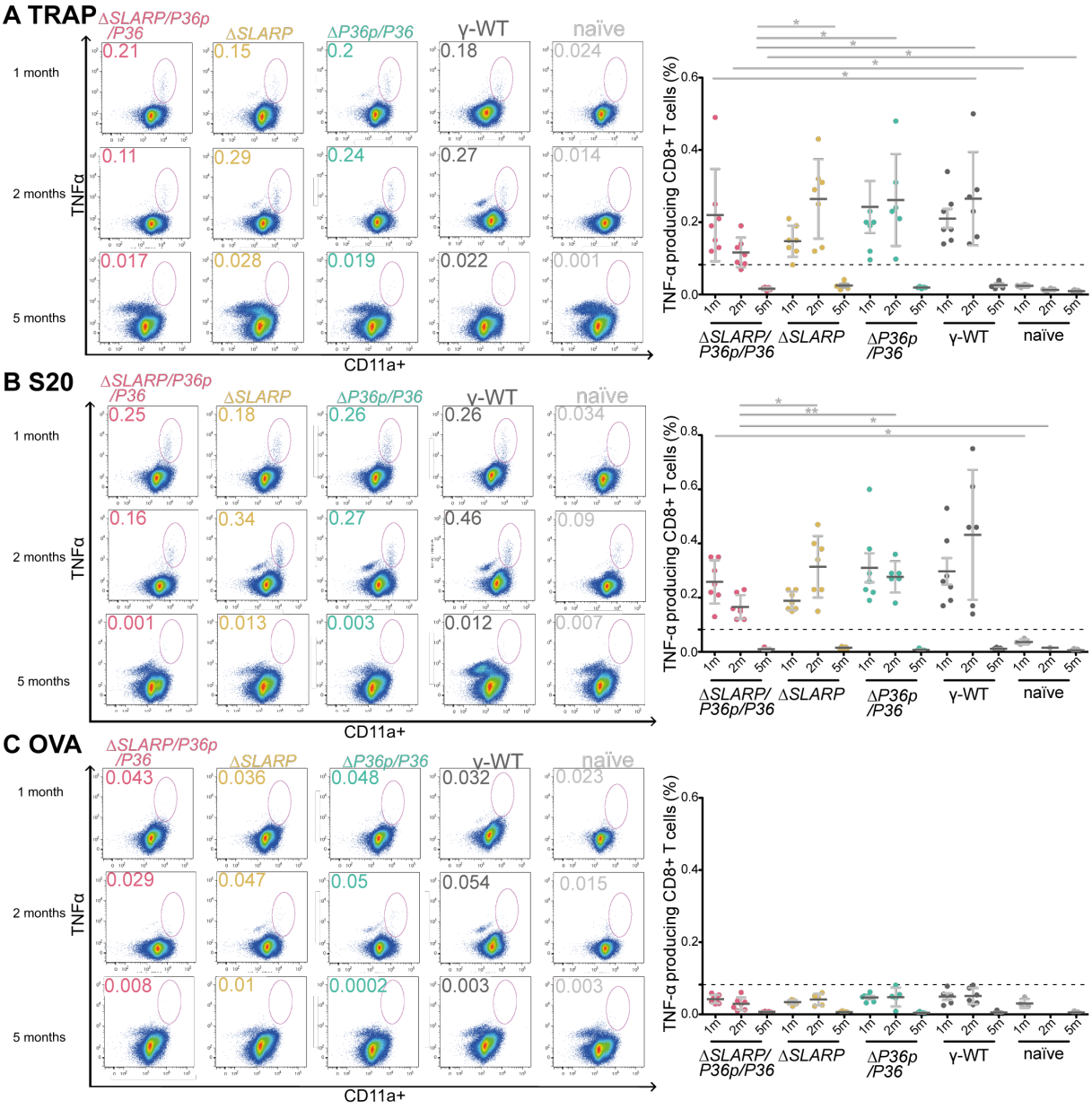

Supplementary Figure 2 TNF-α secreting CD8⁺ T cells in spleen are reduced in *ΔSLARP/P36p/P36* immunized animals

Analysis of CD8⁺ T cells elicited in immunized cohorts. C57BL/6 mice were immunized in a prime/boost regimen (7 days apart), challenged one or two months p.i. and treated with pyrimethamine in the drinking water before excision of spleens one month post challenge. For the excision of spleens from immunized mice 5 months p.i., animals were immunized in a prime/boost regimen (7 days apart) and challenged 5 months p.i.. Spleens were excised 42h post challenge. Splenic cells were restimulated with H2-K^b specific peptide epitopes (TRAP/S20) and a control OVA/H2-D^b and stained with fluorescently labeled antibodies for analysis with MACSQuant. FACS files were processed with FlowJo 8.7.3. **A** Examples of mean CD8⁺ T TNF-α secretion restimulation with TRAP peptide in spleens of immunized cohorts one, two or five months post immunization compared to naïve controls. Statistical analysis: Mann-Whitney-U test, *, $p<0.05$, **B** Examples of mean TNF-α secreting CD8⁺ T cell restimulation with S20 peptide of immunized cohorts one, two and five months post immunization compared to naïve controls. Statistical analysis: Mann-Whitney-U test, *, $p<0.05$, **, $p<0.01$**C** Examples of mean TNF-α secreting CD8⁺ T cell restimulation with OVA peptide, as negative control, of immunized cohorts one, two and five months post immunization compared to naïve controls. Dot blot shows comparison of percentage of CD8⁺ T cell TNF-α secretion in immunized cohorts. Depicted are TNF-α producing CD8⁺ T cells of individual mice (dots), as well as the mean of the cohort ± SD. Only significant statistical differences of cohorts compared to *ΔSLARP/P36p/P36* immunized mice are shown. Statistical analysis: Mann-Whitney-U test.

Supplementary Table 1 Normal development of *ΔSLARP/P36p/P36* mosquito stages

Parasite strain	Midgut infectivity (%) d10-14	Number of salivary gland sporozoites/mosquito d17-25
ΔSLARP/P36p/P36	83	8680± 6.800
ΔSLARP	62	10500± 3.880
ΔP36p/P36	57	13100± 7.360
WT	57	22900± 2.760

[a] Average numbers of three independent biological experiments
[b] Average numbers of six independent biological experiments

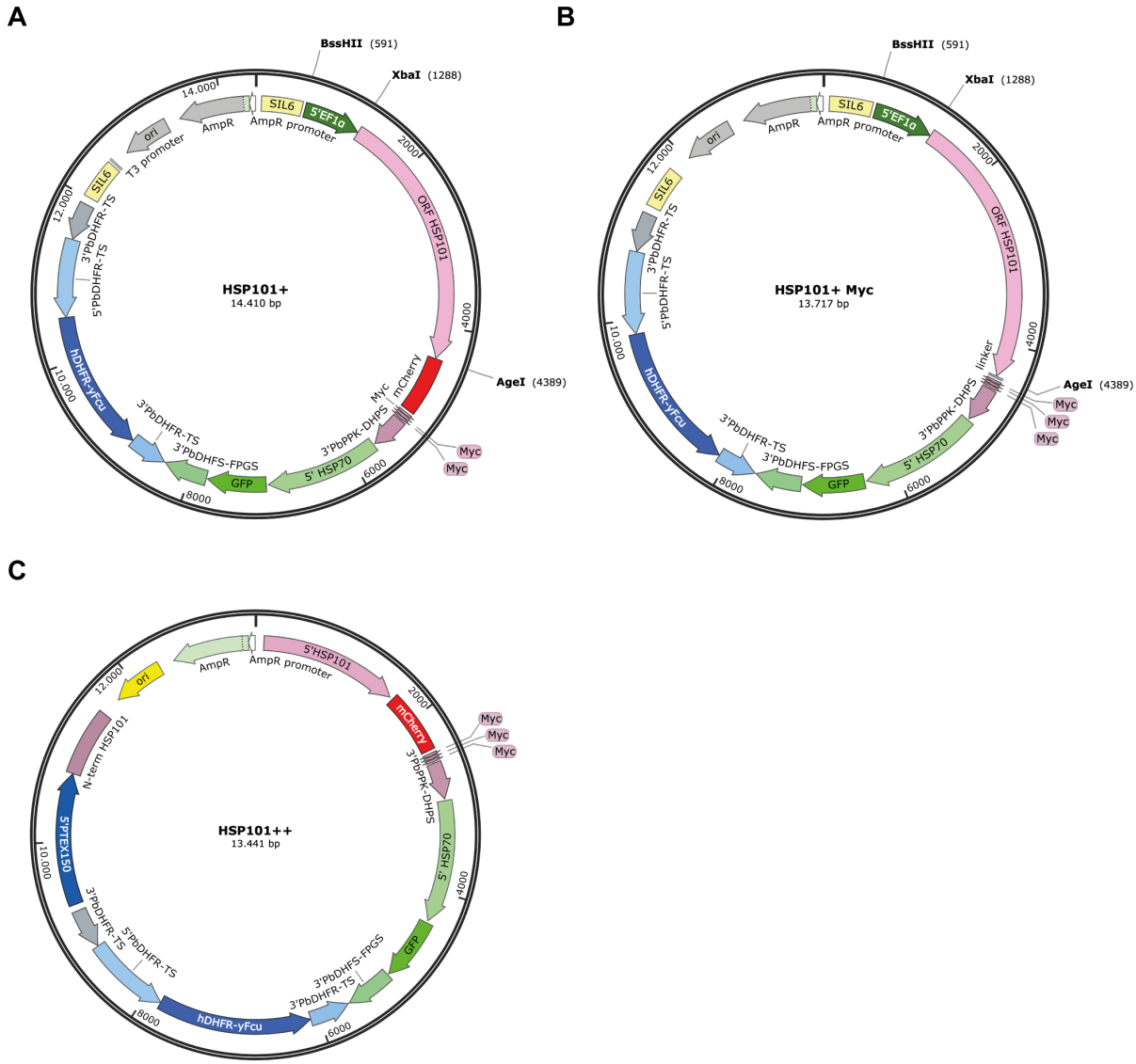

Supplementary Figure 3 Plasmid maps of pHSP101+/Myc and pHSP101++

A+B Schematic plasmid maps of pHSP101+/Myc. Depicted in light yellow are the silent 6 homologous regions for homologous recombination. The *EF1a* promoter (dark green) was inserted in the *Bss*HII-*Xba*I restriction site upstream of the *HSP101* ORF (light pink), which was inserted in the *Xba*I-*Age*I restriction site in frame with mCherry (red) and triple Myc taq (pink) or triple Myc only for pHSP101+Myc. GFP (bright green) under the control of *HSP70* promoter (light green) was included for parasite detection throughout the life cycle and positive selection by FACS sorting. The plasmid additionally harbors an hDHFR-yFcu (dark blue) under the control of *PbDHFR* promoter (light blue) for positive/ negative selection of transgenic or recycled parasites. **C** Schematic plasmid map of pHSP101++. Depicted in light

pink are the *HSP101* 5' UTR and N-terminus for homologous recombination. A mCherry (red) and a triple Myc tag (dark pink) are downstream of the *HSP101* 5' UTR, however, mCherry and Myc are not expressed due to a lack of a start codon. Additionally, a new promoter PTEX150 (dark blue) was inserted upstream of the *HSP101* N-terminus. The plasmid contains a GFP (bright green) under the *HSP70* promoter (light green) for parasite detection throughout the life cycle and positive selection by FACS sorting. Additionally, an hDHFR-yFcu (dark blue) under the control of *PbDHFR* promoter (light blue) is present in the plasmid for positive/ negative selection of transgenic or recycled parasites.

Supplementary Table 2 Normal development of *HSP101+/Myc* and *HSP101++* mosquito stages

Parasites	Midgut infectivity (%)[a]	Numbers of salivary gland Sporozoites/Mosquito[b]
HSP101+	50	14250 ±9889
HSP101++	70	18440 ±4555
HSP101+Myc	73	11750[c]
WT	47	17458 ±15624

[a] Average numbers of three independent biological experiments
[b] Average numbers of six independent biological experiments
[c] Average number of one experiment only

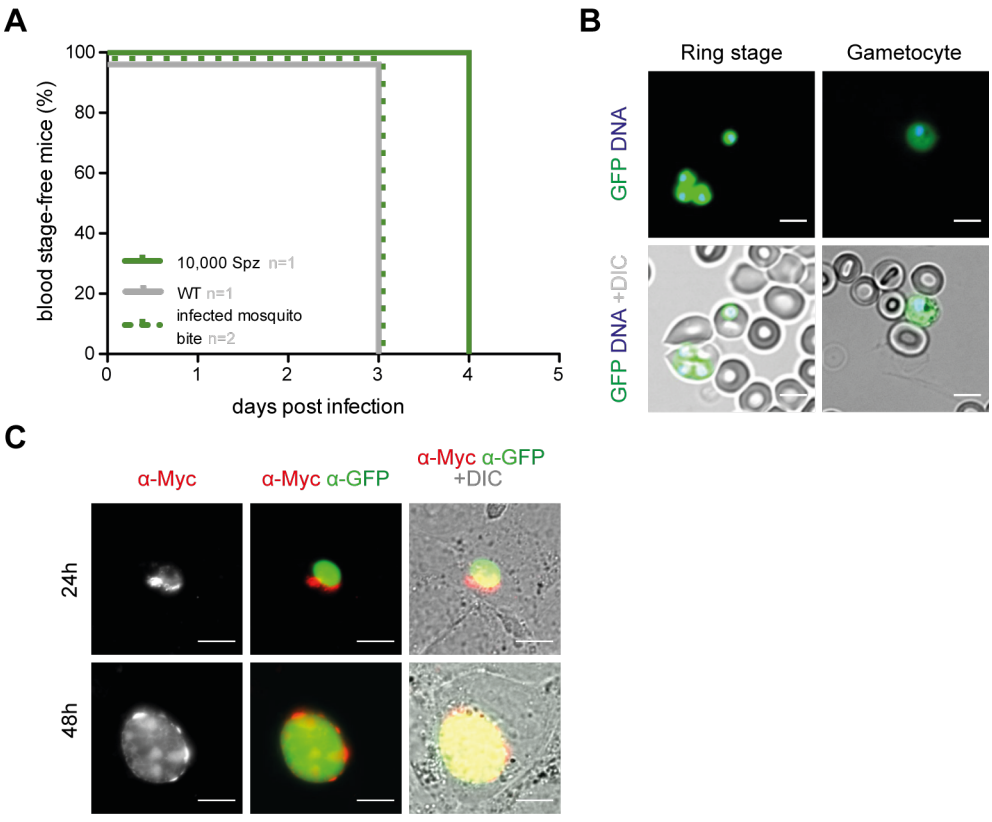

Supplementary Figure 4 Normal life cycle progression of *HSP101+Myc*

A Kaplan-Meier curve analysis of time to patency after sporozoite infection. C57BL/6 mice were infected with $1x10^4$ *HSP101+Myc* (green), or WT (dark grey) sporozoites i.v. or by natural transmission by exposure to 15 *HSP101++* infected mosquitoes and blood infection was monitored by daily microscopic examination of Giemsa-stained blood smears. **B** Live imaging blood stages: ring stage and gametocyte. Cells were stained with Hoechst 33342 1:5,000 (blue) for nuclear staining. Expression of transgenic parasite marker GFP staining the parasite's cytoplasm is displayed in green (Scale bar: 5 µm). **C** Immunofluorescence microscopy analysis (IFA) of α-Myc (HSP101, red) and α-GFP (green) stained *HSP101+* and WT *P.b.* parasites at 24 and 48 hours post hepatoma cell (Huh7) infection shows localization of HSP101 to the parasite's PV. Nuclear staining was performed with Hoechst 33342 (blue). Left panel is showing α-Myc (HSP101) staining only (Scale bar 10 µm).

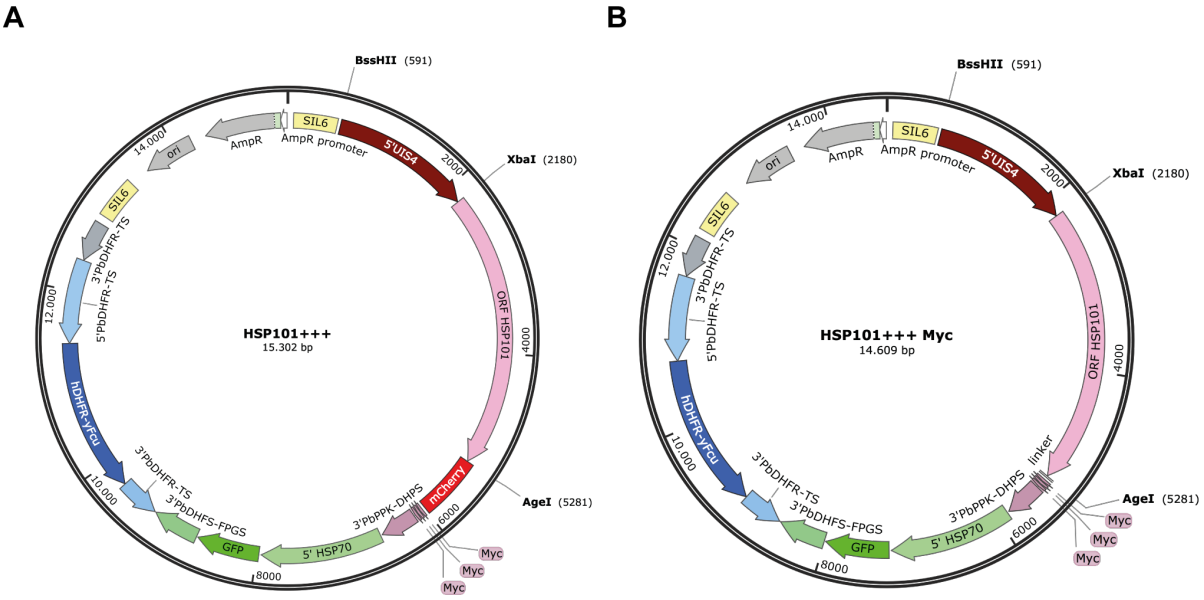

Supplementary Figure 5 Plasmid map of *HSP101+++* and *HSP101+++Myc*

A+B Schematic plasmid maps of pHSP101+++/Myc. Depicted in light yellow are the silent 6 homologous regions for homologous recombination. The *UIS4* promoter (dark red) was inserted in the *Bss*HII-*Xba*I restriction site upstream of the *HSP101* ORF (light pink), which was inserted in the *Xba*I-*Age*I restriction site in frame with mCherry (red) and triple Myc tag (pink) or triple Myc only for pHSP101+++Myc. GFP (bright green) under the control of *HSP70* promoter (light green) was included for parasite detection throughout the life cycle and positive selection by FACS sorting. The plasmid additionally harbors an hDHFR-yFcu (dark blue) under the control of *PbDHFR* promoter (light blue) for positive/ negative selection of transgenic or recycled parasites.

Supplementary Table 3 Normal development of *HSP101+++/Myc* mosquito stages

Parasites	Midgut infectivity (%)[a]	Numbers of salivary gland Sporozoites/Mosquito[b]
HSP101+++	90	9214 ±4856
HSP101+++Myc	90	5160 ±919
WT	60	8710 ±2307

[a] Average numbers of three independent biological experiments
[b] Average numbers of six independent biological experiments

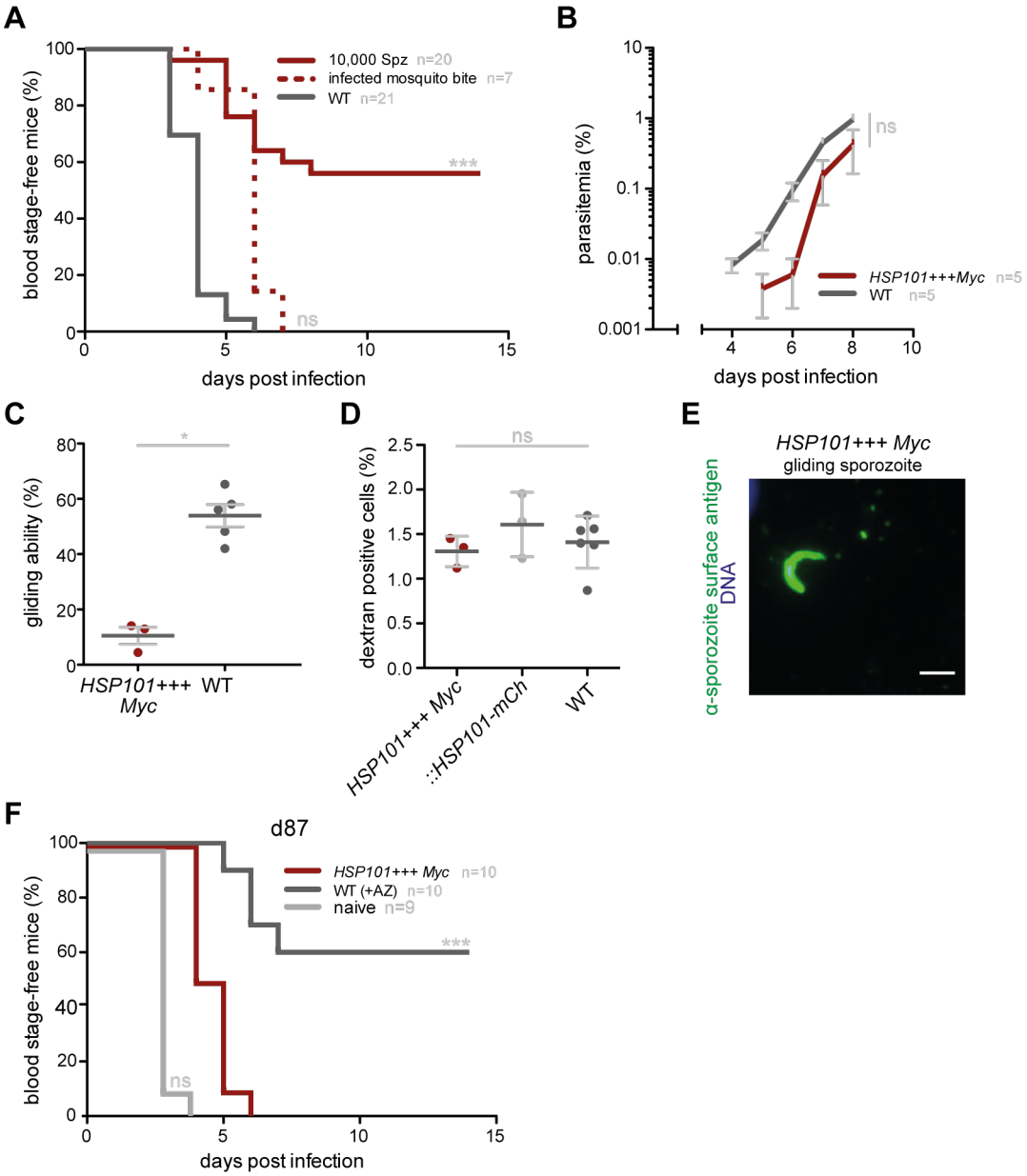

Supplementary Figure 6 Pre-erythrocytic development is severely impaired in *HSP101+++Myc* parasites

A Kaplan-Meier curve of blood infection over time after sporozoites infection. C57BL/6 mice were infected with 1x10^4 *HSP101+++Myc* (dark red) or WT (dark grey) sporozoites or by natural transmission by exposure to 15 *HSP101+++Myc* infected mosquitoes and blood infection was monitored by daily microscopic examination of Giemsa-stained blood smears of four (for 1x10^4 sporozoite infection) and two (for natural transmission) independent biological experiments. Statistical analysis: Log rank (Mantel-Cox) test, n.s., non-significant, ***p<0.001. **B** Blood stage growth (parasitemia %) 3-8 days post sporozoite infection is unaffected in comparison to WT infections. Giemsa-stained thin blood smears from pre-patency analysis were additionally used for quantifying parasitemia of one biological experiment. Shown is the mean of five mice ±SD. Statistical analysis: growth slope difference n.s., non-significant **C** Impaired sporozoite gliding motility of *HSP101+++Myc*. Salivary gland *HSP101+++Myc* and WT *P.b.* sporozoites were excised at day 17 and left to settle and subsequently glide on a BSA-covered 2-dimensional glass slide. Sporozoite surface protein trails shed by gliding sporozoites were stained with α-sporozoite surface antigen and Hoechst 33342 for nuclear staining. Three independent experiments (dots) were used to determine the percentage of gliding sporozoites. Depicted are the mean ±SD. Statistical analysis: Mann-Whitney-U-test *, p<0.05 **D** Normal transmigration of *HSP101+++Myc* sporozoites. Shown is the FACS quantification of dextran-positive hepatoma cells after two hours post sporozoite infection. 1x10^6 Huh7 cells were infected with 7.5x10^4 *HSP101+++Myc* or WT *P.b.* sporozoites or dextran+/sporozoites- (as a control for dextran influx without sporozoite infection) and analyzed with FACS for dextran influx using MACSquant. Examples of gating strategy: FITC (dextran) is blotted against FFC for dextran-/sporozoite-,

dextran+/sporozoite- and dextran+/sporozoite+ (WT) cells. Depicted are individual percentages of dextran positive cells of each replicate of three independent experiments (with three replicates each) ±SD. Statistical analysis: Mann-Whitney-U-test ns: non significant **E** Impaired sporozoite gliding motility of *HSP101+++Myc*. Shown is a representative immunofluorescence image of *HSP101+++Myc* salivary gland sporozoite. The transgenic parasite and the gliding trail were stained with α-sporozoite surface antibody and with Hoechst 33342 for nuclear staining (Scale bar: 5 µm) **F** Kaplan-Meier analysis of blood infection over time after sporozoite challenge reveals no protection in *HSP101+++Myc*-immunized animals. Mice were immunized and boosted after 10 days with *HSP101+++Myc* or WT sporozoites under AZ drug cover. WT *P.b.* sporozoite challenge was performed 87 days post immunization and non-immunized control animals (naïve, light grey) confirmed sporozoite infectivity by patent blood stage infection 3 days post inoculation. Pre-patency was monitored 3-14 days p.i. using Giemsa-stained thin blood smears. Statistical analysis: Log rank (Mantel-Cox) test, n.s., non-significant, ***, $p< 0.001$

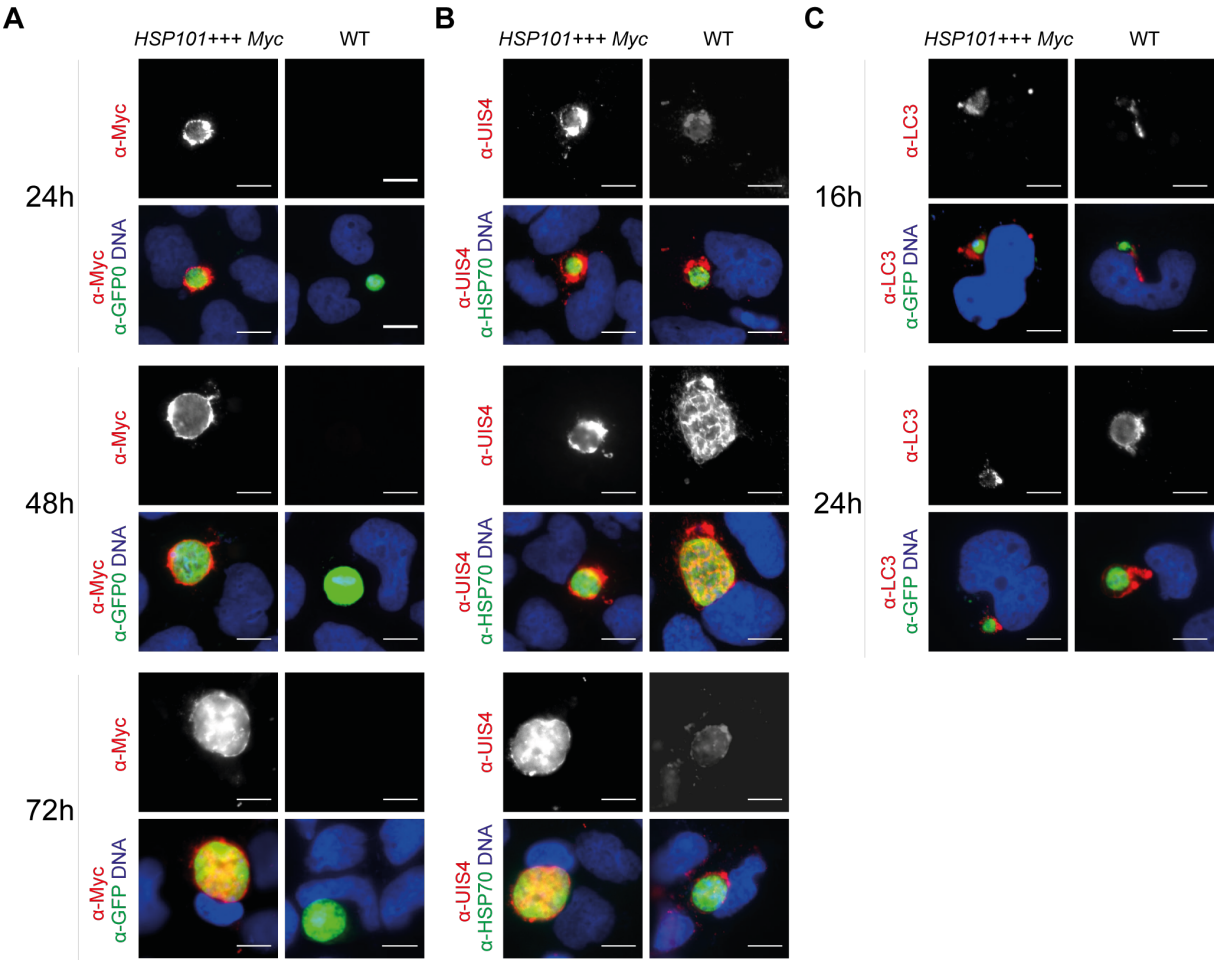

Supplementary Figure 7 *HSP101+++Myc* parasites establish a PVM during liver stage development

A Immunofluorescence microscopy analysis (IFA) of α-Myc (HSP101, red) and α-GFP (staining the parasite's cytoplasm in green) stained *HSP101+++Myc* and WT *P.b.* parasites at 24, 48 and 72 hours post hepatoma cell (Huh7) infection shows localization of HSP101 to the PV. Nuclear staining was performed with Hoechst 33342 (blue). Upper panel is showing Myc (HSP101) staining only, lower panel is displaying the merged image. (Scale bar 10 µm) **B** Localization of UIS4 by IFA in *HSP101+++*Myc and WT *P.b.* parasites infected Huh7 cells at 24, 48 and 72 hours p.i.. Upper panel is showing α-UIS4 (red) staining only, lower panel is depicting the merged image with α-GFP (green) and nuclear staining with Hoechst 33342 (blue). (Scale bar 10 µm) **C** IFA of α-LC3 (red) and α-GFP (green) stained *HSP101+++Myc* and WT *P.b.* parasites at 16 and 24 hours post Huh7 infection reveals LC3, a host autophagy marker, localization to the parasite's PVM. Nuclear staining is displayed with Hoechst 33342 (blue). Upper panel is showing α-LC3 (red) staining only, lower panel is displaying the merged image (Scale bar 10 µm).

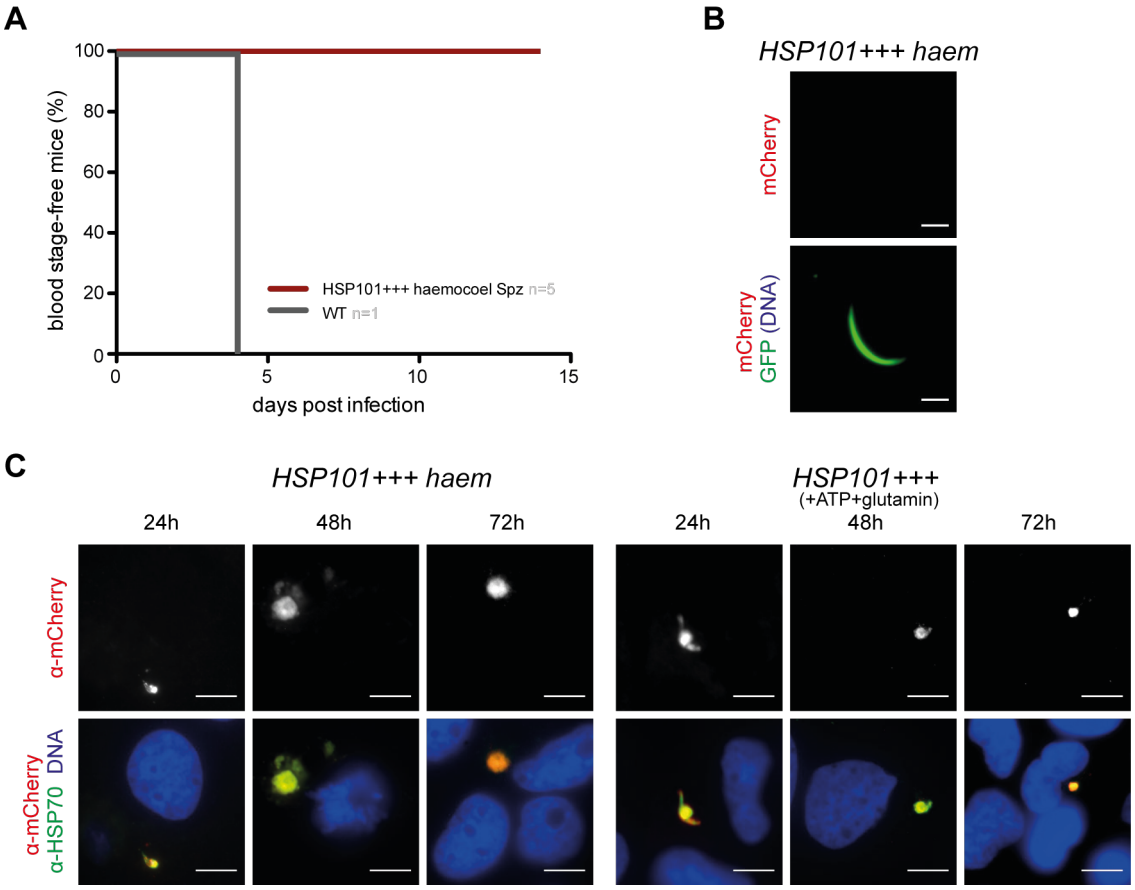

Supplementary Figure 8 Exo-erythrocytic development is still impaired in *HSP101*+++ haemocoel sporozoites or under the addition of ATP

A Kaplan-Meier curve of time to blood stage pre-patency after sporozoites infection reveals pre-erythrocytic developmental arrest of *HSP101*+++ haemocoel sporozoites. C57BL/6 mice were infected with $1x10^4$ *HSP101*+++ (dark red) or WT (dark grey) sporozoites and blood infection was monitored by daily microscopic examination of Giemsa-stained blood smears. Statistical analysis: Log rank (Mantel-Cox) test, n.s., non-significant; *, p<0.05,**, *p*< 0.01, ***p<0.001. **B** Live imaging of *HSP101*+++ haemocoel sporozoites. Expression of HSP101-mCh is not present in haemocoel sporozoites as the *UIS4* promoter is not active (upper panel). The transgenic parasite marker GFP, staining the parasite's cytoplasm, is displayed in green. Nuclear staining was performed with Hoechst 33342 1:5,000 and motility inhibition with 1:50 Phalloidin (Scale bar: 5 µm). **C** Immunofluorescence microscopy analysis of α-mCherry (HSP101, red) and α-HSP70 (green) stained *HSP101*+++ haemocoel or *HSP101*+++ salivary gland sporozoites incubated with 0.01 mM ATP and glucose at 24, 48 and 72 hours post hepatoma cell (Huh7) infection shows liver stage developmental abort. Nuclear staining was performed with Hoechst 33342 (blue). Upper panel is showing α-mCherry (HSP101) staining only (Scale bar 10 µm).

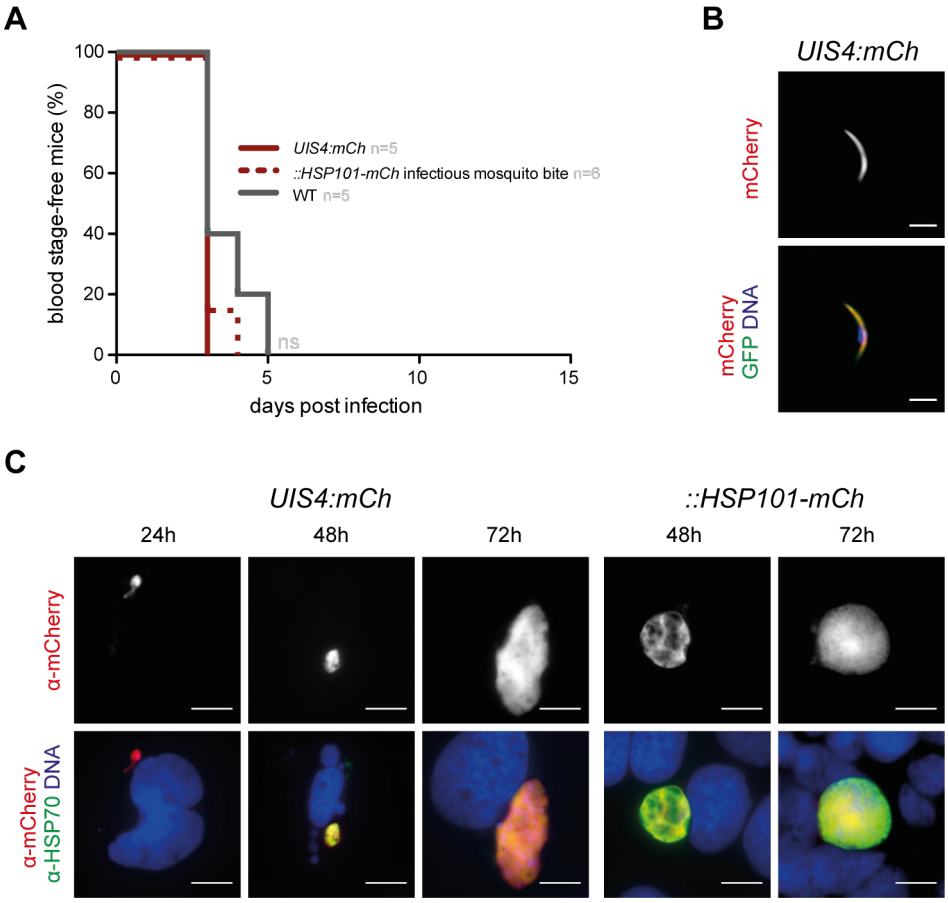

Supplementary Figure 9 Normal pre-erythrocytic development of *UIS4::mCh* and *::HSP101-mCh* parasites

A Kaplan-Meier curve of time to blood stage patency after sporozoite infection reveals normal infection with *UIS4::mCh* and *::HSP101-mCh* parasites *in vivo*. C57BL/6 mice were infected with $1x10^4$ *UIS4::mCh* (dark red) or WT (dark grey) sporozoites or by natural transmission by exposure to 15 *::HSP101-mCh* infected mosquitoes and blood infection was monitored by daily microscopic examination of Giemsa-stained thin blood smears. Statistical analysis: Log rank (Mantel-Cox) test, n.s., non-significant. **B** Live imaging of *UIS4::mCh* sporozoites. Expression of mCherry in sporozoites is displayed in upper panel. The transgenic parasite marker GFP, staining the parasite's cytoplasm, is displayed in green. Nuclear staining was performed with Hoechst 33342 1:5,000 and motility inhibition with 1:50 Phalloidin (Scale bar: 5 µm). **C** Immunofluorescence microscopy analysis (IFA) of α-mCherry (red) and α-HSP70 (green) stained *UIS4::mCh* and *::HSP101-mCh* parasites at 24, 48 and 72 hours post hepatoma cell (Huh7) infection shows normal liver stage development. Nuclear staining was performed with Hoechst 33342 (blue). Upper panel is showing α-mCh (or HSP101-mCh) staining only (Scale bar 10 µm).

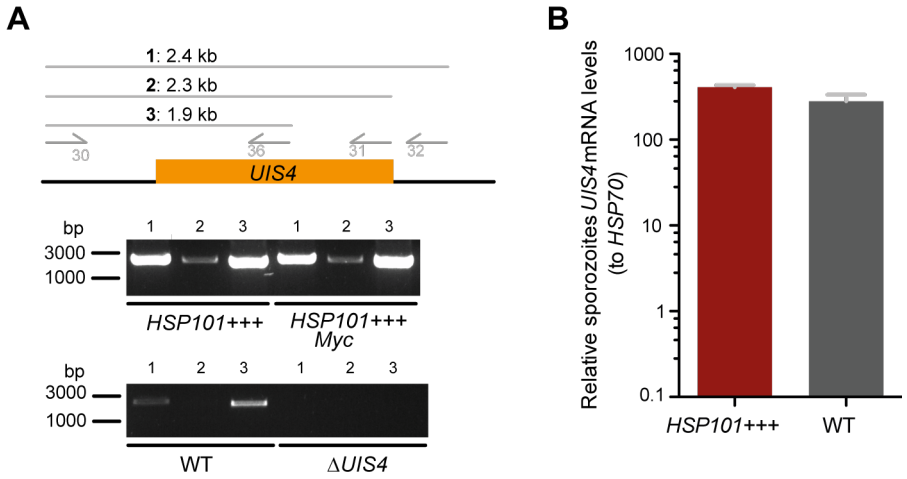

Supplementary Figure 10 *UIS4* is expressed in *HSP101*+++ parasites

A Genotyping of *HSP101*+++ and *HSP101*+++*Myc* parasites by PCR. Presence of an intact *UIS4* locus (orange) in *HSP101*+++ was confirmed with UIS4 5', 3' UTR and ORF specific primer combinations (in grey). *P.b.* ANKA WT gDNA was used as control. **B** Quantitative RT-PCR analysis of *UIS4* mRNA levels in *HSP101*+++ and WT sporozoites. *HSP101*+++ and WT sporozoites were excised from salivary gland of infected mosquitoes at day 17, RNA was extracted from sporozoites relative mRNA levels normalized to *PbHSP70* levels. Data is displayed as mean of two technical replicates.

Supplementary Table 4 Additional transgenic parasite lines and plasmid constructs for liver stage PTEX complex and export analysis

Name	Parasite line/ Plasmid	Purpose
EXP2::HSP101	Parasite line (clonal)	HSP101 overexpression
HSP70::HSP101-Myc	Parasite line (mixed)	HSP101 overexpression
HSP101+ rec	Parasite line (clonal)	recycled parasites for integration of other constructs
HSP101+/ UIS4::CS-PEXEL-OVA	Parasite line (clonal)	export analysis
HSP101++/ UIS4::CS-PEXEL-mCh	Parasite line (clonal)	export analysis
pEXP2::PTEX150		PTEX150 overexpression
pEF1α::PTEX150	Plasmid	PTEX150 overexpression
pEF1α::HA-PTEX150	Plasmid	PTEX150 overexpression and tagging
p::HA-PTEX150	Plasmid	PTEX150 N-terminal tagging
p::mCh-PTEX150	Plasmid	PTEX150 N-terminal tagging
pPTEX150::mCh-PTEX150	Plasmid	double crossover PTEX150 N-terminal tagging
pΔHSP101/IBIS::IBIS-PEXEL-GFP	Plasmid	knockout of endogenous HSP101 while inserting a reporter construct
pΔHSP101/IBIS::IBIS- PEXEL-Myc	Plasmid	see above
pΔHSP101/IBIS::IBIS-GFP	Plasmid	knockout of endogenous HSP101 while inserting a control non-functional reporter construct
pΔHSP101/IBIS::IBIS-Myc	Plasmid	see above
pLISP2::HSP101-Myc	Plasmid	HSP101 overexpression
pEXP2::HSP101-Myc	Plasmid	HSP101 overexpression
pHSP70::HSP101-mCh	Plasmid	HSP101 overexpression